THE NONLINEAR BEHAVIOUR OF SHALLOW SPHERICAL SHELLS

Abstract of Thesis presented for the Degree of Doctor of Philosophy of the University of Glasgow.

by

J.D.W. Hossack, B.Sc., A.R.C.S.T.

March, 1965.

A B S T R A C T

The subject matter of the thesis concerns the instability of shallow spherical shells. It presents an analytical and experimental investigation of the elastic, nonlinear, axisymmetric behaviour of such shells under the action of uniform pressure and point loading at the apex.

Chapter I is a critical survey of the relevant published literature. The survey outlines the development of the theoretical aspects of shell buckling and shows how this was influenced by the results of experimental investigations. It further outlines the development of highly refined experimental techniques which reduced the scatter of results characteristic of previous work. It is then shown that even experimental work using these refined techniques, provides only a partial substantiation of theoretical analyses and it is concluded that the apparent disparity may be due to the uncertain character of the displacement dependent boundary restraints employed.

In Chapter II, the essential equivalence of the governing differential equations adopted by many authors is demonstrated for the first time in an integrated manner. The solution of these equations:

equations is discussed with special reference to an original analysis of the case of a pressure loaded, freely supported shell. Alternative solutions by direct integration and the Galerkin method are discussed but these are shown to lead to excessive computational difficulties. The effect of various boundary conditions is then examined and their influence on critical load values is shown to be significant.

In the research undertaken, displacement dependent boundary conditions were avoided by using only force dependent conditions in the experimental work. The simplest of these conditions are those corresponding to a free support.

In Chapter III, the requirements of experimental technique necessary to obtain the equilibrium path in both the stable and unstable states of equilibrium are discussed. This has led to the development of new techniques of preparation of accurate, stress-free specimens and the adoption of a new, controlled deflection loading technique. The experimental investigation also presents, for the first time, the measurement of surface strains throughout the loading history of the shells.

The:

The results of the experimental investigations are discussed and compared with theory in Chapter IV. A critical comparison with the published experimental work of previous investigators is included where relevant.

Chapter V summarises the main findings of the investigation regarding the basic aspects and shows that good agreement with theory is obtained by the refinement of experimental techniques introduced so as to approach as closely as possible, the assumptions of the theoretical analysis. Thus, for the first time to the author's knowledge, experimental results which are both consistent in themselves and in agreement with theory have been obtained. The application of the results of the investigation to practical engineering problems is considered.

A Bibliography and Author's Index is provided in Chapter VI, followed in Chapter VII by Appendices giving details of analyses considered in the thesis, together with a full presentation of the results of the experimental investigation.

THE NONLINEAR BEHAVIOUR OF SHALLOW SPHERICAL SHELLS

Thesis presented for the Degree of
Doctor of Philosophy of the
University of Glasgow.

by

J.D.W. Hossack, B.Sc., A.R.C.S.T.

March, 1965.

I N D E X

C O N T E N T S

ABSTRACT

The subject matter of the thesis concerns the instability of shallow spherical shells. It presents an analytical and experimental investigation of the elastic, nonlinear, axisymmetric behaviour of such shells under the action of uniform pressure and point loading at the apex.

Chapter I is a critical survey of the relevant published literature. The survey outlines the development of the theoretical aspects of shell buckling and shows how this was influenced by the results of experimental investigations. It further outlines the development of highly refined experimental techniques which reduced the scatter of results characteristic of previous work. It is then shown that even experimental work using these refined techniques, provides only a partial substantiation of theoretical analyses and it is concluded that the apparent disparity may be due to the uncertain character of the displacement dependent boundary restraints employed.

In Chapter II, the essential equivalence of the

governing differential equations adopted by many authors is demonstrated for the first time in an integrated manner. The solution of these equations is discussed with special reference to an original analysis of the case of a pressure loaded, freely supported shell. Alternative solutions by direct integration and the Galerkin method are discussed but these are shown to lead to excessive computational difficulties. The effect of various boundary conditions is then examined and their influence on critical load values is shown to be significant.

In the research undertaken, displacement dependent boundary conditions were avoided by using only force dependent conditions in the experimental work. The simplest of these conditions are those corresponding to a free support.

In Chapter III, the requirements of experimental techniques necessary to obtain the equilibrium path in both the stable and unstable states of equilibrium are discussed. This has led to the development of new techniques of preparation of accurate, stress-free specimens and the adoption of a new, controlled deflection loading technique. The experimental

investigation also presents, for the first time, the measurement of surface strains throughout the loading history of the shells.

The results of the experimental investigations are discussed and compared with theory in Chapter IV. A critical comparison with the published experimental work of previous investigators is included where relevant.

Chapter V summarises the main findings of the investigation regarding the basic aspects and shows that good agreement with theory is obtained by the refinement of experimental techniques introduced so as to approach as closely as possible, the assumptions of the theoretical analysis. Thus, for the first time to the author's knowledge, experimental results which are both consistent in themselves and in agreement with theory have been obtained. The application of the results of the investigation to practical engineering problems is considered.

A Bibliography and Author's Index is provided in Chapter VI, followed in Chapter VII by Appendices giving details of analyses considered in the thesis, together with a full presentation of the results of the experimental investigation.

NOTATION

a	base radius of shallow cap
R	spherical radius of curvature
t	thickness of spherical shell
r, θ	polar co-ordinates
h	rise of spherical cap given by $h = \frac{a^2}{2R}$
ρ, ξ, γ	dimensionless parameters defined by $\rho = \frac{r}{a}$, $\xi = \frac{r}{R}$, $\gamma = \frac{a}{R}$
$\varepsilon_r, \varepsilon_\theta$	meridional and circumferential strain
u, v, w	tangential, axial and normal components of displacement
δ	deflection parameter given by $\delta = \frac{w}{h}$
δ_o	dimensionless deflection at $r = 0$
Ψ	rotation of normal to shell surface
N_r, N_θ	meridional and circumferential membrane force per unit length
M_r, M_θ	meridional and circumferential bending moment per unit length
Q	shear force per unit length
Φ	stress function given by $\Phi = rN_r$
E, ν	Young's modulus and Poisson's ratio

D flexural rigidity $D = \dfrac{Et^3}{12(1-\nu^2)}$

B extensional rigidity $B = \dfrac{Et}{1-\nu^2}$

λ, μ, η dimensionless shell parameters defined by:

$$\lambda = \frac{a^4}{R^2t^2}, \quad \mu = 2\left[3(1-\nu^2)\right]^{\frac{1}{4}}\left(\frac{h}{t}\right)^2 = \left[12(1-\nu^2)\lambda\right]^{\frac{1}{4}}$$

$$\eta = 12(1-\nu^2)\left(\frac{a}{t}\right)^2$$

P axial point load at apex of shell

p uniform pressure load intensity

$\dfrac{PR}{Et^3}$ point load parameter

$\dfrac{pRa^2}{Et^3}$ pressure load parameter

q classical buckling pressure for complete sphere given by

$$q = \frac{2Et^2}{R^2\left[3(1-\nu^2)\right]^{\frac{1}{2}}}$$

CHAPTER I

REVIEW OF PUBLISHED LITERATURE

I.1 Introduction

In view of the inherent complexity of the shell buckling phenomenon, early theoretical treatments were based on relatively simple concepts regarding the assumed behaviour of idealised shells. The results of experimental investigations indicated collapse loads which were considerably lower than those obtained on the basis of these early theoretical analyses. It was obvious, therefore, that the actual mechanism of buckling was appreciably more complex than that assumed in the analysis and that the phenomenon was influenced by factors outwith the scope of the early theoretical treatments. At the same time as the theoretical analysis was extended to take account of these factors, workers in the experimental field attempted to manufacture and test specimens which conformed more closely with the idealised shells of the theory. Thus a continuous process of extension of the theoretical work and refinement of experimental technique was initiated.

It therefore appears reasonable to review the published literature chronologically and thus illustrate this continuous development of the

theoretical analysis and refinement of experimental technique whereby a better understanding of the buckling phenomenon has emerged.

Before examining in detail some of the more recent contributions to the understanding of the phenomenon of instability in shallow shell segments, it is convenient to survey briefly the early approaches to the problem indicating the formulation of the basic concepts of shell buckling. It is also convenient to review the criteria governing instability and to indicate how greater refinement in theoretical treatments became necessary in the light of experimental data. With special reference to the latter, a brief analysis of the factors influencing experimental work is presented so that a more critical assessment may be made of papers dealing with this aspect when these are reviewed later.

The first investigations of the phenomenon of elastic instability were concerned with the problem of the complete sphere subject to external pressure. The work of ZOELLY[1] and SCHWERIN[2] introduced the concept of the classical definition of a critical pressure. Both ZOELLY and SCHWERIN considered

rotationally symmetric deformations but VAN DER NEUT[3] was more general in his assumptions. In their analyses, only linear terms were retained in defining strains in terms of displacements. The resulting governing differential equations were thus linear in character. Their work represented the classical analysis based on the classical criterion of instability. This was defined as the lowest pressure at which an adjacent stable equilibrium configuration was possible.

The first experimental work was reported in 1939 by KARMAN and TSIEN[4]. This work was carried out on a copper hemisphere of 0.02 in. wall thickness and 18 in. radius. The shell snapped into a rotationally symmetric form at about one quarter of the classical pressure. This and later work indicated an apparent failure of the classical theory to predict instability. It therefore became clear that analysis of the post-buckled states was necessary and this problem was assumed to be that of a spherical segment clamped at the boundary. These early analyses were based on the assumption of a simple algebraic term with a single undetermined constant to describe the deformation of the shell. Such an assumption has been shown to yield

substantial error in the light of subsequent experimental work. From this stage, only work relevant to the shallow spherical shell is considered.

The use of so called energy methods to solve the governing differential equations led to the formulation of the energy criterion of buckling. This was defined as the lower limit of all values of the pressure for which a buckled state of equilibrium existed with an energy level below that of the unbuckled state. Several authors subsequently discussed at some length the validity and interpretation of the energy concept. As a criterion, it was artificial and appeared to yield a lower bound on the theoretical and (almost) all the available experimental data and did not contribute materially to the better understanding of the problem.

Later, when the inherent limitations implied in the use of a single term to describe the deformation of the shell had been appreciated, attention was focussed on the numerical difficulties involved when further terms were retained. In 1963 FEODOS'EV[5] introduced dynamic terms into the governing equations,

basing the evaluation of the equilibrium condition on the frequency parameter. He showed that the solution of the resulting algebraic equations in his variational approach could be simplified and thus introduced a new concept of general application into the solution of the problem. The main advantage accruing from his approach, was that the investigator was not bound in advance by definite criteria of stability.

Until fairly recently, the major part of the published literature has been based on assumed symmetrical behaviour of the shell. It has been recognised for some time that the agreement between the theory and experimental data has been disappointing for some ranges of shell form. This has led authors to seek means of explaining the discrepancy. Such a discrepancy may arise from two sources; the theory may be at fault by omitting, for example, the effects of imperfections or the experimental data may be suspect. In considering the theoretical aspect, some authors have investigated the influence of assumed initial irregularity. This by itself has been insufficient to account for some of the disparity. More recent analyses have recognised that collapse of the shell may occur via nonsymmetric modes and this has been shown to have an important effect

on the critical load. Recent research has shown that early authors were insufficiently critical of the available experimental evidence with which they compared their theoretical results. Experimental results are very sensitive to a variety of factors only in part considered by previous workers.

I.2 The Effect of Errors of Measurement

In order to verify any particular theoretical solution, certain basic requirements of the experimental model must be fulfilled. In general, a shell theory will include dependent parameters which define the shell geometry, the load and the elastic properties of the shell itself.

Considering first the shell geometry, the relevant shell parameter may be defined by

$$\mu = a \sqrt[4]{12(1-\nu^2)}/\sqrt{Rt}$$

Similarly, the pressure load parameter may be defined by

$$P = \frac{\sqrt{3(1-\nu^2)}\ R^2 p}{2 E t^2}$$

These definitions are those most commonly adopted, and it is obvious that the parameters depend on the following quantities:

a = base radius of shell

R = spherical radius of shell

t = thickness of shell

which define the shell geometry, and

ν = Poisson's ratio

E = Young's modulus

which represent the material properties of the shell.

Let $K = 1 - \nu^2$, then the relative error in μ and P , expressed as a function of the relative errors in a, R, t, E, p and K will be

$$\frac{\delta\mu}{\mu} = \frac{1}{4}\frac{\delta K}{K} + \frac{\delta a}{a} + \frac{1}{2}\frac{\delta R}{R} + \frac{1}{2}\frac{\delta t}{t}$$

and

$$\frac{\delta P}{P} = \frac{1}{2}\frac{\delta K}{K} + 2\frac{\delta R}{R} + 2\frac{\delta t}{t} + \frac{\delta E}{E} + \frac{\delta p}{p}$$

Consider the relative error in μ . It is clear that this depends largely on a which can, however, be measured with considerable accuracy. The effect of errors in R and t is not so pronounced.

The determination of the error in P is more complicated due to the quadratic dependence on R and t . Errors in t, apart from those due to faulty measurement, may arise from random non-uniformity in the thickness of the shell. Where such random variations occur in the thickness of the shell, it is difficult to decide what value of t should be used in correlating theoretical and experimental work. For example, an error in t of $\pm$ 3% could lead to calculated values of P differing by 12%. Similarly, an error in the determination of the spherical radius has effects of the same order. Thus an uncertainty of the order of $\pm$ 3% in both R and t could lead to values of P differing by 24%. It may be concluded therefore, that extreme care must be exercised in determining as accurately as possible the geometry of the shell.

Accuracy is obviously dependent on the precision with which the elastic constants E and ν are known and hence some care is necessary in measuring them. An error in E has a direct effect on P. The effect of an error in ν is not so easily established. Apart from ν appearing in the both P and μ where its effect is easily assessed, it also enters the solution of the problem through the boundary conditions. The effect

of an error arising from this source may not be readily estimated except by repeating the calculations for a finite variation in ν .

The basic requirements may now be recognised. Since the presence of initial stress is inadmissible if theoretical comparisons are to be made, it is necessary to produce a stress free shell of regular geometry. The shell, measured so that the geometry is defined, must be supported and loaded in accordance with the various conditions assumed in the theoretical analysis.

Most of the papers reviewed have dealt with the case of the clamped shell. The most commonly adopted method of attempting to secure a clamped boundary has been to bolt the shell between rings. Evidence gained from an experimental investigation of this particular method of edge restraint[35] has shown that it offers only a poor approximation to the fully clamped condition. Of even more importance is the fact that this method of mounting shells will almost inevitably apply random force and moment actions to the shell boundary, thereby inducing an initial state of stress. Since instability is total stress dependent, any such initial state of stress, which cannot be incorporated in the theoretical analysis due to its random character, should be avoided.

It is possible that these force and moment actions could produce a state of pre-stress in the shell of sufficient magnitude to precipitate the premature collapse phenomena which has characterised much of the experimental work recorded. At the very least, these actions will introduce a scatter into the experimental results which will greatly diminish the value of the latter in testing a particular solution.

I.3 The Point Loaded Shell

The first theoretical treatment of the buckling of freely supported shallow spherical shells was reported by BIEZENO[6] in 1935. At this time, other investigators were still adhering to the classical linear approach to the problem of the pressure loaded complete sphere. BIEZENO recognised the need to adopt nonlinear strain-displacement relations with the result that the differential equations became nonlinear in form. Indeed, most of the subsequent work was based on equations analogous to those of BIEZENO. He assumed that the deflected form of the shell under a central point load was related to that for a flat plate by an undetermined multiple with the addition of a

linear term. Thus he assumed the deflected form

$$\Psi = C_1 \frac{r}{R} + C_2 \frac{r}{R} \log \frac{a}{r} \qquad \text{I.2.1}$$

where C_1 and C_2 are two undetermined constants. Solving the appropriate differential equation with this substitution, he obtained a solution for Ψ which was, of course, different to the form quoted above. Assuming that both the final form and the approximate form given by I.2.1 would yield the same central deflection and change of slope at the boundary, he obtained the values of C_1 and C_2 and hence calculated the equilibrium path. The effect of his assumption is difficult to estimate but it should be noted that this procedure allowed the deflected form to change as loading progressed. Thus it recognised an inherent feature of the buckling phenomenon and it therefore offered a considerable advantage over the one term 'Galerkin' approach adopted by other authors. It would require a minimum of two such Galerkin terms to provide a similar degree of flexibility in permitting changes in the deflected form during loading. Furthermore, it is unlikely that a general term, unless very carefully selected, would represent the deflected form as accurately as the approximation from the

inextensional flat plate analogy.

Other work relevant to the point load action was reported by CHIEN[7] in 1956. He examined the stability of shells subject to a ring load at the apex and bending moments round the edge of the shell. The equations derived were nonlinear and an attempt was made to solve these by assuming a single term to represent the deflected form. In the limit as the radius of the ring tended to zero, the case of a point load at the apex was obtained.

ASHWELL[8] in 1959 applied Love's principle of applicable surfaces to the problem. According to this principle, the deformed portion of the spherical shell was an inverted spherical surface, or nearly so. By matching the radial displacements and shears at the boundary between the deformed and undeformed portions of the shell, which was assumed to remain spherical, linear differential equations were obtained. He also conducted experimental work on four aluminium alloy shells for values of μ of 4.7, 4.9, 5.8 and 6.4. The results of his experimental work were reported to agree well with the analytical solutions and with BIEZENO'S results.

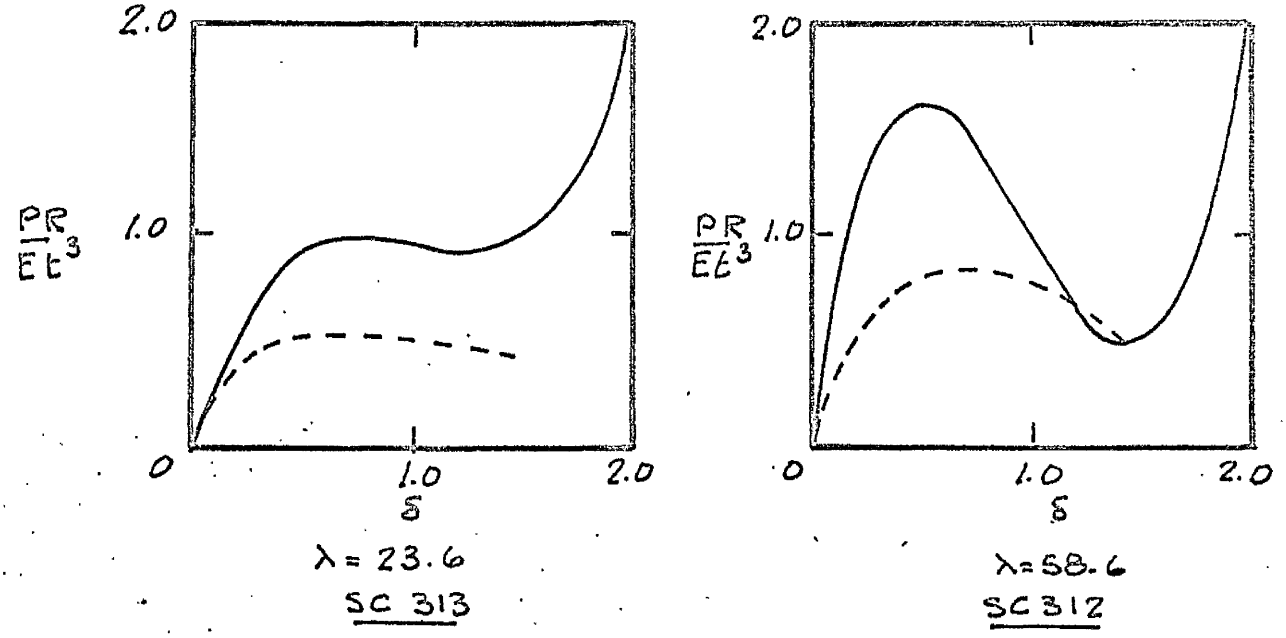

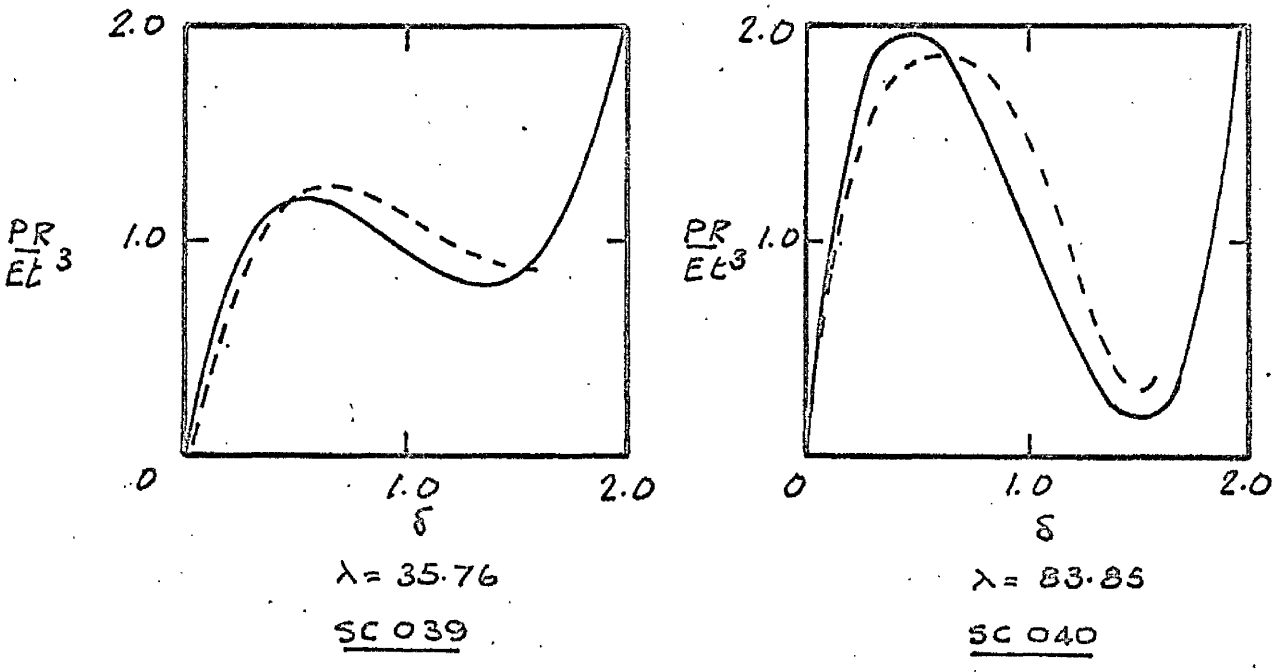

FIG. I.1 Experimental equilibrium paths of EVAN-IWANOWSKI et al. (9) compared with the theory of BIEZENO (6)

An extensive experimental study of buckling under central point loading was reported in 1962 by EVAN-IWANOWSKI, CHENG and LOO[9]. They tested a very wide range of shells in copper, steel, aluminium and vinyl polyethelene. For the metallic specimens, they adopted the hydroform process to produce shells with spherical radii varying from 5 in. to 10 in., base radii varying from 0.953 in. to 3.812 in. and μ varying from 3.72 to 14.95. Both clamped and freely supported shells were tested. For the clamped tests, the shells were restrained at the boundary by rings 'machined to fit' the shell contour. In view of the method of manufacture of the metallic shells, it seems unlikely that the shells were of a stress free character. Their method of obtaining a clamped boundary in the case of the fixed shell tests, also seems open to criticism. No reference was made of the method used to measure the spherical radius of curvature or whether an attempt was made to measure variations in thickness. Their results, while showing considerable scatter due, probably, to their experimental technique, show a tendancy which is in general agreement with the predictions of BIEZENO and ASHWELL. Some of their results are shown in FIG. I.1 and FIG. I.2. where they are compared with the theory

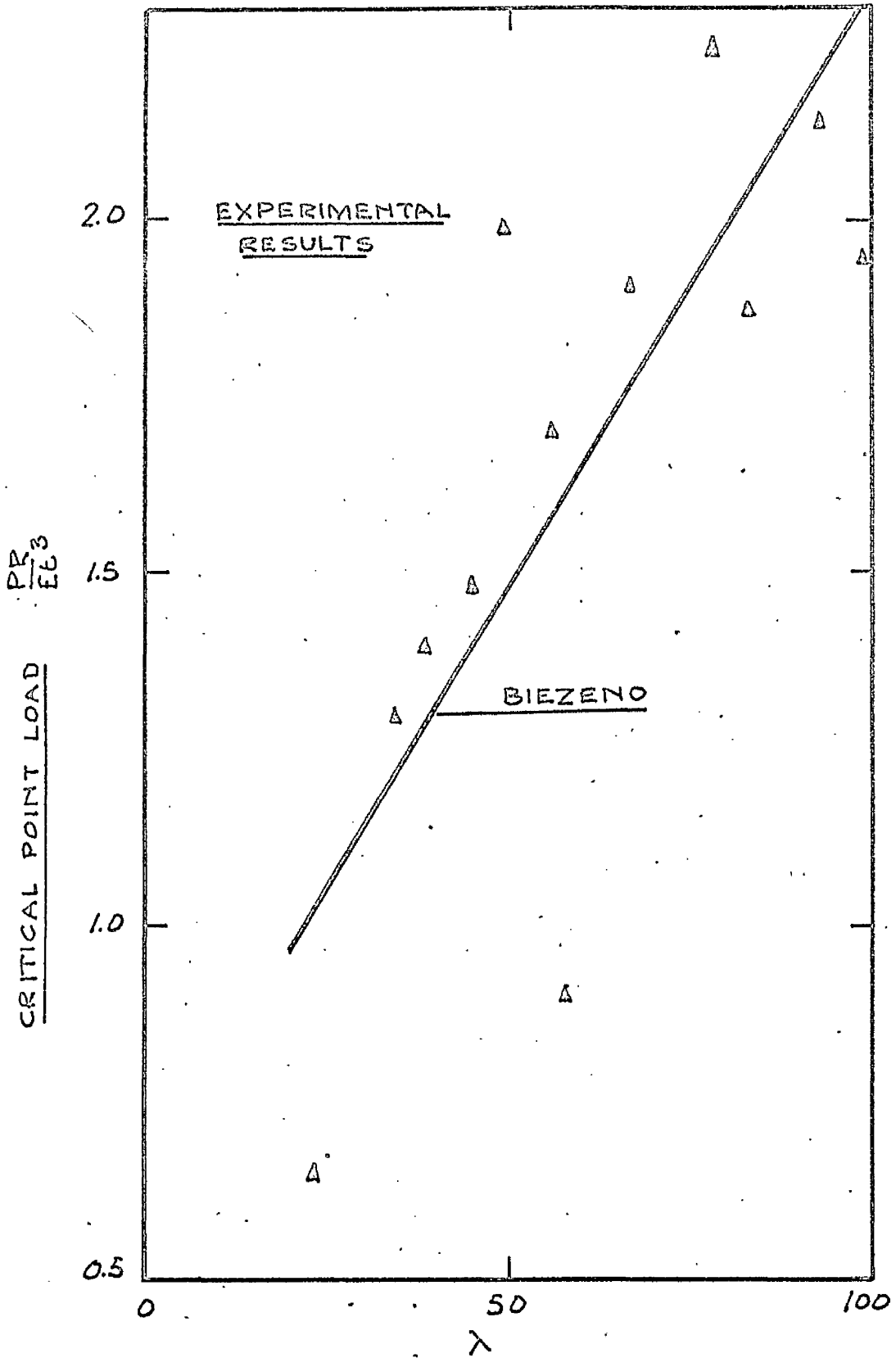

FIG. I.2 Experimental critical loads of EVAN-IWANOWSKI et al. (9) compared with the theory of BIEZENO (6)

of BIEZENO[6] for $\nu = 0.33$. Their work is examined in more detail in Chapter IV.

Their main conclusions were:

(1) Simply supported shells of μ less than 3.7 did not snap but merely deflected in a nonlinear manner.

(2) Known analytical solutions agreed well in the range $3.7 < \mu < 6.5$ for symmetric deformations.

(3) Shells with $\mu > 10.2$ buckled nonsymmetrically.

(4) Very deep shells did not exhibit buckling (probably due to large plastic deformations).

(5) Variations in the parameter h/a did not affect the critical loads but might affect the deflected forms.

Though stresses were measured, they were not correlated to any existing theory. They also tested clamped shells but these did not exhibit any snap through phenomenon.

In the same year EVAN-IWANOWSKI[10] presented results of a further experimental study. In this

investigation, the behaviour of both simply supported and clamped shells was examined under eccentric local load and uniform pressure superimposed on eccentric load action. It was noted that critical combinations of dead-weight and pressure were independent of the order in which the loading was applied - a result which is not surprising. He was, however, disturbed to find that when the concentrated load was applied eccentrically, a higher combination of the total load resulted as compared with the axisymmetrical case. At first sight, this might appear to be unexpected in view of the natural expectation that an eccentric load would tend to encourage nonsymmetric collapse leading to lower collapse loads for certain values of μ . EVAN-IWANOWSKI does not appear to have considered the possibility that the application of an eccentric point load will influence the total potential energy of the system and could therefore raise the critical combination of the buckling load. While it was recognised that initial imperfections influenced the buckling load of a shell subject to external pressure, the corresponding influence was much less pronounced in shells under point load action since, in general, the large local deformations in the neighbourhood of

the load point may well swamp all but very large initial irregularity.

I.4 Pressure Loaded Shells

The behaviour of the pressure loaded shells is characterised by the theoretical and experimental investigations of the clamped shell segment. This definition of the problem arose in the post-buckling analysis of the complete sphere in which the behaviour of a clamped segment was assumed to be representative of the phenomenon of dimple formation.

As mentioned earlier, the problem of the stability of the spherical segment is distinct from that of the complete sphere. The restraint at the boundary of the segment prevents uniform contraction of the shell and bending thus occurs on the first application of the load. The behaviour is therefore one of continuous bending until snap results when the maximum deflection is comparable with the total height of the shell initially. In view of the large bending distortions which occur, it is apparent that nonlinear terms must be retained in the strain analysis if a true picture of the buckling phenomenon is to be

obtained. The inherent nonlinear character of the problem has been recognised by most authors who, with some recent exceptions, have further assumed axisymmetric behaviour.

In the experimental field, work was reported by TSIEN. By using oil as a loading medium, he constrained the shells to snap under approximately constant volume conditions. Later, in 1953, tests on domes were carried out by KLOPPEL and JUNGBLUTH[11]. Since they adopted air pressure for loading the shells, the snap occurred at approximately constant pressure. Using high speed photography, they showed that snap between rotationally symmetric states could occur nonsymmetrically. Much of the work reported above, was carried out on relatively deep shells and hence the nonsymmetric behaviour is not unexpected.

The first detailed investigation of the snapping of shallow shells was carried out by KAPLAN and FUNG[12] in 1954. They assumed rotational symmetry and retained nonlinear terms in presenting their equilibrium equations. The differential equations which they derived were essentially equivalent to those which BIEZENO proposed some eighteen years

previously. In writing their equilibrium equations, it was assumed that the radial membrane stress was influenced by the deformations. The governing equations, which are based on force equilibrium and strain-displacement compatability requirements, are presented as follows:

$$\frac{d}{dr}\frac{1}{r}\frac{d}{dr}(r^2 N_r) + \frac{1}{2}Et\left(\frac{dw}{dr}\right)^2 + Et\frac{r}{R}\frac{dw}{dr} = 0 \qquad \text{I.3.1}$$

$$D\frac{d}{dr}\frac{1}{r}\frac{d}{dr}\left(r\frac{dw}{dr}\right) = N_r\left(\frac{r}{R} + \frac{dw}{dr}\right) + \frac{1}{2}pr \qquad \text{I.3.2}$$

where $$N_r = \frac{Et}{1-\nu^2}\left[\frac{du}{dr} - \frac{w}{R} + \frac{1}{2}\left(\frac{dw}{dr}\right)^2 + \nu\left(\frac{u}{r} - \frac{w}{R}\right)\right]$$

and u, w are the tangential and normal displacements respectively.

They used a perturbation method to solve the above equations by expressing the dependent variables w, N_r and p in terms of $W_o = \frac{w_o}{t}$ as a parameter and expanding all the variables in powers of W_o. The boundary conditions assumed were those of a clamped shell and the critical pressure was obtained by setting $\frac{dp}{dw_o} = 0$. They found that for $\mu = 4$, the convergence of the solution was good but deteriorated

MODE I

$\mu \doteqdot 4$, w_{max} at the centre

MODE II

$\mu \doteqdot 7$, w_{max} not at the centre

MODE III

$\mu \doteqdot 9$, w_{max} at the centre

FIG. I.3 Initial deflection modes
KAPLAN and FUNG (12)

rapidly for higher values. The convergence was, however, good enough for small values of W_o to indicate the mode changes which might be expected to occur. Thus for μ approximately 7, the maximum deflection is no longer at the centre. For μ approximately 9, the mode changes again and the maximum deflection is again at the centre. These modes, which are of course axisymmetric, are shown in FIG. I.3 and will be subsequently referred to as Modes I, II and III respectively. More recent experimental work indicates that for μ greater than about 5, shells may behave nonsymmetrically. Thus their solution, based on assumed axial symmetry, may be considered reasonably adequate for values of μ up to about 5. Whilst they were no doubt concerned about the poor convergence at higher values, the value of effort spent in overcoming this difficulty for assumed axial symmetry is marginal, since the shell may well behave nonsymmetrically.

KAPLAN and FUNG also carried out experimental work on shells of 8 in. base diameter and nominal radii of 20 in. and 30 in. with thicknesses varying from 0.032 in. to 0.102 in. The shells were formed by spinning from hot magnesium plate. Though the

magnitudes were not given, this process almost certainly introduced thickness variations, the effect of which has been discussed earlier. It also seems likely that the process would induce fairly substantial residual stresses. The value of μ was obtained from measurement of the shell rise because 'variations of the specimens from true spherical form' implied that the radius of curvature was in doubt. Initial imperfection amounted to 40% of the thickness at some points. To provide a clamped boundary, the shells were mounted between rings which were bolted together. They conducted tests with both oil and air pressure (corresponding to constant volume and constant pressure conditions) but no perceptable difference in behaviour of the shells was recognised under the two media. They claimed that their experimental results were in fair agreement with their theoretical work for the lower values of μ and for the range up to μ approximately 5, the criterion $\frac{dp}{dw_o} = 0$ for the determination of the collapse pressure appeared valid. At higher values of μ their experimental results were less satisfactory (due probably to limitations on their method of testing and the onset of nonsymmetric buckling) and they supposed that the use of the energy

criterion might be preferable.

There then followed two papers, by SIMONS and ARCHER respectively, attempting to obtain solutions to REISSNER'S[13] equations (1950). These equations are directly analogous to those of KAPLAN and FUNG.

In 1956, SIMONS[14] adopted a power series method in which he expanded $\psi = \frac{dw}{dr}$ and rN_r in terms of the independent variable $\frac{r}{R}$. He intended to use the condition $\frac{dp}{dw} = 0$ to locate the maximum pressure but was unable to obtain any satisfactory solution due to poor convergence of the series. Though his method could be applied to freely supported shells, he considered only the case of the clamped boundary.

In the same year, ARCHER[15] used a perturbation technique expanding the dependent variables in terms of w_{max} the maximum displacement which need not be at the centre. He adopted the condition $\frac{dp}{dw_{max}} = 0$ to locate the turning value of the equilibrium path. His results were higher than the available experimental evidence and he attributed this to finite disturbances during loading.

In 1957 REISS, GREENBERG and KELLER[16] used a power series method similar to that of SIMONS to solve equations equivalent to those of REISSNER. They used a computer to deal with a large number of terms. To obtain the maximum pressure they adopted a computational technique by evaluating as p_{max} the pressure at which the search for an adjacent equilibrium position became fruitless. They also attempted to locate the lower buckling pressure but the convergence of the series was poor in the post-buckled region.

In the following year REISS[17] suggested that the problem could be examined by solving two linear problems. He first solved the eigenvalue problem of a segment supported at the edge in such a manner that only membrane stresses were induced in the shell prior to buckling. Hence he obtained a series of curves of the critical load against μ for different initial modes of buckling. He then solved the linear bending problem of a clamped segment to obtain values of at which the initial mode changed. For μ less than the first mode change position, the initial bending is Mode I; for μ beyond the first mode change, the initial bending is Mode II. He thus developed a continuous curve of the buckling pressure as a function

of μ . This curve passed through the experimental points.

In 1958, WEINITSCHKE[18] adopted the method of SIMONS and used a computer to deal with a large number of terms of the power series. To determine the critical pressure he used the criterion $\frac{dp}{dw_o} = 0$. He expressed a doubt about the validity of the perturbation approach. He considered both clamped and simply supported shells.

VON WILLICH[19] in 1959 used an energy method for solution. Both he and CHEN[20] adopted similar nonlinear terms to those of KAPLAN and FUNG in expressing the total potential energy. Assuming rotational symmetry, VON WILLICH used a single algebraic term to express the deflected form in terms of w, the normal displacement and derived a corresponding expression for the tangential displacement u. Finally, he obtained an energy expression in terms of two parameters only. He assumed that one of these parameters could be considered constant during loading, implying that the deflection at any point was proportional to that at the centre at all times. CHEN, recognising that this assumption

was unjustifiable, used a similar method but avoided this restriction. Both authors defined the critical pressure by setting $\frac{dp}{dw_o} = 0$. CHEN further examined the effect of initial irregularity of the middle surface and showed that this could have considerable effect on the behaviour of the shell.

In the same year, KELLER and REISS[21] attempted a new solution by an iterative process using a finite difference approximation of the nonlinear problem. Confining their attention to the range of μ for which Mode I (FIG. I.3) buckling occurs, they calculated the maximum pressure of the equilibrium path as well as the lower buckling pressure and the energy criterion pressure. They concluded that the latter was of little value in explaining the behaviour of shallow shells. At the same time BUDIANSKY[22] derived the axisymmetric equations of MARGUERRE[23] which are equivalent to those of REISSNER. BUDIANSKY developed corresponding integral equations which he solved by numerical integration and hence located the maximum pressure. He examined both initially perfect and imperfect shells and concluded that at the higher values of μ , assumed initial imperfection could not, in itself, account for the lack of agreement with

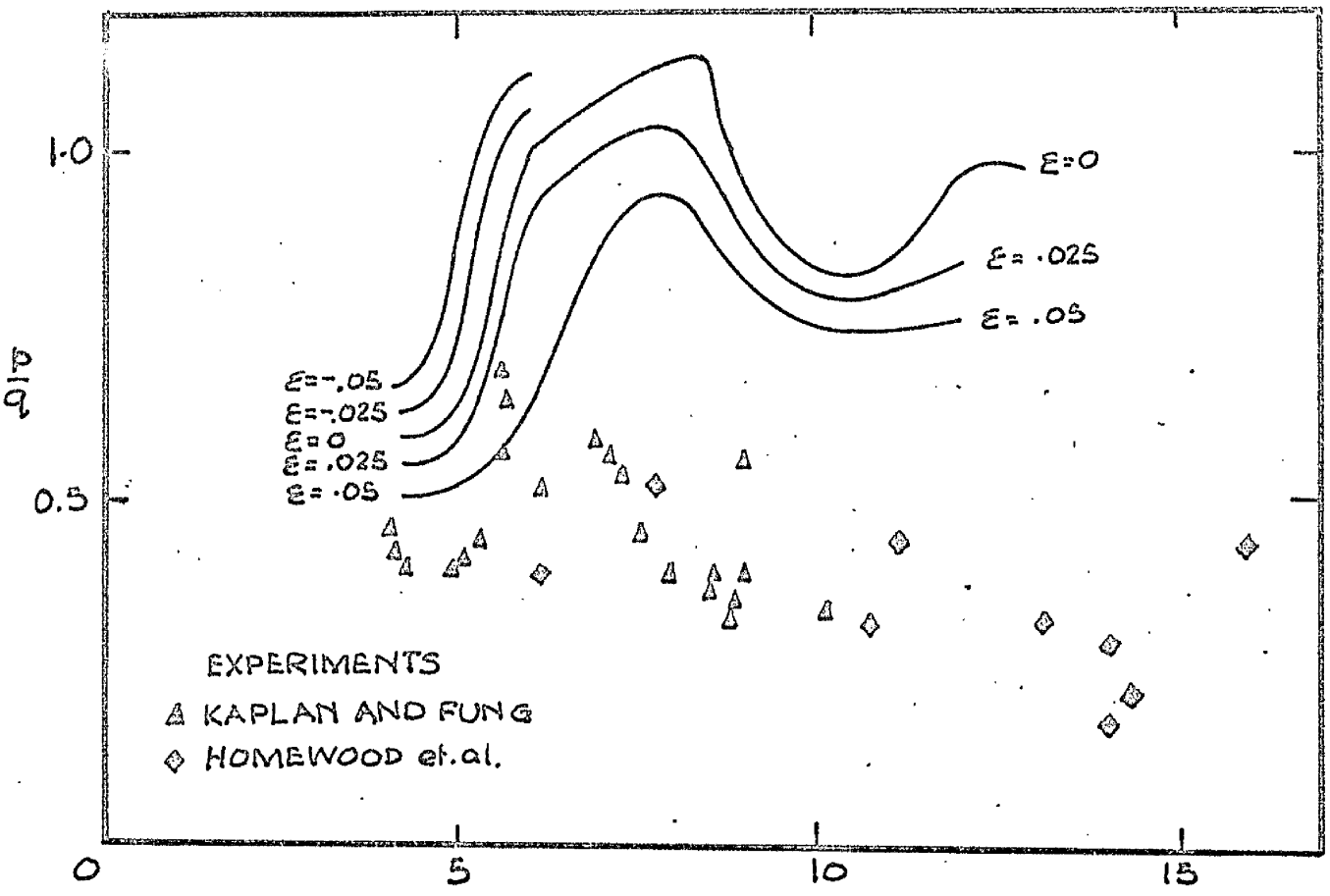

$$\mu = 2[3(1-\nu^2)]^{1/4}\left(\frac{h}{t}\right)^{1/2}$$

FIG. I.4 Effect of axisymmetric initial imperfection
BUDIANSKY (22)

experimental evidence. He came, therefore, to the conclusion that this disparity could only be accounted for by nonsymmetric behaviour. Some of his results are shown in FIG. I.4.

Further experimental work was undertaken by HOMEWOOD, BRINE and JOHNSON[24]. The shells they tested were of 34 in. diameter and nominal radii of curvature of 40 in. and 78 in. with thicknesses ranging from 0.067 in. to 0.260 in. The thickness variation within any one specimen was of the order of $\pm$ 4%. It was not recorded whether any attempt was made to measure initial imperfection nor was there any reference as to how the shell parameter μ was calculated. The shells were spun from hot rolled sheet steel and wrought aluminium alloy. The method of clamping and testing was similar to that used by KAPLAN and FUNG. In view of the experience of KAPLAN and FUNG, it may be inferred that the test results may have been influenced by the presence of residual stress in their specimens.

All the theoretical work so far reviewed has been concerned with the analysis of the shallow shell segment the behaviour of which has been assumed to be

symmetrical. The relatively poor agreement of such analyses with experimental data from shells with μ greater than about 5, has been attributed to the development of nonsymmetric modes. Thus an increasing number of authors have turned their attention to an analysis of this type of behaviour.

The problem of nonsymmetric snap was examined by GRIGOLYUK[25] in 1959. He used a Galerkin method to solve the equations of MARGUERRE. To deal with nonsymmetric deformation, he assumed that the deflection was given by:

$$w = (\rho^2-1)^2(w_0 + w_1\rho^4\cos n\theta)$$

where

$$\rho = \frac{r}{a}$$

This form allows two degrees of freedom and permits the deflected form to change during loading. Substitution of this assumed form into the governing differential equations led to two simultaneous algebraic equations. He did not indicate how he intended to solve these and thus did not present results. He did not discuss criteria by which he would recognise snap.

In 1961, THURSTON[26] carried out numerical

solutions of REISSNER'S equations for the axisymmetric buckling of a clamped spherical cap. The method of solution was to assume an approximate result for the nonlinear differential equations. A correction to this solution was obtained by solving the resulting linear nonhomogeneous 'variational' equations. This correction was used to compute a new assumed solution and the process repeated until the correction approached zero.

BELLINFANTE[27] in 1962, adopted a hydroforming technique to make shells with nominal radii of curvature of 8 in. and 23 in. in aluminium. He considered that this method was superior to spinning as the thickness variations were reduced. The range of thicknesses tested were from 0.028 in. to 0.25 in. with thickness variations of $\pm$ 0.001 in. within a specimen. Initial imperfections and the method of measuring shell geometry were not recorded. The state of residual stress would also appear to be unknown but may be expected to be high. The shells were clamped between rings of internal diameter 10 in. and tested under oil pressure. It should be noted that the general geometry of his shells violated the shallowness assumption.

In 1962 a collection of papers on the instability of shell structures was published. The following five papers are of special interest.

WEINITSCHKE[28] noted that several recent theoretical axisymmetric analyses had shown good agreement with each other but a marked disagreement with experimental work. While he did not contest the validity of the latter, he suggested that the lack of agreement was due to nonsymmetric deformation. He therefore approached the problem by superimposing small asymmetric deflections on finite axisymmetric displacements. He showed that the symmetric states of deformation were unstable over certain ranges of load. He suggested that axisymmetric deformation took place until a critical value was reached at which point bifurcation of solutions of the basic equations occurred. One branch of the solutions corresponded to axisymmetric states, other branches corresponded to asymmetric states which, in the vicinity of the bifurcation point, differed from the axisymmetric states by infinitesimal amounts. He used two different techniques to determine the onset of instability. One amounted to the calculation of the second variation of the appropriate potential energy

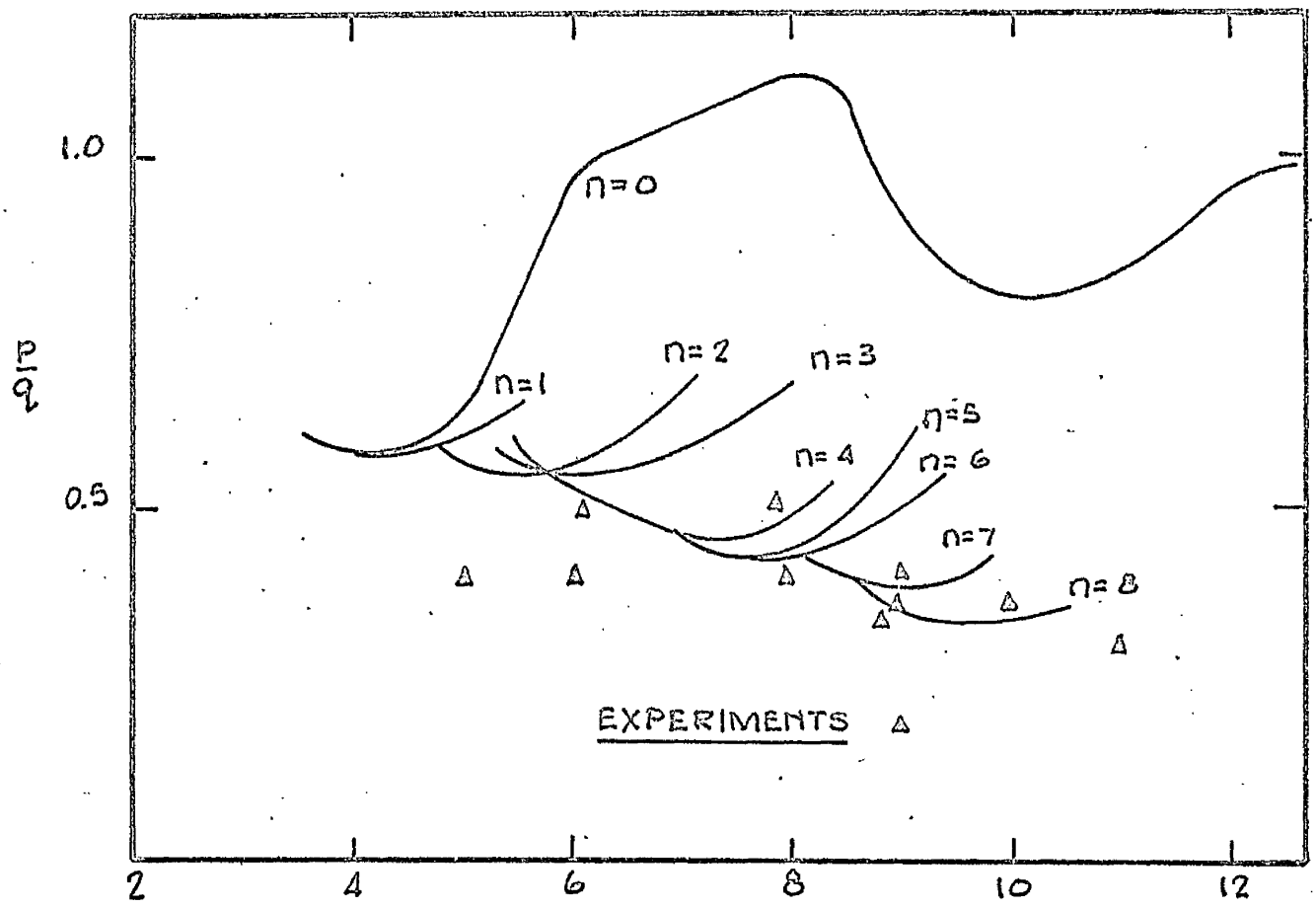

$$\mu = 2\left[3(1-\nu^2)\right]^{1/4}\left(\frac{h}{t}\right)^{1/2}$$

FIG. I.5 Nonsymmetric behaviour of clamped shells
WEINITSCHKE (28)

function, the other reduced the stability problem to a nonlinear eigenvalue form. The results of his analysis is shown in FIG. I.5 and indicate a trend in general agreement with experimental data.

PARMERTER and FUNG[29] also considered nonsymmetric behaviour and adopted a Galerkin method of solution for VON KARMAN'S large deflection equations. They represented the deflection in a form asymmetric with respect to θ by:

$$w(r,\theta) = f(r) + g(r) \cos n\theta$$

where $f(r) \ll g(r)$

They chose the deflected form to include two independent parameters. On substituting the assumed form into the differential equations, two simultaneous algebraic equations were obtained. The paper represented an interim report of work then being undertaken. A full analysis was presented by PARMERTER in 1963 and will be reviewed separately.

KELLER and REISS[30] examined in some detail the possible mechanism of buckling in the light of criteria governing the loss of stability. Their main conclusion

was that while bifurcation of solutions could be predicted, closely controlled experimental work on this feature was desirable.

THURSTON[31] used a computer to solve REISSNER'S finite deflection equations for any shell of revolution with continuous second derivatives of the parametric equations of the shell middle surface. The nonlinear ordinary differential equations of the finite deflection theory were solved by an extension of Newton's method for calculating the roots of algebraic equations. He also calculated the strain energy and potential energy at each equilibrium state by integrating over the shell surface. In considering axisymmetric imperfection, he found that their effect was greater than the corresponding results obtained by BUDIANSKY and he attributed this to the difference in the assumed shape of imperfection. He suggested that his axisymmetric analysis could be extended to allow asymmetric behaviour with the possibility of including asymmetric imperfections in the analysis.

VON KARMAN and KERR[32] examined the total potential energy concept with special reference to its value in interpreting equilibrium states. They also

concluded that the energy criterion was of little value in stability analysis.

Also in 1962, GJELSVIK and BODNER[33] in an investigation of nonsymmetrical behaviour, included an analysis of symmetrical collapse. Their work, based on the total potential of the system, used a single term to describe the deflected form. Thus it did not recognise the changing form as loading progressed.

In 1963 a paper was published by FEODOS'EV[5] in which he introduced a new approach to the solution of the axisymmetric problem of the pressure loaded clamped shell. He noted that the use of variational methods to solve problems of stability had limitations in that they become excessively cumbersome when generalised. He pointed out that, in general, deformations are such that they cannot be represented with acceptable accuracy over the range of load by considering one or two terms. The problem becomes computationally difficult as the variational approach leads, as a rule, to a system of nonlinear algebraic equations (frequently cubic in form), the number of simultaneous equations being equal to the number of variable parameters. In the first part of his paper he solved the axisymmetric bending problem using a

finite difference method with varying interval. In the early stages of the loading history, successive approximations of the load were predicted by linear interpolation. Near critical states, quadratic interpolation became necessary. The critical pressures were determined by the criterion of multiple roots. He thus established the axisymmetric behaviour of the clamped shell with acceptable accuracy. He then went on to show that the use of only one independent parameter in the approximating function in the variational method was only acceptable for a limited range of shells. He indicated that the use of more terms might well lead to insuperable computational difficulties associated with the solution of the resulting algebraic equations. He thus proposed the introduction of a time dependent variable which, rather than complicating the matter, led to a simplification. He therefore introduced inertia terms and linear damping effects into the normal equilibrium equation. Dynamic effects were assumed to have a negligible effect on radial equilibrium. Assuming three independent parameters in his approximating function, he reduced the differential equations to three simultaneous cubic algebraic equations. These he

solved by finite difference methods and the results showed general agreement with his earlier numerical integration approach. The concept is of interest in that the introduction of time dependence has the effect of changing the variable. Elimination of the time dependent terms reduces the algebraic equations to those obtained by the more usual variational approach. It is important to note that the essential nonlinearity of the problem does not materially influence the solution of the time dependent equations. He suggested that the method was of wide application and could be used in the analysis of plastically deformable bodies.

In 1963, KRENZKE and KIERNAN[34] reported the results of an experimental investigation of the collapse of pressure loaded clamped shells. They noted that previous experimental work had been characterised by a lack of repeatability while the results of their own investigations followed a definite pattern. They claimed that this had been achieved by very careful preparation of models in which a high degree of geometric precision had been maintained. They prepared their specimens by machining relatively small caps from solid aluminium stock so that the shell

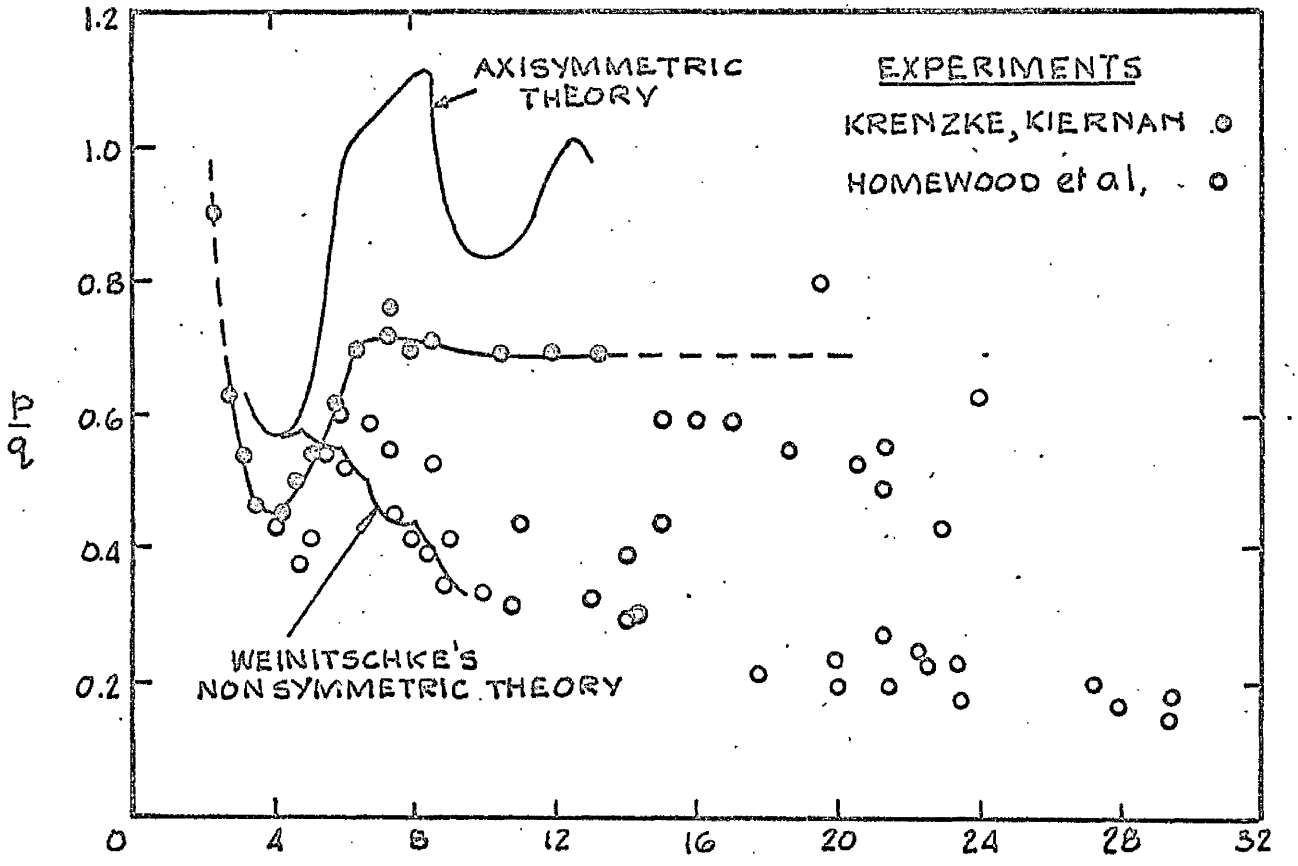

FIG. I.6 Comparison of experimental results of KRENZKE and KIERNAN (34) with theory.

and its supporting ring were continuous. In this way they probably produced the closest possible approximation to a fully clamped shell by ensuring continuity of the shell and its support. From the geometrical stability of the models during the final stages of the machining process, they deduced that negligible residual stresses were present. The spherical radii of curvature of the specimens were 2 in. and 3 in. with base radii varying from 0.43 in. to 1 in. The errors in spherical radii were less than 0.01% with variations in thickness less than 1%. The results of their investigation are shown in FIG. I.6. Though their claim of a definite trend in their results appeared to be substantiated, the values of collapse pressures were consistently low by as much as 20% in comparison with theory. The consistency in their results indicated that a high degree of uniformity had been achieved in the preparation of their specimens and thus factors which had caused varying degrees of scatter in previous work had been eliminated. By machining their specimens from solid material, they had at least achieved symmetrical support conditions. It would appear from the consistently low results which they obtained for the collapse pressures, that even

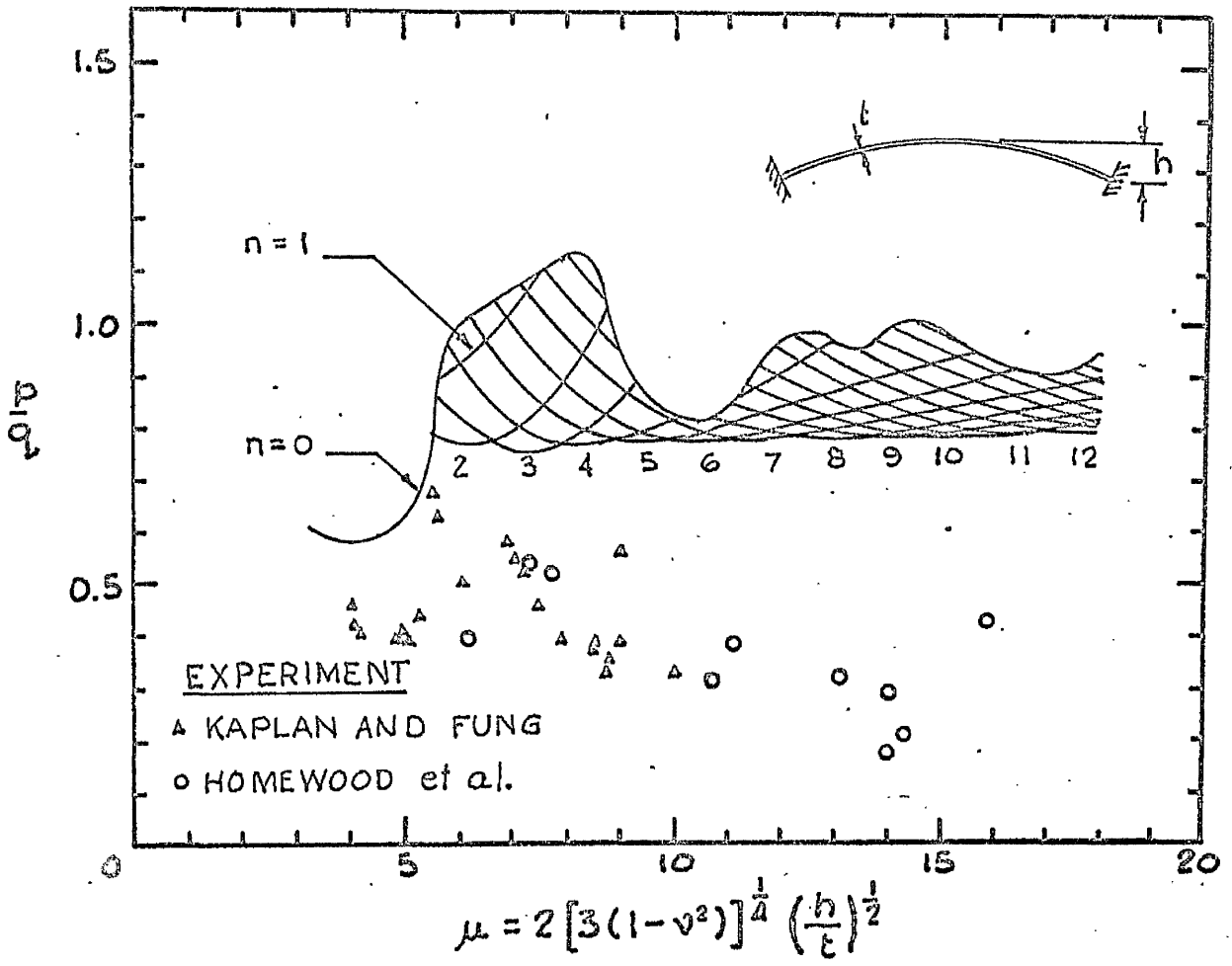

FIG. I.7 The theory of HUANG (36)

this method of attempting to achieve the clamped boundary condition does not in practice reproduce the conditions of no change in slope and no movement of the support as assumed in theoretical treatments. This fact further substantiates the view that such a condition, which is so critical in instability, can never be achieved in practice.

In 1963 PARMERTER[35] published the results of an experimental and theoretical investigation referred to earlier. Using the equations of MARGUERRE, he examined both the symmetric and nonsymmetric modes of collapse for the pressure loaded clamped shell. He adopted a Galerkin procedure using three terms. The resulting cubic algebraic equations were solved iteratively by Newton's method. His results showed a measure of agreement with the work of HUANG[36] whose theory is shown in FIG. I.7. It is of interest to note that his findings were in marked contrast with the work of WEINITSCHKE[28] and PARMERTER suggested that the good agreement with experimental data claimed by Weinitschke was possibly fortuituous in view of the substantial experimental errors of previous work. PARMERTER also carried out very closely controlled experimental investigations on almost perfect shells

made by the electro-forming technique. In this way he was able to produce stress free shells with thickness variations of the order of 1/50th of the thickness. The shells had nominal radii of curvature of 20 in. and 40 in. but the radius of curvature used in the reduction of the data was calculated as the radius of the circle having the minimum least squares deviation from 17 measured ordinates on the surface of the shell. By repeating measurements along other meridians, he deduced that the spherical radius could be determined to within about 0.1%. The base radius of his specimens was 4 in. $\pm$ 0.02%. The shells were loaded by oil pressure and the buckling pressure determined to within 1%. To obtain a clamped boundary, the shell was located in a cavity 0.015 in. wide and the space filled with an epoxy cement. No reference was made as to whether any movements of the shell in the support were detected. PARMERTER went to considerable lengths to obtain accurate values of Young's modulus, E, in tension. Tests were performed on specimens 200 in. long with an estimated error of less than 3%. He obtained Poisson's ratio from transverse strain gauges on the tensile specimen. He reported good agreement between his experimental results and his theoretical

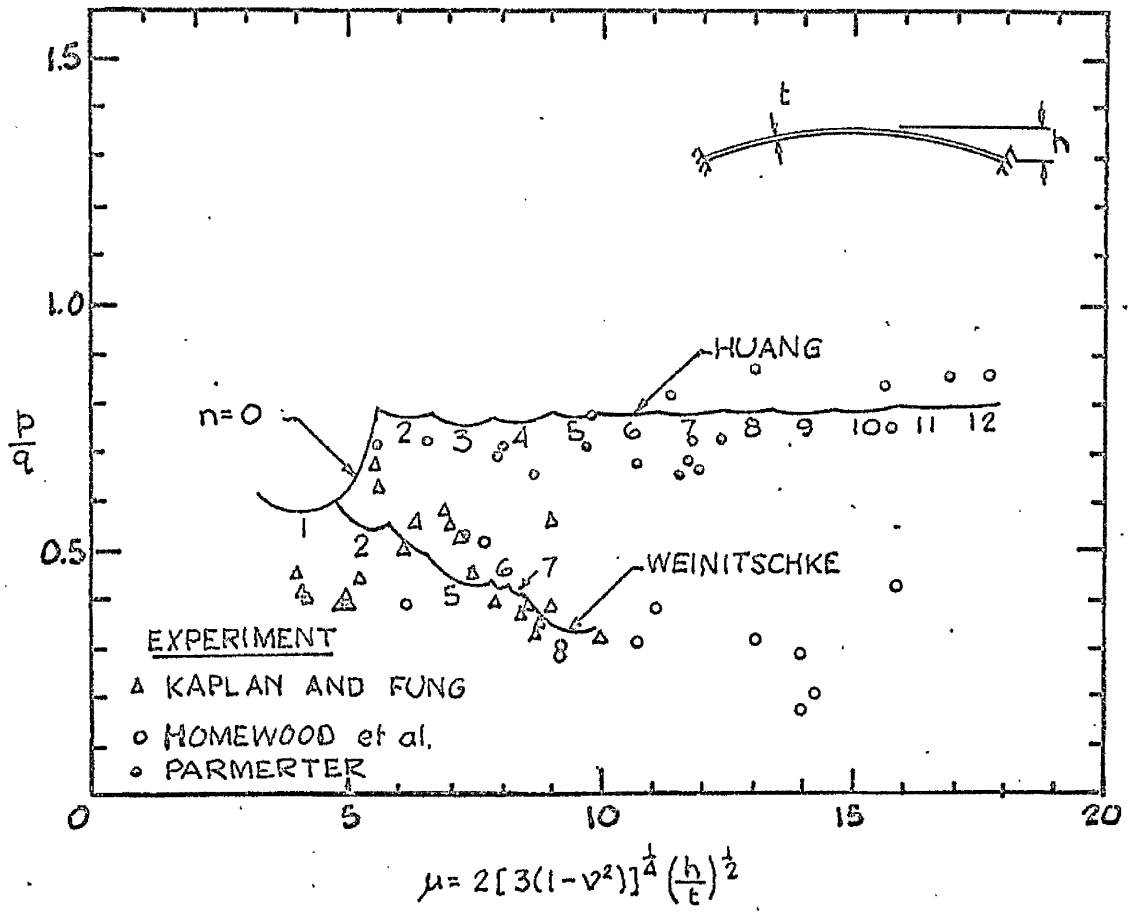

FIG. I.8 Comparison of the theories of HUANG (36) and WEINITSCHKE (28) with the experimental data of References 12, 25 and 35

work. His results are shown in FIG. I.8.

The most recent paper on the subject of instability in shells, was published by THURSTON[37] in 1964. In it he described a computer program for the analysis of any shell of revolution under external pressure, axial load, torsion and axisymmetric temperature gradients or any combination of these load actions. The natural frequencies of free vibration could also be obtained under all loads except torsion. The solution of the nonlinear problem was restricted to thin isotropic shells of revolution in which the thickness and Young's modulus could vary in the meridional direction. The boundary conditions could be any linear combination of stress resultants and deflections. He claimed good agreement with the work of HUANG for the special case of the clamped shell subject to external pressure.

I.5 Critical Summary

In reviewing previous theoretical work, an attempt has been made to show how a basic lack of understanding of the mechanism of buckling forced

investigators of the problem to make far reaching simplifying assumptions such as assumed initial perfection of geometry and axial symmetry of behaviour. Historically, the study of the clamped spherical cap arose in the investigation of the post-buckling behaviour of dimple formation in the complete sphere. Thus most authors have attempted to correlate their findings for the restricted problem of the clamped segment with that of the complete sphere. The basic assumptions which characterised the early theoretical work were;

(i) the shell is initially stress free

(ii) the shell is geometrically perfect

(iii) the behaviour of the shell is symmetrical

in addition to these, most workers on the problem of the pressure loaded sphere have assumed that

(iv) the shell is fully restrained in position and in direction at the boundary (i.e. clamped).

It is only relatively recently that experimental work has been directed towards a more critical examination of the effects of these basic assumptions.

Most of the experimental results were characterised by an appreciable scatter and a disturbing lack of repeatability. It would seem, therefore, that the experimental shells, their conditions of support and their behaviour only in part conformed to the requirements of the theoretical approach. Even with the adoption of highly refined techniques for the preparation of specimens and the most careful test procedures, only partial substantiation of the corresponding theory was possible. Theoretical treatments were extended to include the effects of nonsymmetric behaviour and initial imperfection but on the experimental side, the inconsistent nature of the results indicated that factors such as the reliability of assumed support conditions might be in question.

It can therefore be seen that as the theoretical approach was successively extended to include additional factors, the experimental techniques became more refined so that the actual behaviour of shallow shells was examined from two converging points of view.

Having examined in outline the background of the shell buckling problem, it is appropriate to deal in rather more detail with the main contributions and findings of investigations of the phenomenon.

In general, authors have used very similar differential equations based on those of REISSNER or MARGUERRE for their analyses. The differences therefore lie mainly in the methods adopted to obtain solutions. Until relatively recently, only axisymmetric deformations were considered. For pressure loaded shells with clamped boundaries, the evidence suggests that the range of shells for which such behaviour is valid, is limited to μ less than about 5.5. Over this range, substantial agreement between authors suggests that the problem of axisymmetric buckling is now fully understood and that collapse can be predicted with acceptable accuracy. Shells with other boundary conditions and other types of load action have been the subject of relatively few papers and none of these has examined possible nonsymmetric behaviour analytically. Thus no conclusion can be reached regarding the expected limits of symmetrical deformation for these other cases.

For clamped shells under pressure load, nonsymmetric behaviour must be considered when μ exceeds about 5.5. The problem of nonsymmetric deformation has been the subject of several recent papers which are not in complete agreement with one

another. In this respect, WEINITSCHKE claimed good agreement with experimental data and predicted critical pressures for a clamped shell considerably lower than both PARMERTER and HUANG. Since WEINITSCHKE computed the stability curves for the asymmetric buckling of perfect shells and the experimental data may be in error due to imperfections in the experimental technique and specimens tested, the agreement would appear to be somewhat fortuituous. This view is to some extent strengthened by the results of PARMERTER'S experimental work where collapse occurred at pressures appreciably higher than would have been predicted by WEINITSCHKE.

CHEN and BUDIANSKY have shown that the effect of initial imperfection of the middle surface may have a pronounced influence on the critical pressure. THURSTON also examined the effect of imperfection and found that the effects were more far reaching than suggested by BUDIANSKY. This he attributed to differences in the assumed form of the imperfection. In shells loaded by local loads, the large deflections in the vicinity of the load point tend to swamp all but very large imperfections and hence the effect of assumed irregularity is much less marked.

In the experimental field, it has been shown that very careful attention must be paid to the need to produce accurate stress free specimens, the thickness of which must be uniform. The geometry of the specimens must be capable of accurate measurement so that the shell parameter may be determined with high precision. Furthermore, the shell must be mounted in accordance with the theory to be tested.

Many investigations have been concerned with clamped shells. This particular boundary condition has been shown to be one of the most difficult to achieve in practice. Thus a large volume of experimental work is open to criticism and its value in substantiating the various solutions open to doubt. In this context, the work of PARMERTER is exceptional in that he was the first to appreciate the need for very closely controlled experimental work. In endeavouring to bring their theoretical work into line with experimental data, the majority of authors have been insufficiently critical of experimental technique.

Most of the theoretical work carried out, has had as its objective, the determination of critical states. To predict these it was often sufficient to

carry out approximate analyses such as the Galerkin method adopted by some authors, using one or two terms. While such analyses may be adequate for predicting collapse, there is no guarantee that they would describe the state of stress in a shell with corresponding accuracy. Very little work has been reported on the variations of the stress distribution in the shell as loading progresses. This seems to be a significant omission.

It has also been shown that the behaviour of shells is very sensitive to the boundary support conditions. Thus the work of most authors on the fully clamped edge must represent an upper bound on collapse loads achieved in most practical applications, where such an edge condition is unlikely to obtain. Thus analyses of the fully clamped shell, while valuable in understanding the fundamental phenomenon of instability, are of restricted value in engineering applications.

CHAPTER II

THEORETICAL ANALYSIS

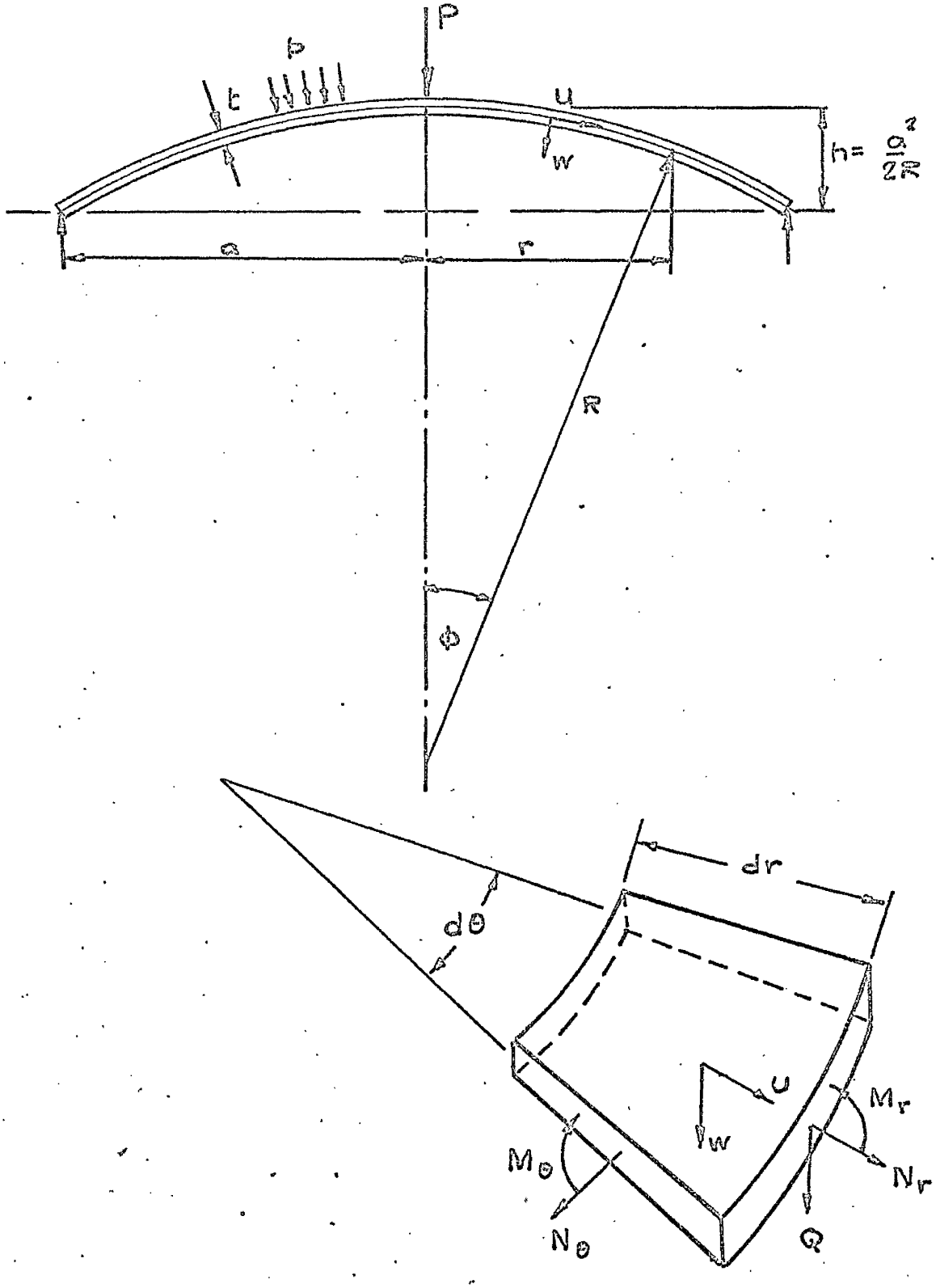

FIG. II.1 Notation for shell analysis

II.1 The Governing Differential Equations

Consider a shallow spherical shell segment as shown in FIG. II.1 where

R - spherical radius of curvature

a - base radius

t - thickness (constant)

r - radial distance from the axis of symmetry

The deformation of the middle surface is assumed to be radially symmetric and is specified by

u displacement measured tangentially on the middle surface

w displacement measured perpendicular to the middle surface

$\psi = \frac{dw}{dr}$ rotation of the normal to the middle surface

Small finite deflections are considered and terms up to the second degree in ψ are retained though ψ^2 is neglected in comparison to unity. In consequence of the assumed thinness of the shell, the Kirchhoff conditions apply:

(i) lines normal to the middle surface remain normal during bending

(ii) stresses normal to the surface are neglected.

The shell is assumed to be sufficiently shallow that if z is the height above the base plane, then

$$\left(\frac{\partial z}{\partial r}\right)^2 \ll 1$$

It is common practice to restrict the term 'shallow' to shells for which

$h < \frac{a}{8}$ where h is the rise of the shell.

Under these conditions, the equations of equilibrium are,

$$\frac{d}{dr}(r M_r) - M_\theta - r Q = 0 \qquad \text{II.1.1a}$$

$$\frac{d}{dr}(r N_r) - N_\theta = 0 \qquad \text{II.1.1b}$$

$$Q = -\frac{1}{r}\int_0^r r p\, dr - N_r\left(\frac{r}{R} + \frac{dw}{dr}\right) \qquad \text{II.1.1c}$$

in which

N_r - meridional membrane force per unit length

N_θ - circumferential membrane force per unit length

M_r - meridional bending moment per unit length

M_θ - circumferential bending moment per unit length

Q - shear force normal to middle surface per unit length

The strains of the middle surface, expressed in terms of displacements are:

$$\varepsilon_r = \frac{du}{dr} + \frac{1}{2}\psi^2 - \frac{w}{R} \qquad \text{II.1.2a}$$

$$\varepsilon_\theta = \frac{u}{r} - \frac{w}{R} \qquad \text{II.1.2b}$$

from which u, w may be eliminated to give the equation of compatability as

$$r\frac{d}{dr}(\varepsilon_\theta) + \varepsilon_\theta - \varepsilon_r + \frac{1}{2}\psi^2 + \frac{r}{R}\psi = 0 \qquad \text{II.1.3c}$$

The force actions per unit length may be expressed in terms of displacements thus,

$$N_r = B\left[\frac{du}{dr} - \frac{w}{R} + \frac{1}{2}\psi^2 + \nu\left(\frac{u}{r} - \frac{w}{R}\right)\right] \qquad \text{II.1.4a}$$

$$N_\theta = B\left[\frac{u}{r} - \frac{w}{R} + \nu\left(\frac{du}{dr} - \frac{w}{R} + \frac{1}{2}\psi^2\right)\right] \qquad \text{II.1.4b}$$

$$M_r = D\left[\frac{d\Psi}{dr} + \nu\frac{\Psi}{r}\right] \qquad \text{II.1.4c}$$

$$M_\theta = D\left[\frac{\Psi}{r} + \nu\frac{d\Psi}{dr}\right] \qquad \text{II.1.4d}$$

where

$$B = \frac{Et}{1-\nu^2}$$

$$D = \frac{Et^3}{12(1-\nu^2)}$$

Substitution of equations II.1.4c,d into the equilibrium equation II.1.1a with II.1.1c yields the first governing differential equation

$$D\frac{d}{dr}\left[\frac{1}{r}\frac{d}{dr}(r\Psi)\right] = N_r\left(\frac{r}{R} + \Psi\right) + \bar{P} \qquad \text{II.1.5}$$

in which

$\bar{P} = \frac{1}{2}$ pr for uniform pressure load

or $\bar{P} = \frac{P}{2\pi r}$ for a point load at the apex

Noting that the force actions of the mid-plane may be expressed in terms of the corresponding strains of the mid-plane

$$N_r = B(\varepsilon_r + \nu\varepsilon_\theta)$$

$$N_\theta = B(\varepsilon_\theta + \nu\varepsilon_r)$$

these expressions, together with the equation of compatibility II.1.3 yield the second governing differential equation

$$r\frac{d}{dr}\frac{1}{r}\frac{d}{dr}(r^2 N_r) + \frac{1}{2}Et\psi^2 + Et\frac{r}{R}\psi = 0 \qquad \text{II.1.6}$$

With the introduction of the parameters $\xi = \frac{r}{R}$ and $\Phi = rN_r$, the governing differential equations II.1.5 and II.1.6 may be expressed in the form derived by REISSNER[13] for the case of the pressure loaded shell as

$$\frac{D}{R}\left[\psi'' + \frac{\psi'}{\xi} - \frac{\psi}{\xi^2}\right] = \Phi + \frac{pR^2\xi}{2} + \frac{\psi}{\xi}\Phi \qquad \text{II.1.7}$$

$$\Phi'' + \frac{\Phi'}{\xi} - \frac{\Phi}{\xi^2} = -REt\left(\psi + \frac{\psi^2}{2\xi}\right) \qquad \text{II.1.8}$$

where the primes indicate differentiation with respect to ξ.

Introducing the dimensionless parameters $\rho = \frac{r}{a}$, $\gamma = \frac{a}{R}$ and $\eta = 12(1-\nu^2)\frac{a^2}{t^2}$ the equations II.1.5 and II.1.6 may be written in the form adopted by MUSHTARI[38], thus

$$\rho\frac{d}{d\rho}\left[\frac{1}{\rho}\frac{d}{d\rho}(\rho\Phi)\right] + \frac{1}{2}\psi^2 + \rho\gamma\psi = 0 \qquad \text{II.1.9}$$

$$\rho \frac{d}{d\rho}\left[\frac{1}{\rho}\frac{d}{d\rho}(\rho\Psi)\right] = \eta\,\Phi(\Psi+\rho\gamma) + \frac{p\rho^2 a^3}{2D} \qquad \text{II.1.10}$$

which are thus directly analogous to those of REISSNER.

The equations of BIEZENO[6] are expressed in terms of the radial and vertical components of the normal and tangential displacements u and w.

$$v = u - \frac{r}{R}w$$

Hence the strain-displacement relations II.1.2a,b may be expressed in terms of v and the rotation Ψ thus,

$$\varepsilon_r = \frac{dv}{dr} + \frac{r}{R}\Psi + \frac{\Psi^2}{2} \qquad \text{II.1.11a}$$

$$\varepsilon_\theta = \frac{v}{r} \qquad \text{II.1.11b}$$

The corresponding force actions may now be expressed in the form derived by BIEZENO thus,

$$N_r = B\left[\frac{dv}{dr} + \nu\frac{v}{r} + \frac{r}{R}\Psi + \frac{\Psi^2}{2}\right] \qquad \text{II.1.12a}$$

$$N_\theta = B\left[\frac{v}{r} + \nu\left(\frac{dv}{dr} + \frac{r}{R}\Psi + \frac{\Psi^2}{2}\right)\right] \qquad \text{II.1.12b}$$

$$M_r = D\left[\frac{d\Psi}{dr} + \nu\frac{\Psi}{r}\right] \qquad \text{II.1.12c}$$

$$M_\theta = D\left[\frac{\Psi}{r} + \nu\frac{d\Psi}{dr}\right] \qquad \text{II.1.12d}$$

The governing equations of BIEZENO may now be obtained by substitution of relations II.1.12a-d into the equations of equilibrium II.1.1a,b. Thus,

$$r^2\frac{d^2v}{dr^2} + r\frac{dv}{dr} - v + r^2\left(\frac{r}{R}+\psi\right)\frac{d\psi}{dr} + (2-\nu)\frac{r^2}{R}\psi + \frac{1-\nu}{2}r\psi^2 = 0 \qquad \text{II.1.13}$$

$$r^2\frac{d^2\psi}{dr^2} + r\frac{d\psi}{dr} - \psi = \frac{r^2}{D}\left[\bar{P} + N_r\left(\frac{r}{R}+\psi\right)\right] \qquad \text{II.1.14}$$

As may be seen from the foregoing derivations, the equations of REISSNER, MUSHTARI and BIEZENO, which are typical of the forms used in most investigations, are merely different expressions of the same basic forms.

Three alternative methods of solution of the governing differential equations have been examined. These are

(1) a new extension of the technique originally proposed by BIEZENO[6]

(2) direct numerical integration

(3) the Galerkin method.

A critical examination of these alternative approaches, indicate overwhelming advantages associated with the technique proposed by BIEZENO. In consequence, this approach is incorporated in the body

of the thesis for the case of the pressure loaded, free shell. The exploratory work associated with the investigation of the other two techniques, is presented in Appendices VII.2 and VII.3.

II.2 The Solution for the Pressure Loaded Shell

The method of solution of the governing differential equations is an extension of the technique originally proposed by BIEZENO[6] in connection with a study of the buckling of a freely supported shallow shell subject to a point load at the apex. In addition to obtaining the equilibrium path, the analysis has been extended to the determination of the distribution of deformation, force actions and surface strains for the case of the pressure loaded shell. A similar analysis for the point load case is presented in Appendix VII.1.

The governing differential equations are II.1.13 and II.1.14. These are repeated here for the case of a shell subject to uniform pressure loading.

$$r^2\frac{d^2v}{dr^2} + r\frac{dv}{dr} - v + r^2\left(\frac{r}{R}+\psi\right)\frac{d\psi}{dr} + (2-\nu)\frac{r^2}{R}\psi + \frac{(1-\nu)}{2}r\psi^2 = 0 \qquad \text{II.2.1}$$

$$r^2\frac{d^2\psi}{dr^2} + r\frac{d\psi}{dr} - \psi = \frac{pr^3}{2D} + \frac{r^2}{D}\left(\frac{r}{R}+\psi\right)N_r \qquad \text{II.2.2}$$

where $$N_r = B\left[\frac{dv}{dr} + \nu\frac{v}{r} + \left(\frac{r}{R}+\frac{\psi}{2}\right)\psi\right] \qquad \text{II.2.3}$$

In order to obtain a suitable solution of the differential equations, a solution for ψ corresponding to the inextensional bending of a freely supported flat plate subject to a uniform pressure loading is taken as a first approximation.

With $R = \infty$ and $N_r = 0$ equation II.2.2 becomes

$$r^2\frac{d^2\psi}{dr^2} + r\frac{d\psi}{dr} - \psi = \frac{pr^3}{2D} \qquad \text{II.2.4}$$

for which the solution is

$$\psi = A_1\frac{r}{R} + A_2\frac{r^3}{a^2R} \qquad \text{II.2.5}$$

The solution for ψ for the shallow spherical shell is taken to be represented by the sum of an unknown multiple of the expression given by II.2.5 with the addition of a linear term in r. Thus a suitable first approximation is

$$\Psi = C_1 \frac{r}{R} + C_2 \frac{r^3}{a^2 R} \qquad \text{II.2.6}$$

and $$\frac{d\Psi}{dr} = \frac{C_1}{R} + 3\frac{C_2 r^2}{a^2 R}$$

Equation II.2.1 becomes

$$r^2\frac{d^2v}{dr^2} + r\frac{dv}{dr} \cdots v + \frac{C_1}{R^2}\left(1+\frac{C_1}{2}\right)(3-\nu)r^3$$

$$+ \frac{C_2}{a^2R^2}(5-\nu)(1+C_1)r^5 + \frac{C_2^2}{2a^4R^2}(7-\nu)r^7 = 0$$

which has the solution

$$v = Ar + \frac{B}{r} - C_1\left(1+\frac{C_1}{2}\right)(3-\nu)\frac{r^3}{8R^2}$$

$$- C_2(1+C_1)(5-\nu)\frac{r^5}{24a^2R^2} - C_2^2\frac{(7-\nu)r^7}{2a^4R^2} \qquad \text{II.2.7}$$

where the arbitrary constants A and B are determined from the conditions

At $r = 0$, v is finite and hence $B = 0$

At $r = a$, $N_r = 0$

ie $$\left[\frac{dv}{dr} + \nu\frac{v}{r} + \frac{r}{R}\Psi + \frac{\Psi^2}{2}\right]_{r=a} = 0$$

from which the constant A is determined as

$$A(1+\nu) = C_1\left(1+\frac{C_1}{2}\right)(3-\nu)(3+\nu)\frac{a^2}{8R^2} + C_2(1+C_1)(5-\nu)(5+\nu)\frac{a^2}{24R^2}$$

$$+ \frac{C_2^2}{2}(7-\nu)(7+\nu)\frac{a^2}{48R^2} - C_1\left(1+\frac{C_1}{2}\right)\frac{a^2}{R^2} - C_2(1+C_1)\frac{a^2}{R^2} - \frac{C_2^2}{2}\frac{a^2}{R^2} \qquad \text{II.2.8}$$

Substitution of II.2.7 and II.2.8 in II.2.3 yields

$$N_r = B(1-\nu^2)\frac{a^2}{8R^2}\left[C_1\left(1+\frac{C_1}{2}\right)\left(1-\frac{r^2}{a^2}\right)\right.$$

$$\left. + \frac{C_2}{3}(1+C_1)\left(1-\frac{r^4}{a^4}\right) + \frac{C_2^2}{12}\left(1-\frac{r^6}{a^6}\right)\right] \qquad \text{II.2.9}$$

With the substitution of II.2.9 with II.2.6 into equation II.2.2, after some manipulation, yields

$$r^2\frac{d^2\psi}{dr^2} + r\frac{d\psi}{dr} - \psi = \frac{pr^3}{2D} + \frac{B}{8D}(1-\nu^2)\frac{a^2}{R^3}\left[\alpha_1 r^3\right.$$

$$\left. + \alpha_2\frac{r^5}{a^2} + \alpha_3\frac{r^7}{a^4} + \alpha_4\frac{r^9}{a^6} + \alpha_5\frac{r^{11}}{a^8}\right] \qquad \text{II.2.10}$$

in which

$$\alpha_1 = C_1(1+C_1)\left(1+\frac{C_1}{2}\right) + \frac{C_2}{3}(1+C_1)^2 + \frac{C_2^2}{12}(1+C_1)$$

$$= \varepsilon_1 + \frac{\varepsilon_3}{3} + \frac{\varepsilon_4}{12}$$

$$\alpha_2 = C_1C_2\left(1+\frac{C_1}{2}\right) - C_1\left(1+\frac{C_1}{2}\right)(1+C_1) + \frac{C_2^2}{12}(1+C_1)$$

$$= -\varepsilon_1 + \varepsilon_2 + \frac{\varepsilon_4}{3} + \frac{\varepsilon_5}{12}$$

$$\alpha_3 = -C_1C_2\left(1+\frac{C_1}{2}\right) - \frac{C_2}{3}(1+C_1)^2 = -\varepsilon_2 - \frac{\varepsilon_3}{3}$$

$$\alpha_4 = -\frac{5}{12}C_2^2(1+C_1) = -\frac{5}{12}\varepsilon_4$$

$$\alpha_5 = -\frac{C_2}{12}^3 = -\frac{\varepsilon_5}{12} \qquad \text{II.2.11a-e}$$

where

$$\varepsilon_1 = C_1(1+C_1)\left(1+\frac{C_1}{2}\right)$$
$$\varepsilon_2 = C_1C_2\left(1+\frac{C_1}{2}\right)$$
$$\varepsilon_3 = C_2(1+C_1)^2$$
$$\varepsilon_4 = C_2^2(1+C_1)$$
$$\varepsilon_5 = C_2^3$$

II.2.12

The solution of equation of II.2.10 takes the form

$$\Psi = Ar + \frac{B}{r} + \frac{Pr^3}{16D} + \frac{B}{8D}(1-\nu^2)\frac{a^2}{R^3}\left[\alpha_1\frac{r}{8}^3 + \alpha_2\frac{r^5}{24a^2} + \alpha_3\frac{r^7}{48a^4} + \alpha_4\frac{r^9}{80a^6} + \alpha_5\frac{r^{11}}{120a^8}\right]$$

where A and B are arbitrary constants which are determined from the condition of symmetry at the origin and from the boundary condition on M_r at r = a.

$$\text{At} \quad r = 0, \quad \Psi = 0 \text{ and hence } B = 0$$
$$\text{At} \quad r = a, \quad M_r = D\left[\frac{d\Psi}{dr} + \nu\frac{\Psi}{r}\right] = 0$$

Hence

$$A(1+\nu) = -(3+\nu)\frac{pa^2}{16D} - \Gamma\frac{a^4}{R^3}\left[(3+\nu)\frac{\alpha_1}{8}\right.$$
$$\left. + (5+\nu)\frac{\alpha_2}{24} + (7+\nu)\frac{\alpha_3}{48} + (9+\nu)\frac{\alpha_4}{80} + (11+\nu)\frac{\alpha_5}{120}\right] \qquad \text{II.2.13}$$

in which $$\Gamma = \frac{B}{8D}(1-\nu^2)$$

The final expression for Ψ becomes

$$\Psi = \frac{p}{16D}\left[r^3 - \frac{(3+\nu)}{1+\nu}a^2r\right] + \Gamma\frac{a^2}{R^3}\left[\left\{r^3 - \frac{(3+\nu)}{1+\nu}a^2r\right\}\frac{\alpha_1}{8}\right.$$
$$+ \left\{\frac{r^5}{a^2} - \frac{(5+\nu)}{1+\nu}a^2r\right\}\frac{\alpha_2}{24} + \left\{\frac{r^7}{a^4} - \frac{(7+\nu)}{1+\nu}a^2r\right\}\frac{\alpha_3}{48}$$
$$\left. + \left\{\frac{r^9}{a^6} - \frac{(9+\nu)}{1+\nu}a^2r\right\}\frac{\alpha_4}{80} + \left\{\frac{r^{11}}{a^8} - \frac{(11+\nu)}{1+\nu}a^2r\right\}\frac{\alpha_5}{120}\right] \qquad \text{II.2.14}$$

Integration of this expression for Ψ gives the deflection in the form

$$\frac{w}{h} = \frac{3}{4}\frac{pa^2R(1-\nu^2)}{Et^3}\left\{\frac{1}{2}\left(\frac{r}{a}\right)^4 - \left(\frac{3+\nu}{1+\nu}\right)\left(\frac{r}{a}\right)^2\right\}$$

$$+ \frac{3}{2}(1-\nu)\lambda\left[\left\{\frac{1}{2}\left(\frac{r}{a}\right)^4 - \left(\frac{3+\nu}{1+\nu}\right)\left(\frac{r}{a}\right)^2\right\}\frac{\alpha_1}{8}\right.$$

$$+\left\{\frac{1}{3}\left(\frac{r}{a}\right)^6 - \left(\frac{5+\nu}{1+\nu}\right)\left(\frac{r}{a}\right)^2\right\}\frac{\alpha_2}{24} + \left\{\frac{1}{4}\left(\frac{r}{a}\right)^8 - \left(\frac{7+\nu}{1+\nu}\right)\left(\frac{r}{a}\right)^2\right\}\frac{\alpha_3}{48}$$

$$\left.+\left\{\frac{1}{5}\left(\frac{r}{a}\right)^{10} - \left(\frac{9+\nu}{1+\nu}\right)\left(\frac{r}{a}\right)^2\right\}\frac{\alpha_4}{80} + \left\{\frac{1}{6}\left(\frac{r}{a}\right)^{12} - \left(\frac{11+\nu}{1+\nu}\right)\left(\frac{r}{a}\right)^2\right\}\frac{\alpha_5}{120}\right] \qquad \text{II.2.15}$$

in which

$$\lambda = \frac{a^4}{R^2t^2} \quad , \quad h = \frac{a^2}{2R}$$

In order to determine the two constants C_1 and C_2, it may be postulated that the expressions II.2.6 and II.2.14 lead to the same change in slope at the boundary r = a. Similarly, the central deflection given by II.2.15 may be equated to that given by II.2.6 when integrated.

Thus equating deflections at the centre leads to

$$p\frac{Ra^2}{Et^3} = \frac{-2a^4}{R^2t^2(5+\nu)}\left[(5+\nu)\frac{\alpha_1}{8} + (7+\nu)\frac{\alpha_2}{18} + (9+\nu)\frac{\alpha_3}{32}\right.$$

$$\left. + (11+\nu)\frac{\alpha_4}{50} + (13+\nu)\frac{\alpha_5}{72}\right] - \frac{8\left(C_1 + \frac{C_2}{2}\right)}{3(1-\nu)(5+\nu)} \qquad \text{II.2.16}$$

Taking $\nu = 0.33$, equation II.2.16 reduces to

$$p\frac{Ra^2}{Et^3} = -\lambda\left[0.25\,\alpha_1 + 0.15280384\alpha_2 + 0.10940431\alpha_3 + 0.08502814\,\alpha_4 + 0.0694705\,\alpha_5\right] - 0.74673537\left(c_1 + \frac{c_2}{2}\right)$$

II.2.17

Equating slopes at r = a leads to

$$p\frac{Ra^2}{Et^3} = -\lambda\left[\frac{\alpha_1}{4} + \frac{\alpha_2}{6} + \frac{\alpha_3}{8} + \frac{\alpha_4}{10} + \frac{\alpha_5}{12}\right] - \frac{2(c_1+c_2)}{3(1-\nu)}$$

II.2.18

For $\nu = 0.33$ this reduces to

$$p\frac{Ra^2}{Et^3} = -\lambda\left[0.25\alpha_1 + 0.16666667\alpha_2 + 0.125\alpha_3 + 0.1\,\alpha_4 + 0.08333333\alpha_5\right] - 0.99502487(c_1 + c_2)$$

II.2.19

Equation II.2.17 and II.2.19 can be written as

$$p\frac{Ra^2}{Et^3} = a_1 + b_1\lambda$$

II.2.20a

and

$$p\frac{Ra^2}{Et^3} = a_2 + b_2\lambda$$

II.2.20b

Hence, on subtraction,

$$(a_1 - a_2) + \lambda(b_1 - b_2) = 0 \qquad \text{II.2.21}$$

with

$$a_1 = -0.74673537\,(c_1 + \tfrac{c_2}{2}) \qquad \text{II.2.22a}$$

$$a_2 = -0.99502487\,(c_1 + c_2) \qquad \text{II.2.22b}$$

$$b_1 = -\Big[0.25\alpha_1 + 0.15280384\,\alpha_2 + 0.10940431\,\alpha_3 + 0.08502814\,\alpha_4 + 0.0694705\,\alpha_5\Big] \qquad \text{II.2.22c}$$

$$b_2 = -\Big[0.25\alpha_1 + 0.16666667\,\alpha_2 + 0.125\alpha_3 + 0.1\,\alpha_4 + 0.083333333\,\alpha_5\Big] \qquad \text{II.2.22d}$$

Integration of II.2.6 yields the deflection at the centre as

$$w = -\frac{a^2}{2R}\,(c_1 + \tfrac{c_2}{2})$$

and noting that the rise of the shell at the centre is given by

$$h = \frac{a^2}{2R}$$

$$\delta = \frac{w}{h} = -(c_1 + \tfrac{c_2}{2}) \qquad \text{II.2.23}$$

From II.2.22a

$$a_1 = 0.74673537\ \delta$$

and from II.2.23

$$C_2 = -2(C_1 + \delta) \qquad \text{II.2.24}$$

From equations II.2.11a-e it can be seen that $\alpha_1, \alpha_2, \alpha_3$ - etc. are defined in terms of C_1 and C_2. Hence, equation II.2.21 is in fact a general cubic equation in terms of C_1 and C_2 only. From II.2.24, C_2 can be expressed explicitly in terms of C_1 and δ, the deflection at the centre. Thus, substitution of equation II.2.24 into equation II.2.21 yields a cubic equation in C_1 and δ.

Equation II.2.21 becomes

$$a_0 C_1^3 + a_1 C_1^2 + a_2 C_1 + a_3 = 0 \qquad \text{II.2.25}$$

where

$$a_0 = -\lambda \left[0.001270755 \right]$$

$$a_1 = \lambda \left[-0.020794245 + 0.003465721\left(1 + \frac{\delta}{2}\right) + 0.010397127(2+\delta) - 0.006469327(1+2\delta) \right]$$

$$a_2 = -0.99502487 + \lambda \left[-0.013862833 + 0.00346572 14\,\delta + 0.010397127(1+2\delta) - 0.00646932 72\,\delta(2+\delta) \right]$$

$$a_3 = -1.24331437\,\delta + \lambda \left[0.010397127\,\delta - 0.00646932 72\,\delta^2 \right]$$

Thus by specifying successive values of δ , the coefficients a_0, a_1, a_2, a_3 can be calculated. Equation II.2.25 can then be solved for C_1 using standard procedures such as Cardan's method. In practice, only one real root is found though for values of λ greater than 300, multiple roots occur. Since the analysis assumes symmetric behaviour, this does not have any real importance since practical shells do not behave symmetrically at such high values of λ .

With C_1 determined, the load parameter can be obtained by substitution in equation II.2.20a. Hence the equilibrium path can be established. Thus

$$p\frac{Ra^2}{Et^3} = 0.74673537\,\delta - \lambda \left[-0.09373046\,\delta + 0.14535819\,\delta^2 - 0.055555556\,\delta^3 + \left\{ 0.09719616 - 0.08679906\,\delta - 0.09373046(1+2\delta) + 0.14535819\,\delta(2+\delta) - 0.16666667\,\delta^2 \right\} C_1 + \right.$$

$$+ \left\{ 0.14579424 - 0.08679906\left(1 + \frac{\delta}{2}\right) - 0.09373046\,(2+\delta) + 0.14535819\,(1+2\delta) - 0.16666667\,\delta \right\} C_1^2 + 0.001270724\, C_1^3 \Bigg] \qquad \text{II.2.26}$$

Determination of Stress Resultants

From equation II.2.9

$$N_r \frac{a^2}{Et^3} = \frac{\lambda}{8}\left[C_1\left(1 + \frac{C_1}{2}\right)\left(1 - \left(\frac{r}{a}\right)^2\right) + \frac{C_2}{3}(1+C_1)\left(1 - \left(\frac{r}{a}\right)^2\right) + \frac{C_2^2}{12}\left(1 - \left(\frac{r}{a}\right)^6\right) \right] \qquad \text{II.2.27}$$

From equation II.1.12b with the relations II.2.14 and II.2.7

$$N_\theta \frac{a^2}{Et^3} = \frac{\lambda}{8}\left[C_1\left(1 + \frac{C_1}{2}\right)\left\{1 - 3\left(\frac{r}{a}\right)^2\right\} + \frac{C_2}{3}(1+C_1)\left\{1 - 5\left(\frac{r}{a}\right)^4\right\} + \frac{C_2^2}{12}\left\{1 - 7\left(\frac{r}{a}\right)^6\right\} \right] \qquad \text{II.2.28}$$

From equation II.1.12c with relation II.2.14

$$M_r \frac{R}{Et^3} = -\frac{pRa^2}{16Et^3}(3+\nu)\left\{1-\left(\frac{r}{a}\right)^2\right\} - \frac{\lambda}{8}\left[(3+\nu)\left\{1-\left(\frac{r}{a}\right)^2\right\}\frac{\alpha_1}{8}\right.$$

$$+ (5+\nu)\left\{1-\left(\frac{r}{a}\right)^4\right\}\frac{\alpha_2}{24} + (7+\nu)\left\{1-\left(\frac{r}{a}\right)^6\right\}\frac{\alpha_3}{48}$$

$$\left. + (9+\nu)\left\{1-\left(\frac{r}{a}\right)^8\right\}\frac{\alpha_4}{80} + (11+\nu)\left\{1-\left(\frac{r}{a}\right)^{10}\right\}\frac{\alpha_5}{120}\right] \qquad \text{II.4.29}$$

From equation II.1.12d with relation II.2.14

$$M_\theta \frac{R}{Et^3} = -\frac{pRa^2}{16Et^3}\left\{(3+\nu) - (1+3\nu)\left(\frac{r}{a}\right)^2\right\} - \frac{\lambda}{8}\left[\left\{(3+\nu) - (1+3\nu)\left(\frac{r}{a}\right)^2\right\}\frac{\alpha_1}{8}\right.$$

$$+ \left\{(5+\nu) - (1+5\nu)\left(\frac{r}{a}\right)^4\right\}\frac{\alpha_2}{24} + \left\{(7+\nu) - (1+7\nu)\left(\frac{r}{a}\right)^6\right\}\frac{\alpha_3}{48}$$

$$\left. + \left\{(9+\nu) - (1+9\nu)\left(\frac{r}{a}\right)^8\right\}\frac{\alpha_4}{80} + \left\{(11+\nu) - (1+11\nu)\left(\frac{r}{a}\right)^{10}\right\}\frac{\alpha_5}{120}\right]$$

II.4.30

Determination of Surface Strains

The membrane strains are given by equations II.1.11a,b. The surface strains can be obtained by adding the rotation components to the membrane strains. Thus

$$\varepsilon_r = \frac{dv}{dr} + \frac{r}{R}\Psi + \frac{\Psi^2}{2} + \frac{t}{2}\frac{d\Psi}{dr} \qquad \text{II.2.31}$$

$$\varepsilon_\theta = \frac{v}{r} + \frac{t}{2}\frac{\Psi}{r} \qquad \text{II.2.32}$$

The surface strains can therefore be computed from II.2.31 and II.2.32 along with II.2.7 and II.2.14.

As can be seen from the foregoing, the solution of the governing differential equations requires considerable algebraic manipulation. Once the algebra has been carried out, however, the numerical computation of the results is readily achieved. Since the solution of the shell problem is based on a first approximation obtained from the inextensional bending of a similarly loaded flat plate, a separate analysis must be carried out for each load condition. Such an analysis for the case of the point loaded shell is presented in Appendix VII.1. The approach can be extended to the case of combined load actions though the algebra would become considerably more tedious.

The success of the method depends largely on the close approximation to the shell problem provided by the solution for Ψ obtained from the inextensional bending of the flat plate. The approach also has the merit that since two independent parameters (C_1 and C_2) contribute to the deflected form, the distribution of stress and deformation is allowed to vary along the equilibrium path.

The equilibrium paths for various shell parameters are presented in FIG. II.2 and FIG. II.3 for both pressure and point loading respectively. The varying distribution of membrane force and bending moment in a typical shell ($\lambda = 48$) at intervals along the equilibrium path, is shown for both cases of loading in FIG. II.4a,b and FIG. II.5a,b.

II.3 The Theoretical Equilibrium Paths

Pressure Loaded Shells The equilibrium paths for pressure loaded shells for various values of shell parameter are shown in FIG. II.2. It may be seen that the behaviour of freely supported shells becomes progressively more nonlinear with increasing shell parameter. The equilibrium paths have no turning value until the value of λ exceeds 17 (approximately). For λ greater than this value but less than 300, the equilibrium path has both a maximum and a minimum turning point. For λ greater than 300, computed equilibrium paths have four turning values though it is doubtful if the theory for this range has physical meaning. Since symmetrical behaviour, which forms the basis of the analysis, is unlikely to obtain at

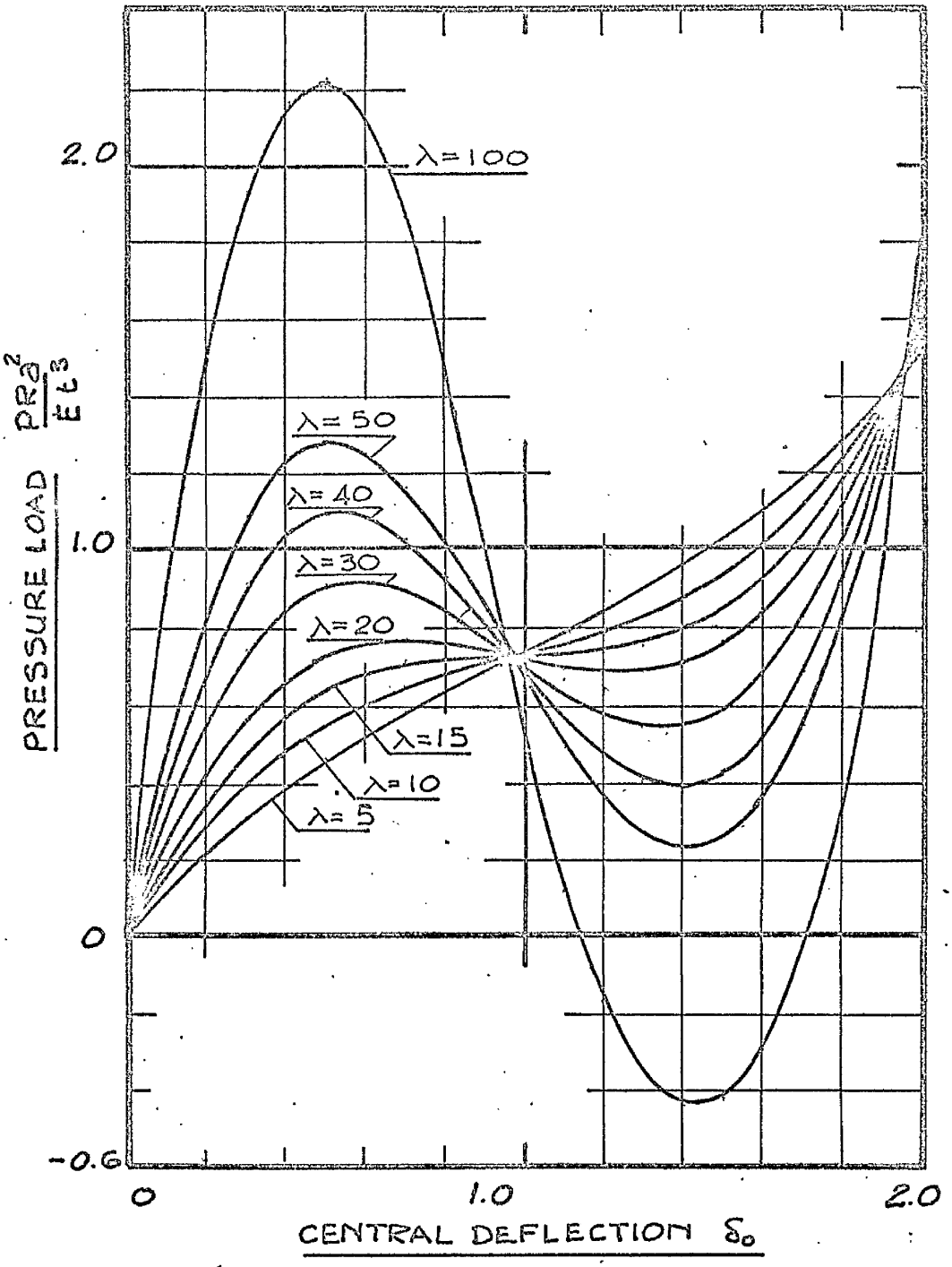

FIG. II.2 The behaviour of pressure loaded, free shells

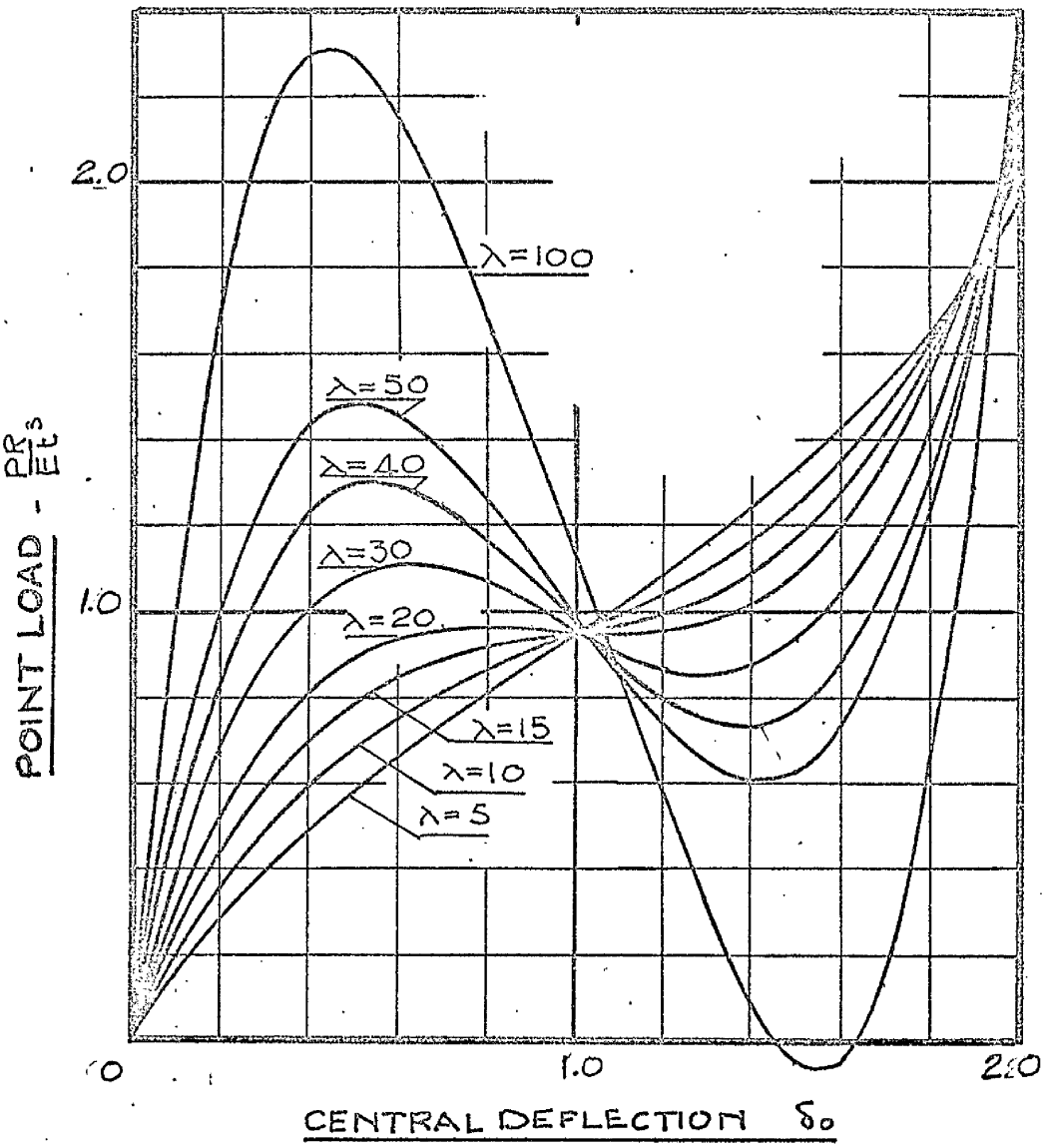

FIG. II.3 The behaviour of point loaded free shells

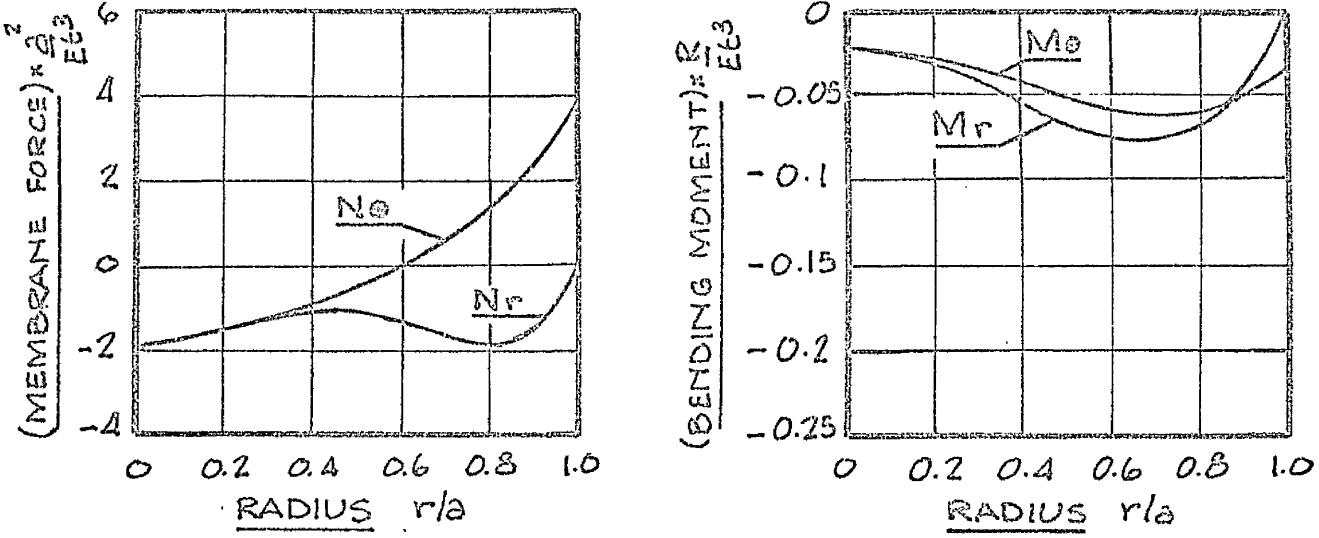

$\delta_0 = 0.4$

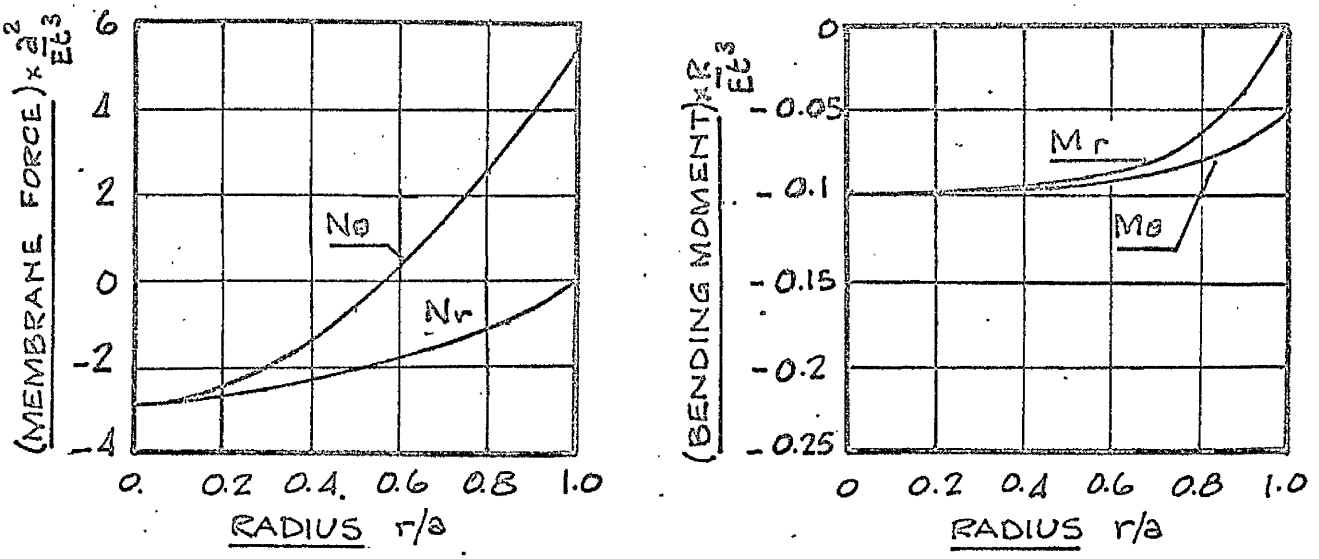

$\delta_0 = 0.72$

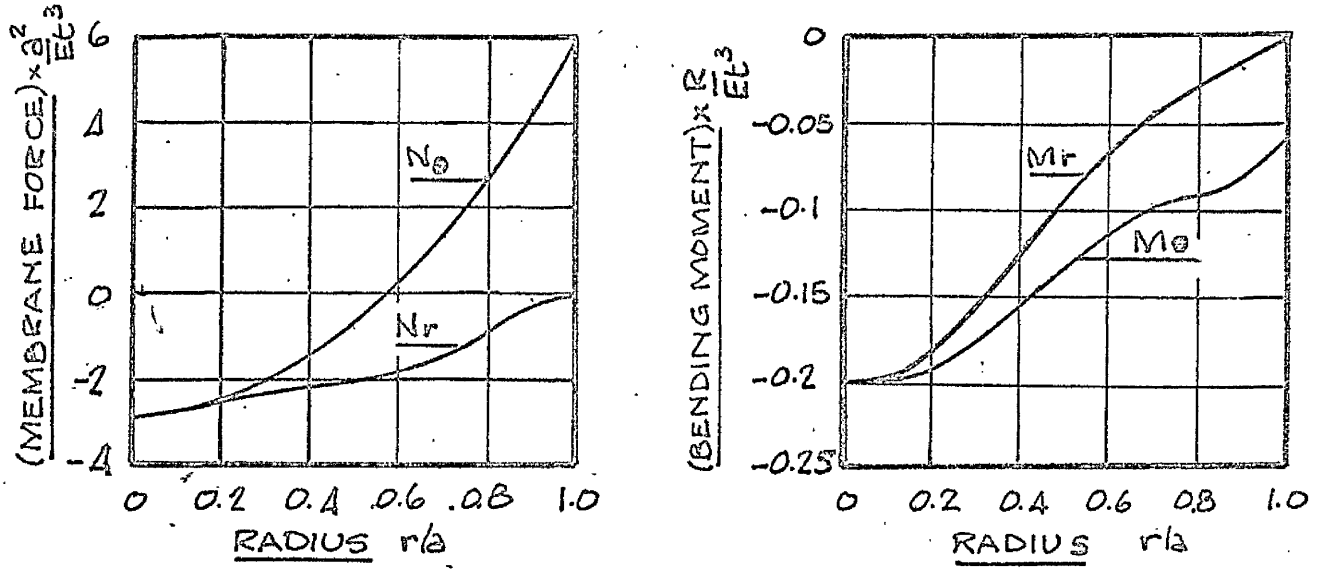

$\delta_0 = 1.04$

FIG. II.4a The variation of membrane and bending actions
PRESSURE LOAD $\lambda = 48$

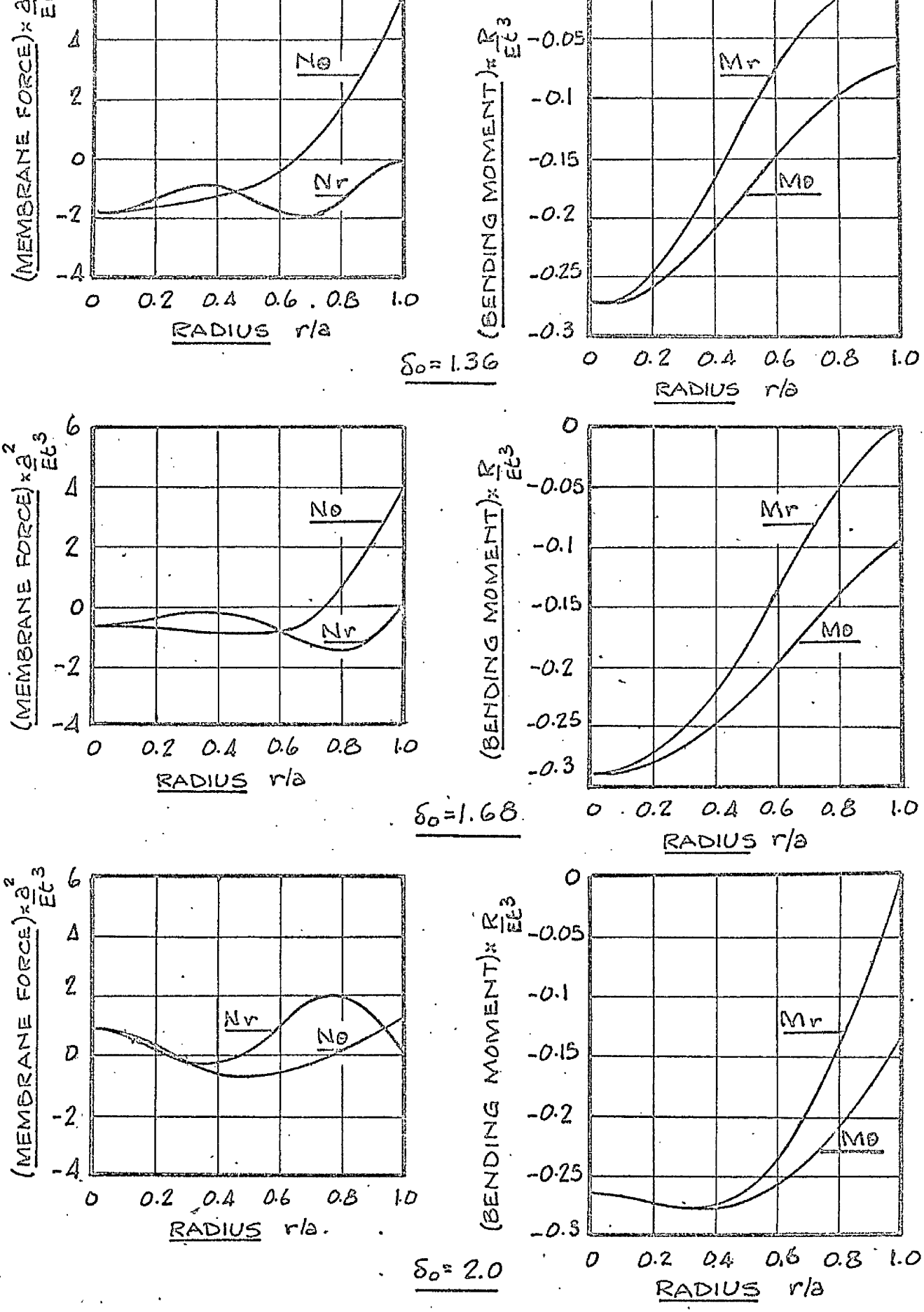

FIG. II.4b The variation of membrane and bending actions
PRESSURE LOAD $\lambda = 48$

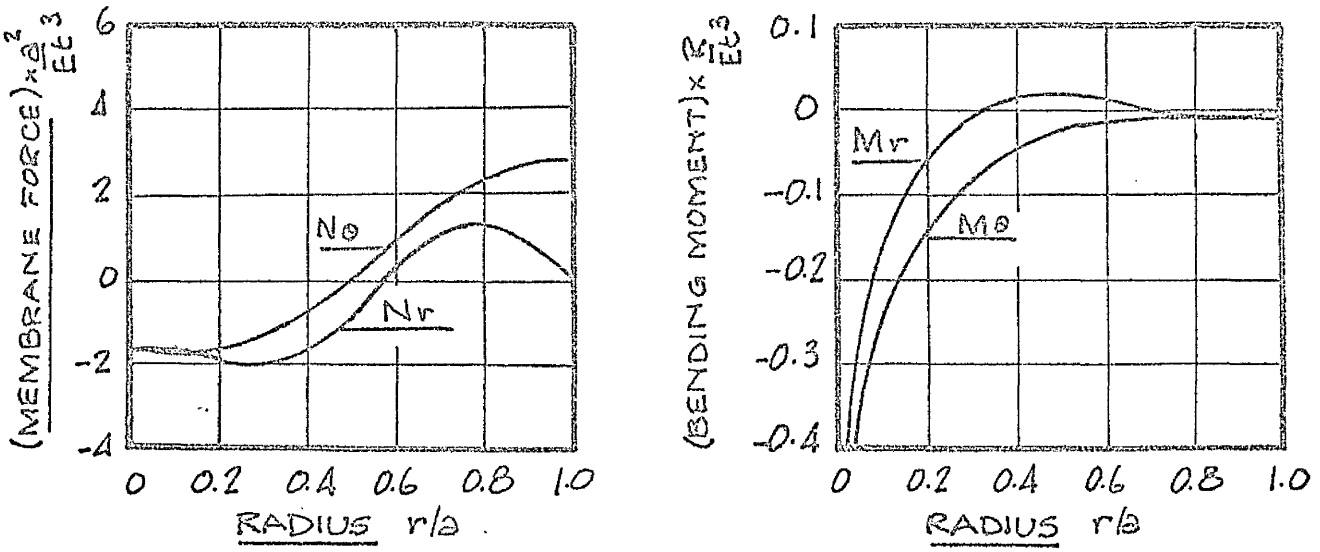

$\delta_0 = 0.4$

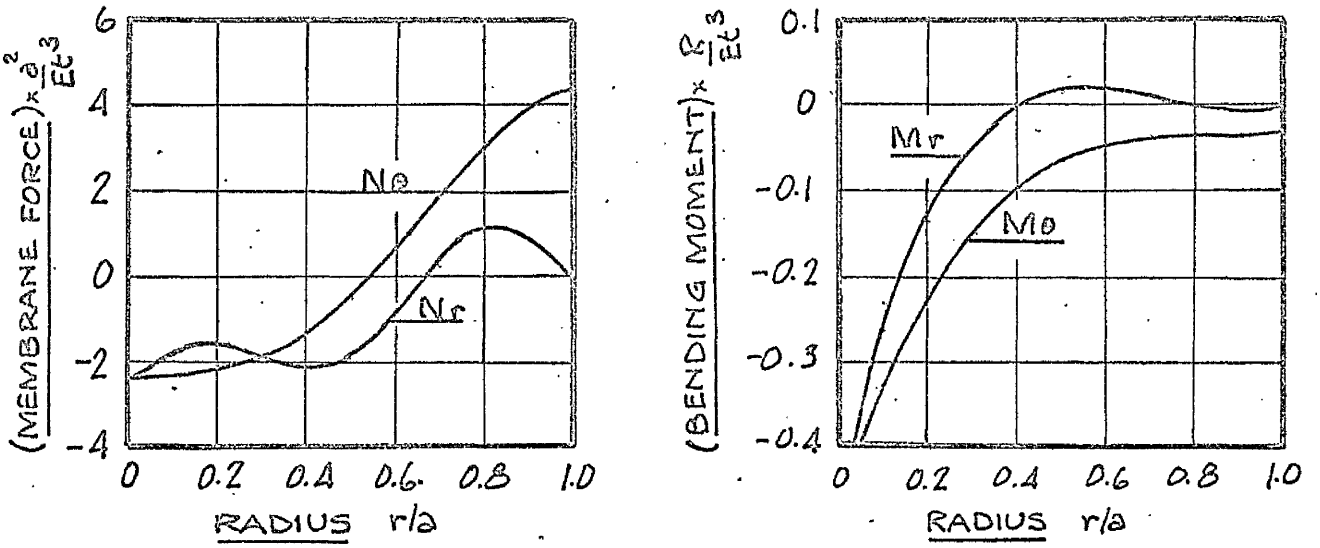

$\delta_0 = 0.72$

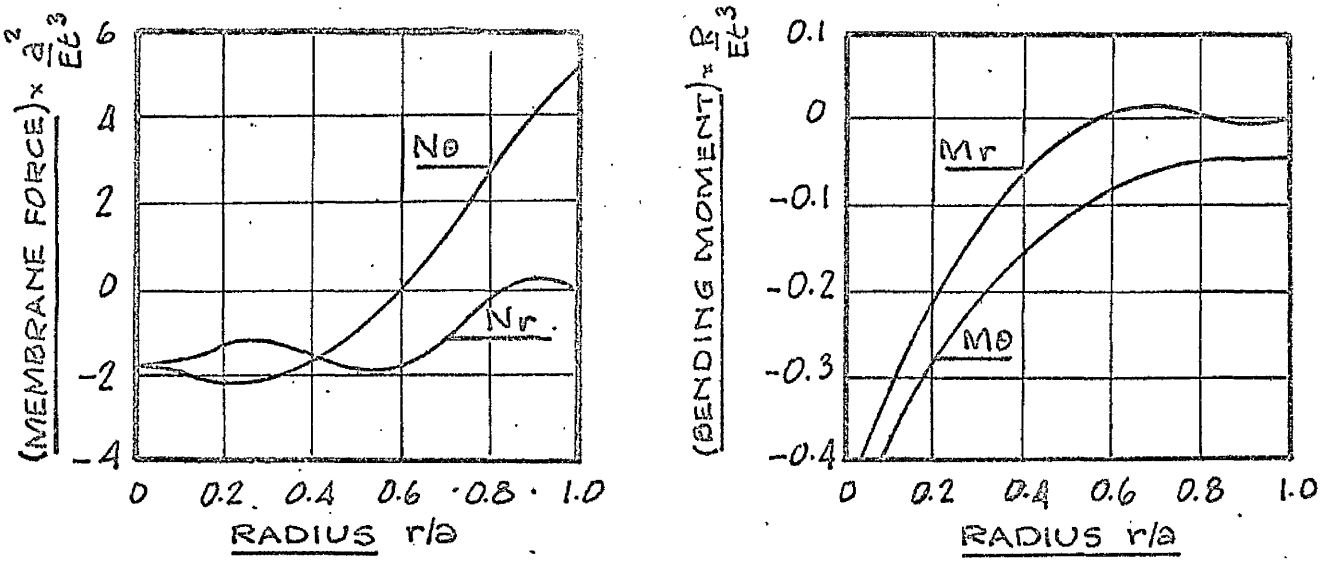

$\delta_0 = 1.04$

FIG. II.5a The variation of membrane and bending actions
POINT LOAD $\lambda = 48$

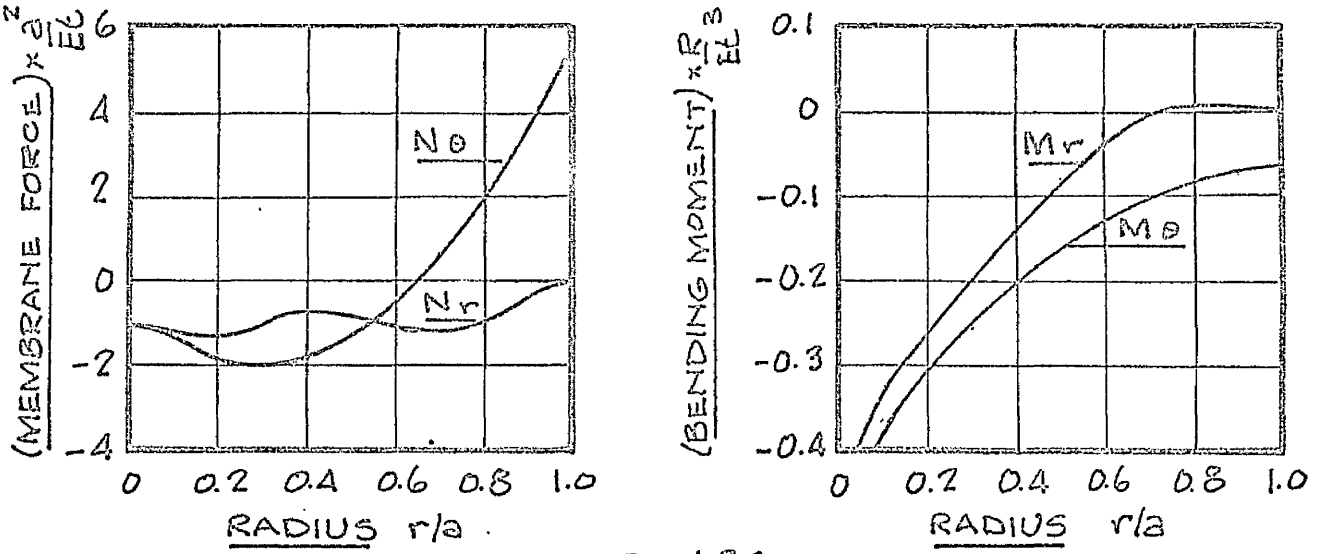

$\delta_o = 1.36$

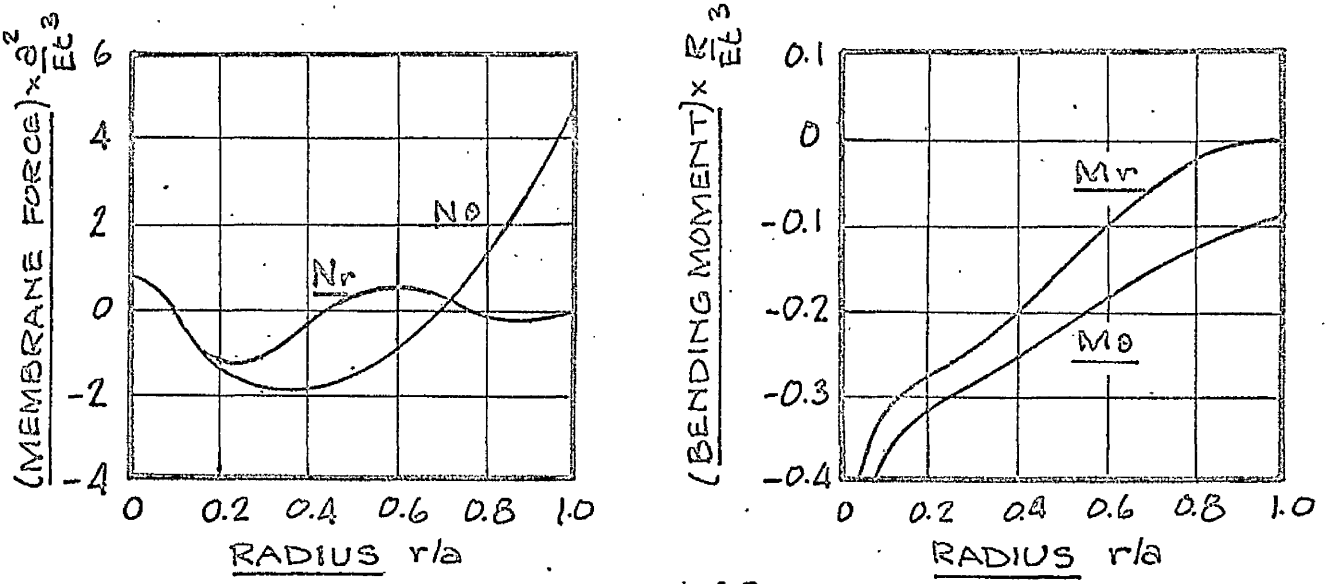

$\delta_o = 1.68$

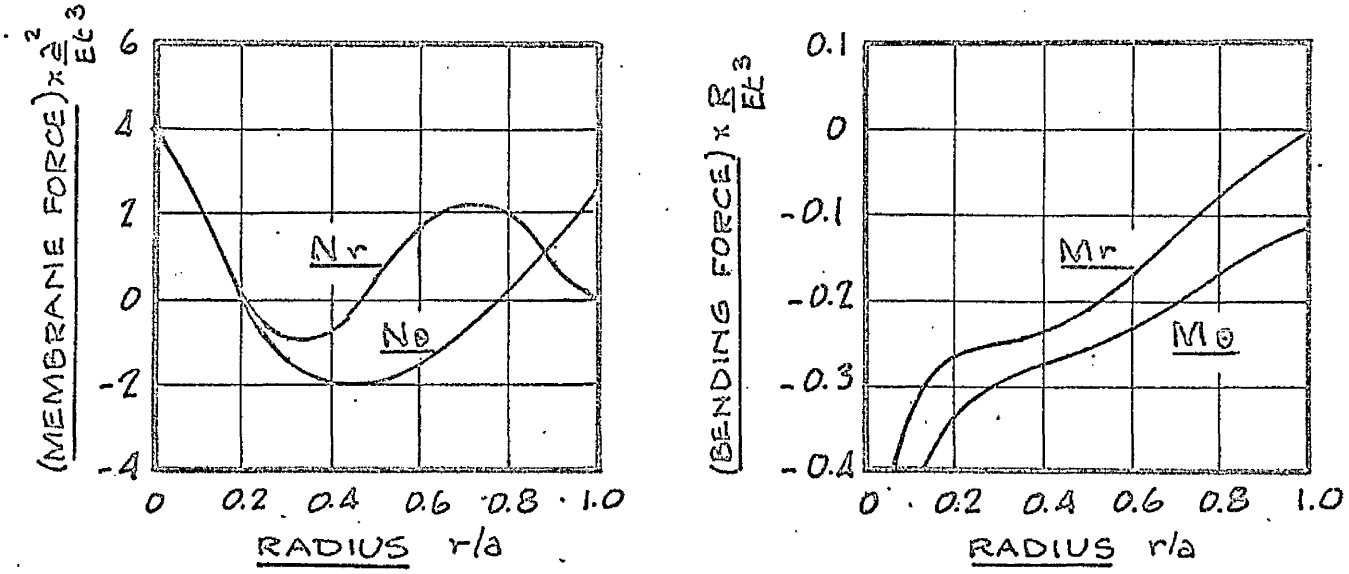

$\delta_o = 2.0$

FIG. II.5b The variation of membrane and bending actions
POINT LOAD $\lambda = 48$

high values of λ , the range has been restricted.

Point Loaded Shells FIG. II.3 shows the corresponding equilibrium paths for point loaded shells for various values of λ . Again, the equilibrium paths become more nonlinear until λ exceeds 17, when subsequent paths exhibit two turning values. When λ exceeds approximately 300, the equilibrium paths have two maxima and two minima though, once again, it is doubtful if the theory has physical meaning in view of the restriction of symmetry.

II.4 Distribution of Membrane Force and Bending Moment

Pressure Load The distribution of membrane force and bending moment in the meridional and circumferential directions is shown in FIG. II.4a and FIG. II.4b at approximately equal intervals along the equilibrium path.

For the pressure load case, the membrane forces in the meridional and circumferential directions are equal at the apex. In addition, since the shell is assumed to be freely supported, the meridional membrane force is zero on the boundary. At small deflections of the order of half the shell rise, the meridional

membrane force has two turning values along the radius. As the deflection increases, N_r becomes monotonic until the distribution at $\delta_o = 1.36$ is very similar to that at $\delta_o = 0.4$. Between $\delta_o = 1.68$ and $\delta_o = 2.0$, the distribution of N_r changes rapidly and in the latter stage has three turning values. The changing distribution of N_θ is rather less marked and varies fairly slowly as the deflection increases.

The bending moments in the meridional and circumferential directions are equal at the apex for a pressure loaded shell. Since the shell is freely supported, M_r is zero on the boundary. As the deflection increases, the distribution of the bending moments changes fairly rapidly initially. For deflections greater than the shell rise, the distribution of bending moment changes less rapidly until at $\delta_o = 2$ the bending moments in both meridional and circumferential directions are substantially the same in magnitude for $r/a < 0.5$.

Point Loaded Shells The distribution of membrane force and bending moment in the meridional and circumferential directions is shown in FIG. II.5a and FIG. II.5b at approximately equal intervals along the equilibrium path.

For the point load case, the meridional membrane forces in the meridional and circumferential directions are again equal at the apex. Since the shell is freely supported, the meridional membrane force and bending moment are zero on the boundary. The distribution of meridional membrane force N_r changes very rapidly until deflections exceed the thickness of the shell and at $\delta_o = 0.4$ a pronounced ripple develops in the distribution along the radius. With increasing deflection, the ripple is intensified until the central deflection approaches the shell rise. At $\delta_o = 1.36$ the ripple in the meridional membrane force is reduced and subsequently changes its character completely with deflections approaching twice the shell rise. As in the case of the pressure loaded shells, the corresponding circumferential membrane action alters its form less radically and the change is more uniformly progressive.

The bending moments in the meridional and circumferential directions are both infinite under the load point and the magnitude of both actions falls very rapidly away from the apex. This rapid fall in magnitude along the radius is characteristic at all values of deflection and it is only at very large

deflections approaching twice the shell rise that distribution of the bending moment actions changes markedly.

II.5 The Influence of Boundary Restraint

It has been shown by FEODOS'EV[5] that a variational solution in which a single term has been used to approximate the deflected form, may predict the behaviour of shallow shells with reasonable accuracy for restricted values of the shell parameter. The range of values of the parameter for which such a solution provides an adequate approximation to the true behaviour is dependent on the type of loading. The results of the present investigation on freely supported shells indicate that for pressure loading, the single term Galerkin solution can be used to infer the behaviour of freely supported shells for values of λ up to about 50. It is possible that the type of boundary condition may influence this limiting value, though direct evidence of this is not available in the present investigation. On the assumption that the effect of boundary support does not radically influence this limiting value, the behaviour of shells within this range have been examined. The Galerkin procedure

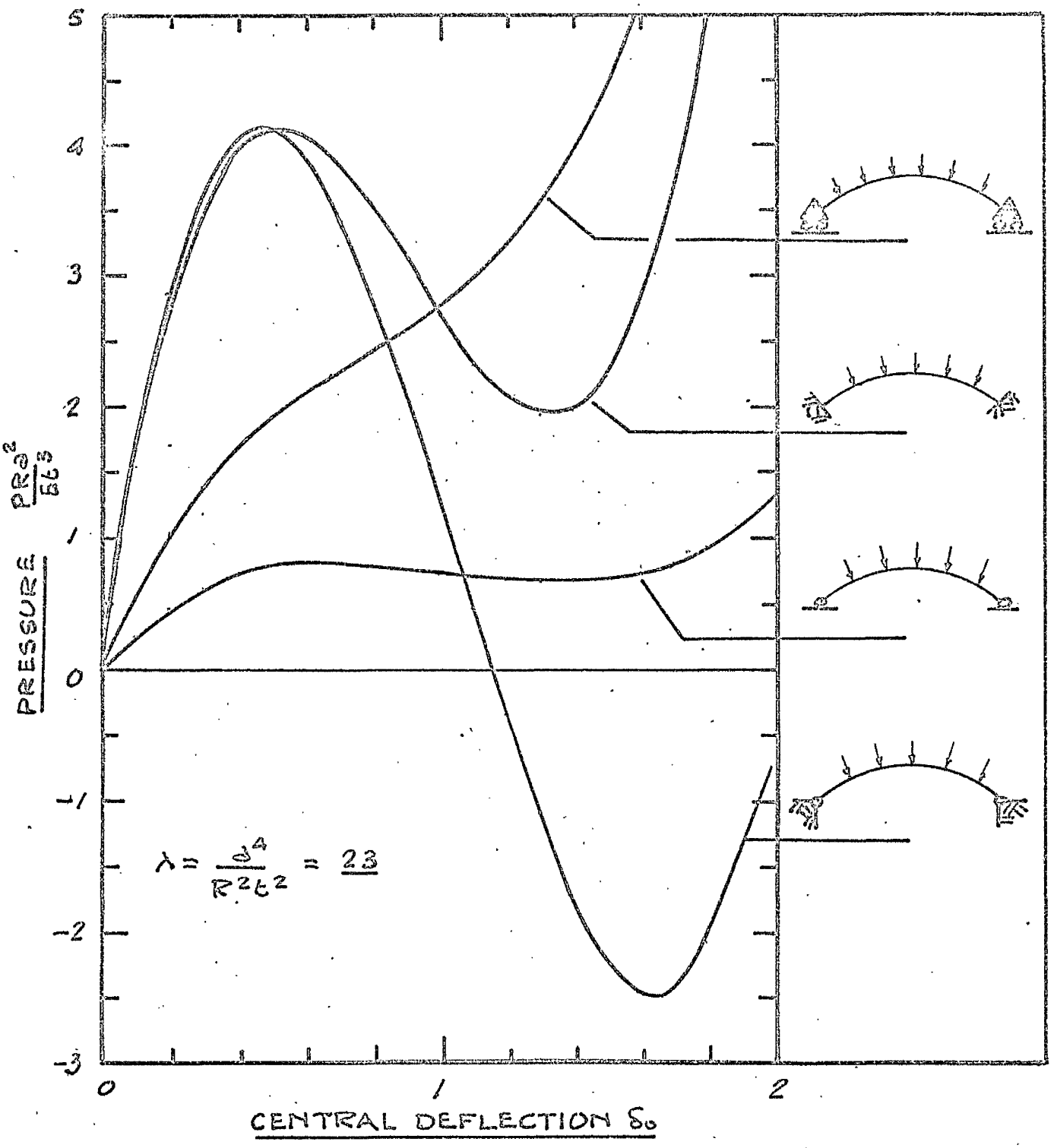

FIG. II.6 The effect of various edge restraints on the behaviour of pressure loaded shells $\lambda = 23$

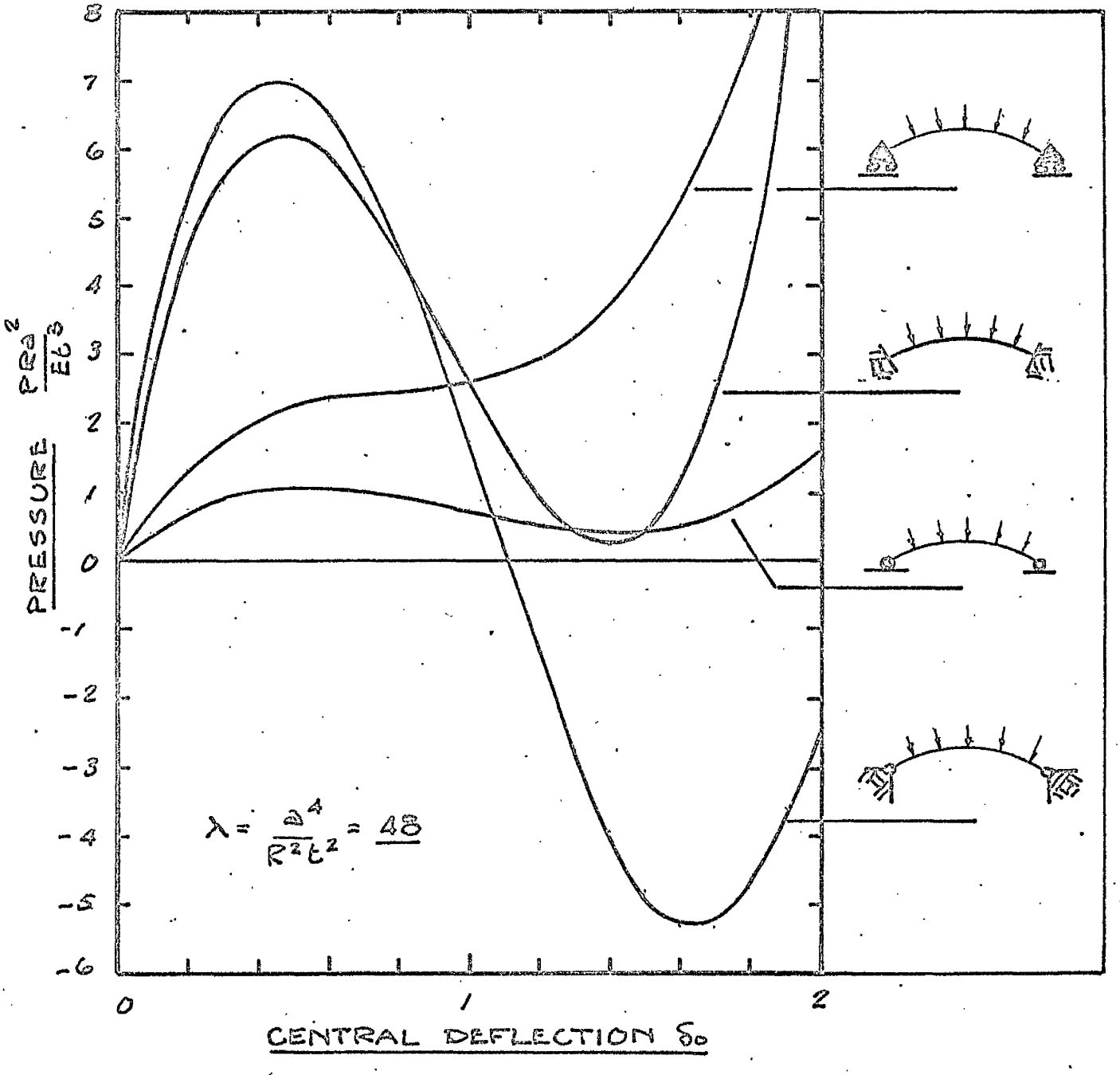

FIG. II.7 The effect of various edge restraints on the behaviour of pressure loaded shells $\lambda = 48$

is suited to this type of investigation since the type of support merely modifies constants involved in the numerical analysis.

The behaviour of shells under pressure loading has been examined for four different boundary conditions in order to assess their influence. The results of these computations are shown graphically in FIG. II.6 and FIG. II.7 for $\lambda = 23$ and $\lambda = 48$ respectively.

FIG. II.6 and FIG. II.7 show the effect of various edge restraints on the behaviour of pressure loaded shells for $\lambda = 23$ and $\lambda = 48$ respectively.

As expected, the freely supported shell has the lowest buckling load as defined by the turning value of the equilibrium path. The effect of radial restraint is to increase the buckling load almost five times in the case of $\lambda = 23$. After the first turning value, the equilibrium path falls very rapidly and becomes negative. This indicates that an internal pressure (approximately two thirds of that required to produce the first snap) would be necessary to 'unbuckle' the shell.

The behaviour of a shell which is rotationally restrained at the boundary but is free to move radially, is nonlinear with no turning value. The combination of this case with that of the radially restrained shell, yields the boundary condition corresponding to the clamped segment. In this case, the effect of rotational restraint is only noticeable at in the latter stages of the equilibrium path since, in the initial stages, the stiffness of the clamped shell derives mainly from its membrane action. Thus the effect of imposing rotational restraint is more marked at large deflections where bending actions contribute significantly to the shell strength. The contribution of these bending actions is sufficient to raise the lower buckling pressure to a positive value about half the upper buckling pressure for $\lambda = 23$.

The behaviour of the freely supported shell is strongly influenced by bending actions. If rotational restraint is first superimposed, the bending strength of the shell is significantly increased and the subsequent behaviour of the shell is of a nonlinear character with no turning value. If edge displacement is now prevented, a clamped condition results. The effect of radial restraint is to increase

the contribution to the shell strength derived from membrane action. This contribution is immediately effective in increasing the initial stiffness of the shell. When the shell is subject to large deflections of the order of the rise, the state of high membrane stress reduces the load carrying capacity of the shell in the presence of large surface rotations which accompany the large deflections.

Thus the behaviour of the clamped shell may be deduced in a qualitative manner by combining the separate effects of different boundary restraints with the behaviour of the free shell.

In the same way, the behaviour of the clamped shell for $\lambda = 48$ (FIG. II.7) may be logically developed in a qualitative manner.

Boundary Condition	Critical Pressure			
	$\lambda = 23$		$\lambda = 48$	
	upper	lower	upper	lower
Rotationally free, radially free.	0.85	0.67	1.10	0.42
Rotationally free, radially restrained.	4.10	-2.50	6.96	-5.29
Rotationally restrained, radially free.	no turning value			
Rotationally restrained, radially restrained.	4.10	2.00	6.19	0.30

It can be seen, therefore, that the behaviour of the shell is influenced to a very considerable extent, by the degree of restraint provided by the support. To the author's knowledge, the influence of such restraints has not previously been investigated with a view to assessing their effect on shell behaviour.

CHAPTER III

EXPERIMENTAL INVESTIGATION

III.1 The Background to the Experimental Investigation

One of the basic assumptions of the theoretical treatment is that the shell remains fully elastic throughout the loading history. If experimental substantiation of the theoretical analysis is to be expected, the requirement of elastic behaviour must be maintained as far as possible.

In any shell under point load action, theoretically infinite stresses exist under the load. Thus the value of the load must be restricted in order to reduce the area of the shell affected by post-elastic stresses to an acceptable size. Since the primary aim of the investigation is an examination of the elastic behaviour of the shell, the shell parameter must be so chosen that nonlinear behaviour obtains and at the same time, the value of the load is restricted. Thus the general geometry of the shell must be, to some extent at least, a compromise.

It has been shown in previous investigations over a wide range of rise to base ratio, that the degree of shallowness has no apparent influence on the behaviour of the shell, provided that the implied

restriction in the term 'shallow' is not violated. This is, of course, in accord with the theoretical considerations where this ratio is not a parameter which influences the behaviour of the shell.

The experimental investigation was directed at the examination of two distinct aspects of instability of shallow spherical shells under uniform pressure and point loading at the apex.

The first of these was the determination of the equilibrium path through both stable and unstable states. To effect this, a new technique using a controlled deflection method was developed.

The second was the examination of stress and deformation states during buckling. These, to the author's knowledge, have not been investigated previously.

Published experimental work to date, has failed to substantiate adequately relevant theoretical treatments. Though many factors may contribute to the apparent divergence, it has been shown that precise measurement of dimensions and freedom from imperfection and initial stress is of considerable importance in meeting the assumptions of the theory. Thus special

attention has been directed to this end. In view of the difficulty of achieving experimentally closely defined displacement dependent support conditions, force dependent conditions have been adopted throughout.

III.2 The Material Characteristics of the Test Specimens

Choice of Material: It was decided to form the test specimens from sheet material in order to ensure uniformity of thickness.

A material was sought which could be formed readily without resorting to the use of very high temperatures. In addition, it was necessary to choose a material which had good linearity of stress-strain properties at normal temperatures. It was recognised that forming the specimens at an elevated temperature would avoid residual stresses which were associated with other forming techniques.

An aluminium alloy, Noral M57S, fulfilled these requirements. The manufacturer's specification for this material was as follows:

(i) Composition Al - 97.75%
Mg - 2.00%
Mn - 0.25%

(ii) Mechanical Properties (annealed, soft)

0.1% Tensile Proof Stress 5 tonf/in^2

Ultimate Tensile Stress 12 tonf/in^2

The two constants of relevance in the experimental analysis were Young's modulus, E, and Poisson's ratio, ν .

Young's Modulus: An attempt to obtain Young's modulus from suitably strain gauged tensile specimens yielded variations in E of the order of 6%. To avoid the use of strain gauges, a more fundamental approach was adopted.

Strips of sheet material were cut from each thickness of sheet and bent under symmetrical four-point loading so that constant bending moment obtained over the central portion. Young's modulus was calculated from observations of the central deflection from which the radius of curvature of the beam specimen was obtained. In this manner, consistent values for E were obtained with an estimated accuracy of 2%. The

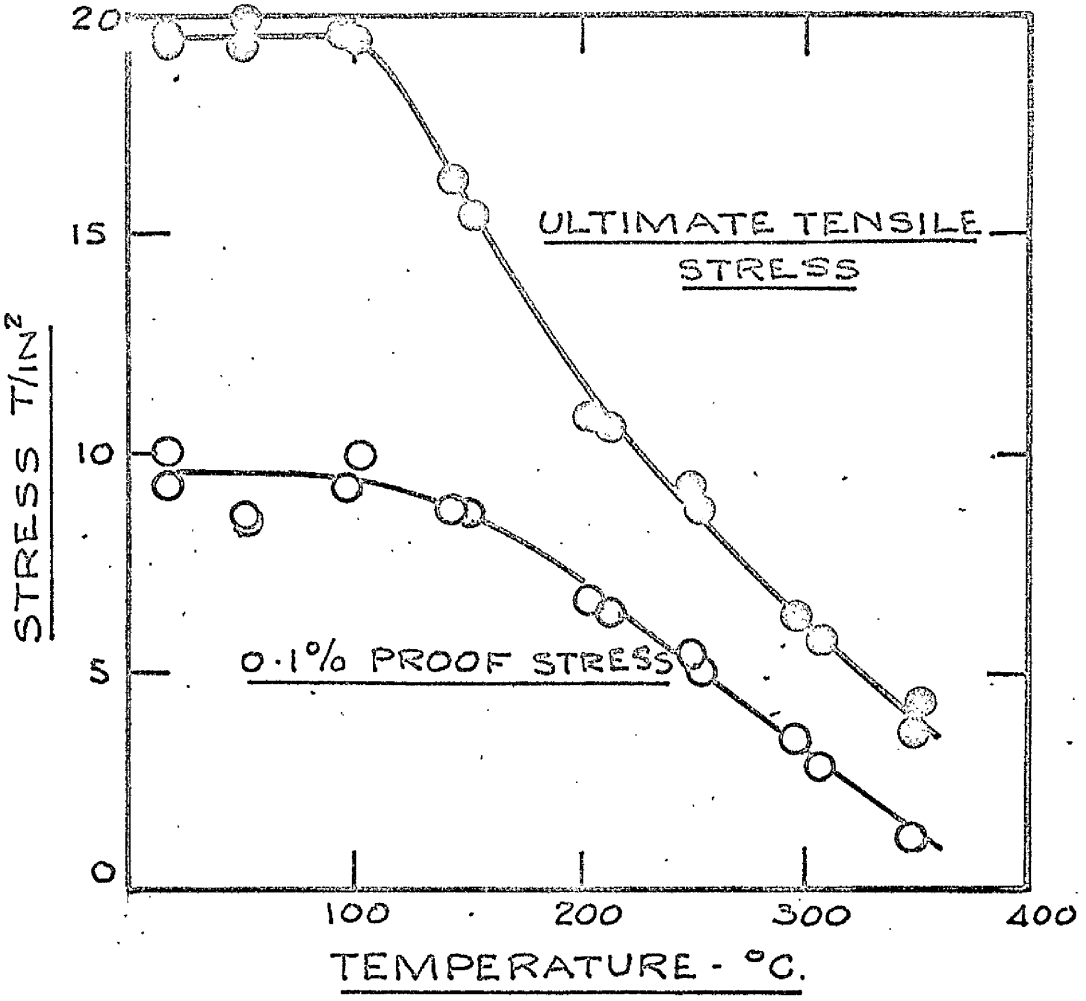

FIG. III.1 The effect of temperature on the mechanical properties of aluminium alloy.

value of Young's modulus was taken as 10.3×10^6 lbf/in^2 throughout.

Poisson's Ratio: Poisson's ratio was obtained from the ratio of transverse to axial strain gauge measurement from four tensile tests. The value $\nu = 0.33$ was adopted for all subsequent calculations.

Isotropic?

III.3 The Fabrication of Test Specimens

Two sets of dies of 10 in base diameter were machined on a profile following lathe to radii of curvature of 80 in and 100 in. The ordinates of the die profiles were subsequently checked for accuracy to within 0.0002 in.

Discs 10 in. diameter were cut from the alloy sheet with a tolerance of 0.0005 in. in the radius. A disc was placed between the dies and heated in an oven to 360°C. The oven was maintained at this temperature for about four hours and then allowed to cool.

It may be seen for FIG. III.1 that the yield stress of the aluminium alloy falls very rapidly

beyond 100°C and that at the forming temperature, the maximum stress that could exist in the specimen was about 1 tonf/in^2. By maintaining the forming temperature, the relatively poor creep properties of the material reduced these stresses still further, obviating in consequence, the possibility of residual stress actions in the final form.

III.4 Dimensional Survey of Test Specimens

On removal from the dies, a dimensional survey including thickness of the specimen was taken at 21 points across the diameter, so that a complete profile of the shell was determined. The radius of curvature of the shell was taken as the radius of the circle which had the minimum least squares deviation from the measured ordinates.

Thus, the equation of the circle, tangent to the X-axis at the origin is

$$x^2 + y^2 + 2Ry = 0$$

In general, the measured points will not satisfy this equation exactly. The square of the error which is assumed to be a function of the radius R

is given by

$$f(R) = \sum (x^2 + y^2 + 2Ry)^2$$

For minimum deviation

$$\frac{\partial f}{\partial R} = 0 = 2 \sum Ry^2 + \sum x^2y + \sum y^3$$

$$\text{Hence} \quad R = \frac{\sum x^2y + \sum y^3}{2 \sum y^2}$$

The results of two typical measurement analyses are presented in Appendix VII.8 where data relevant to an 80 in. and a 100 in. radius shell is analysed.

It was found that the value of the spherical radius obtained in this way, agreed closely with the nominal radius of curvature of the dies, the actual radius of curvature lying usually within 1% of the nominal value. There was no measurable spring back of the specimen on removal from the dies and this provided a further check on the stress free character of the shell. Further measurement of other typical profiles showed good symmetry and consistent curvature. The maximum initial imperfection from the true profile was less than 2% of the thickness.

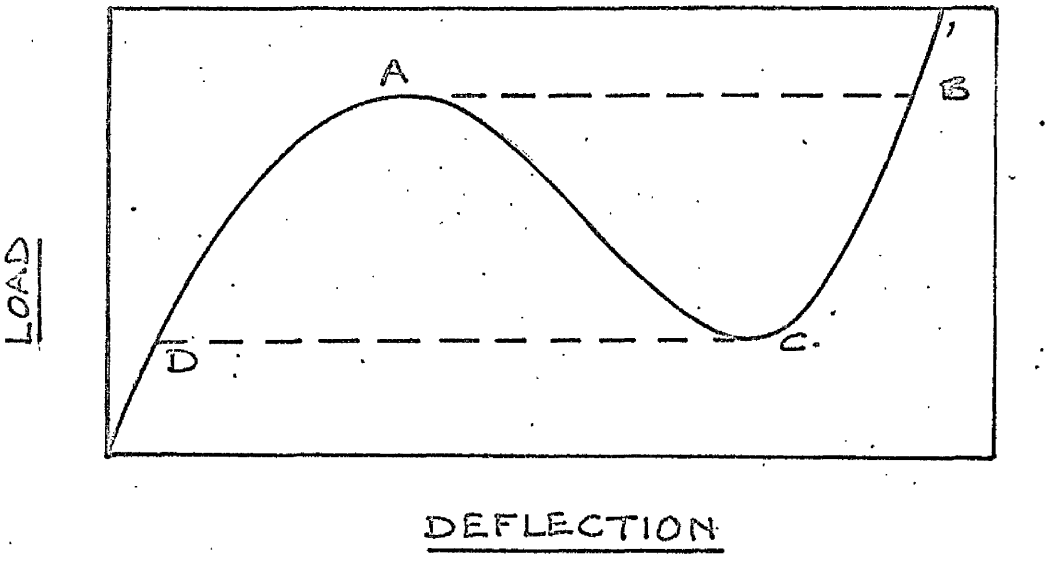

FIG. III.2 A typical equilibrium path.

The nominal dimensions of the shells tested are given below:

No. of specimens	R	a	t	λ
4	80	5	0.036	75.35
4	80	5	0.048	42.39
4	80	5	0.064	23.84
4	100	5	0.036	48.23
4	100	5	0.048	27.13
4	100	5	0.064	15.26

III.5 The Experimental Equipment

In order to obtain the equilibrium path through both stable and unstable ranges, special test techniques were developed. Since equilibrium may be interpreted in terms of energy which is deformation rather than load dependent, a controlled deflection loading technique was adopted. A typical equilibrium path is shown in FIG. III.2.

If the load is applied incrementally, the shell will follow a stable equilibrium path up to the turning point on the path at A. Any further increase in the load causes the shell to snap suddenly from A to B on

the second stable portion of the path. Decrease of the load from B in the second stable range, causes the shell to follow the path down to C. Further decrease in the load produces a second snap to D on the first stable portion of the path. Thus by varying the load, only stable equilibrium states can be achieved. At any intermediate load between the snapping conditions, there will be, in general, three equilibrium displacements, two of which will be stable and one unstable. It is therefore obvious that if the complete equilibrium path is to be achieved, it is necessary to specify the deflection rather than the load. Merely by specifying the deflection and simultaneously measuring the load, the complete equilibrium path can be traversed. Since axial symmetry is assumed in order to simplify the stress analysis, the deflection at the centre of the shell is a convenient parameter to use to determine the equilibrium path.

The test apparatus is shown in FIG. III.3. The shell was placed in a support ring attached to the top of the pressure chamber. A beam ABCD was supported in ball-bearings at B in such a manner that the length AB equalled the length BC. A threaded wheel fitted closely into a slot in the beam at C. By turning the

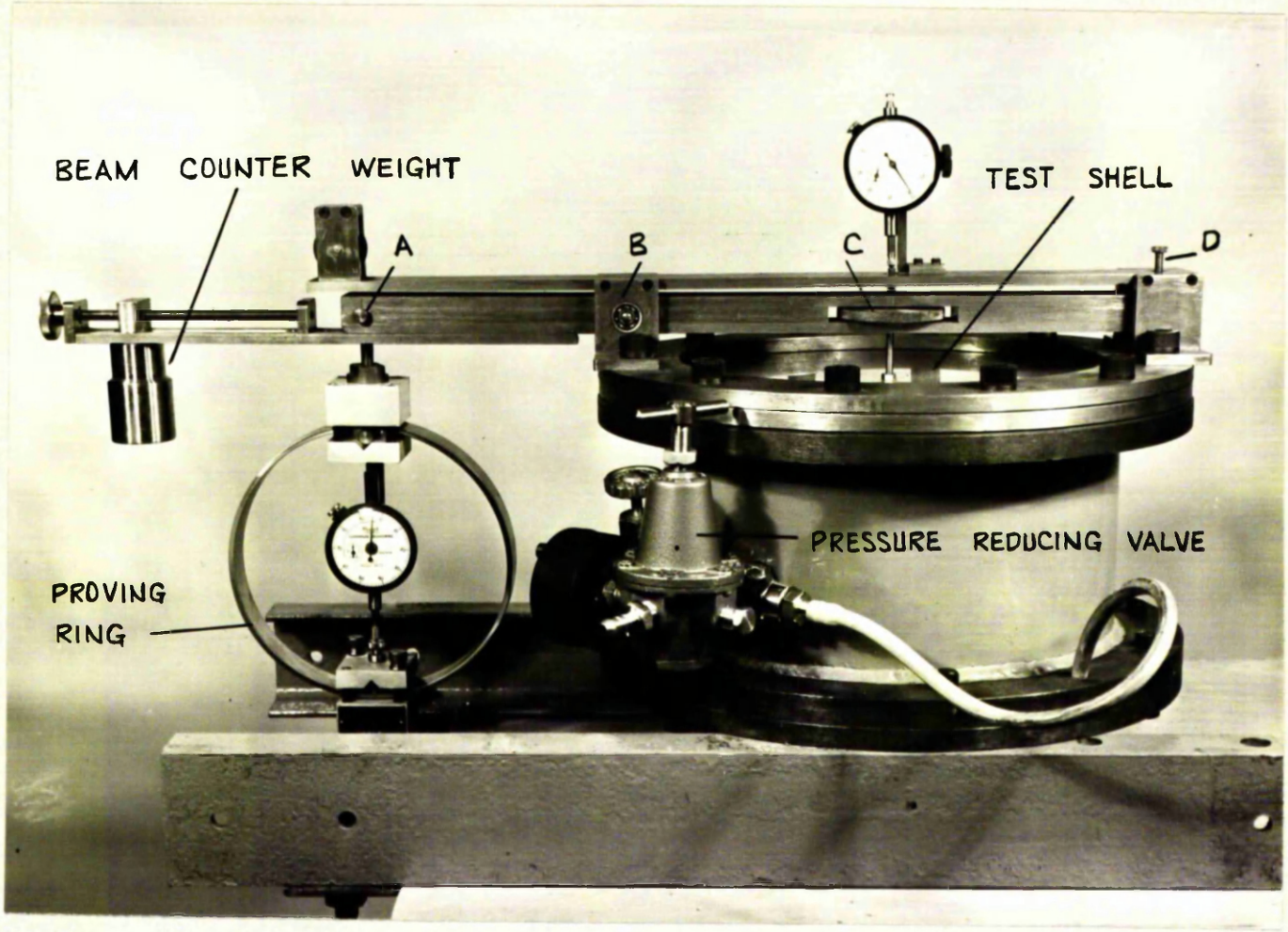

FIG. III.3 Test apparatus

wheel, a threaded rod was advanced axially through the beam. A dial gauge located above the rod recorded the axial movement.

III.6 Test Procedure

Point Load: The shell was placed convex side up for these tests. The load was transmitted to the shell by a ball-bearing located at the lower end of the rod. Since the beam was freely supported at B, the force transmitted by the rod to the shell was recorded on a proving-ring at A. The load was measured at successive increments of 0.01 in. of central deflection. The test was carried through until the central deflection exceeded twice the original rise of the shell. In an average test some thirty points were measured along the equilibrium path depending on the initial rise of the shell. The deflected form of the shell was determined from dial gauges situated at 1 in. intervals from the apex of the shell.

Pressure Load: In the case of the pressure load tests, the shell was penetrated at the apex and attached to the rod so that the concave side was uppermost. In

these tests, the proving-ring was removed and adjustable stops were set at D to restrict the free movement of the beam to 0.001 in. Air pressure was controlled by a reducing valve and a needle valve. The pressure in the chamber was measured on a water manometer with an effective maximum height of 5 ft. To carry out the test, the deflection was given to the shell by setting the wheel at C. This produced a force in the rod connected to the shell and brought the beam against the lower stop at D. The pressure was then gradually increased in the chamber until the beam just 'floated' between the preset limits controlling its free travel. At this pressure, the shell was in equilibrium at the given deflection with no force in the rod at C. In this way the stable and unstable ranges of the equilibrium path were traversed.

Some leakage of air took place at the support since no special measures were adopted to effect a seal. This leakage was fairly constant and, in fact, facilitated the problem of controlling the pressure. In order to assess the effect of the hole at the apex of the shell, the stable ranges of the equilibrium path were examined on similar shells with no such penetrations. No appreciable effect arising from this

source was recognised.

The tests on both point and pressure loaded shells were repeated on further specimens of the same geometric form to assess the degree of consistency in the results. It was found that the critical load could be reproduced to within about 3 - 4%.

III.7 The Measurement of Strain

Six shells were straingauged using 36, $\frac{1}{4}$ in. linear, 70 ohm foil straingauges attached to both surfaces of the shell along a meridional line in the circumferential and radial directions. Thus the state of strain was determined at nine points on both top and bottom surfaces of the shell.

The tests on the straingauged shells were carried out using a similar test procedure to that adopted for the determination of the equilibrium path. The strain readings were recorded using 'Solartron Data Logging Equipment'. This equipment measured voltage changes corresponding to strains on a digital voltmeter and printed out the readings at speeds up to 10 channels per second. All the surface strains were measured at

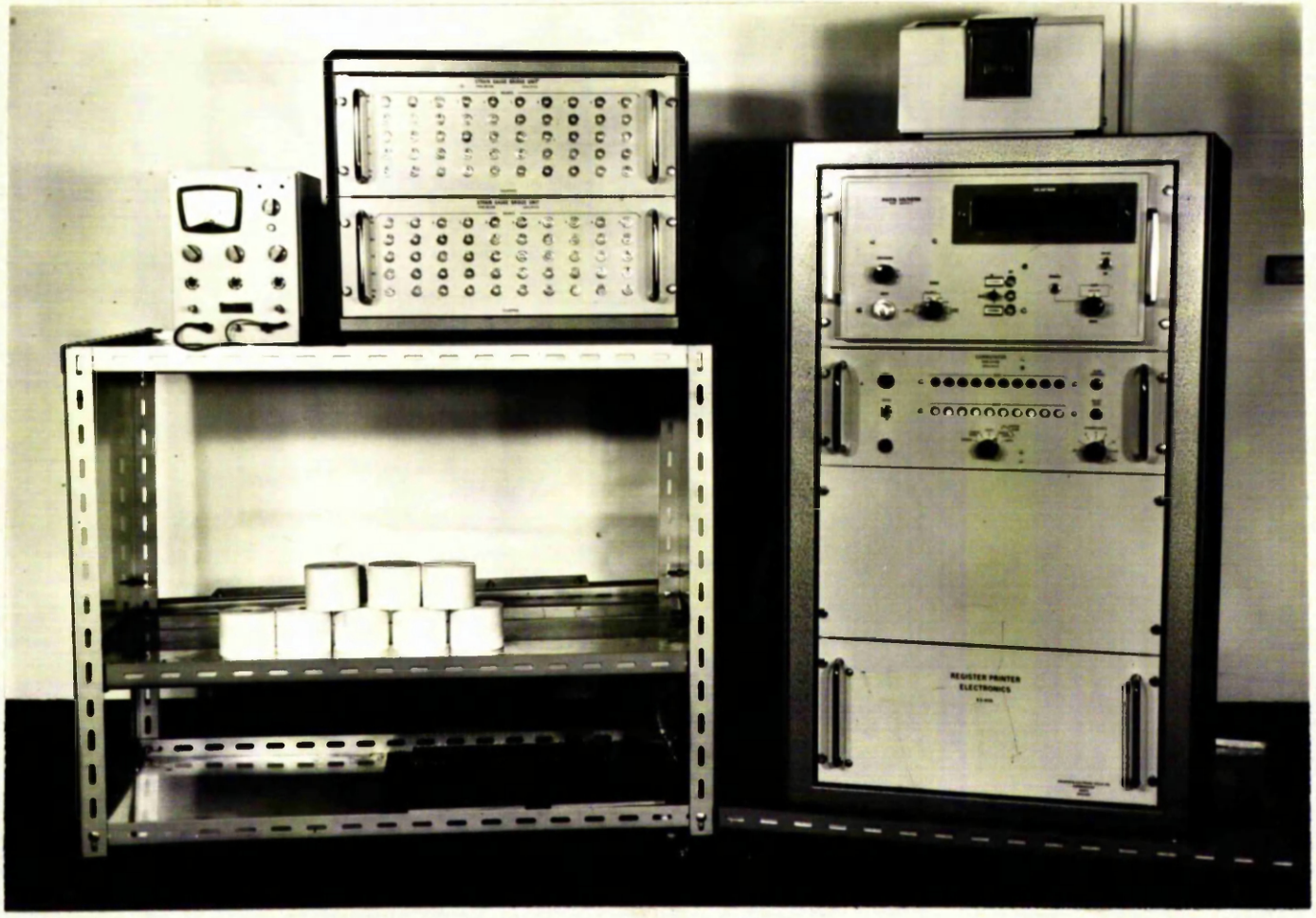

FIG. III.4 Solartron Data Logging Equipment

each increment of deflection so that in an average test, some 1100 strain readings were recorded.

The strain measuring equipment is shown in FIG. III.4.

CHAPTER IV

COMPARISON OF EXPERIMENTAL AND THEORETICAL RESULTS

The comparison of experimental and theoretical results is considered in two parts. In the first part, the behaviour of both point and pressure loaded shells is examined from the point of view of load-deformation and deflected form. In the second part, the comparison of experimental and surface strains is considered.

The results of the investigation are presented in full in Appendix VII.8. In all cases, the experimental results are presented as plotted points and compared with theory which is shown as a full line.

IV.1 The Equilibrium Path and Deflected Form

Pressure Loaded Shells: FIG. VII.1a shows the experimentally determined equilibrium path and variation of deflected form for the shell with $\lambda = 23$. For the equilibrium path, the experimental data and theory are in good agreement for values of central deflection up to the original rise of the shell. Beyond this deflection, the equilibrium path of the shell diverges slightly from theory which is somewhat lower. This may be attributed to the development of plasticity at the higher deflections.

To illustrate the changing deflected form, the deflection at any radius is plotted as a ratio of the value at the centre. The deflected form measured experimentally is in close agreement with theory.

The experimental and theoretical equilibrium paths $\lambda = 42$ are compared in FIG. VII.2a. As in the previous case, good agreement is obtained for central deflections of the order of the shell rise. Thereafter, the experimental path lies above the corresponding theory and gradually diverges from the latter up to central deflections twice the original rise of the shell.

FIG. VII.2a also shows the variation of the deflected form. Here, the theory is fully substantiated by the experimental data. Comparison of the changing deflected form for this shell may be made with the corresponding results for $\lambda = 23$ (FIG. VII.1a). It may be seen that as loading progresses, the thinner shell ($\lambda = 42$) is appreciably more nonlinear in behaviour and this is reflected in greater changes in the deflected form.

For the case of $\lambda = 48$, the experimental and theoretical equilibrium paths are in very good agreement even at large values of central deflection. This shell was one of the thinnest tested and as a result, the stress levels were generally lower than in the thicker shells represented by lower values of the shell parameter. Thus, as expected, the general behaviour of this shell was more elastic with little residual deformation at the end of the test. The behaviour of this shell is compared with theory in FIG. VII.3a which also shows the variation of the deflected form. The deflected form is again in close agreement with theory throughout the range.

From the behaviour of the shells examined, it is clear that the behaviour of the shells becomes more nonlinear with increasing shell parameter. This nonlinearity is reflected in the changing deflected form where the latter varies most in those shells with the highest values of λ .

Equilibrium paths for $\lambda = 15$, $\lambda = 27$ and $\lambda = 75$ are shown in FIG. VII.4. For central deflection of the order of the shell rise, the equilibrium paths for the two lower values of the shell

parameter are in good agreement with relevant theory. At higher deflections, the agreement is less good but the general behaviour of the shells is substantiated by the experimental data though the influence of plasticity is noticeable. For the particular case of $\lambda = 75$, however, the experimental equilibrium path is markedly different from that predicted theoretically. At approximately the first turning value on the path, the experimental results deviate rapidly from the theory and agreement thereafter is relatively poor. During the test on this shell, nonsymmetric behaviour was observed and subsequent tests on shells with the same parameter produced similar results. It would therefore seem that $\lambda = 75$ must represent approximately the limit of symmetric behaviour.

FIG. VII.5 shows a comparison of experimental and theoretical buckling pressures based on the turning values of the corresponding equilibrium paths. It may be seen that experimental values are in good agreement with the theory. Since nonsymmetric behaviour was confined to post buckling states for $\lambda = 75$, the buckling pressure has not been appreciably influenced, though the lower buckling pressure at which the shell would snap back to the first stable

range, has been affected.

Point Loaded Shells: FIG. VII.6a shows a comparison of the experimentally determined equilibrium path and variation of deflected form with relevant theory for the shell with $\lambda = 23$. The behaviour of the shell as determined experimentally, is in close agreement with theory throughout the loading history. The deflected form as measured on the shell is in fair agreement with theory though the latter consistently overestimated the actual deflection at $r/a = 0.4$ by a small amount.

The behaviour of the shell with $\lambda = 42$ is shown in FIG. VII.7a. The experimental and theoretical equilibrium paths are in substantial agreement for deflections up to the order of the shell rise. The effect of plasticity may be recognised subsequently by some divergence at larger deflections. The area affected by plasticity may be assumed to be fairly small since the theory based on assumed elasticity predicts the general behaviour of the shell adequately.

FIG. VII.7a also shows the changing deflected form at intervals along the equilibrium path. As in

the case of the pressure load, shells with higher values of the shell parameter are more nonlinear in behaviour and this is reflected in a more rapidly changing deflected form.

The behaviour of the shell with $\lambda = 48$ is compared with theory in FIG. VII.8a. The experimental and theoretical equilibrium paths are in substantial agreement for most of the loading history though the effects of plasticity may be recognised in the later stages of the path. The measured deflected forms are in good agreement with those predicted theoretically.

Equilibrium paths for $\lambda = 15$, $\lambda = 27$ and $\lambda = 75$ are shown in FIG. VII.9. Again, the paths for the two lower values of the shell parameter are in substantial agreement with relevant theory for central deflections up to the order of the shell rise. For $\lambda = 27$, the effects of gradually developing plasticity may be recognised in the later stages of the path, though the general behaviour is in general agreement with the elastic theory. For $\lambda = 75$, however, the experimental buckling load as defined by the turning point on the equilibrium path, is somewhat lower than that predicted theoretically. Nonsymmetric

behaviour of the shell accounts for the marked divergence which characterises the subsequent portions of the path. Experimentally, this shell was the least consistent in behaviour in that further tests on shells with the same parameter yielded some variations in the experimental equilibrium paths. While nonsymmetric behaviour was noticeably present, the effect on the buckling loads was not very significant.

FIG. VII.10 presents a comparison of experimental and theoretical buckling loads. Here, the general order of agreement is good. The lower buckling loads where the shells would snap back to the first stable range of the equilibrium path show some slight divergence from theory. This may be attributed to the fact that deflections at these positions on the path are fairly large and the effects of plasticity are apparent.

IV.2 Surface Strains

Strain analyses were carried out on six shells; three subject to pressure load and three subject to point load.

The nominal dimensions of the shells tested were:

No. of shells	R	a	t
2	80	5	0.064
2	80	5	0.048
2	100	5	0.036

Some 1100 strain measurements were made in each test and the large volume of experimental data obtained was processed by digital computer to yield the complete deformation history of each shell. Typical results for the surface strain distribution are presented graphically at six points along the equilibrium path. These six points have been chosen arbitrarily at approximately equal intervals of central deflection.

Pressure Load: For $\lambda = 23$, the general agreement of experimentally determined strains with theory is good. It is of interest to note that the measure of agreement is maintained throughout the loading history. The correlation of experimental data with theory is shown in FIG. VII.1b and FIG. VII.1c.

FIG. VII.2b and FIG. VII.2c show the surface strains for the case of $\lambda = 42$. In the initial range up to central deflections of three-quarters of

the original rise of the shell, the experimental strains are in good agreement with theory. Beyond this point, the strains in the circumferential direction are numerically higher than theoretical predictions would indicate. The meridional strains do not show the same divergence and are in better agreement with theory.

For the case of $\lambda = 48$, the thinnest shell tested, the general measure of agreement of the experimentally measured strains with theory is good at all points along the equilibrium path. The comparison of experimental data with theory is shown in FIG. VII.3b and FIG. VII.3c.

Point Load: For the shell parameter $\lambda = 23$, FIG. VII.6b and FIG. VII.6c, the experimental strains indicate similar behaviour to that predicted theoretically. The circumferential strain readings are somewhat higher than those deduced from theoretical considerations particularly in the neighbourhood of the load point. This may be attributed to the development of plasticity near the apex. In addition to this, it must be recognised that the measurement of strain in the presence of high stress gradients is more likely to be somewhat in error.

FIG. VII.7b and FIG. VII.7c show the comparison of experimental and theoretical surface strains for the case of $\lambda = 42$. Again, the experimental surface strains are in general agreement with theory though a significant deviation exists for gauges near the apex.

For the shell parameter $\lambda = 48$, the trend of experimental results is in agreement with theory. Once again, the presence of high stress gradients and the onset of plasticity in the neighbourhood of the load point, caused some divergence between experimental strain values and corresponding theory. The results for this case are compared with theory in FIG. VII.8b and FIG. VII.8c.

IV.3 Commentary on the Experimental Work

From the present investigation, it would appear that $\lambda = 75$ represents the probable limit of symmetric behaviour for both pressure and point loading. For this particular case, nonsymmetric behaviour is limited to the unstable state and appears to have little effect on the first buckling load.

In the case of the point loaded shells, the

effects of plastic deformation could not be avoided. By careful choice of the shell dimensions, the effects were restricted to a fairly small area in the neighbourhood of the load point. Plasticity did not have an appreciable effect on the behaviour of the shells as load carrying structures but it did influence the distribution of surface strain. This factor, together with the presence of high stress gradients in the neighbourhood of the apex, caused a significant divergence between the experimental strain distribution and corresponding theory. In this respect, strain measurement was less satisfactory than in the case of pressure loaded shells where stress levels were, in general, considerably lower. In spite of these factors, the experimental strain distribution was in general agreement with relevant theory.

For pressure loaded shells, the general agreement of experimental data with theory was of a high order. The absence of high stress gradients and generally lower stress levels meant that the assumptions of the theoretical treatment were more nearly fulfilled than in the case of point loaded shells. The presence of a small hole at the apex of these shells, caused a stress concentration which was reflected in the strain

measurements. The effects of the concentration were local to the immediate vicinity of the hole and had no apparent influence on the behaviour of the shell.

The close agreement between shells of similar shell parameter, indicates that the method adopted to manufacture the test specimens produced shells of consistent performance.

A basic assumption of the theoretical treatment is that of symmetric behaviour. Use was made of this assumption in the experimental investigation of surface strain in that strain measurements were made along a typical meridian. It is recognised that by attaching all the strain gauges along a single radial line, the essential symmetry of the shell must be disturbed to some extent. However, since load-deflection relationships were consistent with those for shells without strain gauges, slight nonsymmetric behaviour, if present, may be assumed to be negligible.

IV.4 Comparison with Previous Experimental Work

A considerable volume of literature has been published on the pressure loaded clamped shell but, to

the author's knowledge, no comparable work has been carried out on freely supported shells. In the case of clamped shells, experimental investigations have been directed at the determination of buckling pressures only and no attempts appear to have been made to establish equilibrium paths. There are no recorded instances where the distribution of stresses in shells during buckling have been examined.

In the field of point loaded shells, the most detailed investigation was reported by EVAN-IWANOWSKI, CHENG and LOO[9] in 1962. These authors tested a very wide range of shells most of which were freely supported though some were clamped. Their specimens were formed in a variety of materials including copper, aluminium, steel and rigid polyethelene sheet. The metallic specimens were formed by the hydroform process with spherical radii of curvature varying from 5 in. to 11.2 in. and base radii from 0.697 in. to 3.812 in.

In their paper, no information was presented relating to possible initial stress. They did not indicate how the spherical radius of curvature of their specimens was measured and it would appear that they accepted nominal values as a basis for calculating

their shell parameters. They did not present information from which initial imperfection might be assessed.

They noticed that certain shells exhibited discontinuous load-deflection behaviour. Though this phenomenon would appear to be consistent with a change in the deflection mode, the authors did not comment on this aspect but claimed that, in most cases, rotational symmetry was preserved.

Nearly half of the freely supported shells which they tested may be classed as non-shallow in that h/a was greater than 1/8. Of the non-shallow shells, more than half deformed nonsymmetrically. They claimed symmetrical behaviour for all but two of the shallow shells.

Their results showed a significant scatter which might be attributed to their experimental technique and the difficulty in determining the geometry of their specimens which were very small in some cases (1.394 in base diameter). It would also appear that some of their calculated values of their shell parameters were inconsistent with the published dimensions and, on analysis, gave an imaginary value for Poisson's ratio.

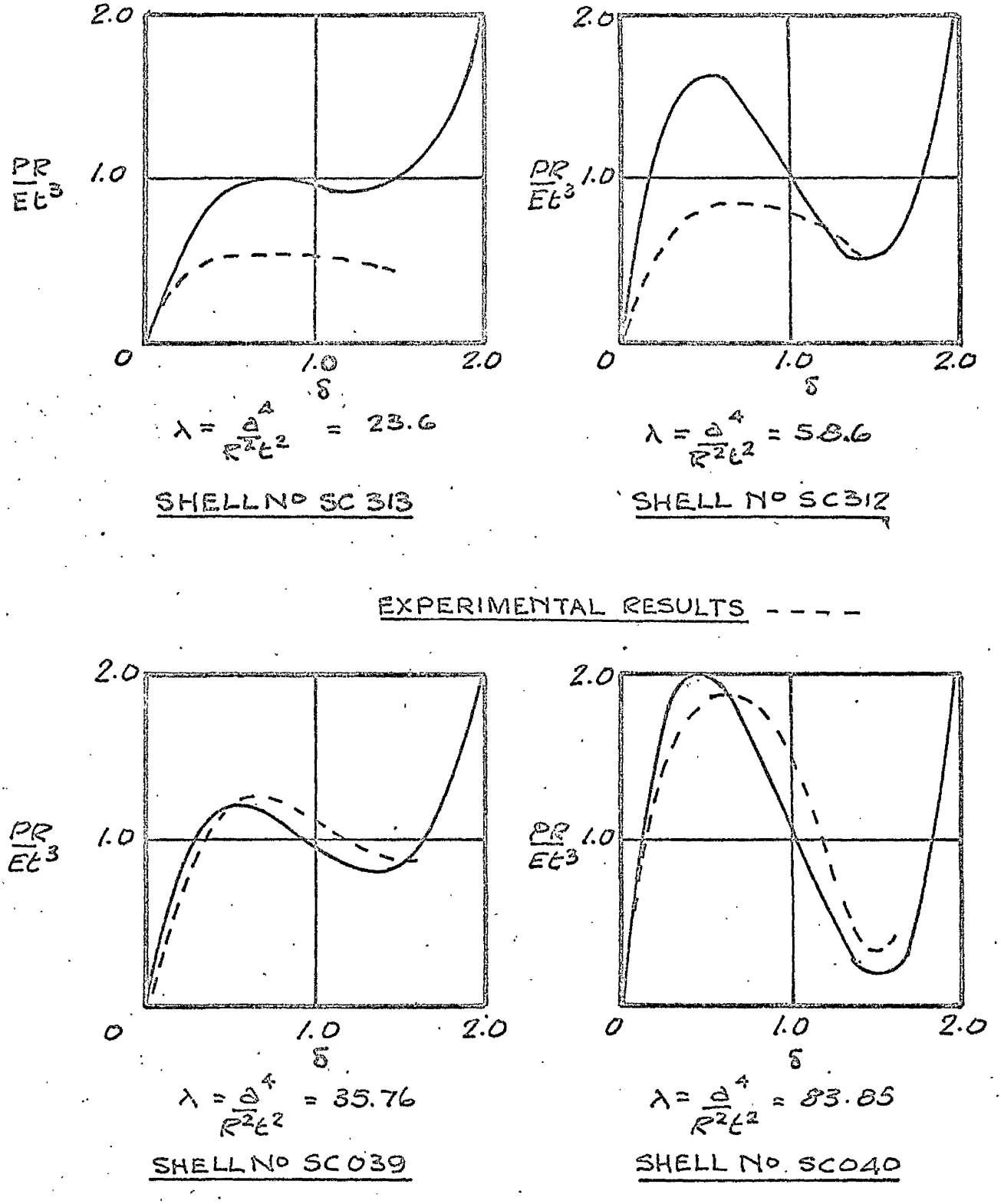

FIG. IV.1 Experimental equilibrium paths of EVAN-IWANOWSKI et al. (9) compared with the theory of BIEZENO (6)

The lack of agreement with theoretical work became more serious in the range of shells exhibiting the discontinuous behaviour and for the shells for which the deformation was recognisably nonsymmetric.

It is significant that the shells which they found to give discontinuous equilibrium paths, had shell parameters which were greater than or equal to the limit found by the present author for symmetrical behaviour.

FIG. IV.1 shows experimental data obtained from the graphs presented by EVAN-IWANOWSKI et al. compared with the theory presented in this thesis. The comparison is intended to show only approximate theoretical behaviour assuming a value of 0.33 for Poisson's ratio, and is restricted to values of less than 80. Within this range, they obtained fair agreement though for some shells, the correlation with theory is poor. At higher values of λ , the agreement with the present work deteriorates and it would appear that $\lambda = 80$ may well represent the probable limit of symmetrical behaviour.

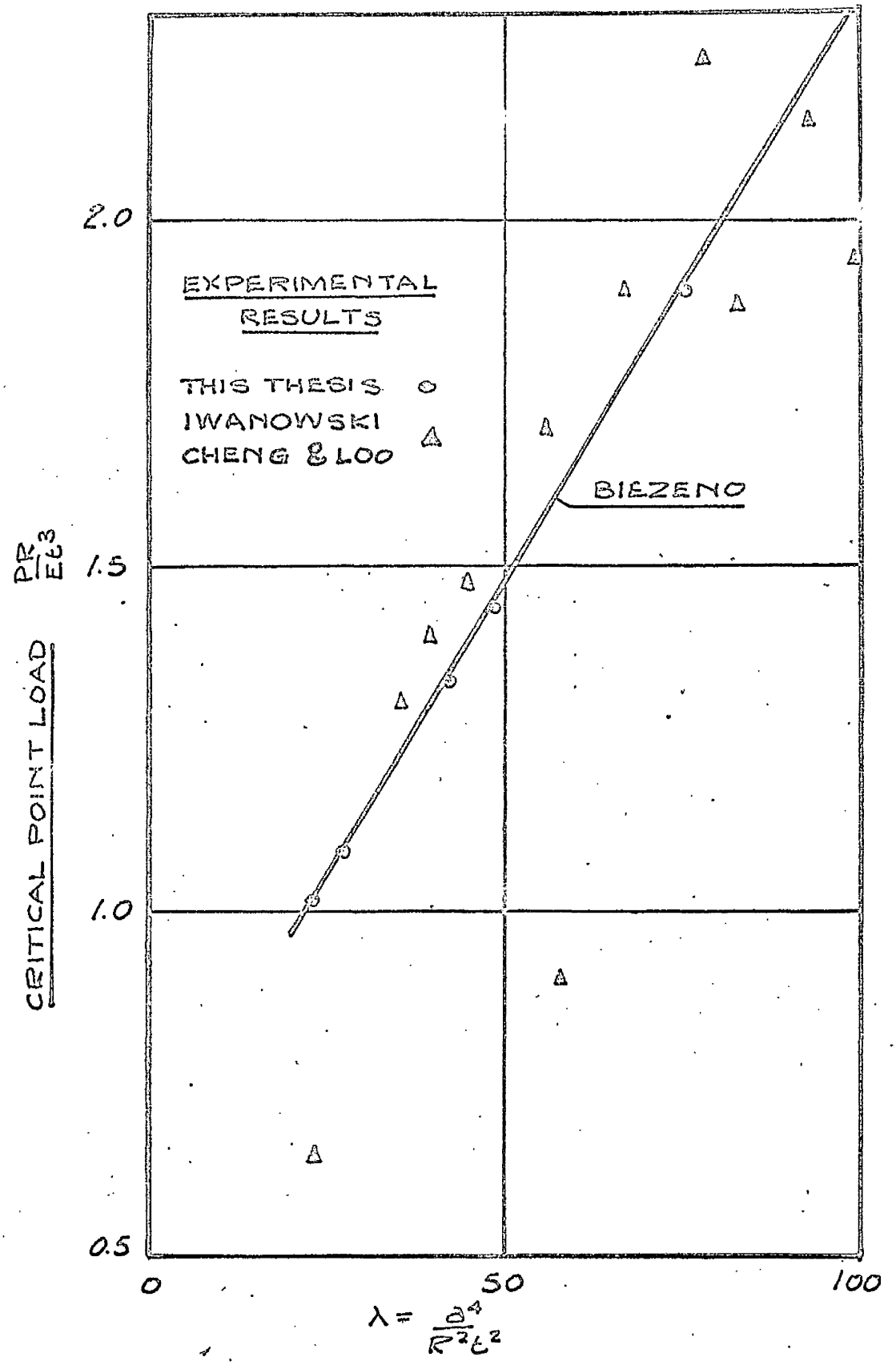

FIG. IV.2 Experimental critical loads of EVAN-IWANOWSKI et al. (9) compared with the theory of BIEZENO (6)

CHAPTER V

SUMMARY AND CONCLUSIONS

V.1 The Nonlinear Behaviour of Shallow Shells

From a survey of literature on the shell buckling phenomenon, it becomes clear that previous experimental data was neither consistent in itself, nor did it offer more than a partial substantiation of relevant theoretical treatments. In this thesis, it has been shown that a major cause of the disparity between theoretical behaviour and previous experimental data lies in the failure of researchers to recognise errors arising from fundamental shortcomings in experimental techniques.

While some previous researchers have appreciated the need to form specimens which conform closely to the conditions implied in relevant theoretical treatments, none have considered fully the true implications of displacement dependent support conditions; and thus none have appreciated that in attempting to achieve these conditions experimentally, they have introduced a major source of error.

In the present work, the effect of degrees of boundary restraint has been clearly demonstrated. From the measure of agreement between several analyses

of the pressure loaded clamped shell, it seems that the academic problem of collapse of these shells is now fully understood, though highly sophisticated treatments of the nonsymmetric problem are largely unsupported by valid experimental data.

In the present investigation, simple force dependent conditions have been adopted. The concepts of shell buckling as incorporated in the theoretical analysis, have been fully substantiated by experimental data which is both consistent in itself and repeatable.

In the experimental investigation, good agreement with theoretical work has been shown to depend on the success with which the shell specimens conform to the assumptions embodied in the theory. In this respect, the method developed to prepare specimens in the present work offered considerable advantages over those adopted in previous work. The method combined the ability to produce shells of accurate and consistent geometry and at the same time maintain the requirement of a stress free character. In addition, the process was relatively simple in concept and has been shown to produce shells of consistent performance. The success of the subsequent experimental work depended to a large measure on these factors.

The development of the controlled deflection technique allowed accurate determination of the equilibrium path and at the same time permitted the measurement of surface strain. Thus, it was possible to examine both the equilibrium path and distribution of deformation experimentally.

In the case of the point load, local plasticity near the load point was reflected in the measurement of surface strains though the behaviour of the shells as load carrying structures has not been influenced. The presence of a hole at the apex of the pressure loaded shells produced a stress concentration which had a slight effect on the strain distribution but, again, the behaviour of the shells was not seriously affected. In the case of both point and pressure loaded shells, it would appear from the results of the experimental work that the onset of nonsymmetric behaviour occurs in the neighbourhood of $\lambda = 80$.

V.2 Shallow Shells in Engineering Practice

It is clear from the present work and that of previous authors, that the theoretical analysis of the buckling problem is only of real value when the basic

assumptions of the analysis are fulfilled in practical applications. The problem is such that even a limited departure from these assumptions may well produce effects which cannot be accurately assessed in the light of present knowledge. The behaviour of shallow shells can only be adequately predicted for a somewhat limited range of problems.

The design of practical shells is usually dependent on factors other than considerations of shell stability. The problem is, therefore, usually one of checking existing designs for possible buckling. For this purpose, the types of analyses at present available are restricted to rotationally symmetric cases. The author feels that in view of the critical influence of such factors as initial stress, imperfection and uncertainty of support restraint, it would be unwise to assume that critical loads deduced from analyses which predict snapping can be relied upon to justify increased carrying capacity. It would similarly be unwise to assume that any useful measure of restraint at the support may be relied upon in practice, though a design based on an assumed free support would undoubtedly be conservative in the absence of other effects. It may, however, be

acceptable to permit large nonlinear deflections provided that these are recognised as such and that buckling does not occur. For this, the shell parameter $\lambda = a^4/R^2T^2$ should be limited to about 17 for both point and pressure load conditions.

In most engineering applications, the behaviour of a shallow cap would probably approximate to that of a freely supported shell even when some measure of restraint is provided. The problem of more extensive shells would most probably be approached by introducing stiffeners arranged in such a manner as to divide the shell into a number of shallow caps of limited shell parameter. In such a structure, the conditions of continuity of the shell over the stiffeners would probably produce some degree of restraint at the cap boundary. Thus the assumption of a free support would be conservative, though this must be balanced against the effect of initial stress and random imperfections.

CHAPTER VI

BIBLIOGRAPHY AND AUTHOR INDEX

VI.1 BIBLIOGRAPHY

1 ZOELLY, R. On a Buckling Problem of a Spherical Shell. Thesis, Zurich University, 1915.

2 SCHWERIN, E. On the Stability of a Thin-walled Hollow Sphere under Uniform External Pressure. Z. angew. Math. Mech. 1922,2,81.

3 NEUT, A van der. The Elastic Stability of a Thin Spherical Shell. Thesis, Delft University, 1932.

4 KARMAN, T.V. and TSIEN, H.S. The Buckling of Spherical Shells by External Pressure. J. aero. Sci. 1939,7,43.

5 FEODOS'EV, V.I. On a Method of Solution of the Nonlinear Problems of Stability of Deformable Systems. PMM 1963,27 No.2. J. Appl. Math. Mech.

6 BIEZENO, C.B. Uber die Bestimmung der Durchschlagkraft einer schwachgekrummten kriesformigen Platte. Z. angew. Math. Mech. 1935,15,10.

7 CHIEN, Wei-Zong and HU, Hai-Chang. On the Snapping of This Spherical Cap. 9th International Congress of Appl. Mechs. 1956, 6, 309-337.

8 ASHWELL, D.G. On the Large Deflection of a Spherical Shell with an Inward Point Load. Proc. of the Symp. on the Theory of Thin Plates, Delft, 1959.

9 EVAN-IWANOWSKI, R.M., CHENG, H.S. and LOO, T.C. Experimental Investigations of Deformations and Stability of Spherical Shells Subjected to Concentrated Load at the Apex. Proceedings of the 4th U.S. National Congress of Applied Mechanics, 1962, 1, 563-575.

10 EVAN-IWANOWSKI, R.M. Deformations and Stability of Spherical Shells Subjected to the Action of Asymmetrical Loadings - Experimental Study. Collected Papers on Instability of Shell Structures. N.A.S.A. TN D-1510, 1962.

11 KLOPPEL, K. and JUNGBLUTH, O. A Contribution to the Durchschlag Problem of Thin-Walled Spherical Shells. Stahlbau 1953,22,121.

12 KAPLAN, A. and FUNG, Y.C. A Nonlinear Theory of Bending and Buckling of Thin Elastic Shallow Spherical Shells. N.A.C.A. TN 3212, 1954.

13 REISSNER, E. On Axisymmetric Deformations of Thin Shells of Revolution. Proceedings of Symposia of Applied Mathematics, 1950,3,27.

14 SIMONS, R.M. On the Nonlinear Theory of Thin Spherical Shells. J. Math. Phys. 1956,35,164.

15 ARCHER, R.R. Stability Limits for a Clamped Spherical Shell under Uniform Pressure. Thesis, Massachusetts Institute of Technology, 1956.

ARCHER, R.R. Stability Limits for a Clamped Spherical Shell Segment under Uniform Pressure. Quart. appl. Math. 1958, 15 No.3, 355.

16 REISS, E.L., GREENBERG, H.J. and KELLER, H.B. Nonlinear Deflexions of Shallow Spherical Shells. J. aero. Sci. 1957,24,533.

17 REISS, E.L. Axially Symmetric Buckling of Shallow Spherical Shells under External Pressure. J. appl. Mech. 1958,25, No. 4, 556.

18 WEINITSCHKE, H.J. On the Nonlinear Theory of Shallow Spherical Shells. J. Soc. industr. appl. Math. 1958,6, No.3,209.

19 WILLICH, G.P.R. Von The Elastic Stability of Thin Spherical Shells. Thesis, Massachusetts Institute of Technology, Department of Civil and Sanitary Engineering, 1957.

WILLICH, G.P.R. Von The Elastic Stability of Thin Spherical Shells. J. eng. Mech. Divis. Amer. Soc. Civil Engrs. 1959,85, No. EMI,51.

20 CHEN, Wen Liang. Effect of Geometrical Imperfections on the Elastic Buckling of Thin Shallow Spherical Shells. Thesis, Massachusetts Institute of Technology, Department of Civil and Sanitary Engineering, 1959.

21 KELLER, H.B. and REISS, E.L. Spherical Cap Snapping. J. aero Sci. 1959,26, No. 10,643.

22 BUDIANSKY, B. Buckling of Clamped Shallow Spherical Shells. Office of Naval Research Tech. Rep. No. 5, 1959.

BUDIANSKY, B. Buckling of Clamped Shallow Spherical Shells. Proceedings of IUTAM Symposium on the Theory of Thin Elastic Shells, Delft, 1959, North Holland Publishing Company, Amsterdam, 1960, pp.64-85.

23 MARGUERRE, K. On the Theory of Large Deformations of Curved Plates. Proceedings of the 5th International Congress of Applied Mechanics. 1938, p93.

24 HOMEWOOD, R.H., BRINE, A.C. and JOHNSON, A.E. Buckling Instability of Monocoque Shells. Society for Experimental Stress Analysis, 1959.

25 GRIGOLYUK, E.L. On the Unsymmetrical Snapping of Shells of Revolution. Proceedings of IUTAM Symposium on the Theory of Thin Elastic Shells, Delft, 1959, North Holland Publishing Company, Amsterdam, 1960, pp.112-121.

26 THURSTON, G.A. A Numerical Solution of the Nonlinear Equations for Axisymmetric Bending of Shallow Spherical Shells. J. appl. Mech. 1961,28,557-562.

27 BELLINFANTE, R.J. Buckling of Spherical Caps under Uniform External Pressure. Douglas Company Report No. SM-38938, 1962.

28 WEINITSCHKE, H.J. Asymmetric Buckling of Clamped Spherical Shells. Collected Papers on Instability of Shell Structures. N.A.S.A. TN D-1510, 1962.

29 PARMERTER, R.R. and FUNG, Y.C. On the Influence of Nonsymmetrical Modes on the Buckling of Shallow Spherical Shells under Uniform Pressure. Collected Papers on Instability of Shell Structures. N.A.S.A. TN D-1510, 1962.

30 KELLER, H.B. and REISS, E.L. Some Recent Results on the Buckling Mechanism of Spherical Caps. Collected Papers on Instability of Shell Structures. N.A.S.A. TN D-1510, 1962.

31 THURSTON, G.A. Comparison of Experimental and Theoretical Buckling Pressures of Spherical Caps. Collected Papers on Instability of Shell Structures. N.A.S.A. TN D-1510, 1962.

32 KARMAN, T. Von and KERR, A.D. Instability of Spherical Shells Subjected to External Pressure. Collected Papers on Instability of Shell Structures. N.A.S.A. TN D-1510, 1962.

33 GJELSVIK, A. and BODNER, S.R. The Nonsymmetrical Snap Buckling of Clamped Spherical Caps. Technical Report No. 30, Engineering Division, Brown University, 1962.

GJELSVIK, A. and BODNER, S.R. Nonsymmetrical Snap Buckling of Clamped Spherical Caps. J. eng. Divis. Amer. Soc. civil Engrs. 1962,88, EM5.

34 KRENZKE, M.A. and KIERNAN, T.J. Elastic Stability of Near-Perfect Shallow Spherical Shells. AIAA Journal, 1963,1, No. 12, 2855-2857.

35 PARMERTER, R.R. The Buckling of Clamped Spherical Shells under Uniform Pressure. AFOSR Report 5362, 1963.

36 HUANG, N.C. Unsymmetrical Buckling of Shallow Spherical Shells. AIAA Journal, 1963,1, No. 4, pp.945-946. Also Harvard University Technical Report No. 15, 1963.

37 THURSTON, G.A. Asymmetrical Buckling of Spherical Caps under Uniform Pressure. AIAA Journal, 1964.

38 MUSHTARI, H.M. On the Theory of Stability of a Spherical Shell Subjected to External Pressure. Appl. Math. Mech., Leningr. 1955, 19, No. 2, 251.

39 MUSHTARI, H.M. and GALIMOV, K.Z. Nonlinear Theory of Thin Elastic Shells. Published for N.A.S.A. by The Israel Program for Scientific Translations. 1961.

40 WARNER, F.J. Solution of Jury Problems with many Degree of Freedom. D.S.I.R., N.P.L., 1959.

VI.2 AUTHOR INDEX

CHAPTER VII

APPENDICES

VII.1 Solution for the Point Loaded Shell

The governing differential equations of a shallow shell subject to a point load at the apex are given by II.1.13 and II.1.14. These are,

$$r^2\frac{d^2v}{dr^2} + r\frac{dv}{dr} - v + r^2\left(\frac{r}{R}+\psi\right)\frac{d\psi}{dr} + (2-\nu)\frac{r^2}{R}\psi + \frac{1-\nu}{2}r\psi^2 = 0 \qquad \text{VII.1.1}$$

$$r^2\frac{d^2\psi}{dr^2} + r\frac{d\psi}{dr} - \psi = \frac{Pr}{2\pi D} + \frac{r^2}{D}N_r\left(\frac{r}{R}+\psi\right) \qquad \text{VII.1.2}$$

where

$$N_r = B\left[\frac{dv}{dr} + \nu\frac{v}{r} + \left(\frac{r}{R}+\frac{\psi}{2}\right)\psi\right] \qquad \text{VII.1.3}$$

In order to obtain a suitable approximate solution for the differential equations VII.1.1 and VII.1.2, a comparable solution for ψ is established for the inextensional bending of a freely supported flat plate subject to a concentrated force P at the centre.

With $R = \infty$ and $N_r = 0$, equation VII.1.2 becomes,

$$r^2\frac{d^2\psi}{dr^2} + r\frac{d\psi}{dr} - \psi = \frac{Pr}{2\pi D} \qquad \text{VII.1.4}$$

for which the solution is

$$\psi = A_1\frac{r}{R} + A_2\frac{r}{R}\log\frac{a}{r} \qquad \text{VII.1.5}$$

The solution for ψ for the shallow spherical shell can be represented by the sum of an unknown multiple of the expression given by VII.1.5 with the addition of a linear term in r . Thus a suitable approximate solution is

$$\psi = C_1 \frac{r}{R} + C_2 \frac{r}{R} \log \frac{a}{r} \qquad \text{VII.1.6}$$

and $$\frac{d\psi}{dr} = \frac{1}{R}(C_1 - C_2) + \frac{C_2}{R} \log \frac{a}{r}$$

Equation VII.1.1 becomes

$$r^2 \frac{d^2 v}{dr^2} + r\frac{dv}{dr} - v = \left[(1+C_1)C_2 - C_1(1+\frac{C_1}{2})(3-\nu)\right]\frac{r^3}{R^2}$$

$$+ \left[C_2^2 - (1+C_1)C_2(3-\nu)\right]\frac{r^3}{R^2}\log\frac{a}{r} - C_2^2\,\frac{3-\nu}{2}\,\frac{r^3}{R^2}\log^2\frac{a}{r}$$

which has the solution

$$v = Ar + \frac{B}{r} - \left[(1+C_1)C_2\left(\frac{5-3\nu}{4}\right) + C_1(1+\frac{C_1}{2})(3-\nu) + C_2^2\left(\frac{9-7\nu}{16}\right)\right]\frac{r^3}{8R^2}$$

$$- \left[C_2^2\left(\frac{5-3\nu}{4}\right) + (1+C_1)C_2(3-\nu)\right]\frac{r^3}{8R^2}\log\frac{a}{r} - C_2^2\left(\frac{3-\nu}{2}\right)\log^2\frac{a}{r} \qquad \text{VII.1.7}$$

where the arbitrary constants A and B are determined for the conditions:

At $r = 0$, v is finite and hence $B = 0$

At $r = a$, $N_r = 0$

i.e. $$\left[\frac{dv}{dr} + \nu\frac{v}{r} + \frac{r}{R}\psi + \frac{\psi^2}{2}\right]_{r=a} = 0$$

from which the constant A is determined.

$$(1+\nu)A = \frac{1-\nu^2}{8}\left[\left\{\frac{3}{4}(1+C_1)C_2 + C_1\left(1+\frac{C_1}{2}\right) + \frac{7}{16}C_2^2\right\}\frac{r^2}{R^2}\right.$$

$$\left. + \left\{\frac{3}{4}C_2^2 + (1+C_1)C_2\right\}\frac{r^2}{R^2}\log\frac{a}{r} + \frac{C_2^2}{2}\frac{r^2}{R^2}\log^2\frac{a}{r}\right] \qquad \text{VII.1.8}$$

Substitution of VII.1.7 and VII.1.8 in VII.1.3 yields

$$N_r = \frac{B(1-\nu^2)}{8R^2}\left[\left\{\frac{3}{4}(1+C_1)C_2 + C_1\left(1+\frac{C_1}{2}\right) + \frac{7}{16}C_2^2\right\}(r^2-a^2)\right.$$

$$\left. + \left\{\frac{3}{4}C_2^2 + (1+C_1)C_2\right\}r^2\log\frac{a}{r} + \frac{C_2^2}{2}r^2\log^2\frac{a}{r}\right] \qquad \text{VII.1.9}$$

Substitution of VII.1.9 with VII.1.6 into VII.1.2 yields, after some simplification,

$$r^2\frac{d^2\psi}{dr^2} + r\frac{d\psi}{dr} - \psi = \frac{Pr}{2\pi D} - \frac{(1-\nu^2)}{8R^2}\frac{B}{D}r^3\left[\alpha_1(r^2-a^2)\right.$$

$$\left. + \alpha_2 a^2\log\frac{a}{r} + \alpha_3 r^2\log\frac{a}{r} + \alpha_4 r^2\log^2\frac{a}{r} + \alpha_5 r^3\log^3\frac{a}{r}\right] \qquad \text{VII.1.10}$$

in which

$$\alpha_1 = C_1\left(1+\frac{C_1}{2}\right)(1+C_1) + \frac{3}{4}(1+C_1)^2 C_2 + \frac{7}{16}(1+C_1)C_2^2 = \varepsilon_1 + \frac{3}{4}\varepsilon_3 + \frac{7}{16}\varepsilon_4$$

$$\alpha_2 = -C_1\left(1+\frac{C_1}{2}\right)C_2 - \frac{3}{4}(1+C_1)C_2^2 - \frac{7}{16}C_2^3 = -\varepsilon_2 - \frac{3}{4}\varepsilon_4 - \frac{7}{16}\varepsilon_5$$

$$\alpha_3 = C_1\left(1+\frac{C_1}{2}\right)C_2 + (1+C_1)^2 C_2 + \frac{3}{2}(1+C_1)C_2^2 + \frac{7}{16}C_2^3 = \varepsilon_2 + \varepsilon_3 + \frac{3}{2}\varepsilon_4 + \frac{7}{16}\varepsilon_5$$

$$\alpha_4 = \frac{3}{2}(1+C_1)C_2^2 + \frac{3}{4}C_2^3 = \frac{3}{2}\varepsilon_4 + \frac{3}{4}\varepsilon_5$$

VII.1.11a-e

$$\alpha_5 = \frac{C_2^3}{2} = \frac{\varepsilon_5}{2}$$

where

$$\varepsilon_1 = C_1\left(1+\frac{C_1}{2}\right)(1+C_1)$$

$$\varepsilon_2 = C_1 C_2\left(1+\frac{C_1}{2}\right)$$

$$\varepsilon_3 = (1+C_1)^2 C_2$$

$$\varepsilon_4 = (1+C_1)C_2^2$$

$$\varepsilon_5 = C_2^3$$

VII.1.12

The solution of equation VII.1.10 takes the form

$$\Psi = Ar + \frac{B}{r} + \varkappa_1 a^2 r^3 + \varkappa_2 r^5 + \varkappa_3 r \log\frac{a}{r} + \varkappa_4 a^2 r^3 \log\frac{a}{r}$$

$$+ \varkappa_5 r^5 \log\frac{a}{r} + \varkappa_6 r^5 \log^2\frac{a}{r} + \varkappa_7 r^5 \log^3\frac{a}{r} \qquad \text{VII.1.13}$$

with the further abreviations

$$\varkappa_1 = \frac{\gamma}{8}\left(\alpha_1 - \frac{3}{4}\alpha_2\right) = \frac{\gamma}{8}\left(\varepsilon_1 + \frac{3}{4}\varepsilon_2 + \frac{3}{4}\varepsilon_3 + \varepsilon_4 + \frac{21}{64}\varepsilon_5\right)$$

$$\varkappa_2 = -\frac{\gamma}{24}\left(\alpha_1 + \frac{5}{12}\alpha_3 + \frac{19}{72}\alpha_4 + \frac{65}{288}\alpha_5\right) = -\frac{\gamma}{24}\left(\varepsilon_1 + \frac{5}{12}\varepsilon_2 + \frac{7}{6}\varepsilon_3 + \frac{35}{24}\varepsilon_4 + \frac{71}{144}\varepsilon_5\right)$$

$$\varkappa_3 = -\frac{P}{4\pi D}$$

$$\varkappa_4 = -\frac{\gamma}{8}\alpha_2 = \frac{\gamma}{8}\left(\varepsilon_2 + \frac{3}{4}\varepsilon_4 + \frac{7}{16}\varepsilon_5\right)$$

$$\varkappa_5 = -\frac{\gamma}{24}\left(\alpha_3 + \frac{5}{6}\alpha_4 + \frac{19}{24}\alpha_5\right) = -\frac{\gamma}{24}\left(\varepsilon_2 + \varepsilon_3 + \frac{11}{4}\varepsilon_4 + \frac{35}{24}\varepsilon_5\right)$$

$$\varkappa_6 = -\frac{\gamma}{24}\left(\alpha_4 + \frac{5}{4}\alpha_5\right) = -\frac{\gamma}{24}\left(\frac{3}{2}\varepsilon_4 + \frac{11}{8}\varepsilon_5\right)$$

$$\varkappa_7 = -\frac{\gamma}{24}\alpha_5 = -\frac{\gamma}{48}\varepsilon_5 \qquad \text{VII.1.14a-g}$$

where

$$\gamma = \frac{(1-\nu^2)}{8R^2}\,\frac{B}{D} = \frac{3(1-\nu^2)}{2t^2R^2}$$

In equation VII.1.13, A and B are arbitrary constants which are determined from the condition of symmetry at the origin and from the boundary condition on M_r .

At $r = 0$, $\Psi = 0$ hence $B = 0$

At $r = a$, $M_r = D\left[\frac{d\Psi}{dr} + \nu\frac{\Psi}{r}\right]_{r=a} = 0$

so that

$$A = -\frac{1}{1+\nu}\left[(3+\nu)\kappa_1 + (5+\nu)\kappa_2 - \kappa_3 - \kappa_4 - \kappa_5\right] \qquad \text{VII.1.15}$$

and equation VII.1.13 now becomes,

$$\Psi = \left(\frac{1}{1+\nu} - \log\frac{r}{a}\right)\kappa_3 r - \frac{a^4}{1+\nu}\left[(3+\nu)\kappa_1 + (5+\nu)\kappa_2 - \kappa_4 - \kappa_5\right]$$

$$+ a^2\kappa_1 r^3 + \kappa_2 r^5 - a^2\kappa_4 r^3 \log\frac{r}{a}$$

$$- r^5\kappa_5 \log\frac{r}{a} + r^5\kappa_6 \log^2\frac{r}{a} - r^5\kappa_7 \log^3\frac{r}{a} \qquad \text{VII.1.16}$$

Integration of this expression for Ψ gives the deflection in the form,

$$\delta = \frac{w}{h} = \frac{-PR}{4\pi D}\left[\frac{1}{1+\nu} - \log\frac{r}{a} + \frac{1}{2}\right]\left(\frac{r}{a}\right)^2 + 3\left(\frac{1-\nu^2}{2}\right)\lambda\left[-\left\{\left(\frac{3+\nu}{1+\nu}\right)\kappa_1\right.\right.$$

$$\left.\left. + \left(\frac{5+\nu}{1+\nu}\right)\kappa_2 - \frac{\kappa_4}{1+\nu} - \frac{\kappa_5}{1+\nu}\right\}\left(\frac{r}{a}\right)^2 + \frac{\kappa_1}{2}\left(\frac{r}{a}\right)^4 + \frac{\kappa_2}{3}\left(\frac{r}{a}\right)^6\right.$$

$$- \frac{\kappa_4}{2}\left(\frac{r}{a}\right)^4\left(\log\frac{r}{a} - \frac{1}{4}\right) - \frac{\kappa_5}{3}\left(\frac{r}{a}\right)^6\left(\log\frac{r}{a} - \frac{1}{6}\right)$$

$$+ \frac{\kappa_6}{3}\left(\frac{r}{a}\right)^6\left(\log^2\frac{r}{a} - \frac{1}{3}\log\frac{r}{a} + \frac{1}{18}\right) \qquad \text{VII.1.17}$$

$$\left. - \frac{\kappa_7}{3}\left(\frac{r}{a}\right)^6\left(\log^3\frac{r}{a} - \frac{1}{2}\log^2\frac{r}{a} + \frac{1}{6}\log\frac{r}{a} - \frac{1}{36}\right)\right]$$

in which

$$\lambda = \frac{a^4}{R^2 t^2} \quad , \qquad h = \frac{a^2}{2R}$$

In order to determine the two constants C_1 and C_2, it may be postulated that when integrated the expression VII.1.6 and VII.1.17 lead to the same value of deflection at the centre. Similarly, these two expressions may lead to the same value of rotation at the boundary.

Integrating VII.1.6 and equating to the result VII.1.17 gives:

$$(3+\nu)\frac{RP}{2\pi D} + \gamma\left[\frac{(17+5\nu)}{36}\varepsilon_1 + \frac{(49+19\nu)}{216}\varepsilon_2 + \frac{(89+29\nu)}{432}\varepsilon_3 + \frac{(105+41\nu)}{576}\varepsilon_4 + \frac{(437+191\nu)}{10368}\varepsilon_5\right] a^4 R = -4(1+\nu)\left(C_1 + \frac{C_2}{2}\right) \qquad \text{VII.1.18}$$

Equating VII.3.6 and VII.3.16 at r = a,

$$\frac{RP}{4\pi D} + \gamma\frac{a^4 R}{8}\left[\frac{2}{3}\varepsilon_1 + \frac{5}{18}\varepsilon_2 + \frac{5}{18}\varepsilon_3 + \frac{2}{9}\varepsilon_4 + \frac{41}{864}\varepsilon_5\right] = -(1+\nu)C_1 \qquad \text{VII.1.19}$$

Taking Poisson's ratio to 0.33, VII.1.18 and VII.1.19 become

$$\frac{PR}{Et^3} = -\lambda\left[0.122186152\,\varepsilon_1 + 0.060350506\,86\,\varepsilon_2 + 0.053815411\,1\,\varepsilon_3 + 0.048534599\,\varepsilon_4 + 0.011374877\,\varepsilon_5\right] - 0.938727\,59\left(C_1 + \frac{C_2}{2}\right) \qquad \text{VII.1.20}$$

$$\frac{PR}{Et^3} = -1.562\,981\,44\,C_1 - \lambda\left[0.130899695\,\varepsilon_1 + 0.0545415397\,\varepsilon_2 + 0.0545415397\,\varepsilon_3 + 0.043633231\,\varepsilon_4 + 0.009317\,5128\,\varepsilon_5\right] \qquad \text{VII.1.21}$$

Equations VII.1.20 and VII.1.21 respectively can be written in the form

$$\frac{PR}{Et^3} = a_1 + b_1\lambda$$

and

$$\frac{PR}{Et^3} = a_2 + b_2\lambda \qquad \text{VII.1.22a,b}$$

in which

$$a_1 = -0.938727\,59\left(C_1 + \frac{C_2}{2}\right)$$

$$a_2 = -1.562\,981\,44\,C_1$$

$$b_1 = -\left[0.122186152\,\varepsilon_1 + 0.060350506\,86\,\varepsilon_2 + 0.053815411\,1\,\varepsilon_3 + 0.048534599\,\varepsilon_4 + 0.011374877\,\varepsilon_5\right]$$

$$b_2 = -\left[0.130899695\,\varepsilon_1 + 0.0545415397\,\varepsilon_2 + 0.0545415397\,\varepsilon_3 + 0.043633231\,\varepsilon_4 + 0.009317\,5128\,\varepsilon_5\right] \qquad \text{VII.1.23a-d}$$

By subtracting equations VII.1.22a,b

$$(a_1 - a_2) + (b_1 - b_2) = 0 \qquad \text{VII.1.24}$$

By integrating VII.1.6, the deflection at the centre is

$$w_o = -\frac{a^2}{2R}\left(c_1 + \frac{c_2}{2}\right)$$

and noting that the rise of the shell at the centre is given by

$$h \doteq \frac{a^2}{2R}$$

$$\delta_o = \frac{w_o}{h} = -\left(c_1 + \frac{c_2}{2}\right) \qquad \text{VII.1.25}$$

From VII.1.23a

$$a_1 = 0.93872759\ \delta$$

and from VII.1.25

$$c_2 = -2(c_1 + \delta) \qquad \text{VII.1.26}$$

It is convenient to solve equation VII.1.24 for specified values of the central deflection δ_o. With VII.1.26, relations VII.1.12 may be written in terms of c_1 and δ. Thus,

$$\varepsilon_1 = c_1(1+c_1)(1+\frac{c_1}{2}) = c_1 + \frac{3}{2}c_1^2 + \frac{c_1^3}{2}$$

$$\varepsilon_2 = c_1c_2(1+\frac{c_1}{2}) = -2c_1\delta - 2c_1^2(1+\frac{\delta}{2}) - c_1^3$$

$$\varepsilon_3 = (1+c_1)^2c_2 = -2\delta - 2c_1(1+2\delta) - 2c_1^2(2+\delta) - 2c_1^3$$

$$\varepsilon_4 = (1+c_1)c_2^2 = 4\delta^2 + 4c_1\delta(2+\delta) + 4c_1^2(1+2\delta) + 4c_1^3$$

$$\varepsilon_5 = c_2^3 = -8c_1^3 - 24c_1^2\delta - 24c_1\delta^2 - 8\delta^3$$

VII.1.27

Equation VII.1.24 may now be expressed as cubic in C_1. Thus,

$$a_0c_1^3 + a_1c_1^2 + a_2c_1 + a_3 = 0 \qquad \text{VII.1.28}$$

in which

$$a_0 = \lambda\left[0.0055669848\right]$$

$$a_1 = \lambda\left[0.0130703145 + 0.0116180578(1+\frac{\delta}{2}) - 0.0014522572(2+\delta) - 0.019605472(1+2\delta) + 0.0493767408\delta\right]$$

$$a_2 = 1.5629814 + \lambda\left[0.0087135543 + 0.0116180578\delta - 0.0014522572(1+2\delta) - 0.019605472\delta(2+\delta) + 0.0493767408\delta^2\right]$$

$$a_3 = 0.093872759\delta + \lambda\left[-0.0014522272\delta - 0.019605472\delta^2 + 0.016458914\delta^3\right] \qquad \text{VII.1.29a-c}$$

For successive values of δ , the coefficients of VII.1.28 can be calculated from VII.1.29. Equation VII.1.28 can be solved numerically using standard procedures such as Cardan's method. In practice, only one real root is found though for values of λ greater than about 300, multiple roots occur. Since practical shells do not behave symmetrically at such high values of the shell parameter, multiple roots are not of real significance.

The solution of equation VII.1.28 yields the value of the constant C_1 . The value of the load can now be computed from either of the equations VII.1.22a,b. Thus, the first of these gives,

$$\frac{PR}{Et^3} = 0.93872759\,\delta - \lambda\left[-0.10763081\,\delta + 0.19413839\,\delta^2 - 0.09099901\,\delta^3\right]$$

$$-\lambda\left[0.01455530 + 0.05231401\,\delta - 0.07885865\,\delta^2\right]C_1$$

$$-\lambda\left[0.04145484 - 0.05270165\,\delta\right]C_1^2 \qquad \text{VII.1.30}$$

$$+\lambda\left[0.00690405\right]C_1^3$$

Determination of Stress Resultants

From VII.1.9,

$$N_r \frac{a^2}{Et^3} = -\frac{\lambda}{8}\left[\left\{\frac{3}{4}(1+c_1)c_2 + c_1\left(1+\frac{c_1}{2}\right) + \frac{7}{16}c_2^2\right\}\left\{\left(\frac{r}{a}\right)^2-1\right\}\right.$$

$$\left.-\left\{\frac{3}{4}c_2^2 + (1+c_1)c_2\right\}\left(\frac{r}{a}\right)^2\log\frac{r}{a} + \frac{1}{2}c_2^2\left(\frac{r}{a}\right)^2\log^2\frac{r}{a}\right] \qquad \text{VII.1.31}$$

From II.1.12b with relations VII.1.7 and VII.1.16

$$N_\theta \frac{a^2}{Et^3} = -\frac{\lambda}{8}\left[\left\{\frac{3}{4}(1+c_1)c_2 + c_1\left(1+\frac{c_1}{2}\right) + \frac{7}{16}c_2^2\right\}\left\{3\left(\frac{r}{a}\right)^2-1\right\}\right.$$

$$\left.-\left\{\frac{3}{4}c_2^2 + (1+c_1)c_2\right\}\left\{3\log\frac{r}{a}+1\right\}\left(\frac{r}{a}\right)^2 + \frac{c_2^2}{2}\left\{3\log^2\frac{r}{a} + 2\log\frac{r}{a}\right\}\left(\frac{r}{a}\right)^2\right] \qquad \text{VII.1.32}$$

From II.1.12c with VII.1.16

$$M_r \frac{R}{Et^3} = \frac{PR}{Et^3}\frac{(1+\nu)}{4\pi}\log\frac{r}{a} + \frac{\lambda}{8}\left[-\kappa_1(3+\nu)\left\{1-\left(\frac{r}{a}\right)^2\right\}\right.$$

$$-\kappa_2(5+\nu)\left\{1-\left(\frac{r}{a}\right)^4\right\} - \kappa_4\left\{\left((3+\nu)\log\frac{r}{a}+1\right)\left(\frac{r}{a}\right)^2-1\right\}$$

$$-\kappa_5\left\{\left((5+\nu)\log\frac{r}{a}+1\right)\left(\frac{r}{a}\right)^4-1\right\} + \kappa_6\left\{(5+\nu)\log^2\frac{r}{a} + 2\log\frac{r}{a}\right\}\left(\frac{r}{a}\right)^4$$

$$\left.-\kappa_7\left\{(5+\nu)\log^3\frac{r}{a} + 3\log^2\frac{r}{a}\right\}\left(\frac{r}{a}\right)^4\right] \qquad \text{VII.1.33}$$

From II.1.12d with VII.1.16

$$M_\theta \frac{R}{Et^3} = \frac{1}{4\pi}\frac{PR}{Et^3}\left[(1+\nu)\log\frac{r}{a} + \nu - 1\right] + \frac{\lambda}{8}\left[\varkappa_1\left\{(1+3\nu)\left(\frac{r}{a}\right)^2 - (3+\nu)\right\}\right.$$

$$+ \varkappa_2\left\{(1+5\nu)\left(\frac{r}{a}\right)^4 - (5+\nu)\right\} - \varkappa_4\left\{\left((1+3\nu)\log\frac{r}{a} + \nu\right)\left(\frac{r}{a}\right)^2 - 1\right\}$$

$$- \varkappa_5\left\{\left((1+5\nu)\log\frac{r}{a} + \nu\right)\left(\frac{r}{a}\right)^4 - 1\right\}$$

$$+ \varkappa_6\left(\frac{r}{a}\right)^4\left\{(1+5\nu)\log^2\frac{r}{a} + 2\nu\log\frac{r}{a}\right\}$$

$$\left. - \varkappa_7\left(\frac{r}{a}\right)^4\left\{(1+5\nu)\log^3\frac{r}{a} + 3\nu\log^2\frac{r}{a}\right\}\right] \qquad \text{VII.1.34}$$

Determination of Surface Strains

The membrane strains are given by equations II.1.11a,b. The surface strains can be obtained by adding the rotation components to the membrane strains. Thus,

$$\varepsilon_r = \frac{u}{r} + \frac{t}{2r}\psi = \frac{1}{r}\left(v + \frac{t}{2}\psi\right) \qquad \text{VII.1.35}$$

$$\varepsilon_\theta = \frac{dv}{dr} + \frac{r}{R}\psi + \frac{\psi^2}{2} + \frac{t}{2}\frac{d\psi}{dr} \qquad \text{VII.1.36}$$

The surface strains can therefore be computed from VII.1.35 and VII.1.36 along with VII.1.7 and VII.1.16

VII.2 Solution by Numerical Integration

To illustrate this approach, the governing equations II.1.13 and II.1.14 may be considered. The basis of this solution is to express these two nonlinear simultaneous second order differential equations as four nonlinear first order differential equations.

Thus, the following quantities may be defined,

Let $$\alpha = \frac{dv}{dr} \quad , \quad \frac{d\alpha}{dr} = \frac{d^2v}{dr^2} \qquad \text{VII.2.1a}$$

$$\beta = \frac{d\psi}{dr} \quad , \quad \frac{d\beta}{dr} = \frac{d^2\psi}{dr^2} \qquad \text{VII.2.1b}$$

Considering the case of the pressure load, the relations VII.2.1a,b may be substituted into equations II.1.13 and II.1.14.

$$r^2\frac{d\alpha}{dr} + r\alpha - v + r^2\left(\frac{r}{R}+\psi\right)\beta + (2-\nu)\frac{r^2}{R}\psi + \frac{(1-\nu)}{2}r\psi^2 = 0 \qquad \text{VII.2.2a}$$

$$r^2\frac{d\beta}{dr} + r\beta - \psi = \frac{pr^3}{2D} + \frac{r^2\beta}{D}\left[\alpha - \nu\frac{v}{r} + \left(\frac{r}{R}+\frac{\psi}{2}\right)\psi\right]\left(\frac{r}{R}+\psi\right) \qquad \text{VII.2.2b}$$

from which

$$\frac{d\alpha}{dr} = \frac{v}{r^2} - \frac{\alpha}{r} - \left(\frac{r}{R} + \Psi\right)\beta - (2-\nu)\frac{\Psi}{R} - \frac{(1-\nu)}{2}\frac{\Psi^2}{r} \qquad \text{VII.2.3a}$$

$$\frac{d\beta}{dr} = \frac{\Psi}{r^2} - \frac{\beta}{r} + \frac{pr}{2D} + \frac{\beta}{D}\left[\alpha + \frac{\nu v}{r} + \left(\frac{r}{R} + \frac{\Psi}{2}\right)\Psi\right]\left(\frac{r}{R} + \Psi\right) \qquad \text{VII.2.3b}$$

$$\frac{dv}{dr} = \alpha \qquad \text{VII.2.3c}$$

$$\frac{d\Psi}{dr} = \beta \qquad \text{VII.2.3d}$$

The problem as formulated by equations VII.2.3a-d was programmed for digital computation using a four stage Runge-Kutta method for integration. The method integrated forward the set of simultaneous equations step by step.

In order to carry out this procedure, it is first necessary to determine the starting values of the equations to be integrated. These are dependent on the boundary conditions. While any consistent set of boundary conditions may be considered, the problem will be illustrated with respect to those for a simply supported shell. These boundary conditions are

$$r = 0, \quad \Psi = 0 \text{ and } v = 0$$
$$r = a, \quad N_r = 0 \text{ and } M_r = 0$$

Thus at the start of the integration at $r = 0$, $\Psi = v = 0$ but α and β are unknown. It is therefore necessary to estimate α and β such that on completing the integration to the remote boundary at $r = a$, N_r and M_r are both zero. In the case of initial trial values of α and β, the condition on N_r and M_r will not be satisfied in general and further trial values of α and β must be assumed. It is important to note that at any one boundary only two of the four possible parameters can be specified. This is known as a 'Jury' problem with two degrees of freedom and special techniques must be developed to set up an iteration procedure to secure the required terminal values of N_r and M_r. The solution of the Jury problem is discussed in general terms in Appendix VII.3.

A computer programme was written to carry out the numerical work for the shell problem in accordance with the procedure described above. The final objective was to obtain the equilibrium path and, in addition, calculate the distribution of deflection, the variation of stress and surface strain along a typical meridian. The programme to carry out this analysis was thus long

with a consequent heavy demand on machine storage. The Ferranti Sirius Computer, which was used in this investigation, had a limited store of 4000 words and was considerably slower than more recent machines. The calculation, therefore, had to be carried out in stages with a consequent loss in efficiency, though the programme was translated into basic machine code in an attempt to speed computation.

The main conclusions of this investigation were that:

(i) numerical integration was an uneconomically slow process,

(ii) convergence of the Jury problem analysis was, in itself, slow, requiring several trial integrations. Convergence deteriorated as the buckling condition was approached as the numerical work became increasingly unstable.

VII.3 Solution of the General Jury Problem

The method outlined below was proposed by WARNER[40] and is an extension of Aitken's method to may variables.

If there are n functions $f(u,v,\ldots,z)$, $g(u,v,\ldots,z)$, ..., $m(u,v,\ldots,z)$ of the same n independent variables, it is necessary to interpolate between n + 1 sets of values of $f,g,\ldots,m$ to find the n values of $u,v,\ldots,z$ required to form the wanted values of the functions. With more than one variable only linear interpolates are possible, as the extension to higher order interpolates become unprofitable and difficult to generalise.

Consider the case of three variables corresponding to three degrees of freedom. The problem is to obtain three parameters u,v,w which have to be estimated at the start of the range so that three functions f,g,h of these parameters are zero at the end of the range.

Now $f = f(u,v,w)$, $g = g(u,v,w)$, $h = h(u,v,w)$ may be inverted to give $u = u(f,g,h)$, $v = v(f,g,h)$, $w = w(f,g,h)$ provided that the Jacobian of the

transformation does not vanish at any of the points in question. This may be assumed for any given set of numerical functions.

Denoting the values of $u, v, w, \frac{\partial u}{\partial f}, \ldots, \frac{\partial w}{\partial h}$ taken when $f = g = h = 0$ by $U, V, W, U_f, \ldots, W_h$, respectively, a Taylor's series truncated after its first order terms may be obtained

$$u = U + fU_f + gU_g + hU_h$$

From four such equations (derived from the approximations u_1, u_2, u_3, u_4)

$$f_1U_f + g_1U_g + h_1U_h + U = u_1$$

$$f_2U_f + g_2U_g + h_2U_h + U = u_2$$

$$f_3U_f + g_3U_g + h_3U_h + U = u_3$$

$$f_4U_f + g_4U_g + h_4U_h + U = u_4$$

U_f, U_g, U_h may be eliminated to give the required interpolate U.

This set of equations may be solved by the Gauss elimination process to give U without back-substitution.

Further sets of equations for V and W differ from the foregoing for U in that u_1 to u_4 are replaced by v_1 to v_4 and w_1 to w_4 respectively. Hence the whole process may be represented in matrix form as

$$\begin{bmatrix} f_1 & g_1 & h_1 & 1 \\ f_2 & g_2 & h_2 & 1 \\ f_3 & g_3 & h_3 & 1 \\ f_4 & g_4 & h_4 & 1 \end{bmatrix} \begin{bmatrix} U_f & V_f & W_f \\ U_g & V_g & W_g \\ U_h & V_h & W_h \\ U & V & W \end{bmatrix} = \begin{bmatrix} u_1 & v_1 & w_1 \\ u_2 & v_2 & w_2 \\ u_3 & v_3 & w_3 \\ u_4 & v_4 & w_4 \end{bmatrix}$$

and the elimination process may be carried out to give the result in the form

$$\begin{bmatrix} FU & FV & FW \end{bmatrix} = \begin{bmatrix} \overline{u} & \overline{v} & \overline{w} \end{bmatrix}$$

whence $U = \overline{u}/F$, $V = \overline{v}/F$, $W = \overline{w}/F$. This process may then be repeated with four sets of values comprising (U, V, W) and the three best approximations from $(u_1, v_1, w_1), \ldots (u_4, v_4, w_4)$.

Formal solution of the matrices gives

$$U = \frac{\begin{vmatrix} u_1 & f_2 & g_3 & h_4 \end{vmatrix}}{\begin{vmatrix} 1 & f_2 & g_3 & h_4 \end{vmatrix}}$$

VII.4 Solution by the Galerkin Method

MUSHTARI[39] obtained the governing differential equations for the pressure loaded shell in the form

$$\rho \frac{d}{d\rho} \frac{1}{\rho} \frac{d}{d\rho}(\rho \Phi) + \frac{\Psi^2}{2} + \rho \frac{a}{R} \Psi = 0 \qquad \text{VII.4.1a}$$

$$\rho \frac{d}{d\rho} \frac{1}{\rho} \frac{d}{d\rho}(\rho \Psi) + \eta \Phi (\Psi + \rho \frac{a}{R}) + p \frac{\rho^2 a^2}{2D} = 0 \qquad \text{VII.4.1b}$$

where $\rho = \frac{r}{a}$, $\eta = 12(1 - \nu^2)(\frac{a}{t})^2$ and Φ is a stress function such that

$$N_r = Et \frac{\Phi}{\rho} \qquad N_\theta = Et \frac{d\Phi}{d\rho} \qquad \text{VII.4.2}$$

The meridional bending moment is given by

$$M_r = \frac{D}{a}\left(\frac{d\Psi}{d\rho} + \nu \frac{\Psi}{\rho}\right) \qquad \text{VII.4.3}$$

It is convenient to consider generalised boundary conditions assuming elastic restraint at the support. Thus the meridional bending moment may be assumed to be proportional to the angle of rotation Ψ at the boundary.

$$M_r = k_1 \Psi_1 \qquad \text{at} \quad \rho = \frac{r}{a} = 1$$

where k_1 is the stiffness of the rotational restraint.

Hence

$$\frac{d\Psi}{d\rho} + m\Psi = 0 \qquad \text{at} \quad \rho = 1 \qquad \text{VII.4.4}$$

where $$m = \nu + \frac{a}{D} K_1 = \nu + \frac{1}{C_1}$$

and $C_1 = \frac{D}{ak_1}$ represents the flexibility of the support.

Similarly, the meridional membrane force action N_r may be assumed to be proportional to the displacement at the boundary thus,

$$N_r = k_2 u \qquad \text{at} \quad \rho = 1 \qquad \text{VII.4.5}$$

where k_2 is the stiffness of the support.
At the boundary, the deflection w = 0 and u, the tangential displacement u is given by

$$u = a\,\varepsilon_\theta \qquad \text{VII.4.6}$$

Combining VII.4.5 and VII.4.6 with the relation

$$\varepsilon_\theta = \frac{1}{Et}\left(N_\theta - \nu N_r\right)$$

the result is

$$\left(\frac{d\Phi}{d\rho}\right)_{\rho=1} + q\,\Phi_{\rho=1} = 0 \qquad \text{VII.4.7}$$

where $q = -\nu - \frac{Et}{k_2 a} = -\nu - C_2$ and $C_2 = \frac{Et}{k_2 a}$

To obtain a solution of the differential equations VII.4.1a,b by the Galerkin approach, an expression for is assumed in the form of a series, thus

$$\Psi = \sum_1^n \omega_n \left(\rho^{2+n} - \nu_n \rho^n \right) \qquad \text{VII.4.8}$$

which satisfies the boundary conditions given by VII.4.4 and VII.4.7 and the conditions implied by symmetry when $\nu_n = \frac{2+n+m}{n+m}$ and ω_n are undetermined constants.

Introducing VII.4.8 into equation VII.4.1a and integrating twice, Φ is obtained. The constants of integration are determined from the condition VII.4.7 and the requirement of boundedness of the solution at the origin.

The expression for Φ and the assumed form for Ψ as given by VII.4.8 are substituted into equation VII.4.1b. The resulting equation is multiplied successively by $\frac{\partial \Psi}{\partial \omega_n}$ and integrated over the range from $\rho = 0$ to $\rho = 1$ to yield n simultaneous algebraic equations in $\omega_1, \omega_2, - - - \omega_n$. These

equations are cubic in form and simultaneous solution yields values of the undetermined constants $\omega_1, \omega_2, - - - - \omega_n$. Hence the final expression for Ψ is obtained. The deflection at any point may be found by integrating the expression for Ψ .

The lengthy algebraic manipulations to obtain the Galerkin integrals is presented in detail in Appendix VII.5.

The advantage of such a Galerkin solution is that the coefficients for the simultaneous cubic equations can be generated merely by specifying the number of terms to be included in the approximating function for Ψ . Once the generalised Galerkin integrals have been evaluated as shown in Appendix VII.5, the numerical computation may be conveniently carried out by computer. A programme was written to do this without difficulty though the computation process was naturally lengthy.

An iterative procedure was adopted to solve the system of cubic algebraic equations. Initially, the iteration process was fairly rapid but, as the deflection increased, the contribution from the higher

order terms increased, leading eventually to an iteration failure in some cases. The problem was further complicated by the occurrence of multiple roots in the solution of the algebraic equations. An extrapolation process was required to discriminate between possible equilibrium states. This latter difficulty became more acute as the number of terms in the approximating function. To avoid some of these difficulties, a new form was assumed for Ψ and the corresponding analysis and evaluation of the associated Galerkin integrals is presented in Appendix VII.6.

It is of interest to note that some time later, FEODOS'EV[5] in a general discussion of the variational approach, noted that simultaneous solution of the associated algebraic equations is not always possible. An analysis of the cause of iteration failure in the present work, showed that a contributory factor was an apparent sensitivity of the solution to slight variations in the coefficient associated with the load term. It would appear that this effect, which is dependent on the type of load, boundary conditions and to some extent the assumed form for ψ , is inherent in systems subject to transverse load action. In the

corresponding analyses of edge loaded plates, for example, the form of the approximating function has relatively little effect on the load term, and so the solution of the edge load problem is appreciably more stable in this respect. FEODOS'EV suggested that the difficulties of this type might be overcome by considering dynamic effects with linear damping. This has the effect of changing the variable and in his analysis, the damping coefficient, which was an essential feature of his method, was chosen arbitrarily and had the effect of stabilising the solution.

VII.5 Galerkin Solution of Shallow Shell Equations - (a)

The governing differential equations may be considered in the form expressed by II.1.9 and II.1.10. These are

$$\rho \frac{d}{d\rho} \frac{1}{\rho} \frac{d}{d\rho}(\rho\Phi) = \frac{\Psi^2}{2} + \rho\gamma\Psi \qquad \text{VII.5.1}$$

$$\rho \frac{d}{d\rho} \frac{1}{\rho} \frac{d}{d\rho}(\rho\Psi) = \eta\Phi(\Psi + \rho\gamma) + p\frac{\rho^2 a^3}{2D} + \frac{Pa}{2\pi D} \qquad \text{VII.5.2}$$

where

$$\rho = \frac{r}{a} \quad , \quad \eta = 12(1-\nu^2)\frac{a^2}{t^2} \quad , \quad \gamma = \frac{a}{R}$$

p = uniformly distributed pressure load

P = point load at apex of shell

A solution is assumed in the form

$$\Psi = \sum_1^n \omega_n (\rho^{2+n} - \nu_n \rho^n) \qquad \text{VII.5.3}$$

which satisfies the boundary conditions when

$$\nu_n = \frac{2 + n + m}{n + m}$$

Substitution of VII.5.3 into VII.5.1 gives

$$\rho \frac{d}{d\rho} \frac{1}{\rho} \frac{d}{d\rho}(\rho\Phi) = \frac{\Psi^2}{2} - \rho\gamma\Psi = \frac{1}{2}\sum_{s=1}^{n}\sum_{r=1}^{n}\omega_r\omega_s\left[\rho^{r+s+4} - (\nu_r+\nu_s)\rho^{r+s+2} - \nu_r\nu_s\rho^{r+s}\right] - \rho\gamma\sum_{r=1}^{n}\omega_r\left[\rho^{r+2} - \nu_r\rho^{r}\right]$$

$$\frac{1}{\rho}\frac{d}{d\rho}(\rho\Phi) = \frac{1}{2}\sum_{s=1}^{n}\sum_{r=1}^{n}\omega_r\omega_s\left[\frac{\rho^{r+s+4}}{r+s+4} - \frac{(\nu_r+\nu_s)\rho^{r+s+2}}{r+s+2} + \frac{\nu_r\nu_s\rho^{r+s}}{r+s}\right] - \gamma\sum_{r=1}^{n}\omega_r\left[\frac{\rho^{r+3}}{r+3} - \frac{\nu_r\rho^{r+1}}{r+1}\right] + A$$

$$\rho\Phi = \frac{1}{2}\sum_{s=1}^{n}\sum_{r=1}^{n}\omega_r\omega_s\left[\frac{\rho^{r+s+6}}{(r+s+4)(r+s+6)} - \frac{(\nu_r+\nu_s)\rho^{r+s+4}}{(r+s+2)(r+s+4)} + \frac{\nu_r\nu_s\rho^{r+s+2}}{(r+s)(r+s+2)}\right] - \gamma\sum_{r=1}^{n}\omega_r\left[\frac{\rho^{r+s}}{(r+3)(r+5)} - \frac{\nu_r\rho^{r+3}}{(r+1)(r+3)}\right] + \frac{A\rho^2}{2} + B$$

At $\rho=0$, Φ is finite $\therefore B=0$

At $\rho=1$, $\left(\frac{d\Phi}{d\rho}\right)_{\rho=1} + q(\Phi)_{\rho=1} = 0$ where $q = -\nu - c_2$

$$\frac{1}{2}\sum_{s=1}^{n}\sum_{r=1}^{n}\omega_r\omega_s\left[\frac{r+s+5}{(r+s+4)(r+s+6)} - \frac{(r+s+3)(\nu_r+\nu_s)}{(r+s+2)(r+s+4)} + \frac{\nu_r\nu_s(r+s+1)}{(r+s)(r+s+2)}\right] - \gamma\sum_{r=1}^{n}\omega_r\left[\frac{r+4}{(r+3)(r+5)} - \frac{\nu_r(r+2)}{(r+1)(r+3)}\right] + \frac{A}{2}$$

$$+q\cdot\frac{1}{2}\sum_{s=1}^{n}\sum_{r=1}^{n}\omega_r\omega_s\left[\frac{1}{(r+s+4)(r+s+6)} - \frac{\nu_r+\nu_s}{(r+s+2)(r+s+4)} + \frac{\nu_r\nu_s}{(r+s)(r+s+2)}\right]$$

$$-q\gamma\sum_{r=1}^{n}\omega_r\left[\frac{1}{(r+3)(r+5)} - \frac{\nu_r}{(r+1)(r+3)}\right] + \frac{A}{2}q = 0$$

$$\therefore A = \frac{-2}{1+q}\left[\frac{1}{2}\sum_{s=1}^{n}\sum_{r=1}^{n}\omega_r\omega_s\left\{\frac{r+s+5}{(r+s+4)(r+s+6)} - \frac{(r+s+3)(\nu_r+\nu_s)}{(r+s+2)(r+s+4)}\right.\right.$$

$$\left. + \frac{\nu_r\nu_s(r+s+1)}{(r+s)(r+s+2)}\right\} - \gamma\sum_{r=1}^{n}\omega_r\left\{\frac{r+4}{(r+3)(r+5)} - \frac{\nu_r(r+2)}{(r+1)(r+3)}\right\}$$

$$+ \frac{q}{2}\sum_{s=1}^{n}\sum_{r=1}^{n}\omega_r\omega_s\left\{\frac{1}{(r+s+4)(r+s+6)} - \frac{\nu_r+\nu_s}{(r+s+2)(r+s+4)}\right.$$

$$\left.\left. + \frac{\nu_r\nu_s}{(r+s)(r+s+2)}\right\} - q\gamma\sum_{r=1}^{n}\omega_r\left\{\frac{1}{(r+3)(r+5)} - \frac{\nu_r}{(r+1)(r+3)}\right\}\right]$$

Hence

$$\Phi = \frac{1}{2}\sum_{s=1}^{n}\sum_{r=1}^{n}\omega_r\omega_s\left[\frac{\rho^{r+s+5}}{(r+s+4)(r+s+6)} - \frac{(\nu_r+\nu_s)\rho^{r+s+3}}{(r+s+2)(r+s+4)} + \frac{\nu_r\nu_s\rho^{r+s+1}}{(r+s)(r+s+2)}\right]$$

$$-\gamma\sum_{r=1}^{n}\omega_r\left[\frac{\rho^{r+4}}{(r+3)(r+5)} - \frac{\nu_r\rho^{r+2}}{(r+1)(r+3)}\right]$$

$$-\frac{\rho}{1+q}\left[\frac{1}{2}\sum_{s=1}^{n}\sum_{r=1}^{n}\omega_r\omega_s\left\{\frac{r+s+5}{(r+s+4)(r+s+6)} - \frac{(r+s+3)(\nu_r+\nu_s)}{(r+s+2)(r+s+4)} + \frac{\nu_r\nu_s(r+s+1)}{(r+s)(r+s+2)}\right\}\right.$$

$$-\gamma\sum_{r=1}^{n}\omega_r\left\{\frac{r+4}{(r+3)(r+5)} - \frac{\nu_r(r+2)}{(r+1)(r+3)}\right\}$$

$$+\frac{q}{2}\sum_{s=1}^{n}\sum_{r=1}^{n}\omega_r\omega_s\left\{\frac{1}{(r+s+4)(r+s+6)} - \frac{\nu_r+\nu_s}{(r+s+2)(r+s+4)} + \frac{\nu_r\nu_s}{(r+s)(r+s+2)}\right\}$$

$$\left.-q\gamma\sum_{r=1}^{n}\omega_r\left\{\frac{1}{(r+3)(r+5)} - \frac{\nu_r}{(r+1)(r+3)}\right\}\right]$$

The expression for Ψ given by VII.5.3 and the expression for Φ given by VII.5.4 are substituted into equation VII.5.2. Thus,

$$\sum_{r=1}^{n}\omega_r\left[(r+1)(r+3)\rho^{r+1}-(r-1)(r+1)\nu_r\rho^{r-1}\right]$$

$$+\eta\left[\frac{1}{2}\sum_{t=1}^{n}\sum_{s=1}^{n}\sum_{r=1}^{n}\omega_r\omega_s\omega_t\left\{\frac{\rho^{r+s+t+7}}{(r+s+4)(r+s+6)}-\frac{(\nu_r+\nu_s)\rho^{r+s+t+5}}{(r+s+2)(r+s+4)}\right.\right.$$

$$+\frac{\nu_r\nu_s\rho^{r+s+t+3}}{(r+s)(r+s+2)}-\frac{\nu_t\rho^{r+s+t+5}}{(r+s+4)(r+s+6)}$$

$$\left.\left.+\frac{(\nu_r+\nu_s)\nu_t\rho^{r+s+t+3}}{(r+s+2)(r+s+4)}-\frac{\nu_r\nu_s\nu_t\rho^{r+s+t+1}}{(r+s)(r+s+2)}\right\}\right.$$

$$-\gamma\sum_{s=1}^{n}\sum_{r=1}^{n}\omega_r\omega_s\left\{\frac{\rho^{r+s+6}}{(r+3)(r+5)}-\frac{\nu_r\rho^{r+s+4}}{(r+1)(r+3)}\right.$$

$$\left.-\frac{\nu_s\rho^{r+s+4}}{(r+3)(r+5)}+\frac{\nu_r\nu_s\rho^{r+s+2}}{(r+1)(r+3)}\right\}$$

$$-\frac{1}{2(1+q)}\sum_{t=1}^{n}\sum_{s=1}^{n}\sum_{r=1}^{n}\omega_r\omega_s\omega_t\left\{\frac{(r+s+5)\rho^{t+3}}{(r+s+4)(r+s+6)}-\frac{(r+s+3)(\nu_r+\nu_s)\rho^{t+3}}{(r+s+2)(r+s+4)}\right.$$

$$+\frac{\nu_r\nu_s(r+s+1)\rho^{t+3}}{(r+s)(r+s+2)}-\frac{(r+s+5)\nu_t\rho^{t+1}}{(r+s+4)(r+s+6)}$$

$$\left.+\frac{(r+s+3)(\nu_r+\nu_s)\nu_t\rho^{t+1}}{(r+s+2)(r+s+4)}-\frac{\nu_r\nu_s\nu_t(r+s+1)\rho^{t+1}}{(r+s)(r+s+2)}\right\}$$

$$+\frac{1}{1+q}\gamma\sum_{s=1}^{n}\sum_{r=1}^{n}\omega_r\omega_s\left\{\frac{(r+4)\rho^{s+3}}{(r+3)(r+5)}-\frac{(r+2)\nu_r\rho^{s+3}}{(r+1)(r+3)}-\frac{(r+4)\nu_s\rho^{s+1}}{(r+3)(r+5)}+\frac{(r+2)\nu_r\nu_s\rho^{s+1}}{(r+1)(r+3)}\right\}$$

$$-\frac{q}{2(1+q)}\sum_{t=1}^{n}\sum_{s=1}^{n}\sum_{r=1}^{n}\omega_r\omega_s\omega_t\left\{\frac{\rho^{t+3}}{(r+s+4)(r+s+6)}-\frac{(\nu_r+\nu_s)\rho^{t+3}}{(r+s+2)(r+s+4)}+\frac{\nu_r\nu_s\rho^{t+3}}{(r+s)(r+s+2)}\right.$$

$$\left.-\frac{\nu_t\rho^{t+1}}{(r+s+4)(r+s+6)}+\frac{(\nu_r+\nu_s)\nu_t\rho^{t+1}}{(r+s+2)(r+s+4)}-\frac{\nu_r\nu_s\nu_t\rho^{t+1}}{(r+s)(r+s+2)}\right\}$$

$$+\frac{q}{1+q}\gamma\sum_{s=1}^{n}\sum_{r=1}^{n}\omega_r\omega_s\left\{\frac{\rho^{s+3}}{(r+3)(r+5)}-\frac{\nu_r\rho^{s+3}}{(r+1)(r+3)}-\frac{\nu_s\rho^{s+1}}{(r+3)(r+5)}+\frac{\nu_r\nu_s\rho^{s+1}}{(r+1)(r+3)}\right\}\Bigg]$$

$$-7\gamma\Bigg[\frac{1}{2}\sum_{s=1}^{n}\sum_{r=1}^{n}\omega_r\omega_s\left\{\frac{\rho^{r+s+6}}{(r+s+4)(r+s+6)}-\frac{(\nu_r+\nu_s)\rho^{r+s+4}}{(r+s+2)(r+s+4)}+\frac{\nu_r\nu_s\rho^{r+s+2}}{(r+s)(r+s+2)}\right\}$$

$$-\gamma\sum_{r=1}^{n}\omega_r\left\{\frac{\rho^{r+6}}{(r+3)(r+5)}-\frac{\nu_r\rho^{r+3}}{(r+1)(r+3)}\right\}$$

$$-\frac{\rho^2}{1+q}\left\{\frac{1}{2}\sum_{s=1}^{n}\sum_{r=1}^{n}\omega_r\omega_s\left\{\frac{r+s+5}{(r+s+4)(r+s+6)}-\frac{(r+s+3)(\nu_r+\nu_s)}{(r+s+2)(r+s+4)}+\frac{\nu_r\nu_s(r+s+1)}{(r+s)(r+s+2)}\right\}\right.$$

$$\left.-\gamma\sum_{r=1}^{n}\omega_r\left\{\frac{r+4}{(r+3)(r+5)}-\frac{\nu_r(r+2)}{(r+1)(r+3)}\right\}\right.$$

$$+\frac{q}{2}\sum_{s=1}^{n}\sum_{r=1}^{n}\omega_r\omega_s\left\{\frac{1}{(r+s+4)(r+s+6)}-\frac{(\nu_r+\nu_s)}{(r+s+2)(r+s+4)}+\frac{\nu_r\nu_s}{(r+s)(r+s+2)}\right\}$$

$$\left.-q\gamma\sum_{r=1}^{n}\omega_r\left\{\frac{1}{(r+3)(r+5)}-\frac{\nu_r}{(r+1)(r+3)}\right\}\right\}\Bigg]$$

$$+\frac{p\rho^2a^3}{2D}+\frac{Pa}{2\pi D}=0$$

Equation VII.5.5 may now be multiplied through by $\frac{\partial \Psi}{\partial \omega_n}$ and integrated over the range $\rho = 0$ to $\rho = 1$. This yields an algebraic cubic equation of which the coefficients may be determined as follows.

Coefficients of third power terms

$$\eta \; \frac{1}{2} \sum_{t=1}^{n} \sum_{s=1}^{n} \sum_{r=1}^{n} \omega_r \omega_s \omega_t \left\{ \frac{1}{(r+s+4)(r+s+6)(r+s+t+u+10)} \right.$$

$$- \frac{\nu_u}{(r+s+4)(r+s+6)(r+s+t+u+8)} - \frac{\nu_r + \nu_s}{(r+s+2)(r+s+4)(r+s+t+u+8)}$$

$$+ \frac{(\nu_r + \nu_s)\nu_u}{(r+s+2)(r+s+4)(r+s+t+u+6)} + \frac{\nu_r \nu_s}{(r+s)(r+s+2)(r+s+t+u+6)}$$

$$- \frac{\nu_r \nu_s \nu_u}{(r+s)(r+s+2)(r+s+t+u+4)} - \frac{\nu_t}{(r+s+4)(r+s+6)(r+s+t+u+8)}$$

$$+ \frac{\nu_u \nu_t}{(r+s+4)(r+s+6)(r+s+t+u+6)} + \frac{(\nu_r + \nu_s)\nu_t}{(r+s+2)(r+s+4)(r+s+t+u+6)}$$

$$- \frac{(\nu_r + \nu_s)\nu_u \nu_t}{(r+s+2)(r+s+4)(r+s+t+u+4)} - \frac{\nu_r \nu_s \nu_t}{(r+s)(r+s+2)(r+s+t+u+4)}$$

$$\left. \frac{\nu_r \nu_s \nu_t \nu_u}{(r+s)(r+s+2)(r+s+t+u+2)} \right\}$$

$$-\frac{1}{2(1+q)}\sum_{t=1}^{n}\sum_{s=1}^{n}\sum_{r=1}^{n}\omega_r\omega_s\omega_t\Bigg\{\frac{r+s+s}{(r+s+4)(r+s+6)(t+u+6)}-\frac{(r+s+s)\nu_u}{(r+s+4)(r+s+6)(t+u+4)}$$

$$-\frac{(r+s+3)(\nu_r+\nu_s)}{(r+s+2)(r+s+4)(t+u+6)}+\frac{(r+s+3)(\nu_r+\nu_s)\nu_u}{(r+s+2)(r+s+4)(t+u+4)}$$

$$+\frac{(r+s+1)\nu_r\nu_s}{(r+s)(r+s+2)(t+u+6)}-\frac{(r+s+1)\nu_r\nu_s\nu_u}{(r+s)(r+s+2)(t+u+4)}$$

$$-\frac{(r+s+s)\nu_t}{(r+s+4)(r+s+6)(t+u+4)}+\frac{(r+s+s)\nu_t\nu_u}{(r+s+4)(r+s+6)(t+u+2)}$$

$$+\frac{(r+s+3)(\nu_r+\nu_s)\nu_t}{(r+s+2)(r+s+4)(t+u+4)}-\frac{(r+s+3)(\nu_r+\nu_s)\nu_t\nu_u}{(r+s+2)(r+s+4)(t+u+2)}$$

$$-\frac{(r+s+1)\nu_r\nu_s\nu_t}{(r+s)(r+s+2)(t+u+4)}+\frac{(r+s+1)\nu_r\nu_s\nu_t\nu_u}{(r+s)(r+s+2)(t+u+2)}\Bigg\}$$

$$-\frac{q}{1+q}\frac{1}{2}\sum_{t=1}^{n}\sum_{s=1}^{n}\sum_{r=1}^{n}\omega_r\omega_s\omega_t\Bigg\{\frac{1}{(r+s+4)(r+s+6)(t+u+6)}-\frac{\nu_u}{(r+s+4)(r+s+6)(t+u+4)}$$

$$-\frac{(\nu_r+\nu_s)}{(r+s+2)(r+s+4)(t+u+6)}+\frac{(\nu_r+\nu_s)\nu_u}{(r+s+2)(r+s+4)(t+u+4)}$$

$$+\frac{\nu_r\nu_s}{(r+s)(r+s+2)(t+u+6)}-\frac{\nu_r\nu_s\nu_u}{(r+s)(r+s+2)(t+u+4)}$$

$$-\frac{\nu_t}{(r+s+4)(r+s+6)(t+u+4)}+\frac{\nu_t\nu_u}{(r+s+4)(r+s+6)(t+u+2)}$$

$$+\frac{(\nu_r+\nu_s)\nu_t}{(r+s+2)(r+s+4)(t+u+4)}-\frac{(\nu_r+\nu_s)\nu_t\nu_u}{(r+s+2)(r+s+4)(t+u+2)}$$

$$-\frac{\nu_r\nu_s\nu_t}{(r+s)(r+s+2)(t+u+4)}+\frac{\nu_r\nu_s\nu_t\nu_u}{(r+s)(r+s+2)(t+u+2)}\Bigg\}\Bigg]$$

Coefficients of second power terms

$$\eta\gamma\Bigg[-\sum_{s=1}^{n}\sum_{r=1}^{n}\omega_r\omega_s\Bigg\{\frac{1}{(r+3)(r+5)(r+s+t+9)}-\frac{\nu_t}{(r+3)(r+5)(r+s+t+7)}$$

$$-\frac{\nu_r}{(r+1)(r+3)(r+s+t+7)}+\frac{\nu_r\nu_t}{(r+1)(r+3)(r+s+t+5)}$$

$$-\frac{\nu_s}{(r+3)(r+5)(r+s+t+7)}+\frac{\nu_s\nu_t}{(r+3)(r+5)(r+s+t+5)}$$

$$+\frac{\nu_r\nu_s}{(r+1)(r+3)(r+s+t+5)}-\frac{\nu_r\nu_s\nu_t}{(r+1)(r+3)(r+s+t+3)}\Bigg\}$$

$$+\frac{1}{1+q}\sum_{s=1}^{n}\sum_{r=1}^{n}\omega_r\omega_s\Bigg\{\frac{r+4}{(r+3)(r+5)(s+t+6)}-\frac{(r+4)\nu_t}{(r+3)(r+5)(s+t+4)}$$

$$-\frac{(r+2)\nu_r}{(r+1)(r+3)(s+t+6)}+\frac{(r+2)\nu_r\nu_t}{(r+1)(r+3)(s+t+4)}$$

$$-\frac{(r+4)\nu_s}{(r+3)(r+5)(s+t+4)}+\frac{(r+4)\nu_s\nu_t}{(r+3)(r+5)(s+t+2)}$$

$$+\frac{(r+2)\nu_r\nu_s}{(r+1)(r+3)(s+t+4)}-\frac{(r+2)\nu_r\nu_s\nu_t}{(r+1)(r+3)(s+t+2)}\Bigg\}$$

$$+\frac{q}{1+q}\sum_{s=1}^{n}\sum_{r=1}^{n}\omega_r\omega_s\Bigg\{\frac{1}{(r+3)(r+5)(s+t+6)}-\frac{\nu_t}{(r+3)(r+5)(s+t+4)}$$

$$-\frac{\nu_r}{(r+1)(r+3)(s+t+6)}+\frac{\nu_r\nu_t}{(r+1)(r+3)(s+t+4)}-\frac{\nu_s}{(r+3)(r+5)(s+t+4)}$$

$$+\frac{\nu_s\nu_t}{(r+3)(r+5)(s+t+2)}+\frac{\nu_r\nu_s}{(r+1)(r+3)(s+t+4)}-\frac{\nu_r\nu_s\nu_t}{(r+1)(r+3)(s+t+2)}\Bigg\}$$

$$-\frac{1}{2}\sum_{s=1}^{n}\sum_{r=1}^{n}\omega_r\omega_s\left\{\frac{1}{(r+s+4)(r+s+6)(r+s+t+9)}-\frac{\nu_t}{(r+s+4)(r+s+6)(r+s+t+7)}\right.$$

$$-\frac{\nu_r+\nu_s}{(r+s+2)(r+s+4)(r+s+t+7)}+\frac{(\nu_r+\nu_s)\nu_t}{(r+s+2)(r+s+4)(r+s+t+5)}$$

$$\left.+\frac{\nu_r\nu_s}{(r+s)(r+s+2)(r+s+t+5)}-\frac{\nu_r\nu_s\nu_t}{(r+s)(r+s+2)(r+s+t+3)}\right\}$$

$$+\frac{1}{1+q}\left\{\frac{1}{(t+5)}-\frac{\nu_t}{(t+3)}\right\}\left\{\frac{1}{2}\sum_{s=1}^{n}\sum_{r=1}^{n}\omega_r\omega_s\left\{\frac{r+s+5}{(r+s+4)(r+s+6)}-\frac{(r+s+3)(\nu_r+\nu_s)}{(r+s+2)(r+s+4)}+\frac{(r+s+1)\nu_r\nu_s}{(r+s)(r+s+2)}\right\}\right\}$$

$$+\frac{q}{1+q}\left\{\frac{1}{(t+5)}-\frac{\nu_t}{(t+3)}\right\}\left\{\frac{1}{2}\sum_{s=1}^{n}\sum_{r=1}^{n}\omega_r\omega_s\left\{\frac{1}{(r+s+4)(r+s+6)}-\frac{\nu_r+\nu_s}{(r+s+2)(r+s+4)}+\frac{\nu_r\nu_s}{(r+s)(r+s+2)}\right\}\right\}\Bigg]$$

Coefficients of linear terms

$$\sum_{r=1}^{n}\omega_r\left\{\frac{(r+1)(r+3)}{(r+s+4)}-\frac{(r-1)(r+1)\nu_r}{(r+s+2)}-\frac{(r+1)(r+3)\nu_s}{(r+s+2)}+\frac{(r-1)(r+1)\nu_r\nu_s}{(r+s)}\right\}$$

$$+\eta\gamma^2\Bigg[\sum_{r=1}^{n}\omega_r\left\{\frac{1}{(r+3)(r+5)(r+s+8)}-\frac{\nu_s}{(r+3)(r+5)(r+s+6)}\right.$$

$$\left.-\frac{\nu_r}{(r+1)(r+3)(r+s+6)}+\frac{\nu_r\nu_s}{(r+1)(r+3)(r+s+4)}\right\}$$

$$-\frac{1}{1+q}\left\{\frac{1}{(t+5)}-\frac{\nu_t}{(t+3)}\right\}\sum_{r=1}^{n}\omega_r\left\{\frac{(r+4)}{(r+3)(r+5)}-\frac{(r+2)\nu_r}{(r+1)(r+3)}\right\}$$

$$-\frac{q}{1+q}\left\{\frac{1}{(t+5)}-\frac{\nu_t}{(t+3)}\right\}\sum_{r=1}^{n}\omega_r\left\{\frac{1}{(r+3)(r+5)}-\frac{\nu_r}{(r+1)(r+3)}\right\}\Bigg]$$

Coefficients of load terms

$$\frac{pa^3}{2D}\left[\frac{1}{(\epsilon+5)} - \frac{\nu\epsilon}{(\epsilon+3)}\right]$$

$$\frac{Pa}{2\pi D}\left[\frac{1}{(\epsilon+3)} - \frac{\nu\epsilon}{(\epsilon+1)}\right]$$

VII.6 Galerkin Solution of Shallow Shell Equations - (b)

The governing differential equations may be considered in the form expressed by II.1.9 and II.1.10. These are

$$\rho \frac{d}{d\rho} \frac{1}{\rho} \frac{d}{d\rho} (\rho \Phi) = \frac{\psi^2}{2} + \rho \gamma \psi \qquad \text{VII.6.1}$$

$$\rho \frac{d}{d\rho} \frac{1}{\rho} \frac{d}{d\rho} (\rho \psi) = \eta \Phi (\psi + \rho \gamma) + \frac{p \rho^2 a^3}{2D} + \frac{Pa}{2\pi D} \qquad \text{VII.6.2}$$

where

$$\rho = \frac{r}{a}, \quad \eta = 12(1-\nu^2)\frac{a^2}{t^2}, \quad \gamma = \frac{a}{R}$$

p = uniformly distributed pressure load

P = point load at apex of shell

A solution is assumed in the form

$$\psi = \gamma \sum_{n=0}^{n} \omega_n \left[(n+4) a_n \rho^{n+3} + (n+2) b_n \rho^{n+1} + n c_n \rho^{n-1} \right] \qquad \text{VII.6.3}$$

which satisfies the boundary conditions when

$$a_n = 1$$

$$b_n = - \frac{4n + 2m + 6}{2n + m + 1}$$

$$c_n = \frac{2n + m + 5}{2n + m + 1} = - (b_n + 1)$$

and n is an even integer.

Substitution of VII.6.3 into VII.6.1 gives

$$\rho \frac{d}{d\rho} \frac{1}{\rho} \frac{d}{d\rho} (\rho \Phi) = \frac{\Psi^2}{2} - \rho \gamma \Psi$$

$$= \frac{1}{2} \gamma^2 \sum_{s=0}^{n} \sum_{r=0}^{n} \omega_r \omega_s \Big[(r+4)(s+4) \rho^{r+s+6} + \Big\{ (r+4)(s+2) b_s + (r+2)(s+4) b_r \Big\} \rho^{r+s+4}$$

$$+ \Big\{ (r+4) s c_s + (r+2)(s+2) b_r b_s + r(s+4) c_r \Big\} \rho^{r+s+2}$$

$$+ \Big\{ (r+2) s b_r c_s + r(s+2) b_s c_r \Big\} \rho^{r+s} + r.s\, c_r c_s \rho^{r+s-2} \Big]$$

$$- \gamma^2 \sum_{r=0}^{n} \omega_r \Big[(r+4) \rho^{r+4} + (r+2) b_r \rho^{r+2} + r c_r \rho^{r} \Big]$$

Integrating

$$\frac{1}{\rho} \frac{d}{d\rho} (\rho \Phi) = \frac{1}{2} \gamma^2 \sum_{s=0}^{n} \sum_{r=0}^{n} \omega_r \omega_s \Big[\frac{(r+4)(s+4)}{r+s+6} \rho^{r+s+6} + \Big\{ \frac{(r+4)(s+2) b_s + (r+2)(s+4) b_r}{r+s+4} \Big\} \rho^{r+s+4}$$

$$+ \Big\{ \frac{(r+4) s c_s + (r+2)(s+2) b_r b_s + r(s+4) c_r}{r+s+2} \Big\} \rho^{r+s+2}$$

$$+ \Big\{ \frac{(r+2) s b_r c_s + r(s+2) b_s c_r}{r+s} \Big\} \rho^{r+s} + \frac{r.s\, c_r c_s}{r+s-2} \rho^{r+s-2} \Big]$$

$$- \gamma^2 \sum_{r=0}^{n} \omega_r \Big\{ \frac{(r+4)}{(r+4)} \rho^{r+4} + \frac{(r+2)}{(r+2)} b_r \rho^{r+2} + \frac{r c_r \rho^r}{r} \Big\} + A$$

Integrate again

$$\rho\Phi = \frac{1}{2}\gamma^2 \sum_{s=0}^{n}\sum_{r=0}^{n}\omega_r\omega_s \left[\frac{(r+4)(s+4)\rho^{r+s+8}}{(r+s+6)(r+s+8)} + \left\{\frac{(r+4)(s+2)b_s + (r+2)(s+4)b_r}{(r+s+4)(r+s+6)}\right\}\rho^{r+s+6} \right.$$

$$+ \left\{\frac{(r+4)sC_s + (r+2)(s+2)b_r b_s + r(s+4)C_r}{(r+s+2)(r+s+4)}\right\}\rho^{r+s+4}$$

$$\left. + \left\{\frac{(r+2)s\,b_r C_s + r(s+2)b_s C_r}{(r+s)(r+s+2)}\right\}\rho^{r+s+2} + \frac{r.s\,C_r C_s \rho^{r+s}}{(r+s-2)(r+s)} \right]$$

$$-\gamma^2\sum_{r=0}^{n}\omega_r\left[\frac{\rho^{r+6}}{r+6} + \frac{b_r\rho^{r+4}}{r+4} + \frac{C_r\rho^{r+2}}{r+2}\right] + \frac{A}{2}\rho^2 + B$$

At $\rho=0$, Φ is finite $\quad\therefore B=0$

At $\rho=1$, $\left(\frac{d\Phi}{d\rho}\right)_{\rho=1} + q(\Phi)_{\rho=1} = 0$ where $q = -\nu - C_2$

$$\therefore \frac{1}{2}\gamma^2 \sum_{s=0}^{n}\sum_{r=0}^{n}\omega_r\omega_s \left[\frac{(r+4)(s+4)(r+s+7)}{(r+s+6)(r+s+8)} + \left\{\frac{(r+4)(s+2)b_s + (r+2)(s+4)b_r}{(r+s+4)(r+s+6)}\right\}(r+s+5) \right.$$

$$+ \left\{\frac{(r+4)sC_s + (r+2)(s+2)b_r b_s + r(s+4)C_r}{(r+s+2)(r+s+4)}\right\}(r+s+3)$$

$$\left. + \left\{\frac{(r+2)s\,b_r C_s + r(s+2)b_s C_r}{(r+s)(r+s+2)}\right\}(r+s+1) + \frac{r.s\,(r+s-1)C_r C_s}{(r+s-2)(r+s)} \right]$$

$$-\gamma^2\sum_{r=0}^{n}\omega_r\left[\frac{(r+s)}{(r+6)} + \frac{(r+3)b_r}{(r+4)} + \frac{(r+1)C_r}{(r+2)}\right] + \frac{A}{2}$$

$$+q\left[\frac{1}{2}\gamma^2\sum_{s=0}^{n}\sum_{r=0}^{n}\omega_r\omega_s\left\{\frac{(r+4)(s+4)}{(r+s+6)(r+s+8)}+\left\{\frac{(r+4)(s+2)b_s+(r+2)(s+4)b_r}{(r+s+4)(r+s+6)}\right\}\right.\right.$$

$$+\left\{\frac{(r+4)sc_s+(r+2)(s+2)b_rb_s+r(s+4)c_r}{(r+s+2)(r+s+4)}\right\}$$

$$\left.+\left\{\frac{(r+2)sb_rc_s+r(s+2)b_sc_r}{(r+s)(r+s+2}\right\}+\frac{r.sc_rc_s}{(r+s-2)(r+s)}\right\}$$

$$\left.-\gamma^2\sum_{r=0}^{n}\omega_r\left\{\frac{1}{r+6}+\frac{b_r}{r+4}+\frac{c_r}{r+2}\right\}+\frac{A}{2}\right]$$

$$\therefore\quad A=\frac{-2}{1+q}\left\{\frac{1}{2}\gamma^2\sum_{s=0}^{n}\sum_{r=0}^{n}\omega_r\omega_s\left[\frac{(r+4)(s+4)(r+s+7+q)}{(r+s+6)(r+s+8)}\right.\right.$$

$$+\left\{\frac{(r+4)(s+2)b_s+(r+2)(s+4)b_r}{(r+s+4)(r+s+6)}\right\}(r+s+5+q)$$

$$+\left\{\frac{(r+4)sc_s+(r+2)(s+2)b_rb_s+r(s+4)c_r}{(r+s+2)(r+s+4)}\right\}(r+s+3+q)$$

$$\left.+\left\{\frac{(r+2)sb_rc_s+r(s+2)b_sc_r}{(r+s)(r+s+2)}\right\}(r+s+1+q)+\frac{r.sc_rc_s(r+s-1+q)}{(r+s-2)(r+s)}\right]$$

$$\left.-\gamma^2\sum_{r=0}^{n}\omega_r\left\{\frac{r+s+q}{r+6}+\frac{(r+3+q)b_r}{r+4}+\frac{(r+1+q)c_r}{r+2}\right\}\right\}$$

$$\therefore\quad \Phi=\frac{1}{2}\gamma^2\sum_{s=0}^{n}\sum_{r=0}^{n}\omega_r\omega_s\left[\frac{(r+4)(s+4)}{(r+s+6)(r+s+8)}\left\{\rho^{r+s+7}-\left((r+s+7)K_2+K\right)\rho\right\}\right.$$

$$\rho\Psi = \gamma \sum_{r=0}^{n} \omega_r \left[(r+4)\rho^{r+4} + (r+2) b_r \rho^{r+2} + r C_r \rho^{r} \right]$$

$$\frac{d}{d\rho}(\rho\Psi) = \gamma \sum_{r=0}^{n} \omega_r \left[(r+4)^2 \rho^{r+3} + (r+2)^2 b_r \rho^{r+1} + r^2 C_r \rho^{r-1} \right]$$

$$\frac{d}{d\rho}\frac{1}{\rho}\frac{d}{d\rho}(\rho\Psi) = \gamma \sum_{r=0}^{n} \omega_r \left[(r+2)(r+4)^2 \rho^{r+1} + r(r+2)^2 b_r \rho^{r-1} + (r-2) r^2 C_r \rho^{r-3} \right]$$

$$\rho\frac{d}{d\rho}\frac{1}{\rho}\frac{d}{d\rho}(\rho\Psi) = \gamma \sum_{r=0}^{n} \omega_r \left[(r+2)(r+4)^2 \rho^{r+2} + r(r+2)^2 b_r \rho^{r} + (r-2) r^2 C_r \rho^{r-2} \right]$$

The equation VII.6.2 with VII.6.3 and VII.6.4 becomes

$$\gamma \sum_{r=0}^{n} \omega_r \left[(r+2)(r+4)^2 \rho^{r+2} + r(r+2)^2 b_r \rho^{r} + (r-2) r^2 C_r \rho^{r-2} \right]$$

$$+ \eta\gamma^3 \left[\frac{1}{2} \sum_{t=0}^{n} \sum_{s=0}^{n} \sum_{r=0}^{n} \omega_r \omega_s \omega_t \left[\frac{(r+4)(s+4)}{(r+s+6)(r+s+8)} \left\{ (t+4)\left(\rho^{r+s+t+10} - \left\{ (r+s+7)K_2 + K_1 \right\} \rho^{t+4} \right) \right.\right.\right.$$

$$+ (t+2) b_t \left(\rho^{r+s+t+8} - \left\{ (r+s+7)K_2 + K_1 \right\} \rho^{t+2} \right) + t C_t \left(\rho^{r+s+t+6} - \left\{ (r+s+7)K_2 + K_1 \right\} \rho^{t} \right) \Big\}$$

$$+ \frac{(r+4)(s+2)}{(r+s+4)(r+s+6)} b_s + (r+2)(s+4) b_r \left\{ (t+4)\left(\rho^{r+s+t+8} - \left\{ (r+s+5)K_2 + K_1 \right\} \rho^{t+4} \right) \right.$$

$$+(t+2)b_t\left(\rho^{r+s+t+6}-\{(r+s+5)K_2+K_1\}\rho^{t+2}\right)+tC_t\left(\rho^{r+s+t+4}-\{(r+s+5)K_2+K_1\}\rho^{t}\right)\Big\}$$

$$+\frac{(r+4)sC_s+(r+2)(s+2)b_rb_s+r(s+4)C_r}{(r+s+2)(r+s+4)}\Big\{(t+4)\left(\rho^{r+s+t+6}-\{(r+s+3)K_2+K_1\}\rho^{t+4}\right)$$

$$+(t+2)b_t\left(\rho^{r+s+t+4}-\{(r+s+3)K_2+K_1\}\rho^{t+2}\right)+tC_t\left(\rho^{r+s+t+2}-\{(r+s+3)K_2+K_1\}\rho^{t}\right)\Big\}$$

$$+\frac{(r+2)sb_rC_s+r(s+2)b_sC_r}{(r+s)(r+s+2)}\Big\{(t+4)\left(\rho^{r+s+1\,t+4}-\{(r+s+1)K_2+K_1\}\rho^{t+4}\right)$$

$$+(t+2)b_t\left(\rho^{r+s+t+2}-\{(r+s+1)K_2+K_1\}\rho^{t+2}+tC_t\left(\rho^{r+s+t}-\{(r+s+1)K_2+K_1\}\rho^{t}\right)\Big\}\right.$$

$$+\frac{r.s\,C_rC_s}{(r+s-2)(r+s)}\Big\{(t+4)\left(\rho^{r+s+t+2}-\{(r+s-1)K_2+K_1\}\rho^{t+4}\right)$$

$$\left.+(t+2)b_t\left(\rho^{r+s+t}-\{(r+s-1)K_2+K_1\}\rho^{t+2}\right)-tC_t\left(\rho^{r+s+t-2}-\{(r+s-1)K_2+K_1\}\rho^{t}\right)\Big\}\right]$$

$$-\sum_{s=0}^{n}\sum_{r=0}^{n}\omega_r\omega_s\left[\frac{1}{(r+6)}\Big\{(s+4)\left(\rho^{r+s+8}-\{(r+5)K_2+K_1\}\rho^{s+4}\right)\right.$$

$$+(s+2)b_s\left(\rho^{r+s+6}-\{(r+5)K_2+K_1\}\rho^{s+2}\right)+sC_s\left(\rho^{r+s+4}-\{(r+5)K_2+K_1\}\rho^{s}\right)\Big\}$$

$$+\frac{b_r}{r+4}\Big\{(s+4)\left(\rho^{r+s+6}-\{(r+3)K_2+K_1\}\rho^{s+4}\right)$$

$$+(s+2)b_s\left(\rho^{r+s+4}-\{(r+3)K_2+K_1\}\rho^{s+2}\right)+sC_s\left(\rho^{r+s+2}-\{(r+3)K_2+K_1\}\rho^{s}\right)\Big\}$$

$$+ \frac{c_r}{r+2}\left\{(s+4)\left(\rho^{r+s+4} - \{(r+1)K_2 + K_1\}\rho^{s+4}\right)\right.$$

$$\left. + (s+2)b_s\left(\rho^{r+s+2} - \{(r+1)K_2 + K_1\}\rho^{s+2}\right) + sc_s\left(\rho^{r+s} - \{(r+1)K_2 + K_1\}\rho^{s}\right)\right\}\Bigg]\Bigg]$$

$$+ \eta\gamma^3\rho\left[\frac{1}{2}\sum_{s=0}^{n}\sum_{r=0}^{n}\omega_r\omega_s\left[\frac{(r+4)(s+4)}{(r+s+6)(r+s+8)}\left\{\rho^{r+s+7} - \{(r+s+7)K_2 + K_1\}\rho\right\}\right.\right.$$

$$+ \frac{(r+4)(s+2)b_s + (r+2)(s+4)b_r}{(r+s+4)(r+s+6)}\left\{\rho^{r+s+6} - \{(r+s+5)K_2 + K_1\}\rho\right\}$$

$$+ \frac{(r+4)sc_s + (r+2)(s+2)b_r b_s + r(s+4)c_r}{(r+s+2)(r+s+4)}\left\{\rho^{r+s+3} - \{(r+s+3)K_2 + K_1\}\rho\right\}$$

$$+ \frac{(r+2)s\,b_r c_s + r(s+2)b_s c_r}{(r+s)(r+s+2)}\left\{\rho^{r+s+1} - \{(r+s+1)K_2 + K_1\}\rho\right\}$$

$$\left.\left. + \frac{r.s\,c_r c_s}{(r+s-2)(r+s)}\left\{\rho^{r+s-1} - \{(r+s-1)K_2 + K_1\}\rho\right\}\right]$$

$$- \sum_{r=0}^{n}\omega_r\left[\frac{\rho^{r+5} - \{(r+5)K_2 + K_1\}\rho}{r+6} + b_r\left(\frac{\rho^{r+3} - \{(r+3)K_2 + K_1\}\rho}{r+4}\right)\right.$$

$$\left.\left. + c_r\left(\frac{\rho^{r+1} - \{(r+1)K_2 + K_1\}\rho}{r+2}\right)\right]\right]$$

$$+ \frac{p\rho^2 a^3}{2D} + \frac{Pa}{2\pi D} = 0 \qquad \text{VII.6.5}$$

Equation VII.6.5 may now be multiplied through by $\frac{\partial w}{\partial \omega_n}$ and integrated over the range $\rho = 0$ to $\rho = 1$. This yields an algebraic cubic equation of which the coefficients may be determined as follows.

Coefficients of third power terms

$$7\gamma^4 \Bigg[\frac{1}{2} \sum_{t=0}^{n} \sum_{s=0}^{n} \sum_{r=0}^{n} \omega_r \omega_s \omega_t \Bigg[\frac{(r+4)(s+4)}{(r+s+6)(r+s+8)} \Bigg\{ (t+4) \Bigg\{ \Bigg(\frac{1}{r+s+t+u+15} - \frac{(r+s+7)K_2 + K_1}{t+u+9} \Bigg)$$

$$+ b_u \Bigg(\frac{1}{r+s+t+u+13} - \frac{(r+s+7)K_2 + K_1}{t+u+7} \Bigg) + C_u \Bigg(\frac{1}{r+s+t+u+11} - \frac{(r+s+7)K_2 + K_1}{t+u+5} \Bigg) \Bigg\}$$

$$+ (t+2) b_t \Bigg\{ \Bigg(\frac{1}{r+s+t+u+13} - \frac{(r+s+7)K_2 + K_1}{t+u+7} \Bigg) + b_u \Bigg(\frac{1}{r+s+t+u+11} - \frac{(r+s+7)K_2 + K_1}{t+u+5} \Bigg)$$

$$+ C_u \Bigg(\frac{1}{r+s+t+u+9} - \frac{(r+s+7)K_2 + K_1}{t+u+3} \Bigg) \Bigg\} + t C_t \Bigg\{ \Bigg(\frac{1}{r+s+t+u+11} - \frac{(r+s+7)K_2 + K_1}{t+u+5} \Bigg)$$

$$+ b_u \Bigg(\frac{1}{r+s+t+u+9} - \frac{(r+s+7)K_2 + K_1}{t+u+3} \Bigg) + C_u \Bigg(\frac{1}{r+s+t+u+7} - \frac{(r+s+7)K_2 + K_1}{t+u+1} \Bigg) \Bigg\} \Bigg\}$$

$$+ \frac{(r+4)(s+2) b_s + (r+2)(s+4) b_r}{(r+s+4)(r+s+6)} \Bigg\{ (t+4) \Bigg\{ \Bigg(\frac{1}{r+s+t+u+13} - \frac{(r+s+5)K_2 + K_1}{t+u+9} \Bigg)$$

$$+ b_u \Bigg(\frac{1}{r+s+t+u+11} - \frac{(r+s+6)K_2 + K_1}{t+u+7} \Bigg) + C_u \Bigg(\frac{1}{r+s+t+u+9} - \frac{(r+s+5)K_2 + K_1}{t+u+5} \Bigg) \Bigg\}$$

$$+ (t+2) b_t \Bigg\{ \Bigg(\frac{1}{r+s+t+u+11} - \frac{(r+s+5)K_2 + K_1}{t+u+7} \Bigg) + b_u \Bigg(\frac{1}{r+s+t+u+9} - \frac{(r+s+5)K_2 + K_1}{t+u+5} \Bigg)$$

$$+ Cu\left(\frac{1}{r+s+t+u+7} - \frac{(r+s+5)K_2+K_1}{t+u+3}\right)\Big\} + tCt\Big\{\Big(\frac{1}{r+s+t+u+9} - \frac{(r+s+5)K_2+K_1}{t+u+5}\Big)$$

$$+ bu\left(\frac{1}{r+s+t+u+7} - \frac{(r+s+5)K_2+K_1}{t+u+3}\right) + Cu\left(\frac{1}{r+s+t+u+5} - \frac{(r+s+5)K_2+K_1}{t+u+1}\right)\Big\}\Big\}$$

$$+ \frac{(r+4)sCs + (r+2)(s+2)brbs + r(s+4)Cr}{(r+s+2)(r+s+4)}\Big\{(t+4)\Big\{\Big(\frac{1}{r+s+t+u+11} - \frac{(r+s+3)K_2+K_1}{t+u+9}\Big)$$

$$+ bu\left(\frac{1}{r+s+t+u+9} - \frac{(r+s+3)K_2+K_1}{t+u+7}\right) + Cu\left(\frac{1}{r+s+t+u+7} - \frac{(r+s+3)K_2+K_1}{t+u+5}\right)\Big\}$$

$$+ (t+2)bt\Big\{\Big(\frac{1}{r+s+t+u+9} - \frac{(r+s+3)K_2+K_1}{t+u+7}\Big) + bu\Big(\frac{1}{r+s+t+u+7} - \frac{(r+s+3)K_2+K_1}{t+u+5}\Big)$$

$$+ Cu\left(\frac{1}{r+s+t+u+5} - \frac{(r+s+3)K_2+K_1}{t+u+3}\right)\Big\} + tCt\Big\{\Big(\frac{1}{r+s+t+u+7} - \frac{(r+s+3)K_2+K_1}{t+u+5}\Big)$$

$$+ bu\left(\frac{1}{r+s+t+u+5} - \frac{(r+s+3)K_2+K_1}{t+u+3}\right) + Cu\left(\frac{1}{r+s+t+u+3} - \frac{(r+s+3)K_2+K_1}{t+u+1}\right)\Big\}\Big\}$$

$$+ \frac{(r+2)sbrCs + r(s+2)bsCr}{(r+s)(r+s+2)}\Big\{(t+4)\Big\{\Big(\frac{1}{r+s+t+u+9} - \frac{(r+s+1)K_2+K_1}{t+u+9}\Big)$$

$$+ bu\left(\frac{1}{r+s+t+u+7} - \frac{(r+s+1)K_2+K_1}{t+u+7}\right) + Cu\left(\frac{1}{r+s+t+u+5} - \frac{(r+s+1)K_2+K_1}{t+u+5}\right)\Big\}$$

$$+ (t+2)bt\Big\{\Big(\frac{1}{r+s+t+u+7} - \frac{(r+s+1)K_2+K_1}{t+u+7}\Big) + bu\Big(\frac{1}{r+s+t+u+5} - \frac{(r+s+1)K_2+K_1}{t+u+5}\Big)$$

$$+ Cu\left(\frac{1}{r+s+t+u+3} - \frac{(r+s+1)K_2+K_1}{t+u+3}\right)\Big\} + tCt\Big\{\Big(\frac{1}{r+s+t+u+5} - \frac{(r+s+1)K_2+K_1}{t+u+5}\Big)$$

$$+ b_u\left(\frac{1}{r+s+t+u+3} - \frac{(r+s+1)K_2+K_1}{t+u+3}\right) + C_u\left(\frac{1}{r+s+t+u+1} - \frac{(r+s+1)K_2+K_1}{t+u+1}\right)\Bigg\}\Bigg\}$$

$$+ \frac{r.s\,C_r C_s}{(r+s-2)(r+s)}\Bigg\{(t+4)\Bigg\{\left(\frac{1}{r+s+t+u+7} - \frac{(r+s-1)K_2+K_1}{t+u+9}\right) + b_u\left(\frac{1}{r+s+t+u+5} - \frac{(r+s-1)K_2+K_1}{t+u+7}\right)$$

$$+ C_u\left(\frac{1}{r+s+t+u+3} - \frac{(r+s-1)K_2+K_1}{t+u+5}\right)\Bigg\} + (t+2)b_t\Bigg\{\left(\frac{1}{r+s+t+u+5} - \frac{(r+s-1)K_2+K_1}{t+u+7}\right)$$

$$b_u\left(\frac{1}{r+s+t+u+3} - \frac{(r+s-1)K_2+K_1}{t+u+5}\right) + C_u\left(\frac{1}{r+s+t+u+1} - \frac{(r+s-1)K_2+K_1}{t+u+3}\right)\Bigg\}$$

$$+ tC_t\Bigg\{\left(\frac{1}{r+s+t+u+3} - \frac{(r+s-1)K_2+K_1}{t+u+5}\right) + b_u\left(\frac{1}{r+s+t+u+1} - \frac{(r+s-1)K_2+K_1}{t+u+3}\right)$$

$$+ C_u\left(\frac{1}{r+s+t+u-1} - \frac{(r+s-1)K_2+K_1}{t+u+1}\right)\Bigg\}\Bigg\}\Bigg]\Bigg]$$

Coefficients of second power terms

$$-\eta\gamma^4\Bigg[\sum_{s=0}^{n}\sum_{r=0}^{n}\omega_r\omega_s\Bigg[\frac{1}{(r+6)}\Bigg\{(s+4)\Bigg\{\left(\frac{1}{r+s+t+13} - \frac{(r+s)K_2+K_1}{s+t+9}\right)$$

$$+ b_t\left(\frac{1}{r+s+t+11} - \frac{(r+s)K_2+K_1}{s+t+7}\right) + C_t\left(\frac{1}{r+s+t+9} - \frac{(r+s)K_2+K_1}{s+t+5}\right)\Bigg\}$$

$$+ (s+2)b_s\Bigg\{\left(\frac{1}{r+s+t+11} - \frac{(r+s)K_2+K_1}{s+t+7}\right) + b_t\left(\frac{1}{r+s+t+9} - \frac{(r+s)K_2+K_1}{s+t+5}\right)$$

$$+ C_t\left(\frac{1}{r+s+t+7} - \frac{(r+5)K_2+K_1}{s+t+3}\right)\Big\} + SC_s\Big\{\Big(\frac{1}{r+s+t+9} - \frac{(r+5)K_2+K_1}{s+t+5}\Big)$$

$$+ b_t\left(\frac{1}{r+s+t+7} - \frac{(r+5)K_2+K_1}{s+t+3}\right) + C_t\left(\frac{1}{r+s+t+5} - \frac{(r+5)K_2+K_1}{s+t+1}\right)\Big\}\Big\}$$

$$+ \frac{br}{r+4}\Big\{(s+4)\Big\{\Big(\frac{1}{r+s+t+11} - \frac{(r+3)K_2+K_1}{s+t+9}\Big)$$

$$+ b_t\left(\frac{1}{r+s+t+9} - \frac{(r+3)K_2+K_1}{s+t+7}\right) + C_t\left(\frac{1}{r+s+t+7} - \frac{(r+3)K_2+K_1}{s+t+5}\right)\Big\}$$

$$+ (s+2)b_s\Big\{\Big(\frac{1}{r+s+t+9} - \frac{(r+3)K_2+K_1}{s+t+7}\Big) + b_t\left(\frac{1}{r+s+t+7} - \frac{(r+3)K_2+K_1}{s+t+5}\right)$$

$$+ C_t\left(\frac{1}{r+s+t+5} - \frac{(r+3)K_2+K_1}{s+t+3}\right)\Big\} + SC_s\Big\{\Big(\frac{1}{r+s+t+7} - \frac{(r+3)K_2+K_1}{s+t+5}\Big)$$

$$+ b_t\left(\frac{1}{r+s+t+5} - \frac{(r+3)K_2+K_1}{s+t+3}\right) + C_t\left(\frac{1}{r+s+t+3} - \frac{(r+3)K_2+K_1}{s+t+1}\right)\Big\}\Big\}$$

$$+ \frac{Cr}{r+2}\Big\{(s+4)\Big\{\Big(\frac{1}{r+s+t+9} - \frac{(r+1)K_2+K_1}{s+t+9}\Big)$$

$$+ b_t\left(\frac{1}{r+s+t+7} - \frac{(r+1)K_2+K_1}{s+t+7}\right) + C_t\left(\frac{1}{r+s+t+5} - \frac{(r+1)K_2+K_1}{s+t+5}\right)\Big\}$$

$$+ (s+2)b_s\Big\{\Big(\frac{1}{r+s+t+7} - \frac{(r+1)K_2+K_1}{s+t+7}\Big) + b_t\left(\frac{1}{r+s+t+5} - \frac{(r+1)K_2+K_1}{s+t+5}\right)$$

$$+ C_t\left(\frac{1}{r+s+t+3} - \frac{(r+1)K_2+K_1}{s+t+3}\right)\Big\} + SC_s\Big\{\Big(\frac{1}{r+s+t+5} - \frac{(r+1)K_2+K_1}{s+t+5}\Big)$$

$$+ b_t\left(\frac{1}{r+s+t+3} - \frac{(r+1)K_2+K_1}{s+t+3}\right) + C_t\left(\frac{1}{r+s+t+1} - \frac{(r+1)K_2+K_1}{s+t+1}\right)\Big\}\Big\}\Big]$$

$$+ \frac{1}{2}\sum_{s=0}^{n}\sum_{r=0}^{n}\omega_r\omega_s\Big[\frac{(r+4)(s+4)}{(r+s+6)(r+s+8)}\Big\{\Big(\frac{1}{r+s+t+13} - \frac{(r+s+7)K_2+K_1}{t+7}\Big)$$

$$+ b_t\left(\frac{1}{r+s+t+11} - \frac{(r+s+7)K_2+K_1}{t+5}\right) + C_t\left(\frac{1}{r+s+t+9} - \frac{(r+s+7)K_2+K_1}{t+3}\right)\Big\}$$

$$+ \frac{(r+4)(s+2)b_s + (r+2)(s+4)b_r}{(r+s+4)(r+s+6)}\Big\{\Big(\frac{1}{r+s+t+11} - \frac{(r+s+5)K_2+K_1}{t+7}\Big)$$

$$+ b_t\left(\frac{1}{r+s+t+9} - \frac{(r+s+5)K_2+K_1}{t+5}\right) + C_t\left(\frac{1}{r+s+t+7} - \frac{(r+s+5)K_2+K_1}{t+3}\right)\Big\}$$

$$+ \frac{(r+4)sC_s + (r+2)(s+2)b_rb_s + r(s+4)C_r}{(r+s+2)(r+s+4)}\Big\{\Big(\frac{1}{r+s+t+9} - \frac{(r+s+3)K_2+K_1}{t+7}\Big)$$

$$+ b_t\left(\frac{1}{r+s+t+7} - \frac{(r+s+3)K_2+K_1}{t+5}\right) + C_t\left(\frac{1}{r+s+t+5} - \frac{(r+s+3)K_2+K_1}{t+3}\right)\Big\}$$

$$+ \frac{(r+2)sb_rC_s + r(s+2)b_sC_r}{(r+s)(r+s+2)}\Big\{\Big(\frac{1}{r+s+t+7} - \frac{(r+s+1)K_2+K_1}{t+7}\Big)$$

$$+ b_t\left(\frac{1}{r+s+t+5} - \frac{(r+s+1)K_2+K_1}{t+5}\right) + C_t\left(\frac{1}{r+s+t+3} - \frac{(r+s+1)K_2+K_1}{t+3}\right)\Big\}$$

$$+ \frac{r.sC_rC_s}{(r+s-2)(r+s)}\Big\{\Big(\frac{1}{r+s+t+5} - \frac{(r+s-1)K_2+K_1}{t+7}\Big)$$

$$+ b_t\left(\frac{1}{r+s+t+3} - \frac{(r+s-1)K_2+K_1}{t+5}\right) + C_t\left(\frac{1}{r+s+t+1} - \frac{(r+s-1)K_2+K_1}{t+3}\right)\Big\}\Big]\Big]$$

Coefficients of linear terms

$$\gamma^2 \sum_{r=0}^{n} \omega_r \left[\frac{(r+2)(r+4)^2}{r+s+7} + \frac{(r+2)(r+4)^2 b_s}{r+s+5} + \frac{(r+2)(r+4)^2 c_s}{r+s+3} \right.$$

$$+ \frac{r(r+2)^2 b_r}{r+s+5} + \frac{r(r+2)^2 b_r b_s}{r+s+3} + \frac{r(r+2)^2 b_r c_s}{r+s+1}$$

$$\left. + \frac{(r-2)r^2 c_r}{r+s+3} + \frac{(r-2)r^2 b_s c_r}{r+s+1} + \frac{(r-2)r^2 c_r c_s}{r+s-1} \right]$$

$$+ 7\gamma^4 \sum_{r=0}^{n} \omega_r \left[\frac{1}{r+6} \left\{ \left(\frac{1}{r+s+11} - \frac{(r+5)K_2 + K_1}{s+7} \right) \right. \right.$$

$$+ b_s \left(\frac{1}{r+s+9} - \frac{(r+5)K_2 + K_1}{s+5} \right) + c_s \left(\frac{1}{r+s+7} - \frac{(r+5)K_2 + K_1}{s+3} \right) \Big\}$$

$$+ \frac{b_r}{r+4} \left\{ \left(\frac{1}{r+s+9} - \frac{(r+3)K_2 + K_1}{s+7} \right) + b_s \left(\frac{1}{r+s+7} - \frac{(r+3)K_2 + K_1}{s+5} \right) \right.$$

$$\left. + c_s \left(\frac{1}{r+s+5} - \frac{(r+3)K_2 + K_1}{s+3} \right) \right\} + \frac{c_r}{r+2} \left\{ \left(\frac{1}{r+s+7} - \frac{(r+1)K_2 + K_1}{s+7} \right) \right.$$

$$\left. \left. + b_s \left(\frac{1}{r+s+5} - \frac{(r+1)K_2 + K_1}{s+5} \right) + c_s \left(\frac{1}{r+s+3} - \frac{(r+1)K_2 + K_1}{s+3} \right) \right\} \right]$$

Coefficients of load terms

$$\frac{pR^3}{2Eta^2} \left[\frac{1}{r+7} + \frac{b_r}{r+6} + \frac{c_r}{r+3} \right]$$

$$\frac{pR^3}{2\pi Eta^4} \left[\frac{1}{r+5} + \frac{b_r}{r+3} + \frac{c_r}{r+1} \right]$$

VII.7 The Determination of Spherical Radius

The spherical radius of curvature was calculated as the radius of the circle having the minimum least squares deviation from ordinates measured at $\frac{1}{2}$ in intervals across a diameter of the shell. Typical data is presented for two shells of nominal radius of curvature of 80 in and 100 in. respectively.

(a)

X	Y_0	Y_{90}	Y_{180}	Y_{270}
0.0	0.0000	0.0000	0.0000	0.0000
0.5	0.0015	0.0013	0.0014	0.0014
1.0	0.0062	0.0065	0.0060	0.0064
1.5	0.0141	0.0138	0.0145	0.0138
2.0	0.0245	0.0253	0.0258	0.0259
2.5	0.0390	0.0394	0.0394	0.0395
3.0	0.0568	0.0558	0.0567	0.0568
3.5	0.0770	0.0760	0.0770	0.0761
4.0	0.0985	0.1010	0.1008	0.1000
4.5	0.1270	0.1270	0.1268	0.1255
5.0	0.1568	0.1573	0.1570	0.1559
RADIUS	80.00	80.32	79.64	80.27

Mean radius of curvature = 80.06 in.

(b) Nominal Radius of Curvature - 100 in.

X	Y_0	Y_{90}	Y_{180}	Y_{270}
0.0	0.0000	0.0000	0.0000	0.0000
0.5	0.0013	0.0012	0.0011	0.0015
1.0	0.0054	0.0050	0.0045	0.0054
1.5	0.0114	0.0112	0.0120	0.0113
2.0	0.0205	0.0190	0.0210	0.0205
2.5	0.0313	0.0312	0.0315	0.0314
3.0	0.0450	0.0440	0.0456	0.0456
3.5	0.0613	0.0613	0.0614	0.0612
4.0	0.0806	0.0805	0.0808	0.0801
4.5	0.1020	0.1010	0.1014	0.1020
5.0	0.1250	0.1258	0.1252	0.1260
RADIUS	99.69	99.91	99.61	99.36

Mean radius of curvature = 99.64 in.

VII.8 Results of Experimental Investigation

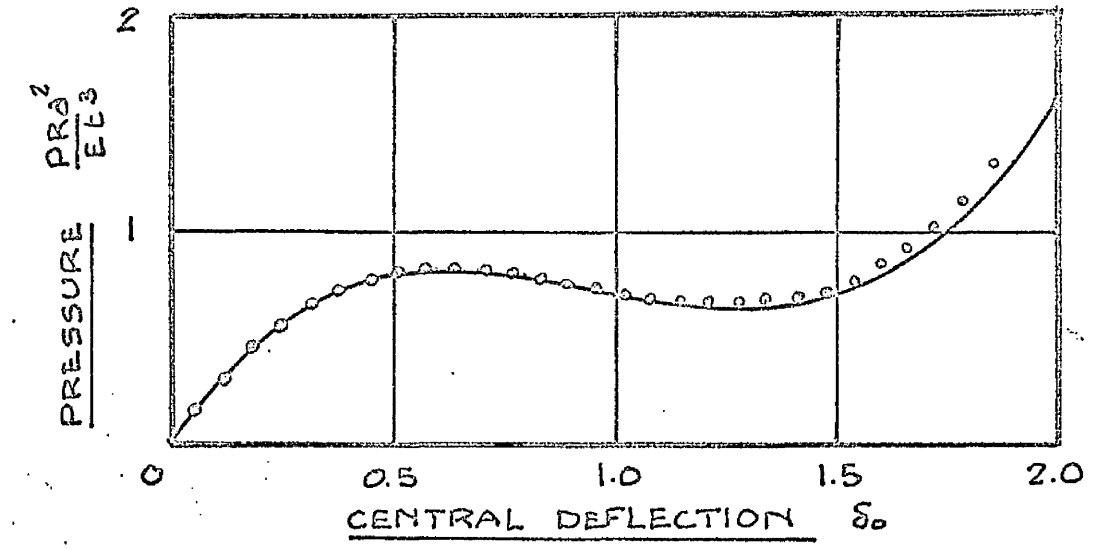

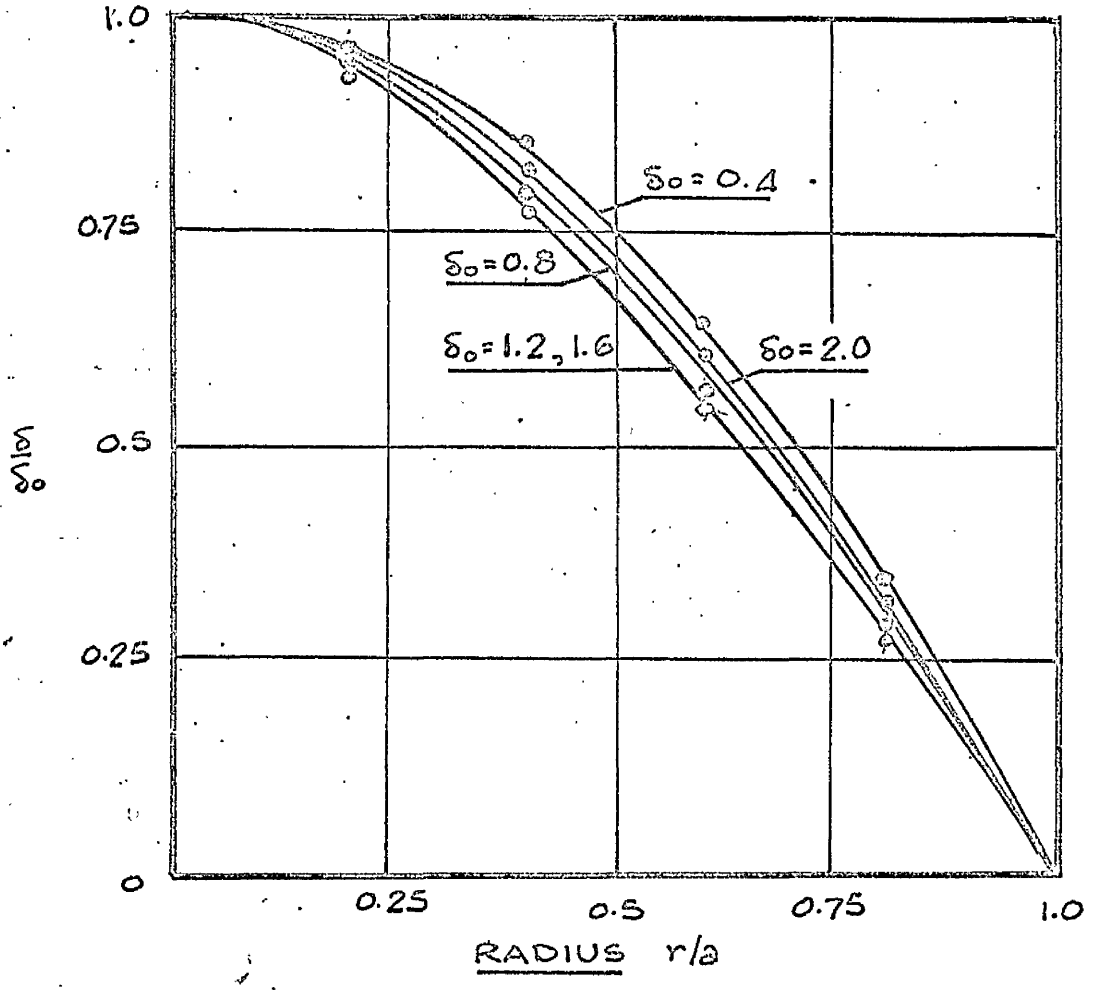

FIG. VII.1a Comparison of experimental and theoretical equilibrium paths and variation of deflected form.
PRESSURE LOAD $\lambda = 23$

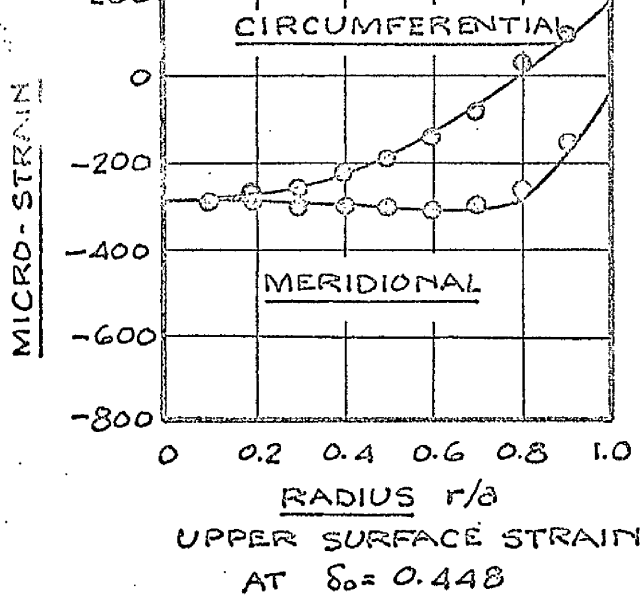

UPPER SURFACE STRAIN
AT $\delta_o = 0.448$

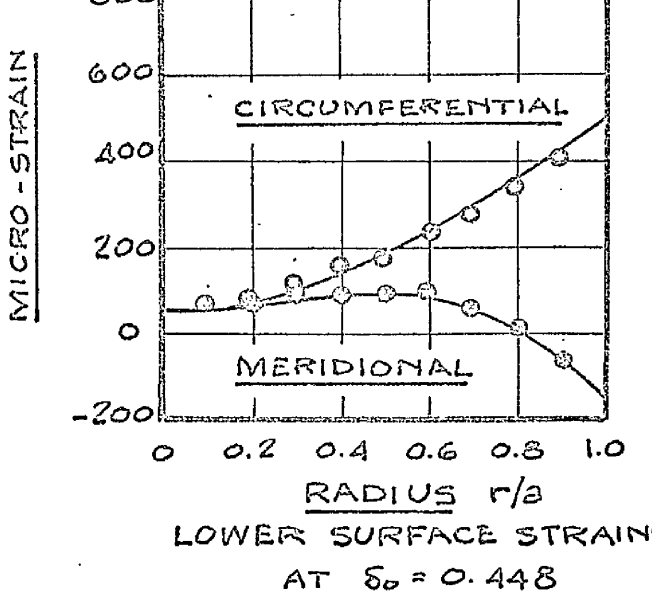

LOWER SURFACE STRAIN
AT $\delta_o = 0.448$

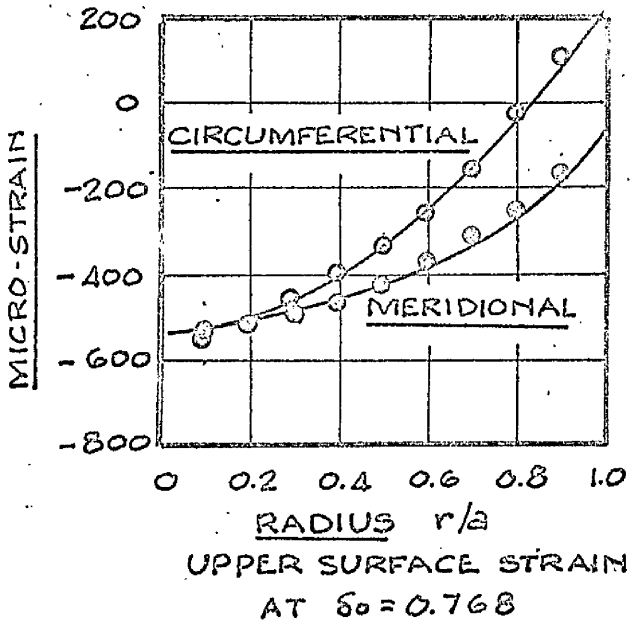

UPPER SURFACE STRAIN
AT $\delta_o = 0.768$

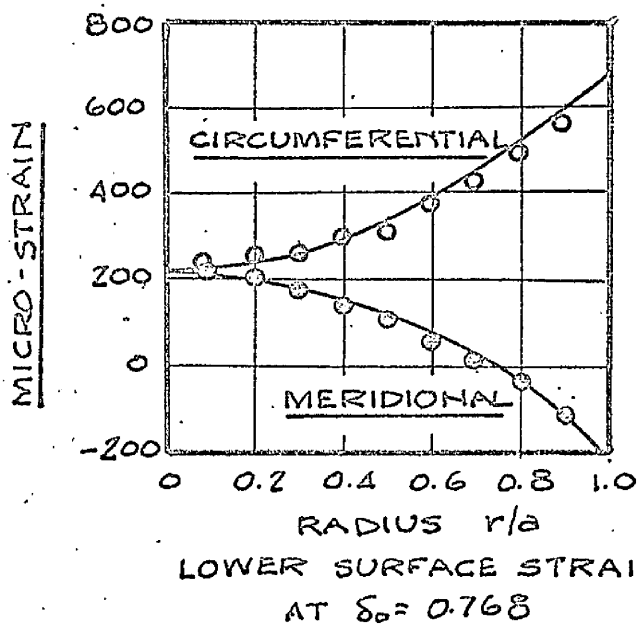

LOWER SURFACE STRAIN
AT $\delta_o = 0.768$

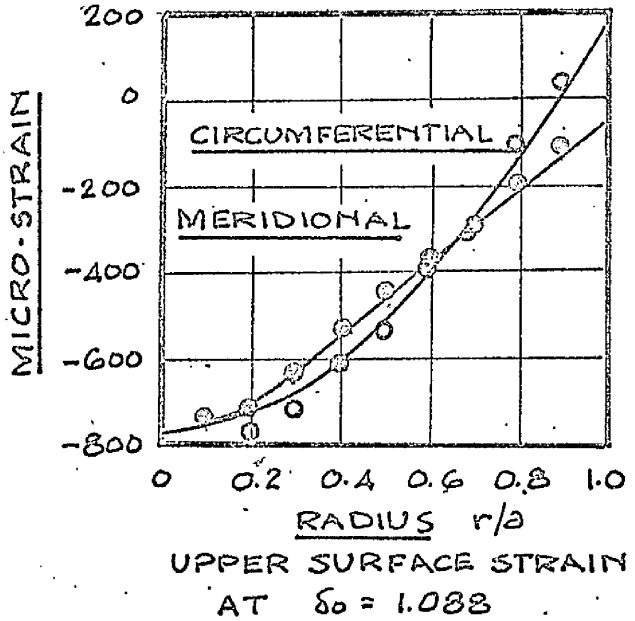

UPPER SURFACE STRAIN
AT $\delta_o = 1.088$

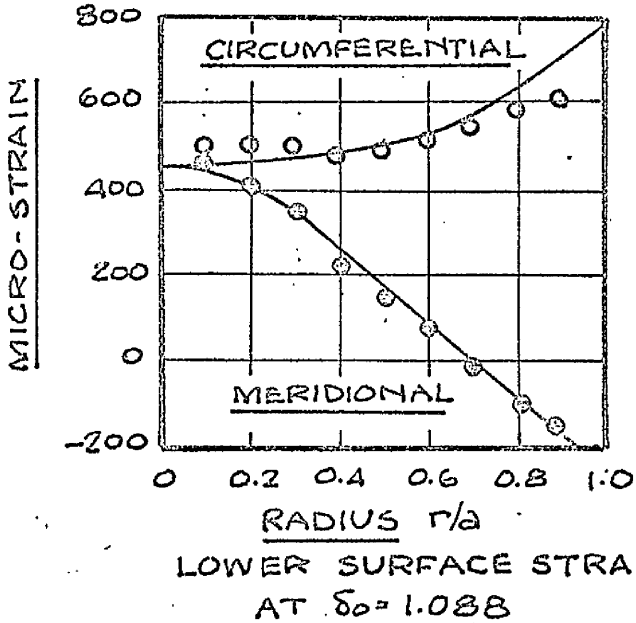

LOWER SURFACE STRAIN
AT $\delta_o = 1.088$

FIG. VII.1b Comparison of experimental and theoretical surface strains. PRESSURE LOAD $\lambda = 23$

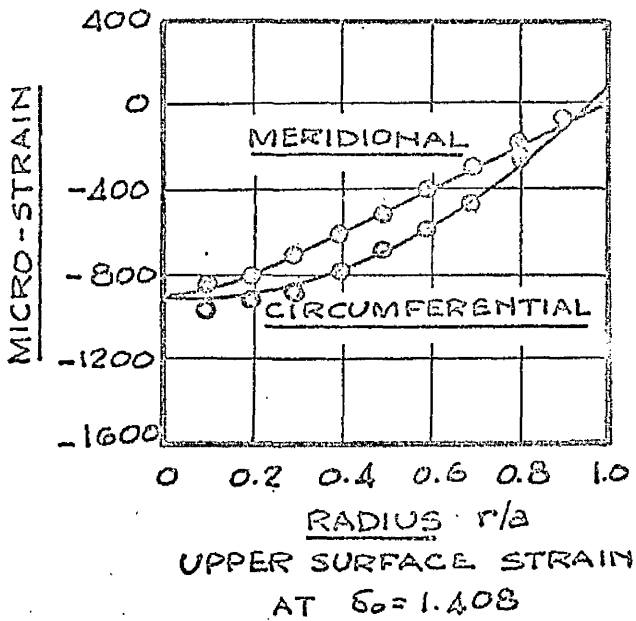

UPPER SURFACE STRAIN
AT $\delta_0 = 1.408$

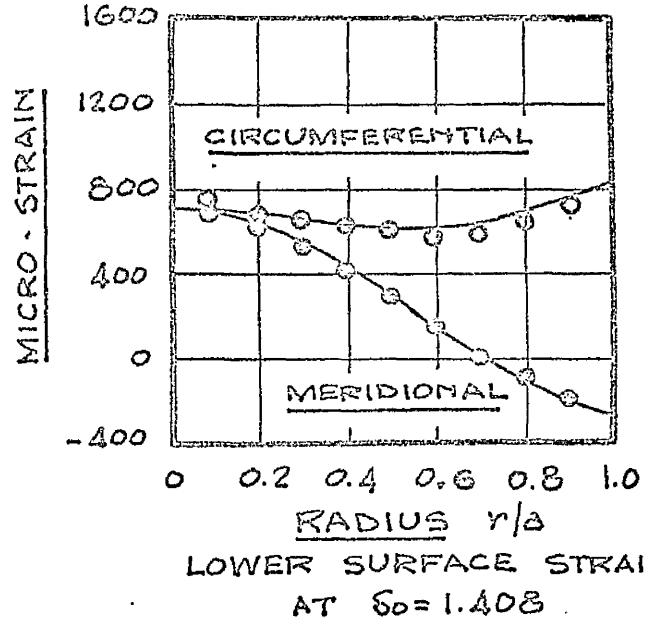

LOWER SURFACE STRAIN
AT $\delta_0 = 1.408$

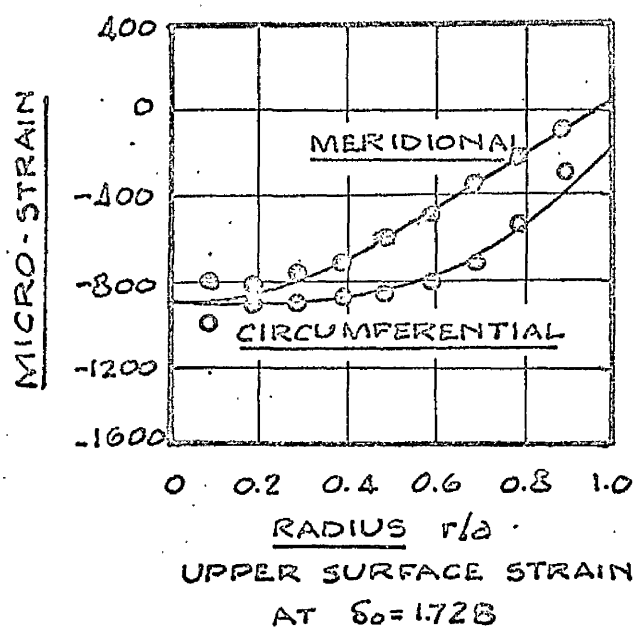

UPPER SURFACE STRAIN
AT $\delta_0 = 1.728$

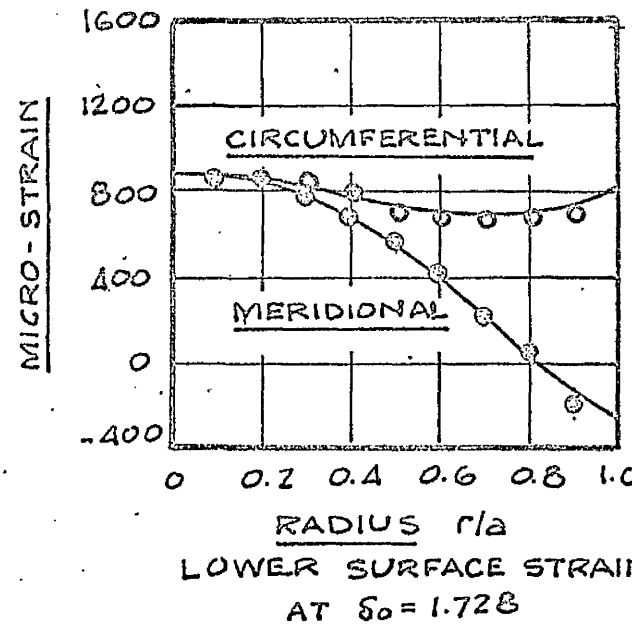

LOWER SURFACE STRAIN
AT $\delta_0 = 1.728$

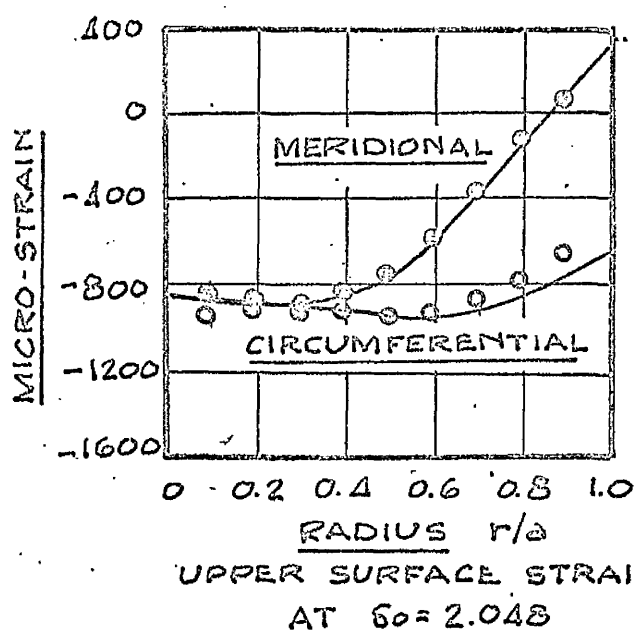

UPPER SURFACE STRAIN
AT $\delta_0 = 2.048$

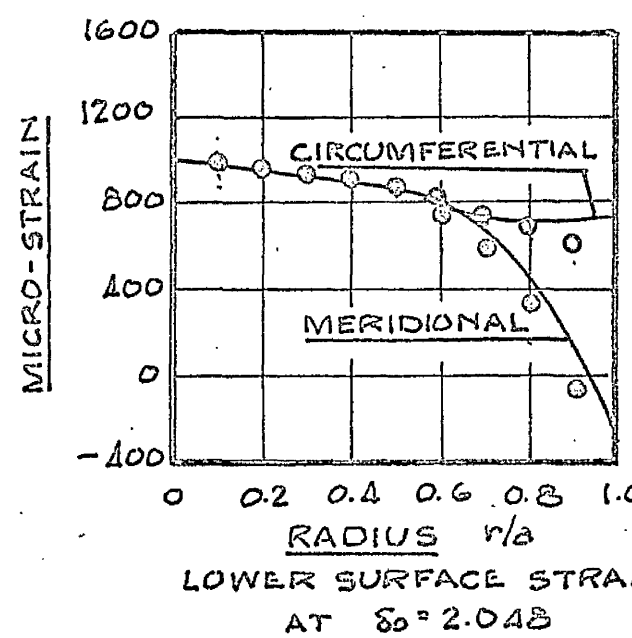

LOWER SURFACE STRAIN
AT $\delta_0 = 2.048$

FIG. VII.1c Comparison of experimental and theoretical surface strains. PRESSURE LOAD $\lambda = 23$

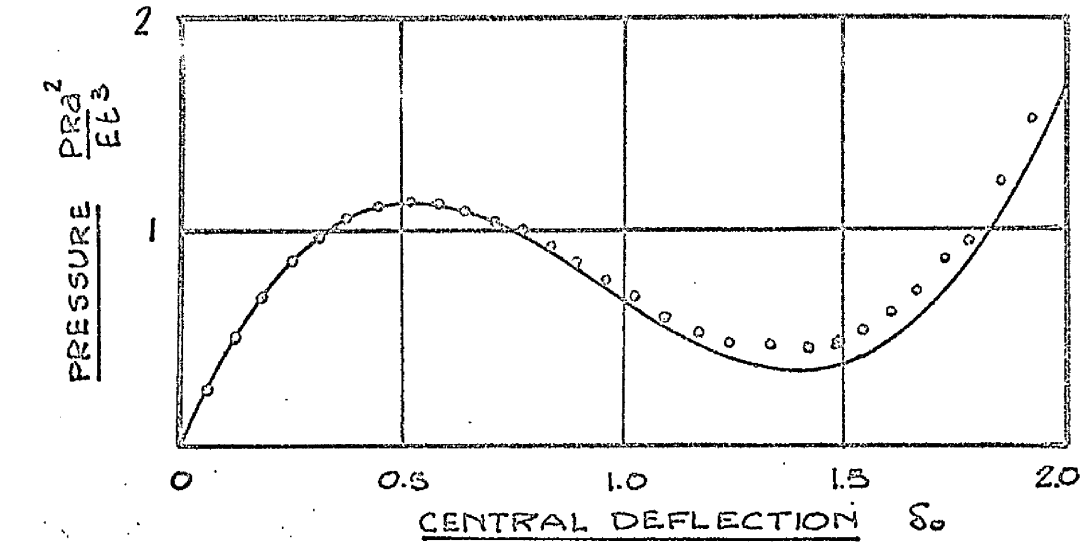

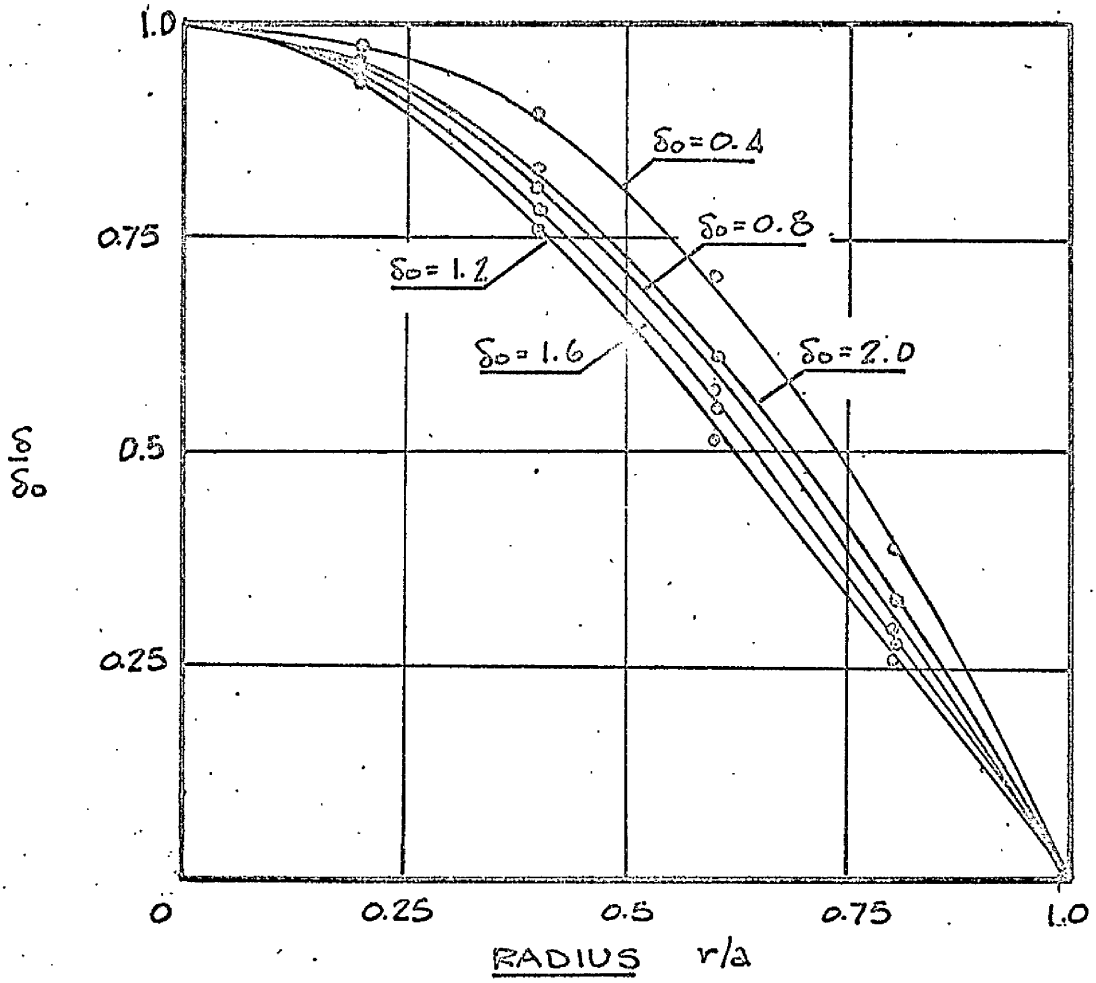

FIG. VII.2a Comparison of experimental and theoretical equilibrium paths and variation of deflected form.
PRESSURE LOAD $\lambda = 42$

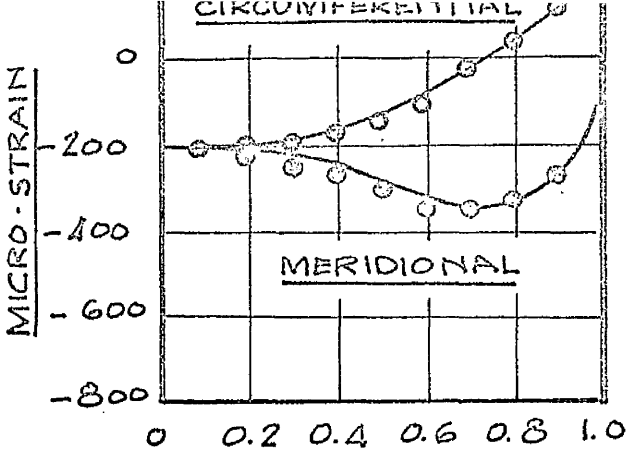

UPPER SURFACE STRAIN
AT $\delta_0 = 0.448$

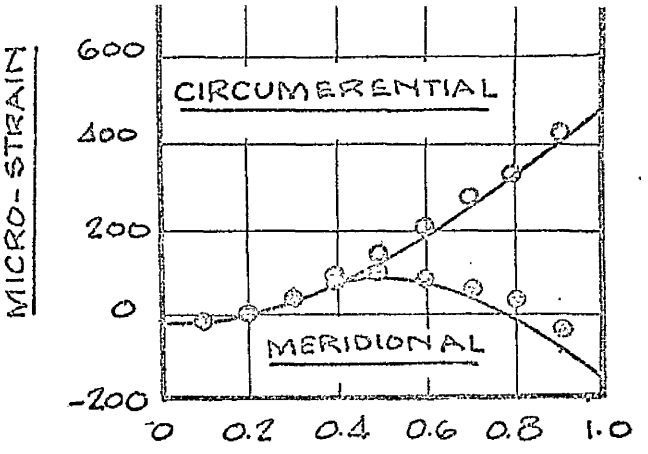

LOWER SURFACE STRAIN
AT $\delta_0 = 0.448$

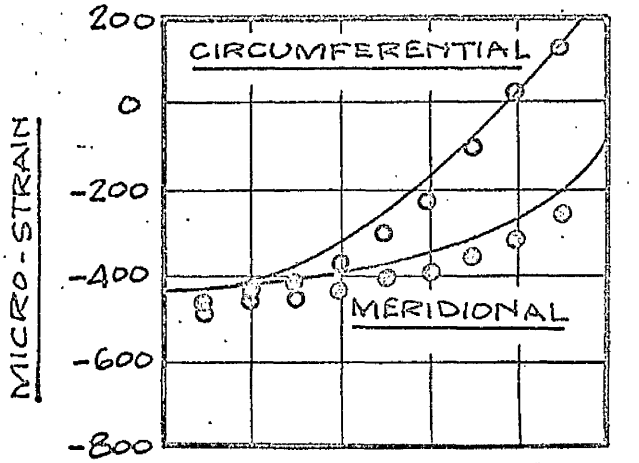

UPPER SURFACE STRAIN
AT $\delta_0 = 0.768$

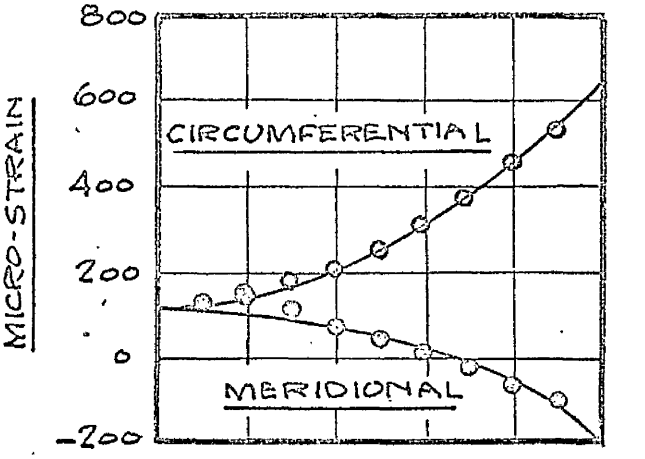

LOWER SURFACE STRAIN
AT $\delta_0 = 0.768$

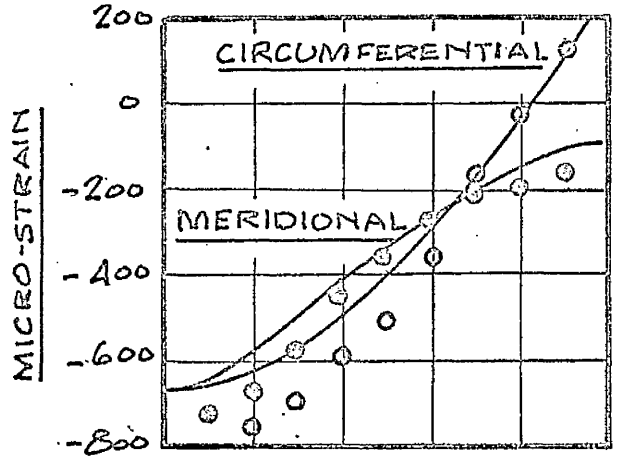

UPPER SURFACE STRAIN
AT $\delta_0 = 1.088$

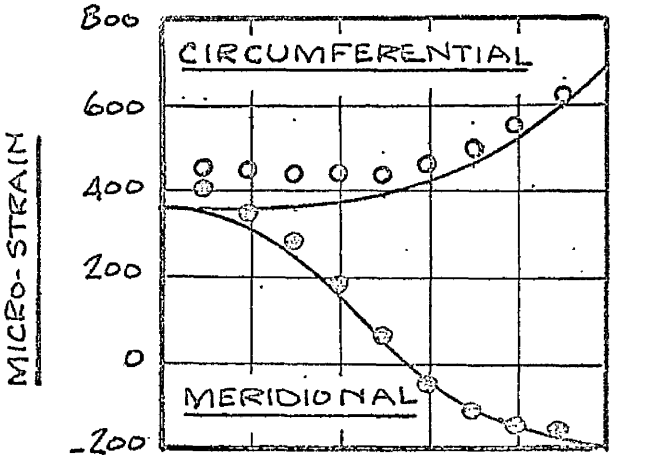

LOWER SURFACE STRAIN
AT $\delta_0 = 1.088$

FIG. VII.2b Comparison of experimental and theoretical surface strains. PRESSURE LOAD $\lambda = 42$

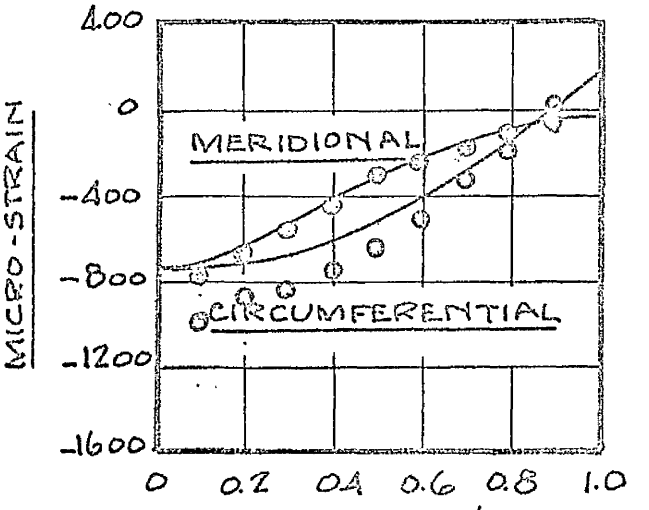

UPPER SURFACE STRAIN
AT $\delta_0 = 1.408$

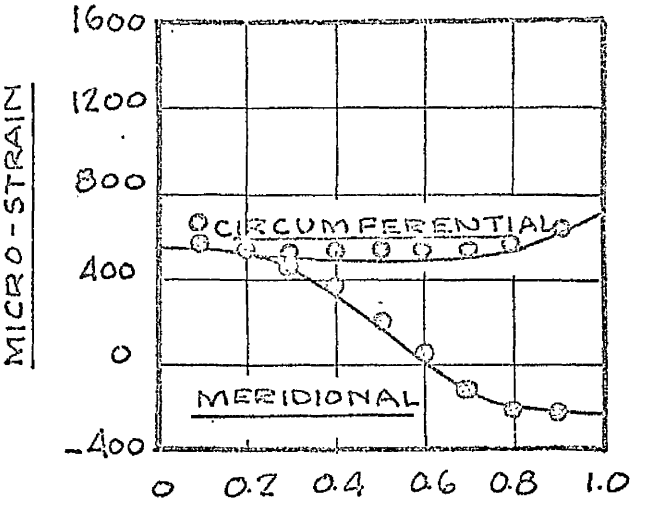

LOWER SURFACE STRAIN
AT $\delta_0 = 1.408$

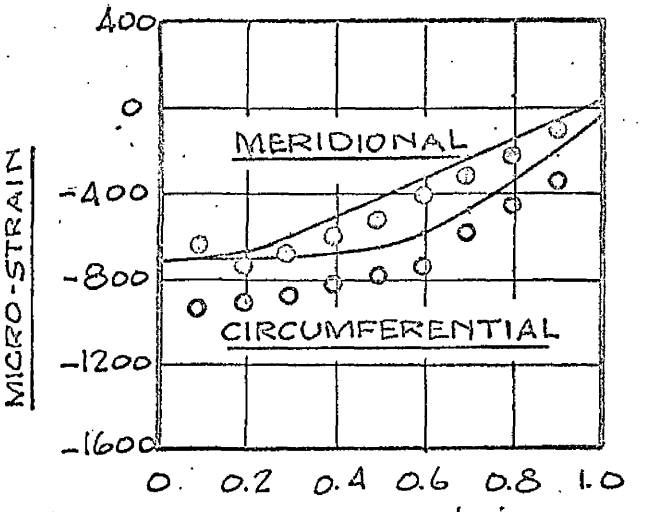

UPPER SURFACE STRAIN
AT $\delta_0 = 1.728$

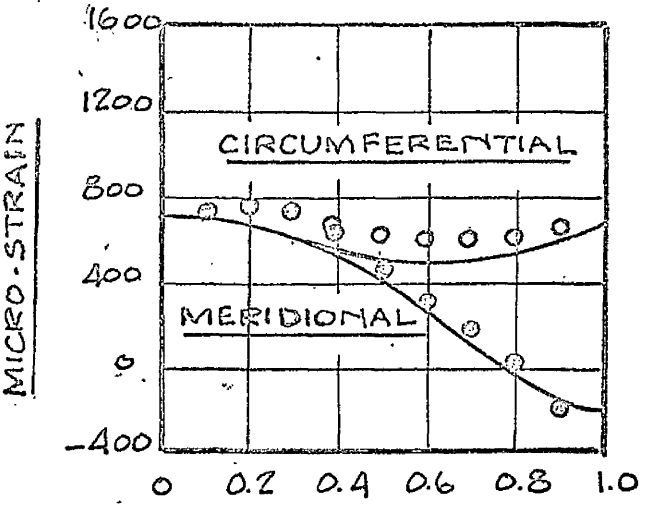

LOWER SURFACE STRAIN
AT $\delta_0 = 1.408$

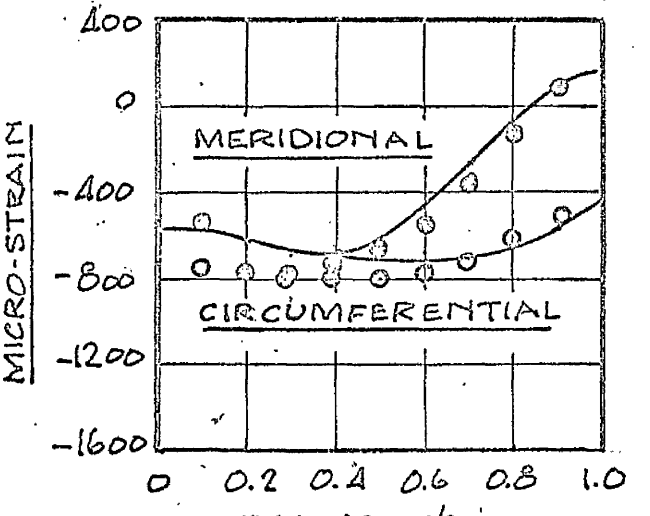

UPPER SURFACE STRAIN
AT $\delta_0 = 2.048$

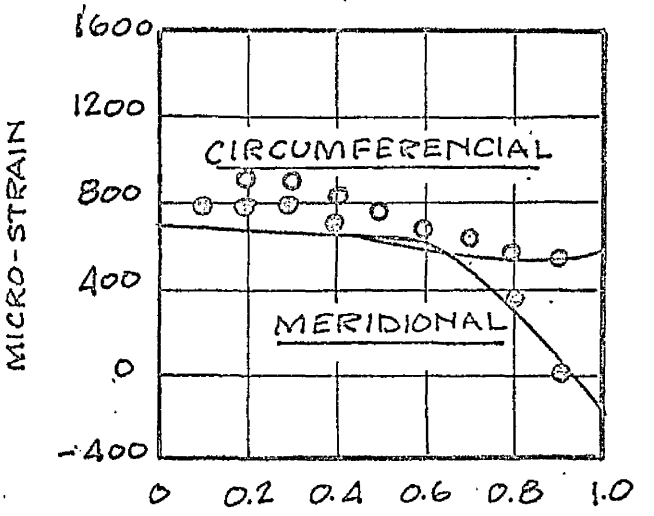

LOWER SURFACE STRAIN
AT $\delta_0 = 2.048$

FIG. VII.2c Comparison of experimental and theoretical surface strains. PRESSURE LOAD $\lambda = 42$

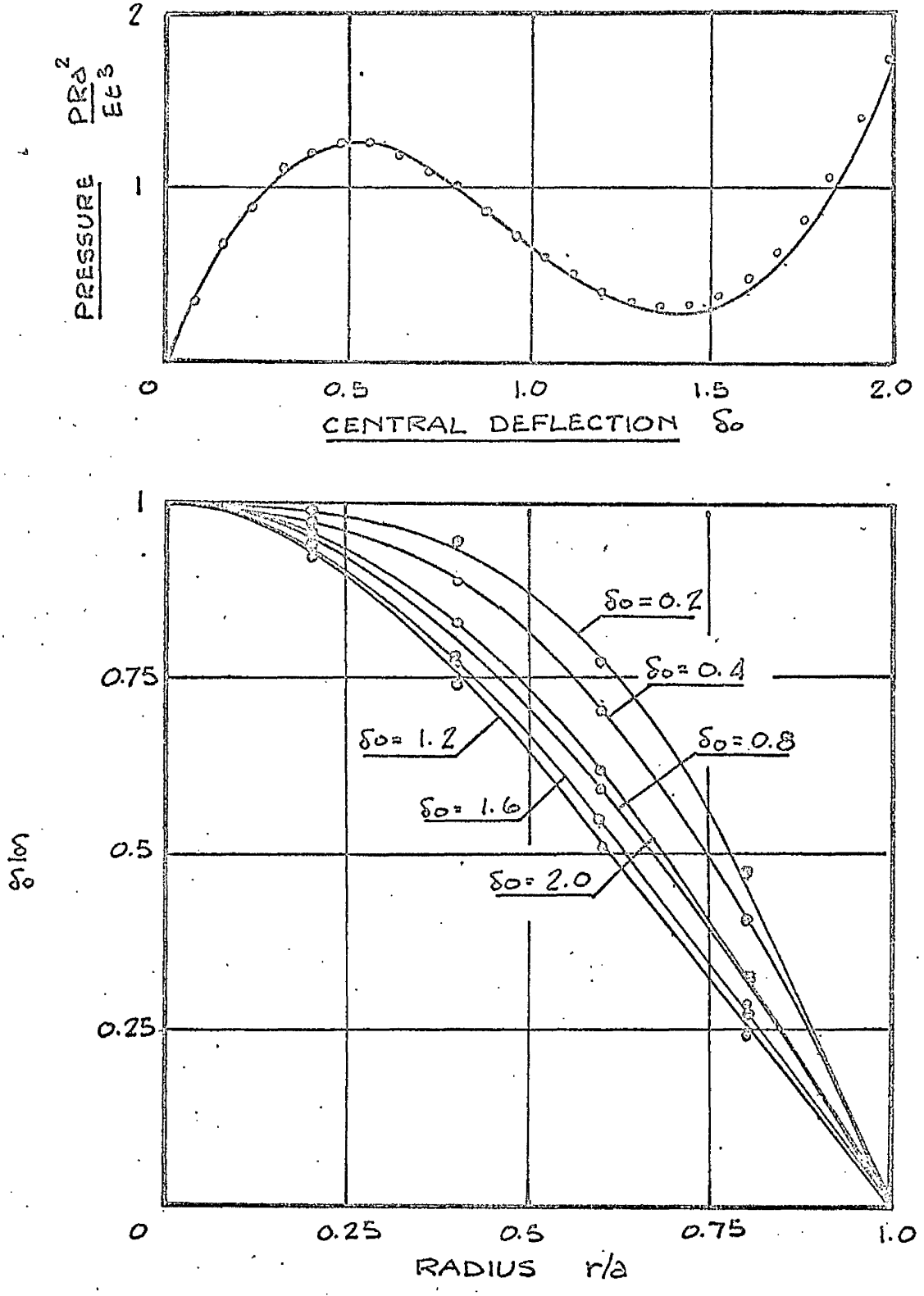

FIG. VII.3a Comparison of experimental and theoretical equilibrium paths and variation of deflected form.
PRESSURE LOAD $\lambda = 48$

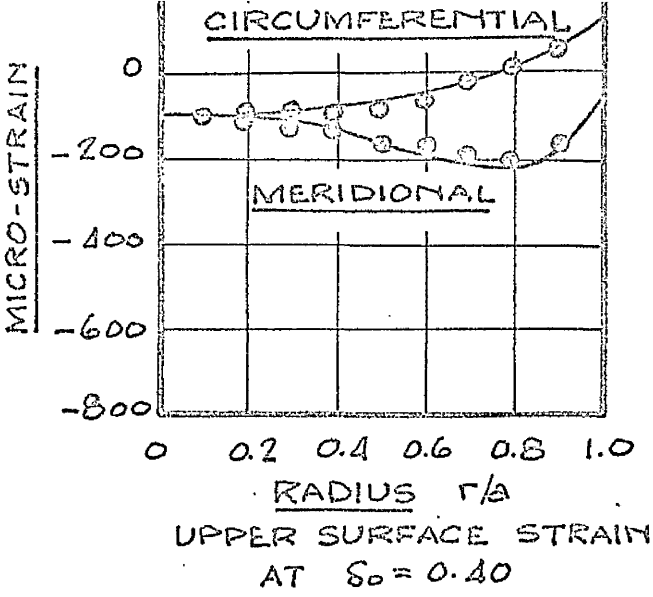

UPPER SURFACE STRAIN AT $\delta_0 = 0.40$

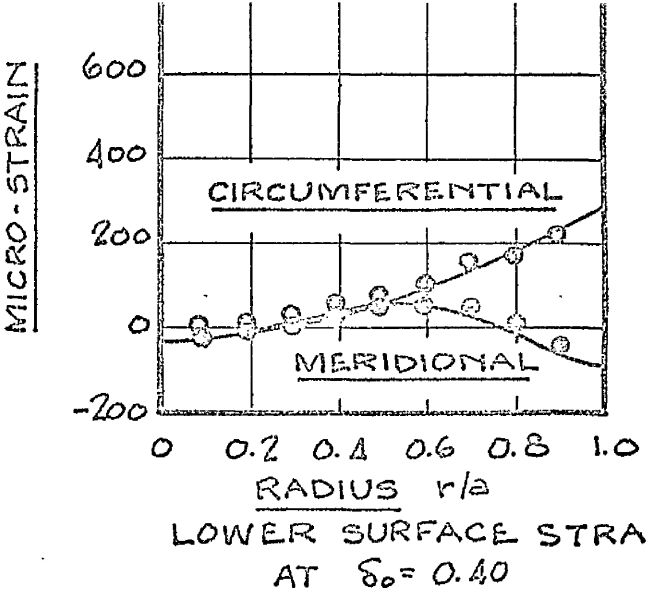

LOWER SURFACE STRAIN AT $\delta_0 = 0.40$

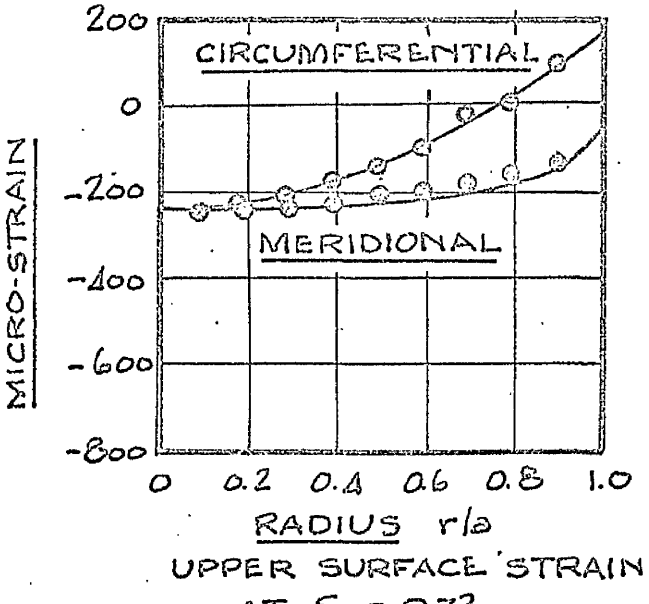

UPPER SURFACE STRAIN AT $\delta_0 = 0.72$

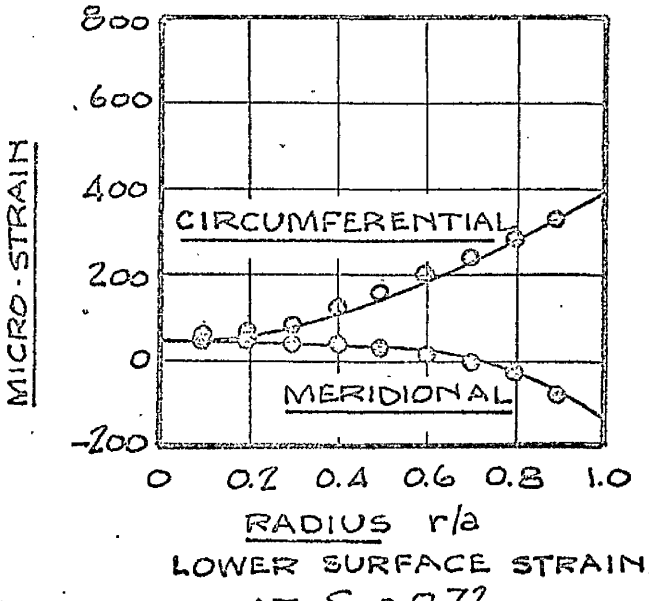

LOWER SURFACE STRAIN AT $\delta_0 = 0.72$

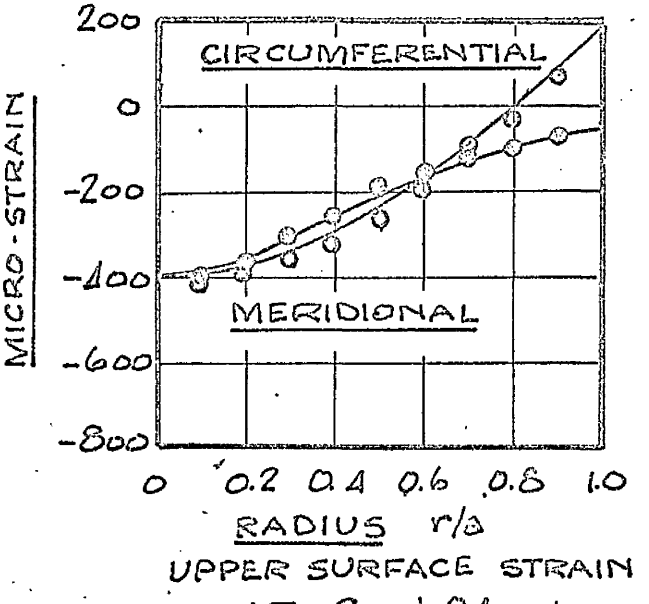

UPPER SURFACE STRAIN AT $\delta_0 = 1.04$.

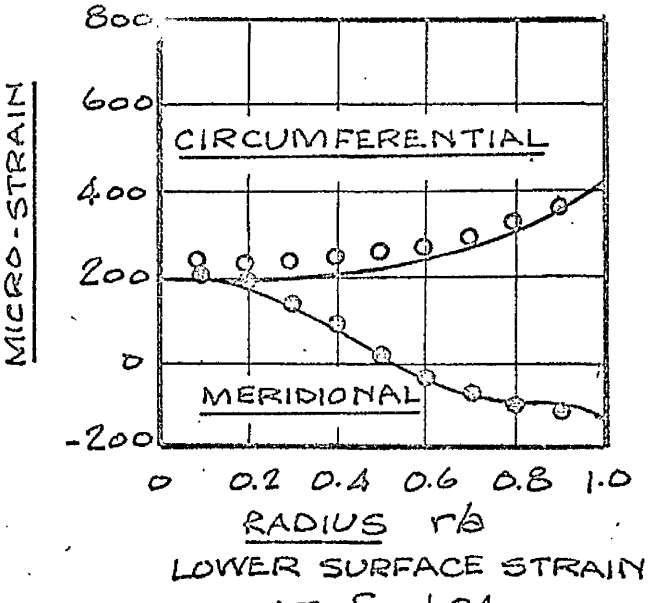

LOWER SURFACE STRAIN AT $\delta_0 = 1.04$

FIG. VII.3b Comparison of experimental and theoretical surface strains. PRESSURE LOAD $\lambda = 48$

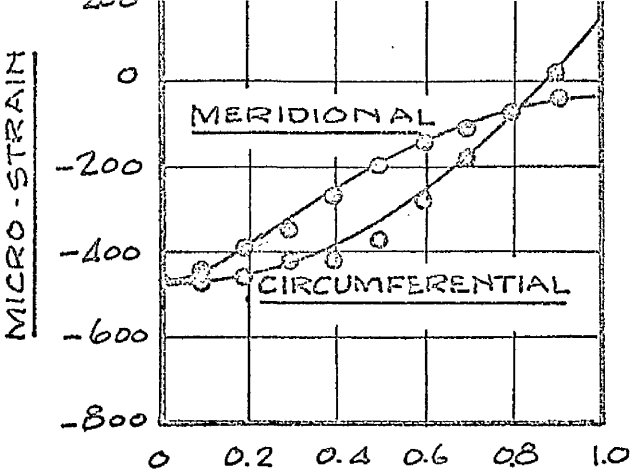

UPPER SURFACE STRAIN
AT $\delta_0 = 1.36$.

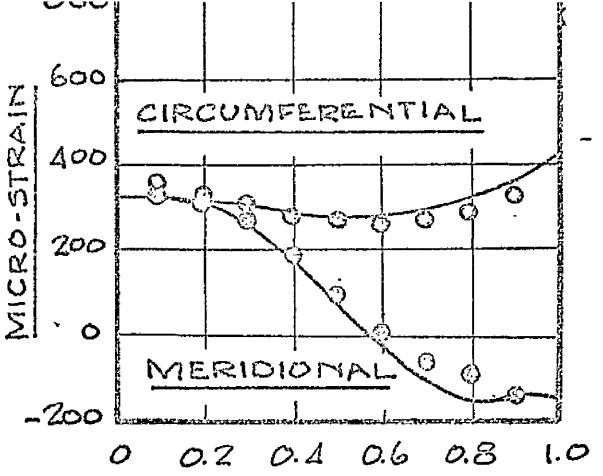

LOWER SURFACE STRAIN
AT $\delta_0 = 1.36$

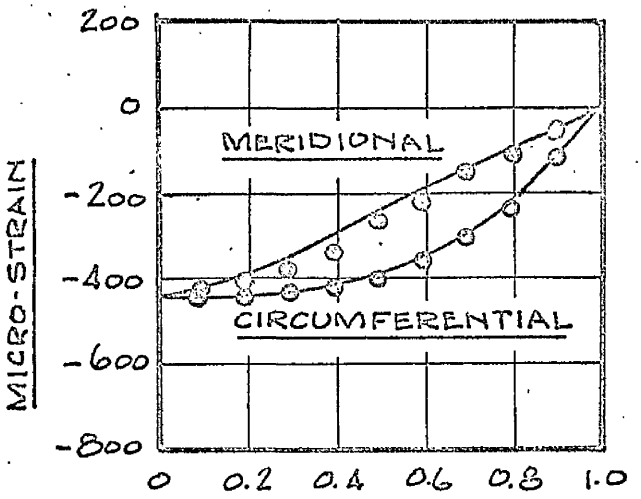

UPPER SURFACE STRAIN
AT $\delta_0 = 1.68$

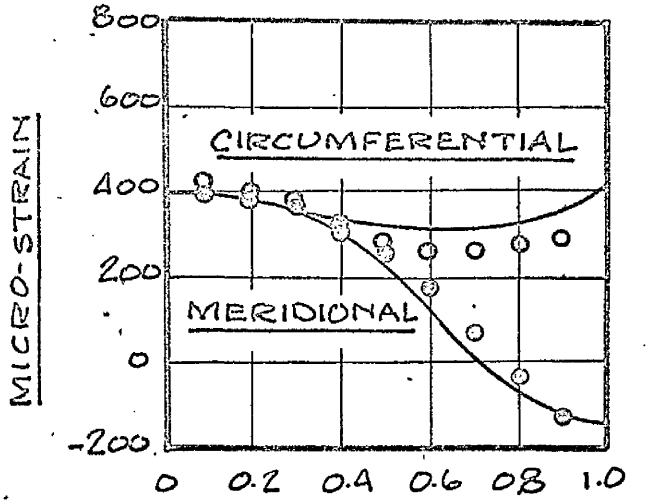

LOWER SURFACE STRAIN
AT $\delta_0 = 1.68$

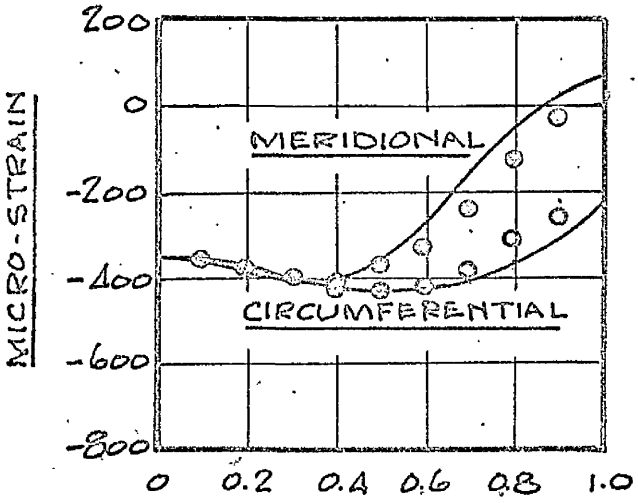

UPPER SURFACE STRAIN
AT $\delta_0 = 2.0$

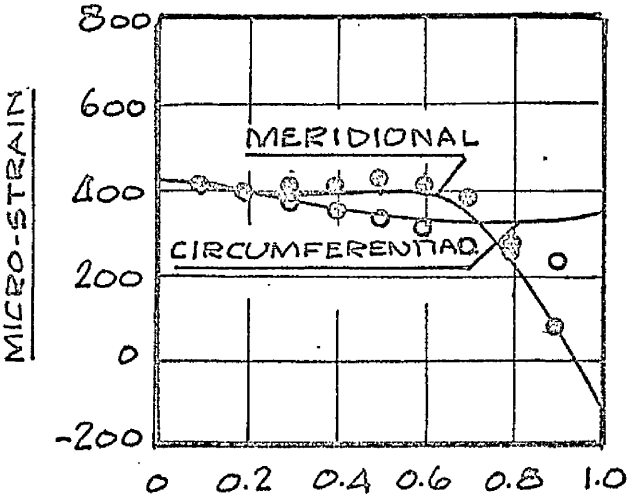

LOWER SURFACE STRAIN
AT $\delta_0 = 2.0$

FIG. VII.3c Comparison of experimental and theoretical surface strains. PRESSURE LOAD $\lambda = 48$

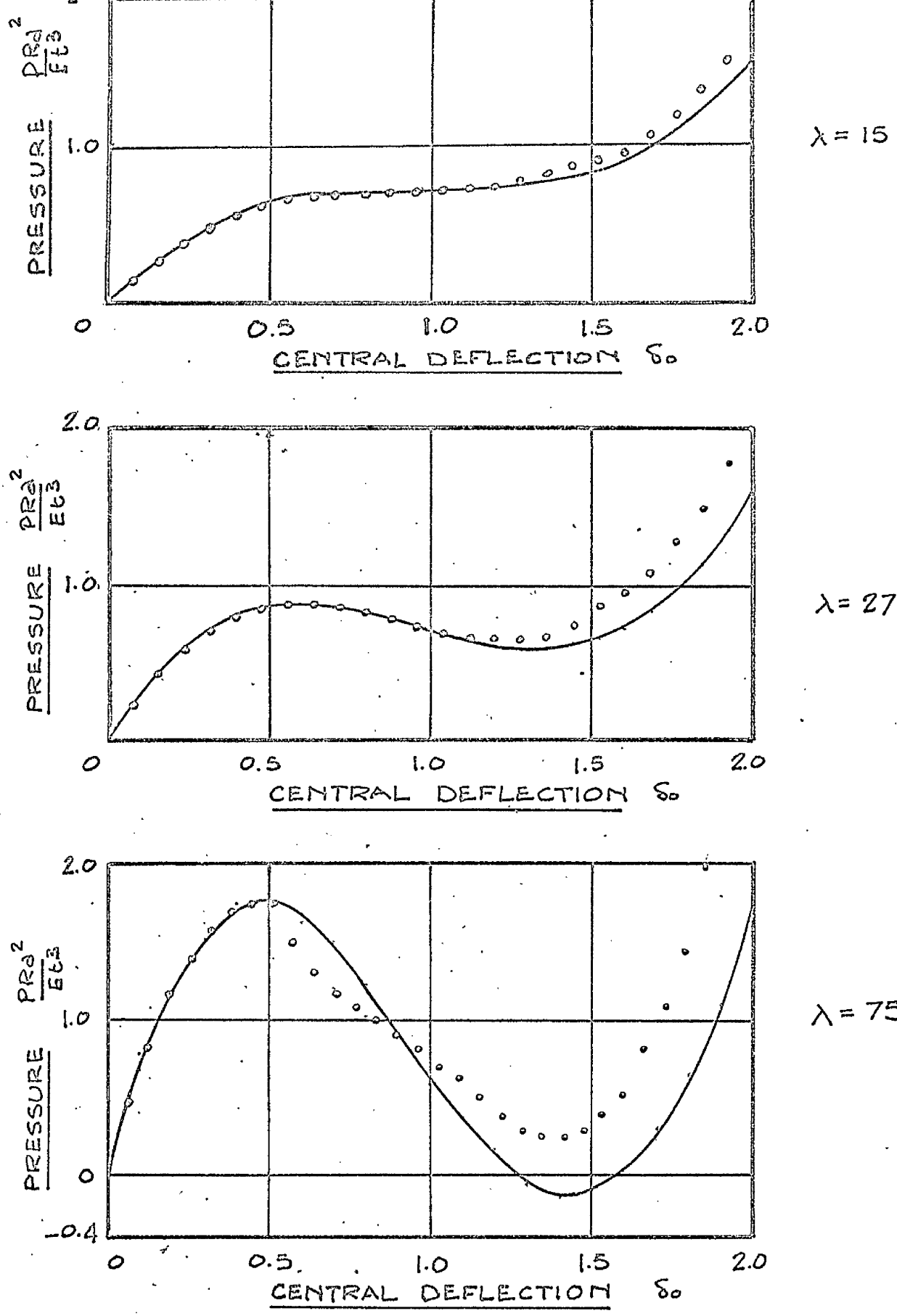

FIG. VII.4 Comparison of experimental and theoretical equilibrium paths
PRESSURE LOAD

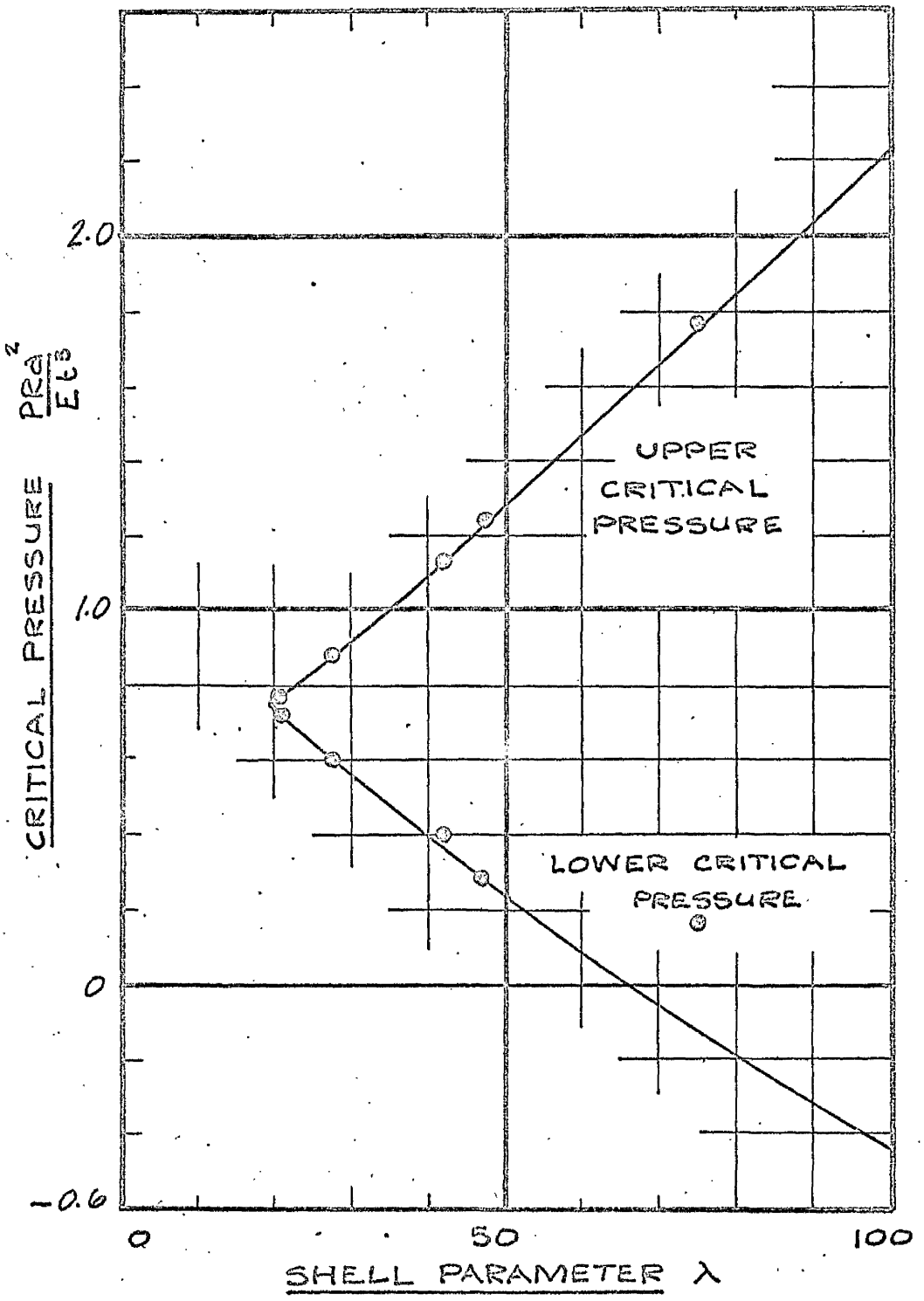

FIG. VII.5 The comparison of experimental and theoretical critical pressure of freely supported shallow spherical shells

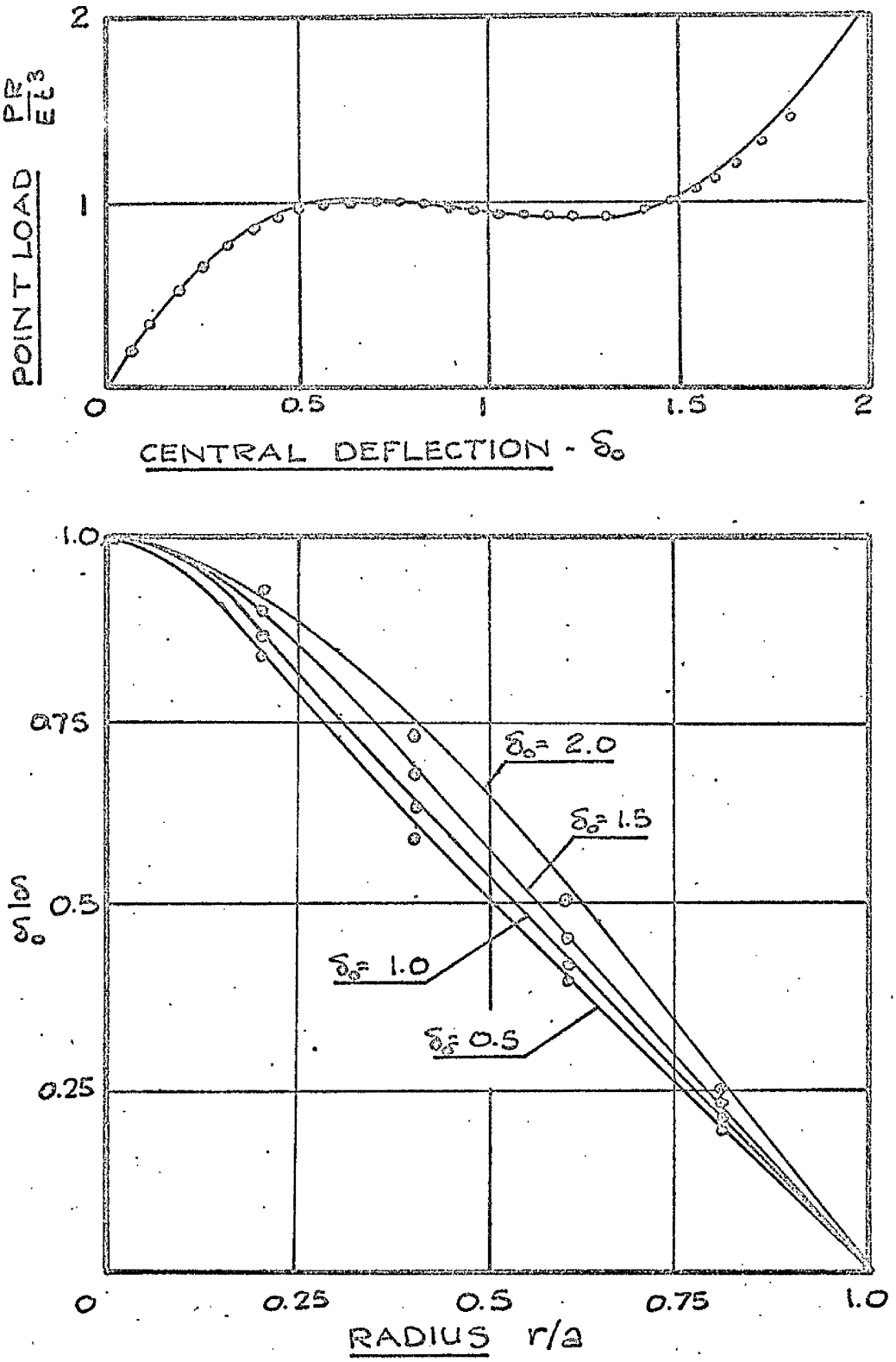

FIG. VII.6a Comparison of experimental and theoretical equilibrium paths and variation of deflected form.
POINT LOAD $\lambda = 23$

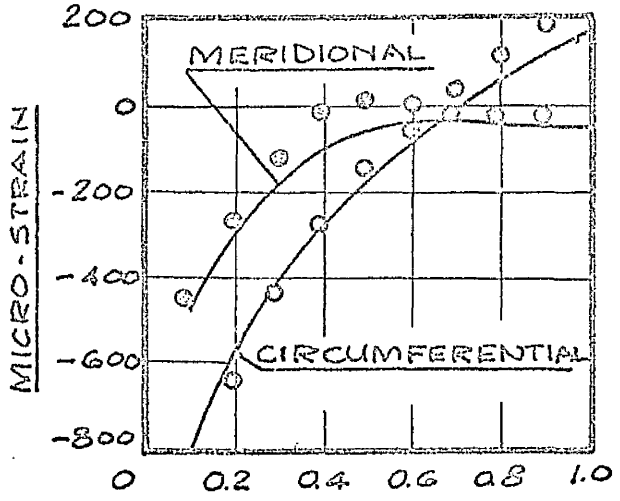

UPPER SURFACE STRAIN AT $\delta_0 = 0.448$

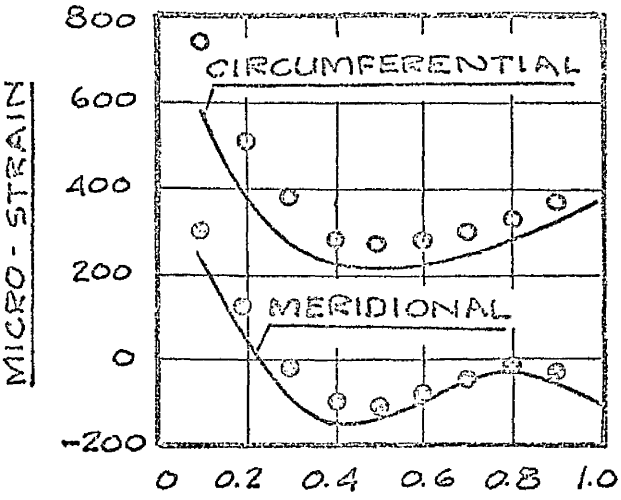

LOWER SURFACE STRAIN AT $\delta_0 = 0.448$

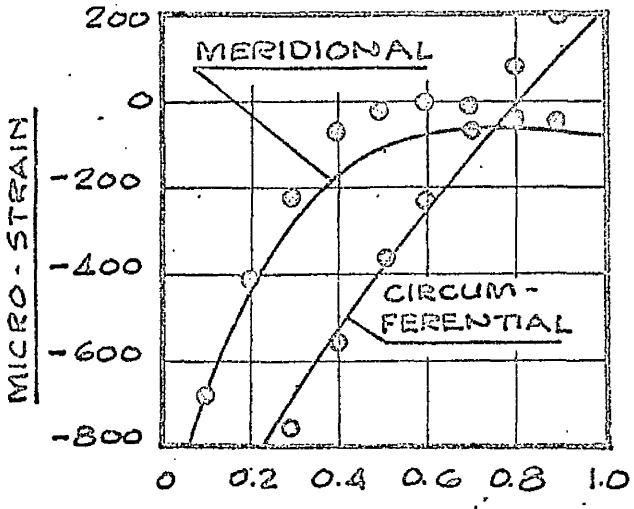

UPPER SURFACE STRAIN AT $\delta_0 = 0.768$

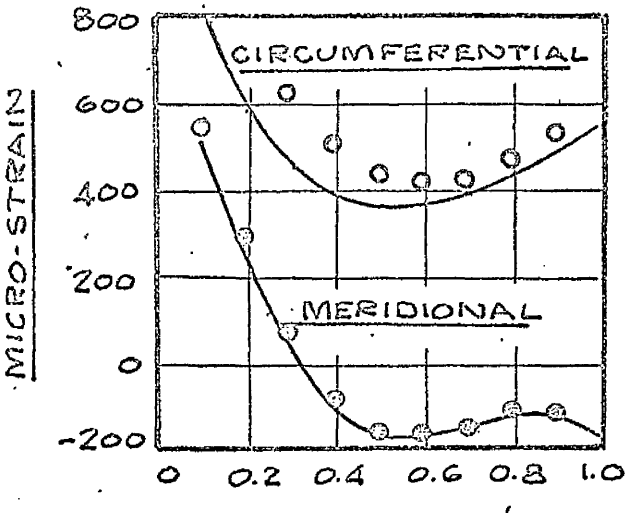

LOWER SURFACE STRAIN AT $\delta_0 = 0.768$

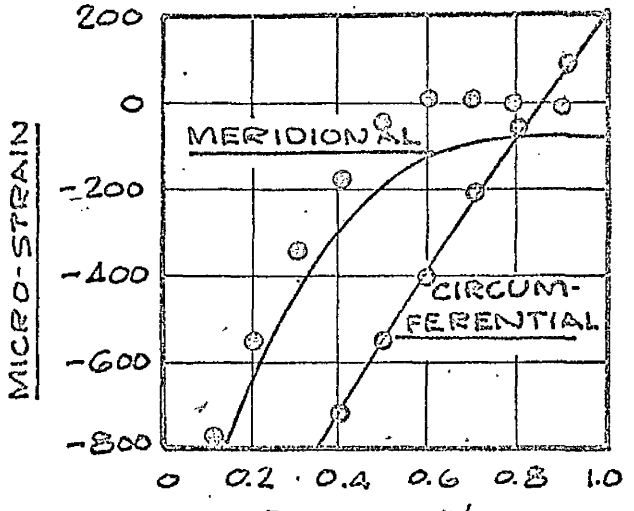

UPPER SURFACE STRAIN AT $\delta_0 = 1.088$

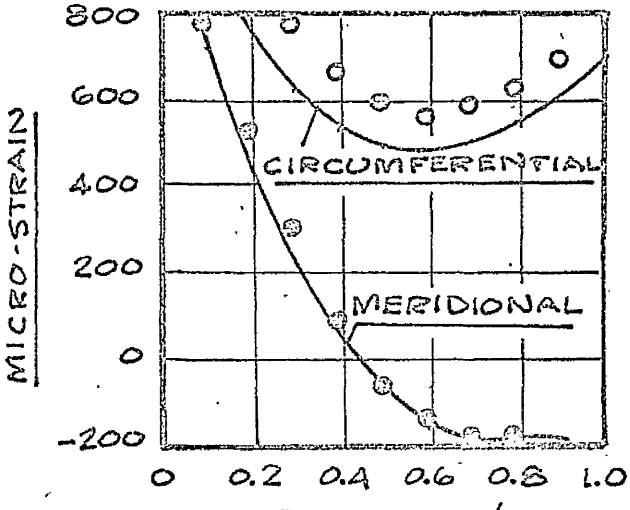

LOWER SURFACE STRAIN AT $\delta_0 = 1.088$

FIG. VII.6b Comparison of experimental and theoretical surface strains. POINT LOAD $\lambda = 23$

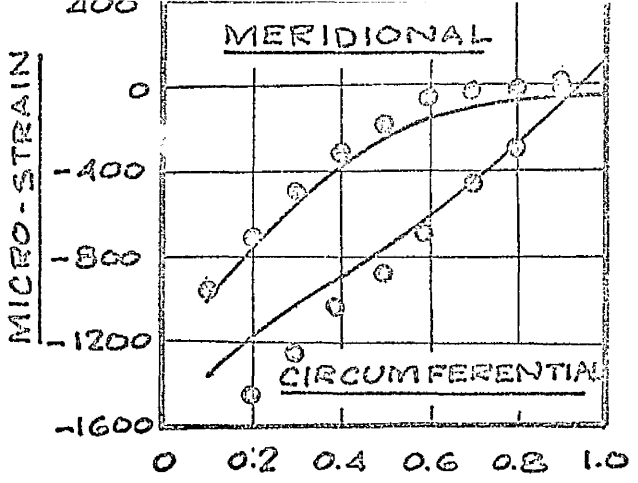

UPPER SURFACE STRAINS
AT $\delta_0 = 1.408$

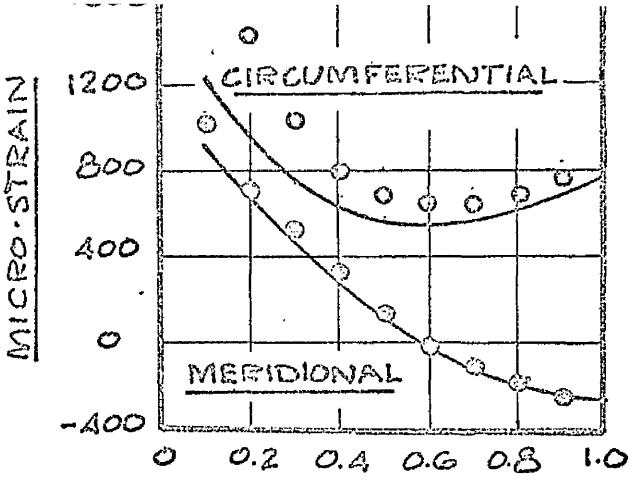

LOWER SURFACE STRAINS
AT $\delta_0 = 1.408$

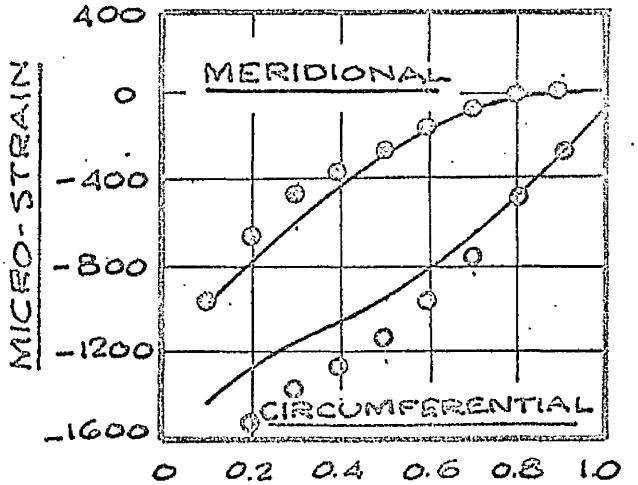

UPPER SURFACE STRAINS
AT $\delta_0 = 1.728$

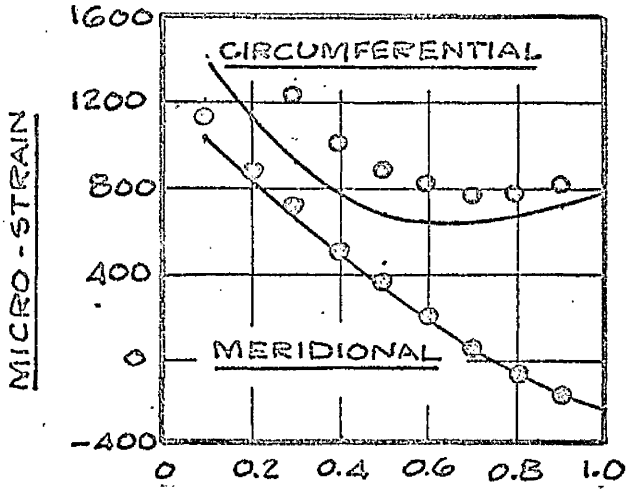

LOWER SURFACE STRAINS
AT $\delta_0 = 1.728$

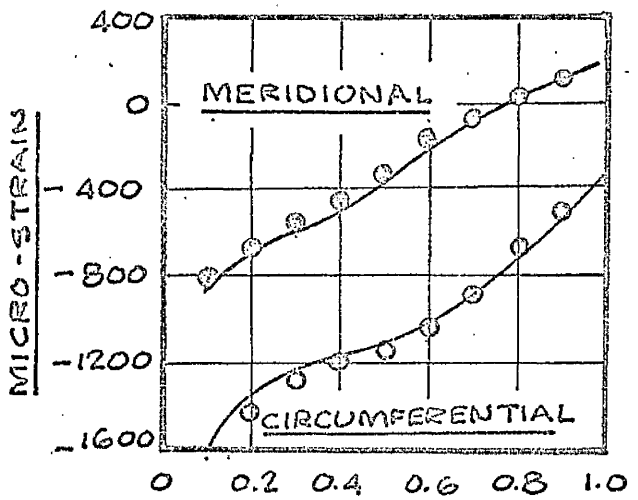

UPPER SURFACE STRAINS
AT $\delta_0 = 2.048$

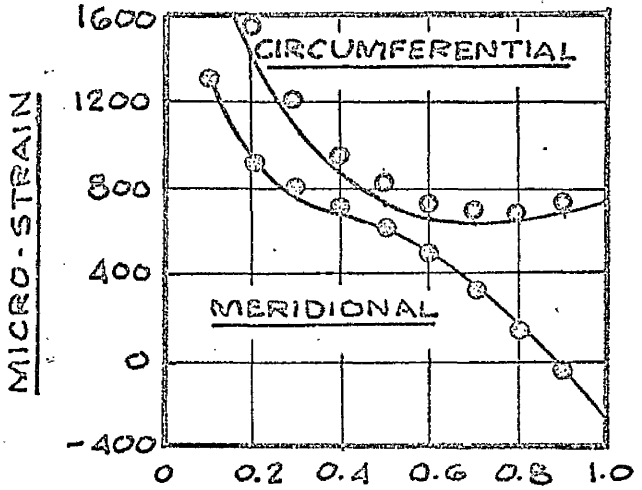

LOWER SURFACE STRAINS
AT $\delta_0 = 2.048$

FIG. VII.6c Comparison of experimental and theoretical surface strains. POINT LOAD $\lambda = 23$

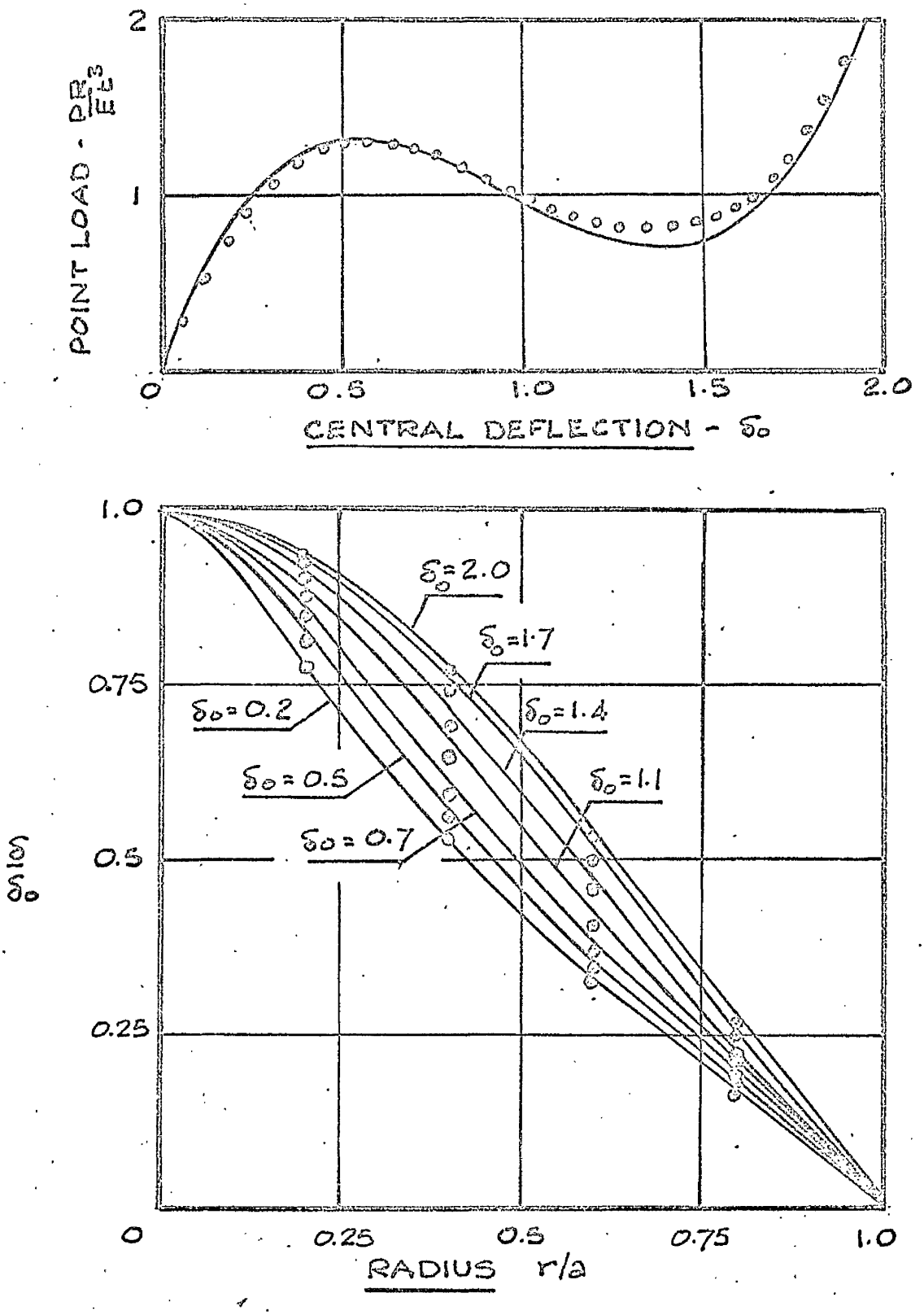

FIG. VII.7a Comparison of experimental and theoretical equilibrium paths and variation of deflected form.
POINT LOAD λ = 42

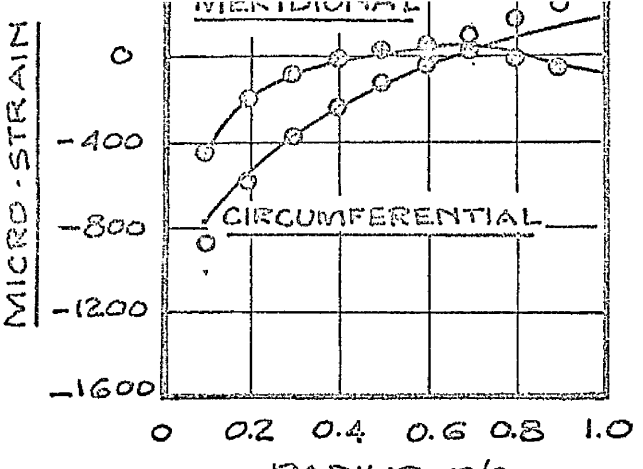

UPPER SURFACE STRAIN
AT $\delta_o = 0.448$

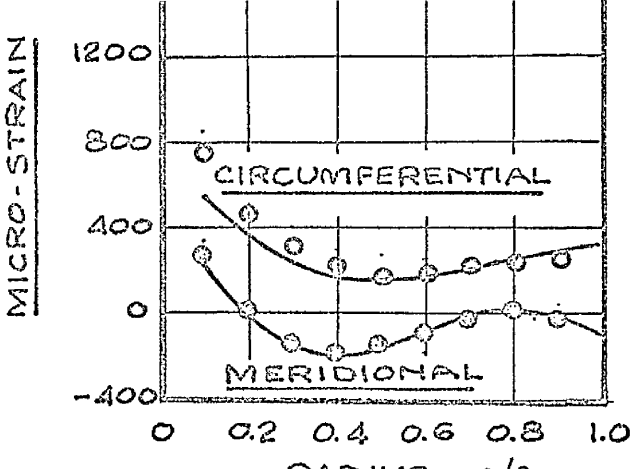

LOWER SURFACE STRAIN
AT $\delta_o = 0.448$

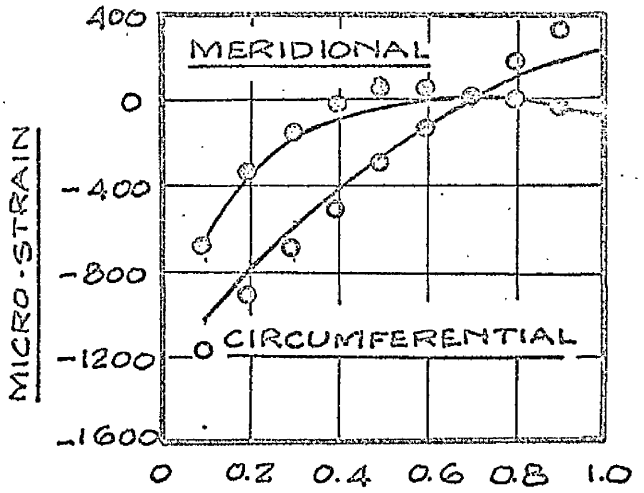

UPPER SURFACE STRAIN
AT $\delta_o = 0.768$

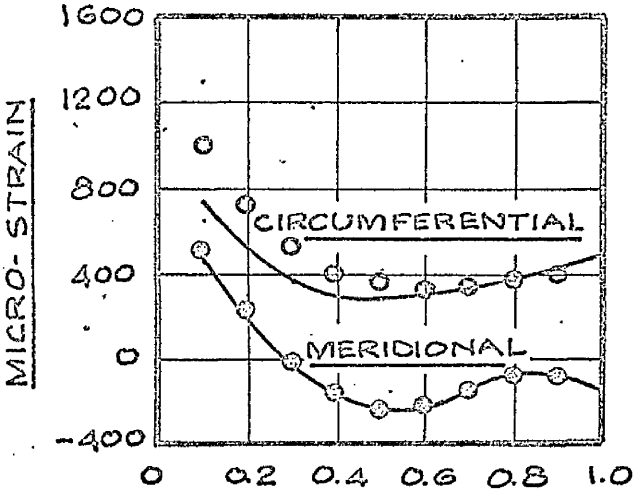

LOWERSURFACE STRAIN
AT $\delta_o = 0.768$

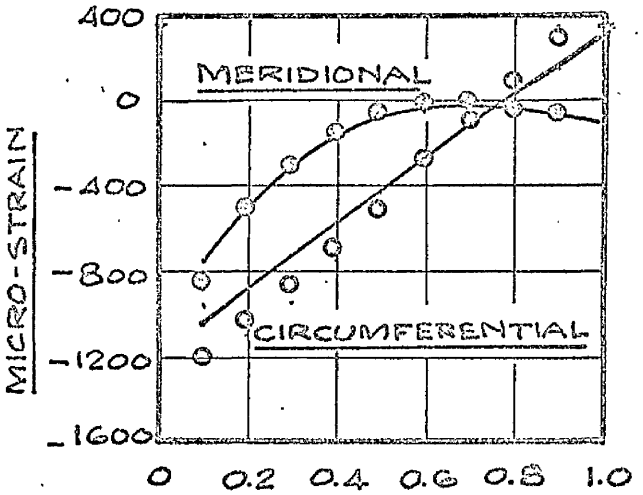

UPPER SURFACE STRAIN
AT $\delta_o = 1.088$

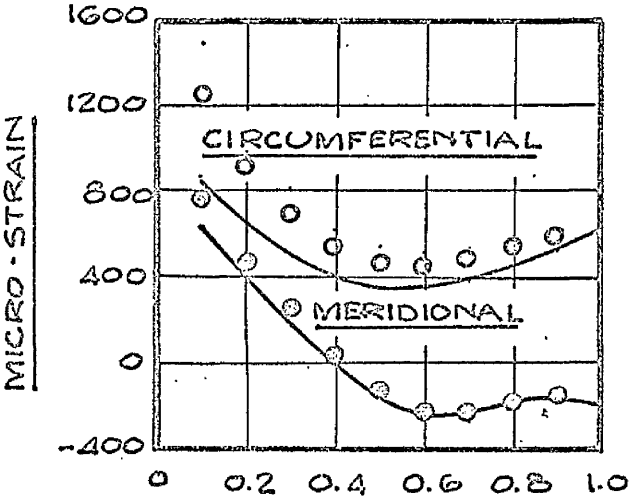

LOWER SURFACE STRAIN
AT $\delta_o = 1.088$

FIG. VII.7b Comparison of experimental and theoretical surface strains. POINT LOAD $\lambda = 42$

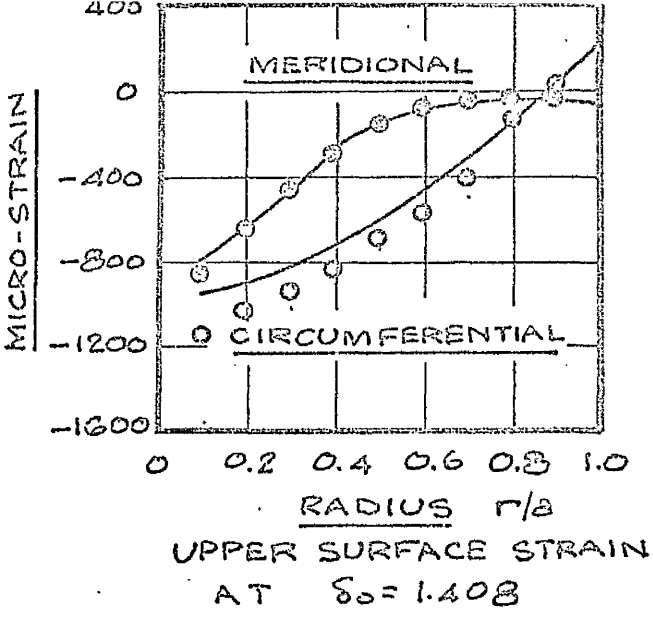

UPPER SURFACE STRAIN AT $\delta_0 = 1.408$

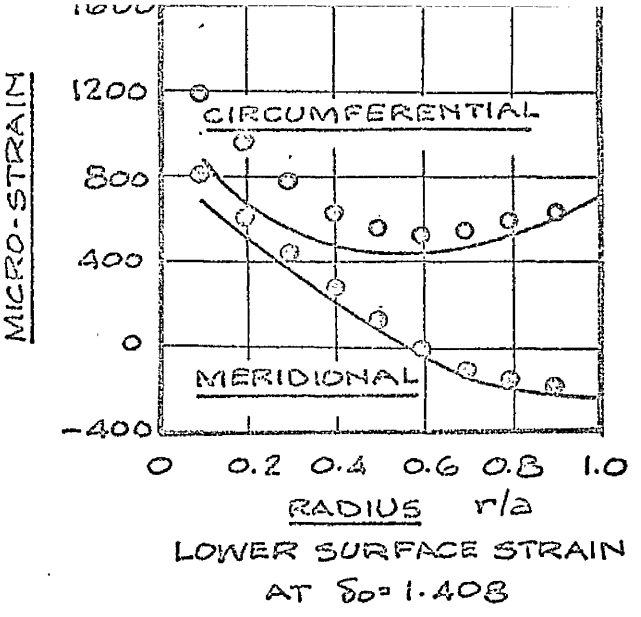

LOWER SURFACE STRAIN AT $\delta_0 = 1.408$

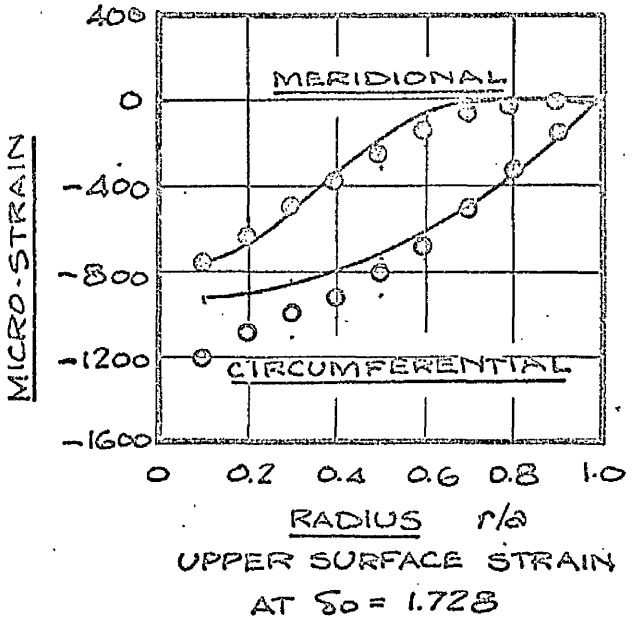

UPPER SURFACE STRAIN AT $\delta_0 = 1.728$

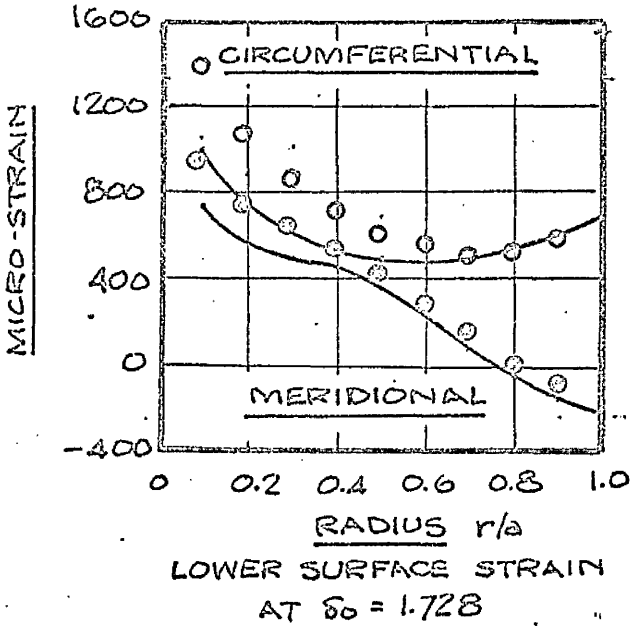

LOWER SURFACE STRAIN AT $\delta_0 = 1.728$

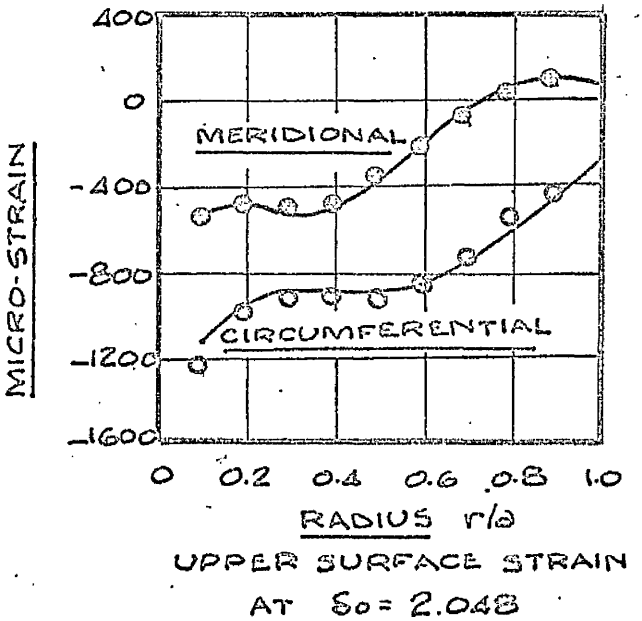

UPPER SURFACE STRAIN AT $\delta_0 = 2.048$

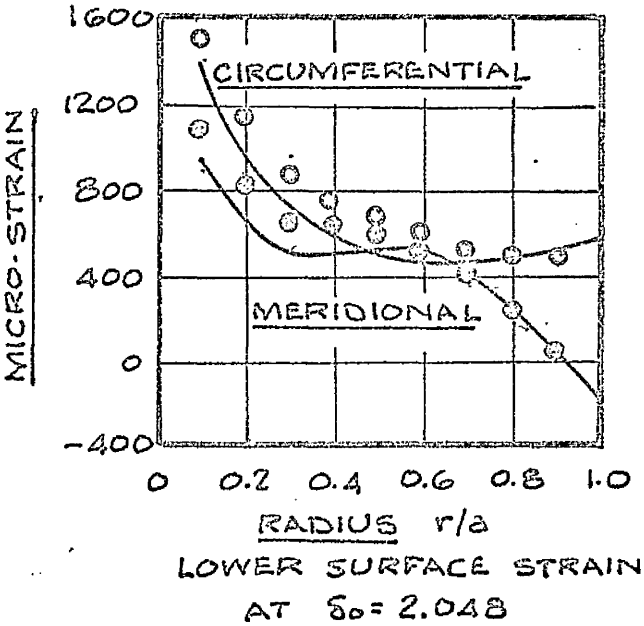

LOWER SURFACE STRAIN AT $\delta_0 = 2.048$

FIG. VII.7c Comparison of experimental and theoretical surface strains. POINT LOAD $\lambda = 42$

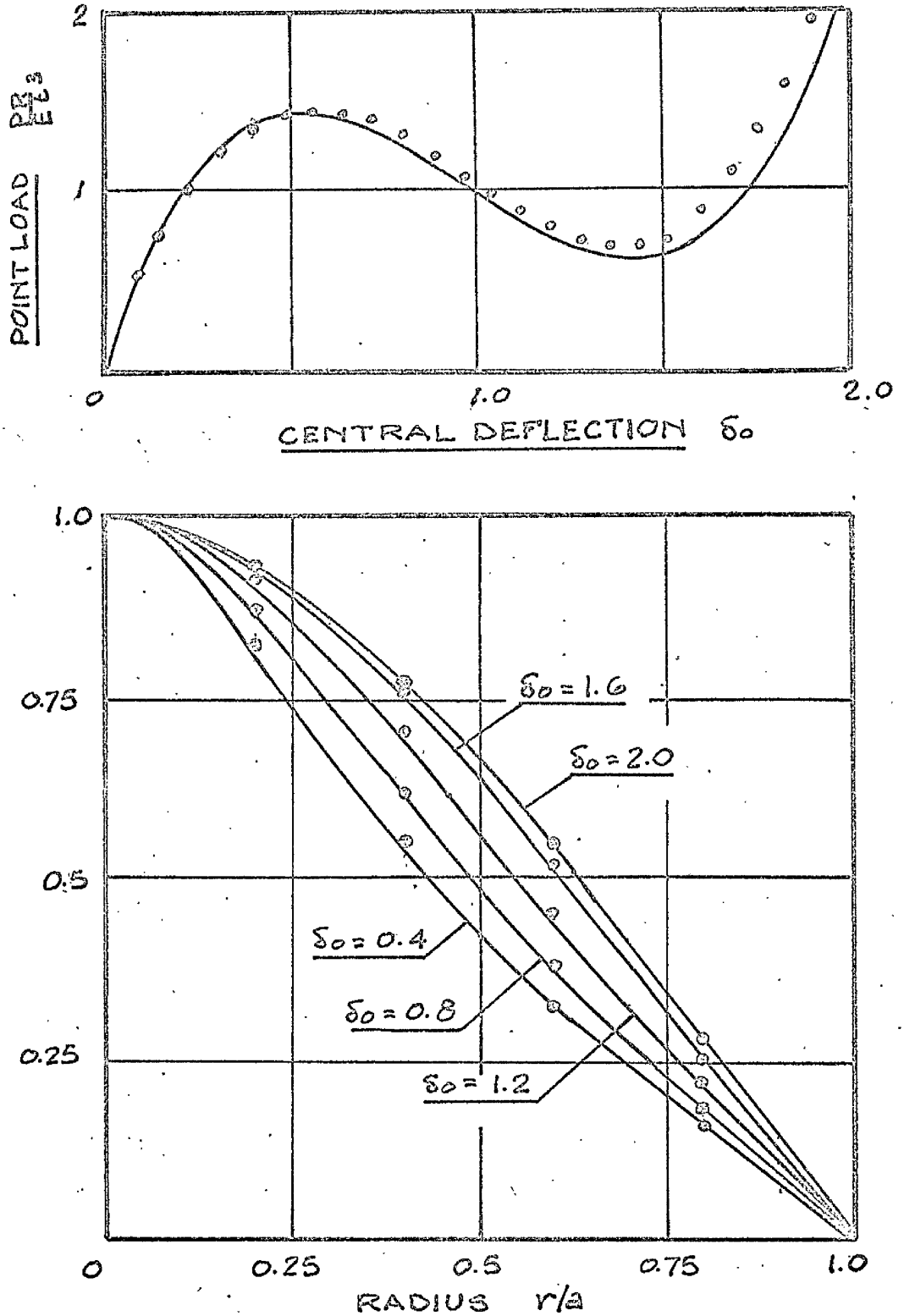

FIG. VII.8a Comparison of experimental and theoretical equilibrium paths and variation of deflected form.
POINT LOAD $\lambda = 48$

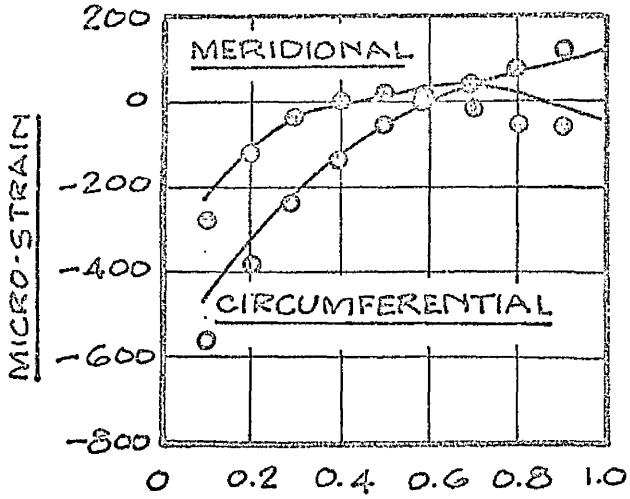

UPPER SURFACE STRAIN AT $\delta_0 = 0.40$

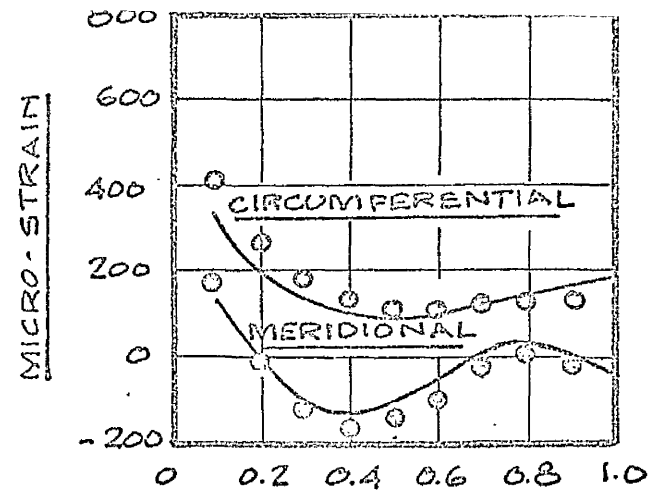

LOWER SURFACE STRAIN. AT $\delta_0 = 0.40$

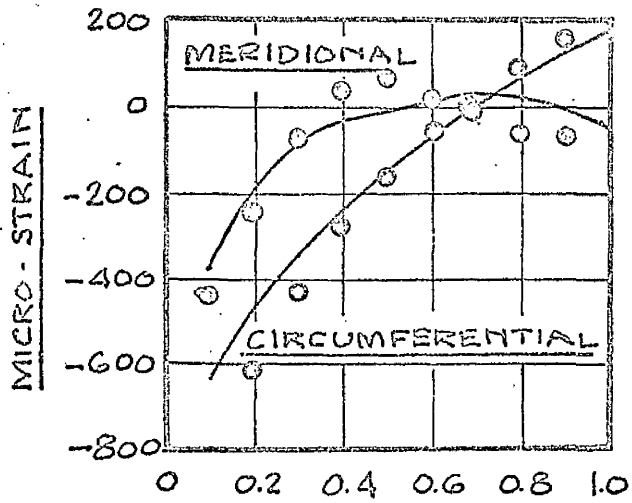

UPPER SURFACE STRAIN AT $\delta_0 = 0.72$

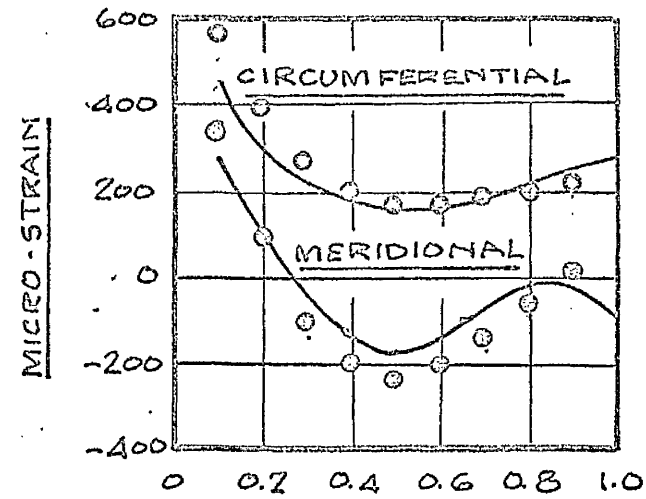

LOWER SURFACE STRAIN AT $\delta_0 = 0.72$

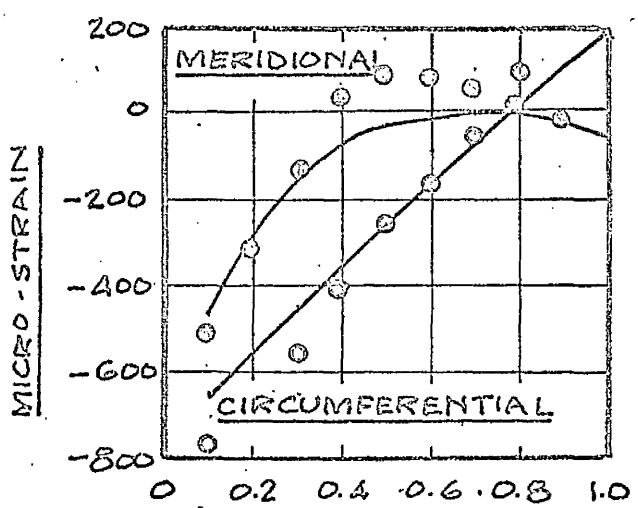

UPPER SURFACE STRAIN AT $\delta_0 = 1.04$

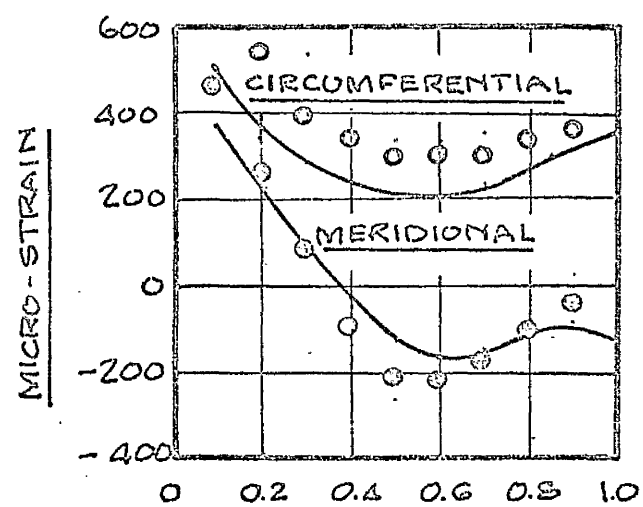

LOWER SURFACE STRAIN AT $\delta_0 = 1.04$.

FIG. VII.8b Comparison of experimental and theoretical surface strains. POINT LOAD $\lambda = 48$

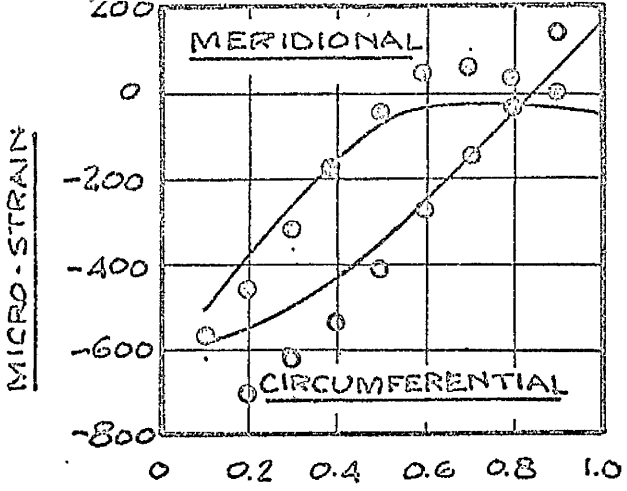

UPPER SURFACE STRAIN
AT $\delta_0 = 1.36$

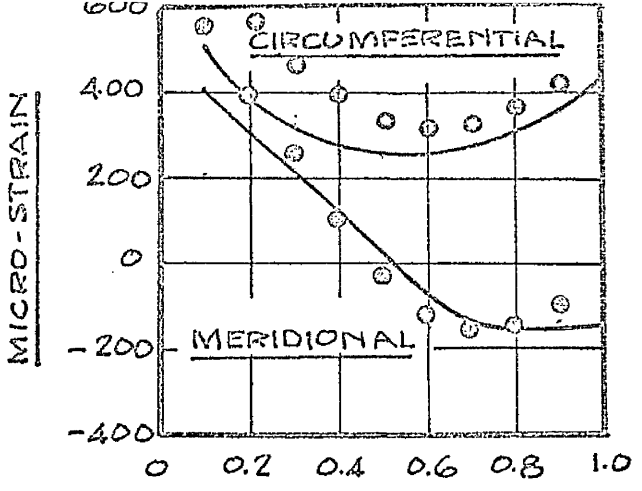

LOWER SURFACE STRAIN
AT $\delta_0 = 1.36$

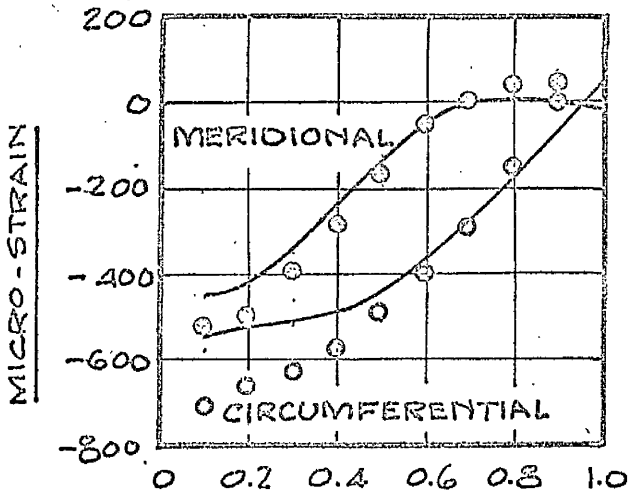

UPPER SURFACE STRAIN
AT $\delta_0 = 1.68$

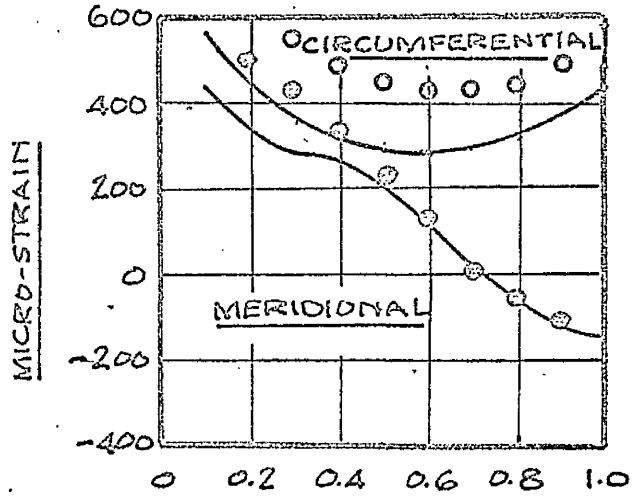

LOWER SURFACE STRAIN
AT $\delta_0 = 1.68$

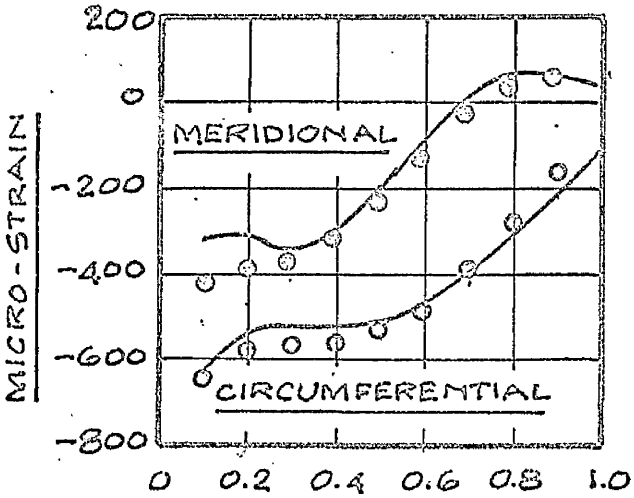

UPPER SURFACE STRAIN
AT $\delta_0 = 2.0$

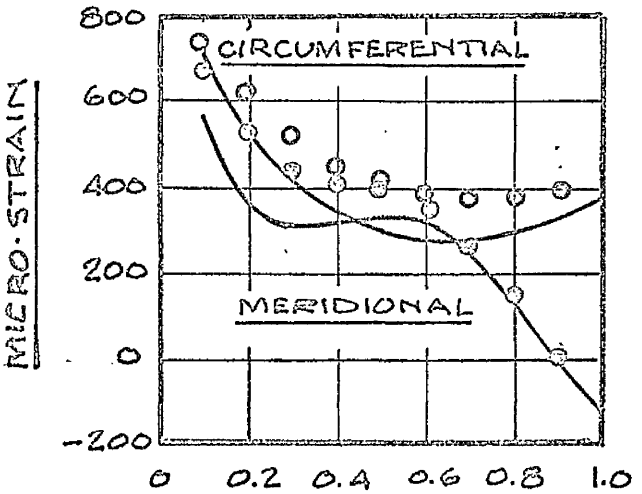

LOWER SURFACE STRAIN
AT $\delta_0 = 2.0$

FIG. VII.8c Comparison of experimental and theoretical surface strains. POINT LOAD $\lambda = 48$

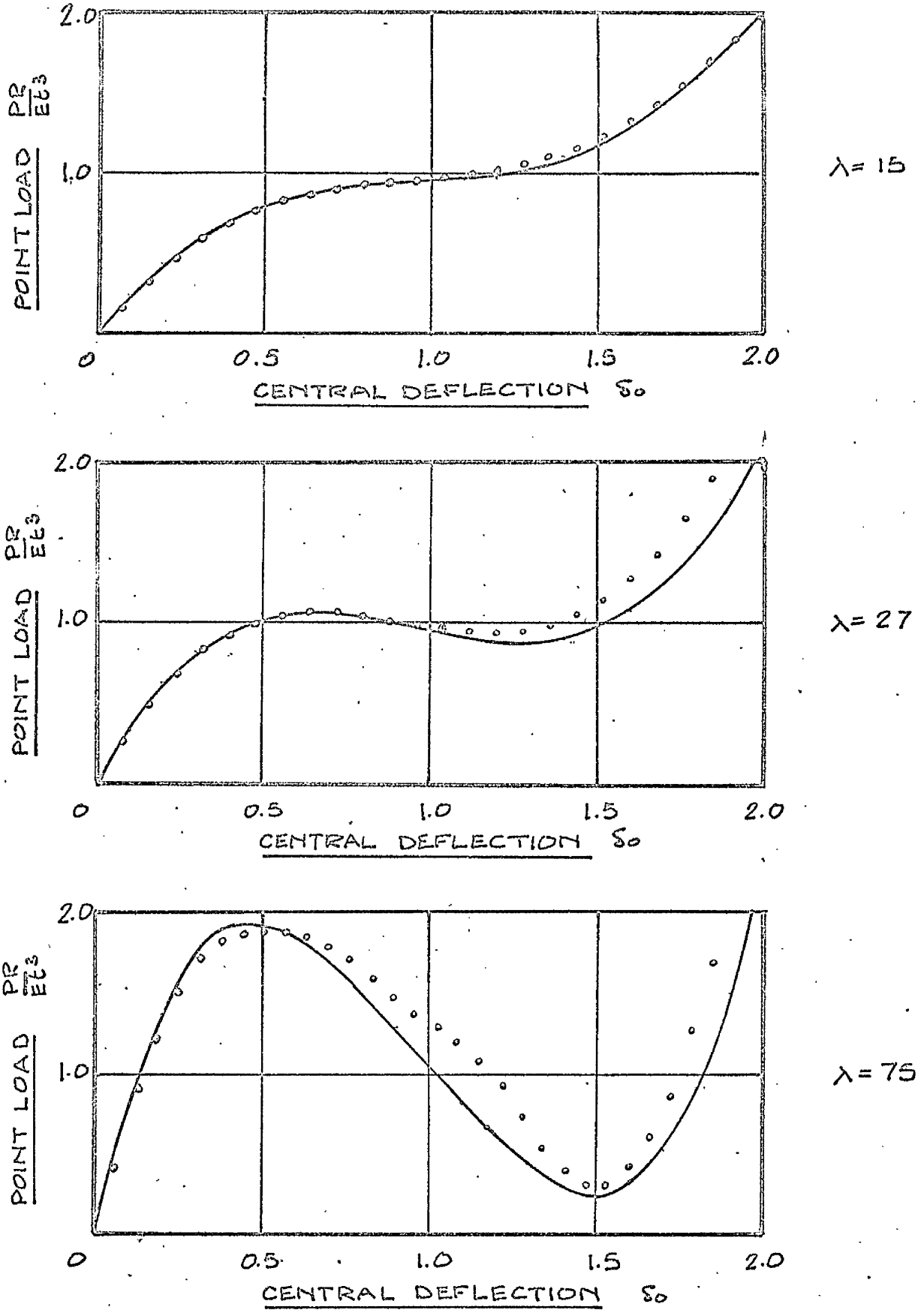

FIG. VII.9 Comparison of experimental and theoretical equilibrium paths
POINT LOAD

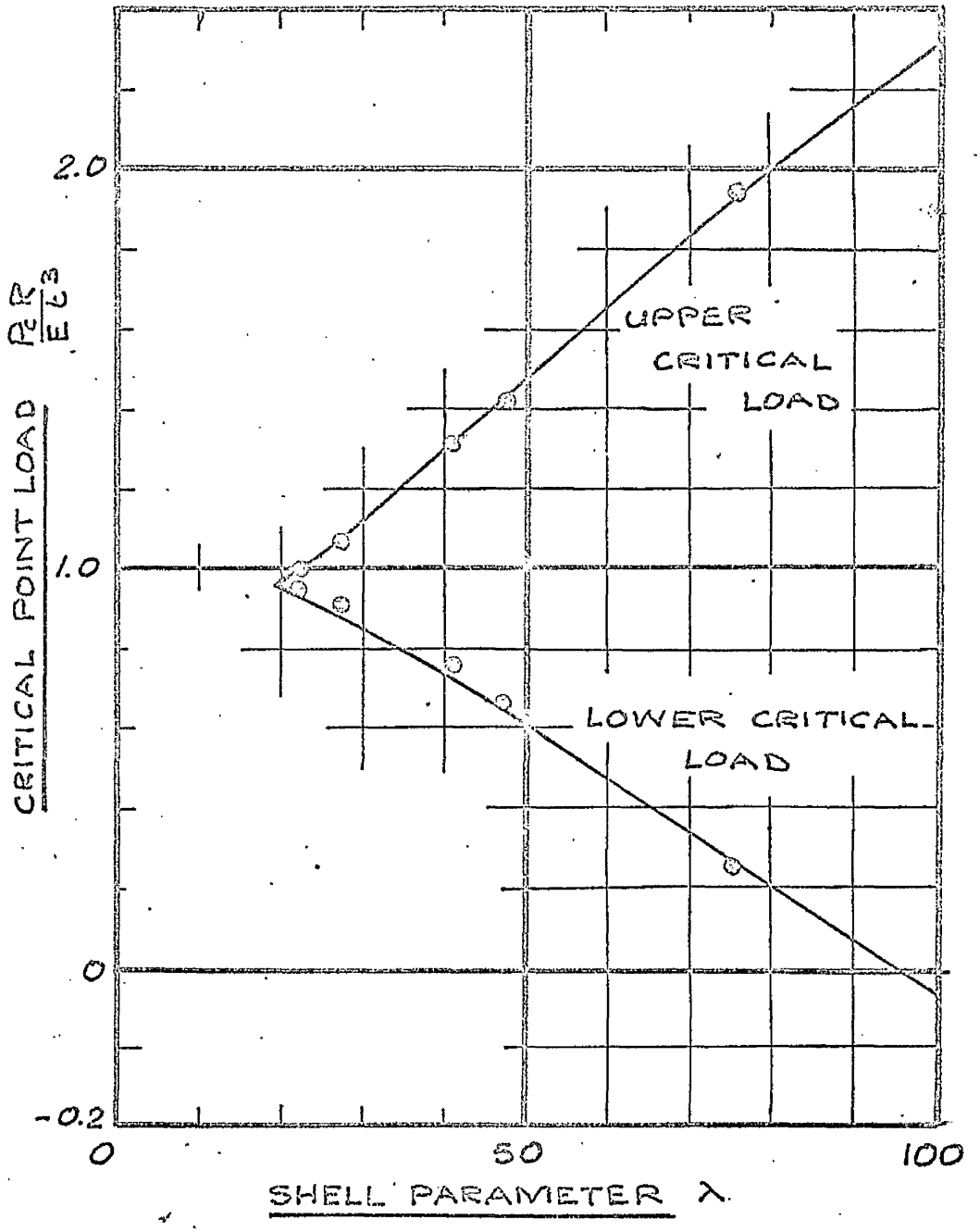

FIG. VII.10 Comparison of experimental and theoretical critical point loads for freely supported shallow spherical shells

ACKNOWLEDGEMENTS

ACKNOWLEDGEMENTS

The author wishes to express his thanks to Professor A.S.T. Thomson, Head of the Division of Mechanical, Civil and Chemical Engineering at the University of Strathclyde, Glasgow, for the use of the facilities of the Division.

Thanks are also due to Professor R.M. Kenedi, Research Professor in Bio-Engineering at the University, for his continued interest and guidance during the period of this investigation. The author also wishes to thank Dr. A.S. Tooth for his advice and encouragement over the period of research.

John D.W. Hossack.